SECT III

OPTICAL TECHNOLOGY APOLLO EXTENSION SYSTEM PHASE A

VOL II

FINAL TECHNICAL REPORT
NAS 8-20256

EXPERIMENTS

SPACE DIVISION CHRYSLER CORPORATION

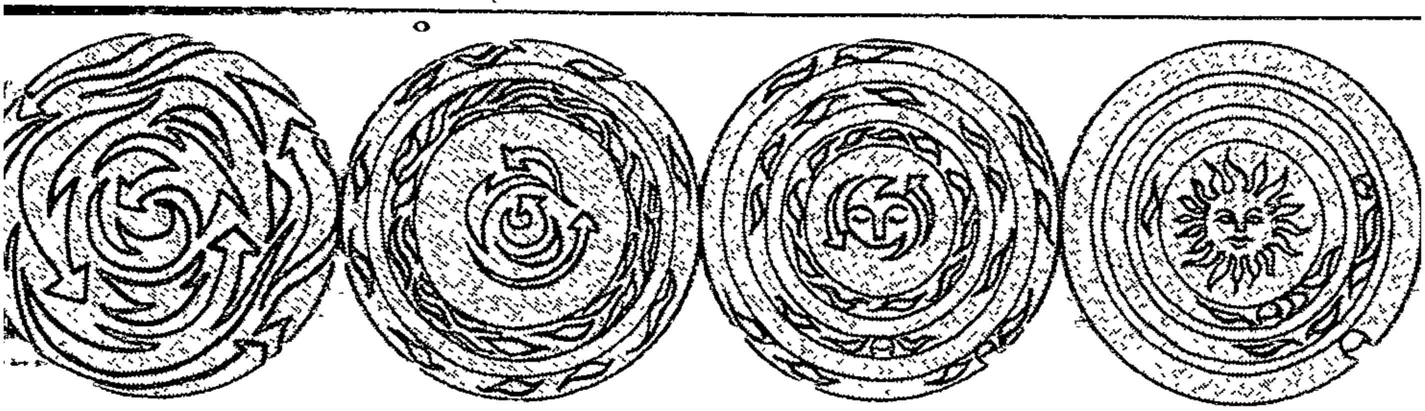

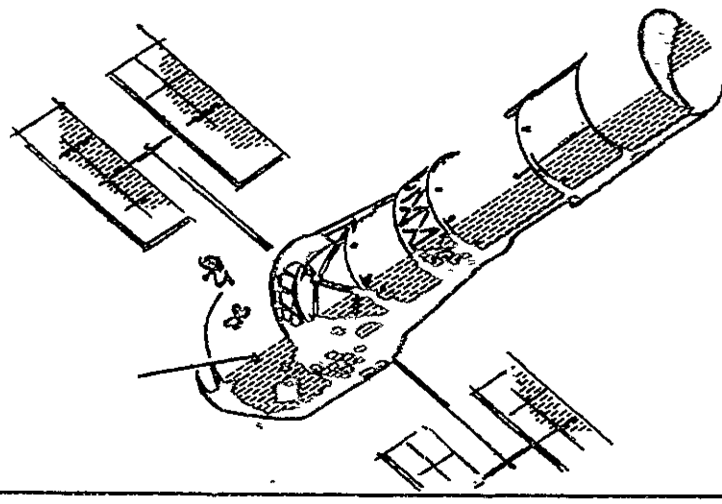

N68-11105 (ACCESSION NUMBER) (THRU) 1
355 (PAGES) (CODE) 23
CR-61925 (NASA CR OR TMX OR AD NUMBER) (CATEGORY)
FACILITY FORM 602

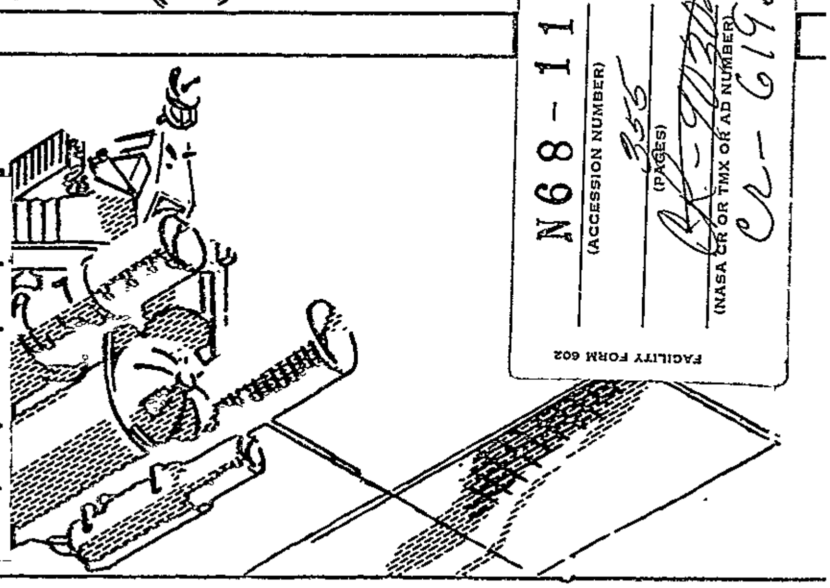

GPO PRICE $ ______

CFSTI PRICE(S) $ ______

Hard copy (HC) 3.00

Microfiche (MF) .65

ff 653 July 65

OPTICAL TECHNOLOGY
APOLLO EXTENSION SYSTEM
PHASE A

FINAL TECHNICAL REPORT

VOLUME II

SECTION III

EXPERIMENTS

OCTOBER 18, 1967

CONTRACT NAS 8-20256

Approved by: William W. Kloepfer

William W. Kloepfer
Program Manager

CHRYSLER-KOLLSMAN-SYLVANIA

CHRYSLER CORPORATION SPACE DIVISION
P.O. BOX 29200, NEW ORLEANS, LA. 70129

PREFACE

The final report of the Optical Technology Apollo Extension System study prepared for NASA/Marshall Space Flight Center under Contract Number NAS8-20256 is presented in six volumes. The study was a team effort by Chrysler Corporation Space Division (CCSD) (prime contractor), Kollsman Instrument Corporation (KIC) and Sylvania Electronic Systems (SES).

Volume 1, containing the Program Results (1.0, 2.0, 3.0 and 4.0) and the Optical Technology Development Plan (5.0, 6.0, 7.0 and 8.0) was the responsibility of CCSD.

Volumes 2 and 3 contain the Recommended Experiments (9.0 through 11.0) Integrated Experiment Requirements (12.0) and Other Experiments (13.0)

The SES experiments are:

- 9.6.1 Optical Heterodyne Detection on Earth
- 9.6.2 Optical Heterodyne Detection in Space
- 9.6.3 Direct Detection on Earth
- 9.6.4 Megahertz Optical Communication
- 9.6.8 10 Micron Phase and Amplitude Correlation
- 9.6.9 Pulse Distortion Measurements

The KIC experiments are:

- 9.6.5 Precision Tracking of a Ground Beacon
- 9.6.6 Point Ahead and Space-to-Ground-to-Space Loop Closure
- 9.6.7 Precision Tracking from One Ground Station to Another
- 10.2.1 Fine Guidance
- 11.4.1 Thin Mirror Nesting Principle
- 11.4.2 Primary Mirror Figure Test and Correction

The CCSD experiment is:

- 10.2.2 Comparison of Isolation Techniques

Integrated Experiment Requirements (12.0) and Other Experiments (13.0) were the responsibility of CCSD except for Residual Atmosphere Scattering Experiments (13.2.4) which was the responsibility of SES and Astronomical Uses of the OTAES Fine Guidance Telescope (13.3.2) which was the responsibility of KIC.

Volume 4 contains Systems Integration. CCSD prepared Candidate Missions (14.0), Manned Operations (15.0), Mission Analyses (16.0), Baseline Space Environment (17.0), Reliability (18.0) and System Requirements (20.0). SES prepared Ground Stations (19.0).

Volume 5 containing Subsystem Design was the responsibility of CCSD except for the Data Management Subsection which was prepared by SES and the Fine Guidance Thermal Analysis (27.5 and 27.6) which was prepared by KIC. This volume includes Design Integration (21.0), Structural and Mechanical Subsystem Design (22.0), Guidance, Navigation and Control (23.0), Propulsion and Reaction Control (24.0), Electrical Power (25.0), Environmental Control (26.0), Thermal Control (27.0), Data Management (28.0), Weight and Mass Properties (29.0) and Crew Equipment (30.0).

Volume 6 containing the Resource Analysis (31.0, 32.0 and 33.0) was the responsibility of CCSD.

MASTER

TABLE OF CONTENTS

PRECEDING PAGE BLANK NOT FILMED.

VOLUME II

TABLE OF CONTENTS

TABLE OF CONTENTS (Continued)

VOLUME II

TABLE OF CONTENTS (Continued)

Section III

EXPERIMENTS

9.0 OPTICAL PROPAGATION EXPERIMENTS

The scientific accomplishments of future NASA space missions will depend upon a continuing broad research and technology program. Many manned and unmanned space programs essential to our national scientific objectives will depend upon major technological advancements during the next few years. This is particularly true of atmospheric science and of planetary explorations -- the continuing improvement in knowledge of our own planet and its atmosphere, the long-standing goal to begin intensive exploration of Mars and Venus in the mid 1970's, and the renewed interest in probes of Jupiter and Mercury later in that decade.(1) The practicality of such missions will depend heavily upon the exploitation of electromagnetic techniques. The inherent precision of optical technology can offer solutions or alternatives to those present mission constraints that relate to sensor resolution and energy transmission.

If new techniques are to be ready when these new programs are defined, today's research and technology development efforts must be directed toward broad areas of potential applications. Therefore, the best strategy is to pursue a program of timely development of alternatives through methods which have the broadest possible prospect of success. Optical technology offers such a set of alternatives and should, therefore, be prosecuted in this broad fashion. This is particularly true for those optical techniques which apply to atmospheric science, communication, and those planetology measurements which depend upon remote optical sensing through planetary atmospheres.

Each of these applications require additional research in propagation -- the interaction of wave energy with the medium through which it passes. Atmospheric physics offers a valid theory for propagation through a turbulent medium; yet, viable mathematical solutions have not been derived for optical frequencies. Section 9.1, First Justification -- Optical Propagation in a Turbulent Atmosphere, discusses the present state of turbulence theory and the empirical contributions needed. The OTAES experiments are essential to these needs.

Such propagation research also constitutes the essential first step in optical communication research. Indeed, the most promising operational application for lasers is wideband communication over extremely long distances. The communicator

(1) E. M. Cortright, "Future Automated Space Mission Requirements," NASA/Electronic Industries Association Briefing on Aerospace Electronic Systems Technology, May 3, 1967.

must consider both the propagation disturbances which distort the received signal and other noise which appears in that signal due to the environment of his receiver.

In the eyes of the communicator, optical techniques simply offer a new electromagnetic frequency band. From a communication engineering viewpoint, there are two approaches by which to exploit a new band: the postulate or the diagnostic. In the past, such exploitation has frequently been solution oriented; i.e., each of the feasible communication system forms have been postulated and tested -- frequently resulting in dramatic forward strides in communication technology. However, this traditional approach occasionally proves less than optimum. A case in point is troposcatter communication, a valid form for which progress has been slowed due to heterogeneous results from the early solution-oriented test programs. In retrospect, the diagnostic approach would have been quite effective in the troposcatter case since most of the early test program difficulties are traceable to the state of knowledge of the transmission medium at that time. To avoid similar difficulties, it is essential that a foundation of spaceborne optical communication diagnostic data must be obtained. The diagnostic approach is discussed in section 9.2, Second Justification -- Optical Communication Diagnostics.

The OTAES optical propagation experiments, singly and as a group, are advanced as a means for studying both the Earth's atmosphere and as a prerequisite to wide-band optical communication from space to Earth:

1. Optical Heterodyne Detection on Earth (section 9.6.1)
2. Optical Heterodyne Detection in the Spacecraft (section 9.6.2)
3. Direct Detection on Earth (section 9.6.3)
4. Megahertz Optical Communication (section 9.6.4)
5. Precision Tracking of a Ground Beacon (section 9.6.5)
6. Point Ahead and Space-to-Ground-to-Space Loop Closure (section 9.6.6)
7. Transfer Tracking from One Ground Station to Another (section 9.6.7)
8. 10 Micron Phase and Amplitude Correlation (section 9.6.8)
9. Pulse Distortion Measurements (section 9.6.9).

9.1 FIRST JUSTIFICATION — OPTICAL PROPAGATION IN A TURBULENT ATMOSPHERE

Earth orbital laser tests are initially justified by the currently limited physical description of the atmosphere. Although a rigorous fundamental theory of turbulence exists, its solutions are characterized either by simplifying assumptions, or by unevaluated forms. The OTAES Optical propagation experiments are designed to verify or define many of these theoretical predictions.

The various manifestations of the atmosphere degradation of a laser beam are interrelated and their separation into rigorously defined, distinct observables is not possible. Nevertheless, it is physically meaningful to distinguish certain qualitative characteristics and their influence on direct-detection and optical heterodyne receivers. The effects of molecular and aerosol scattering and absorption are omitted, recognizing that these effects may also be quite important since they give rise to (possibly time-varying) attenuation and spreading of the beam. The effects due to turbulence are:

a. Amplitude flucutations (scintillation). At short ranges, a laser beam remains intact, and the amplitude variations are simply due to fluctuations in the overall cross-section ("breathing").(1) At ranges exceeding a few hundred meters (i.e., in the far-field of the "inner scale of turbulence" to be discussed below), the beam takes on a "boiling" appearance with light and dark patches throughout. The instantaneous intensity is no longer correlated across the entire beam. At still longer ranges, depending on the amount of turbulence, severe breakup of the beam is observed ("tearing").(2,3) This effect necessitates the use of a large receiver aperture in order to smooth out the fluctuations in the total received signal; in certain cases such as an optical heterodyne receiver, this requirement for a large aperture may conflict with other considerations.

b. Steering of the beam. The overall beam in the receiver plane is observed to move laterally. This dictates the use of large or multiple receivers and increased transmitter beam-divergence angles.

---

(1) P. Beckmann, "Signal Degradation in Laser Beams Propagated Through a Turbulent Atmosphere," Radio Science J. of Res., vol. 69D, April 1965, pp. 629-640.

(2) W. R. Hinchman and A. L. Buck, "Fluctuations in a Laser Beam Over 9 and 90 Mile Paths," Proc. IEEE (Correspondence), vol. 52, March 1964, pp. 305-306.

(3) J. R. Whitten, G. F. Prehmus, and K. Tomiyasu, "Q-Switched Laser Beam Propagation over a 10-Mile Path," Proc. IEEE (Correspondence), vol. 53, July 1965, p. 736.

c. Destruction of lateral phase coherence. Turbulence largely destroys the spatial coherence of the received beam, and the phase-correlation or coherence area becomes small — on the order of centimeters or millimeters, depending on conditions.[4] This coherence area represents the maximum effective aperture of a fixed heterodyne receiver,[5] but is largely immaterial in the operation of a direct-detection system. (An exception to this is in the case of a detector with a very small active area.[6] The spatial coherence effect may be conceptually (and even rigorously)[7] divided into two sub-effects, image "dancing" and image "blurring."

d. Transit-time fluctuations in the beam. This effect may limit the maximum information bandwidth in wideband systems, but is generally small and difficult to measure.[8]

e. Depolarization of the beam. It has been commonly assumed that atmospherically induced changes in beam polarization will be negligible. This assumption is especially pertinent to the consideration of polarization-modulation systems. Although, there have been reports of significant depolarization effects due to turbulence or aerosol scattering,[9] recent experiments showed no measurable depolarization.

The phase and amplitude effects associated with turbulence occur at low- and sub-audio rates. However, amplitude modulations caused by the atmosphere cannot be eliminated through the use of high modulation frequencies, contrary to some statements in the literature, because the effects are multiplicative rather than additive, and hence are not spectrally separable.

---

(4) I. Goldstein, A. Chabot, and P.A. Miles, "Heterodyne Measurements of Light Propagation Through Atmospheric Turbulence," Proc. IEEE, vol. 53, September 1965, pp. 1172-1180.

(5) A. E. Siegman, "The Antenna Properties of Optical Heterodyne Receivers," Proc. IEEE, vol. 54, October 1966, pp. 1350-1356.

(6) J.R. Kerr, "Microwave Bandwidth Optical Communications Systems," Proc. IEEE (to be published).

(7) D. L. Fried, "Statistics of a Geometric Representation of Wavefront Distortion," J. Opt. Soc. Am., vol. 55, November 1965, pp. 1427-1435.

(8) F. E. Goodwin, "The Measurement of Optical Phase Noise Over Long Atmospheric Paths," Proceedings of the Conference on Atmospheric Limitations to Optical Propagation, Boulder, Colo., March 1965, p. 293.

(9) D. L. Fried and G.E. Mevers, "Atmospheric Optical Effects--Polarization Fluctuation," J. Opt. Soc. Am., vol. 55, June 1965, pp. 740-741.

The above phenomenological descriptions have been mathematically described using geometrical optics.[1,10] Unfortunately, these descriptions also use an incorrect representation of turbulence, as discussed below. The "correct" theory of turbulence used with geometric or physical optics leads to expressions in which the above effects are all lumped into a total scintillation, phase fluctuation, or loss of coherence.

9.1.1 Theoretical Description of Turbulence Effects on Optical Propagation

The central physical quantity in the theory of turbulence effects is the refractive index, and its statistical description is in terms of a spatial correlation or structure function. These statistics are in turn related to meteorological variables and the altitude.[11] A rigorous theory of turbulence derives a somewhat complicated correlation function known as the Obukhov-Kolmogorov (O-K) function, in which the refractive index variations are characterized by a so-called "macroscale" (outer scale) and "microscale" (inner scale). The O-K function is used in the well-known work of Tatarski,[12] and by many of the authors in the current literature. Although the optical propagation descriptions are quite incomplete, the Kolmogorov turbulence theory per se is considered to be completely verified by experiment.[12,13]

A much simpler approach is to ignore the microscale, which is on the order of millimeters, and formulate the correlation function of refractive index as Gaussian. The remaining authors use this approach.[1,10,14] The difficulty with the Gaussian theory is that the mutual interference of beamlets deflected by the microscale is ignored, which has led to the erroneous inference that geometrical optics may be applied over any terrestrial path.[1] Also, a serious error arises in the functional dependence of some of the results obtained with this theory, even in the range of validity of geometrical optics. This will be discussed in paragraph 9.1.1.2.

---

(10) H. Hodara, "Laser Wave Propagation Through the Atmosphere," Proc. IEEE, vol. 54, March 1966, pp. 368-375.

(11) R. E. Hufnagel and N. R. Stanley, "Modulation Transfer Function Associated with Image Transmission Through Turbulent Media," J. Opt. Soc. Am., vol. 54, January 1964, pp. 52-61.

(12) V. I. Tatarski, Wave Propagation in a Turbulent Medium, McGraw-Hill Book Co., Inc., N. Y., 1961.

(13) J. L. Lumley and H. A. Panofsky, The Structure of Atmospheric Turbulence, John Wiley and Sons (Interscience), N. Y., 1964.

(14) L. A. Chernov, Wave Propagation in a Random Medium, McGraw-Hill Book Co., Inc., N. Y., 1960.

Use of the Obukhov-Kolmogorov turbulence theory is unavoidable if realistic results are to be obtained. For its derivation, the structure function, covariance, and correlation function of a physical quantity (x) are defined as follows:

$$\text{Structure function} = D_x(r) = \langle (x_1 - x_2)^2 \rangle$$

$$\text{Covariance} = C_x(r) = \langle (x_1 - \bar{x})\ (x_2 - \bar{x}) \rangle$$

$$\text{Correlation function} = \langle x_1 x_2 \rangle$$

where $\bar{x}$ is the mean value of x, and points 1 and 2 are separated (in the transverse plane) by a distance r. Isotropy and lateral stationarity of the statistics are also assumed. Note that

$$\text{Variance} = C_x(0)$$

and

$$D_x(r) = 2C_x(0) - 2C_x(r)$$

In essence, the result of this theory is an expression for the structure function of the refractive index (n) as follows:

$$D_n(r) = C_n^2(h) r^{2/3} \tag{1}$$

The quantity $C_n^2(h)$ is the refractive index "structure constant," and is a function of height and the strength of the turbulence. It is also simply related to a structure constant of temperature.[11] This is known as the "two-thirds law." The other pertinent parameter is the microscale of turbulence, which we denote by ℓ_o.

9.1.1.1 Basic Results of the Theory

The statistical solution for optical propagation in a turbulent medium is expressed basically in terms of structure functions and variances for the phase and logarithm of the amplitude, and in terms of the mutual coherence function of the received beam. These functions are expressed in terms of the refractive index structure constant, C_n, the inner scale, ℓ_o, the wavelength, λ, or wavenumber, $(2\pi/\lambda)$, and the distance or range, L. Until recently, the solutions were mostly limited to consideration of an infinite plane wave incident on the turbulent region, which unfortunately only applies to the case of starlight or a spaceborne laser. A detailed solution has now been obtained for the case of a point source (spherical wave propagation) in the turbulent medium, and a partial solution, in terms of unevaluated integrals, has been obtained for the actual case of a laser beam. However, important unresolved questions remain.

The solutions are obtained in most cases by means of a solution of the wave equation for propagation through an inhomogeneous medium.[12] The two principal mathematical techniques used are those of geometrical optics (the WKB approximation) and a perturbation approach ascribed to Rytov.[12] Geometrical optics fail to take into account interference between refracted beam-components, and hence are not valid beyond the near field of the inner scale (a few hundred meters, typically). The Rytov approach, which allows the use of physical optics, extends the solution to the far field of the inner scale. This approach has been questioned by a number of authors on mathematical grounds.[11,15,16] These particular questions have apparently been satisfactorily answered by Fried[17] and DeWolf.[18] However, there is still a range beyond which the Rytov approach must be viewed with caution.

The situation for the mutual coherence function or Modulation Transfer Function (MTF)[15] is unique, in that the wave equation need not be involved, and the Rytov approximation can be circumvented. The MTF, however, contains only limited information, i.e., the resolution of an image in the focal plane of the receiver optics (which is directly related to the performance of an optical heterodyne receiver). The solution for the MTF for infinite plane wave propagation over a horizontal path, is

$$M(r) = \exp\left[-\frac{1}{2} D(r)\right] \tag{2a}$$

where D(r) is the "wave structure function" given by

$$D(r) = \left(2.91\, k^2\, L\, C_n^2\right) r^{5/3} \quad , \qquad k = 2\pi/\lambda. \tag{2b}$$

This solution was first obtained by Hufnagel and Stanley[11] using an approach which circumvented the Rytov approximation. In their solution it was stated that "diffraction and scintillation cancel" insofar as the MTF is concerned, so that the

---

(15) M. J. Beran, "Coherence Properties of Radiation Passing Through a Random Medium," Stanford Electronics Laboratories, Stanford, Calif., Technical Report SU-SEL-65-086, September 1965.

(16) W. P. Brown, Jr., "Validity of the Rytov Approximation in Optical Propagation Calculations," J. Opt. Soc. Am., vol. 56, August 1966, pp. 1045-1052.

(17) D. L. Fried, "A Diffusion Analysis for the Propagation of Mutual Coherence," (to be published).

(18) D. A. DeWolf, (to be published). Also see D. A. DeWolf, "Wave Propagation Through Quasi-Optical Irregularities," J. Opt. Soc. Am., vol. 55, July 1965, pp. 812-817.

results are valid for any range L. Their method was questioned in regard to an averaging procedure,[15,19,20] but this objection has been explicitly answered by Fried.[17] Furthermore, this result has now been obtained using an entirely different and highly physical argument[17] and by other mathematical means.[15] Finally, it has been obtained by Fried using the Rytov approximation[21] which is taken as further indicating a general validity for the Rytov approach. Fried has also dropped certain small-angle approximations.

The solution of Eq. (2) thus seems well established. Beran[22] and Fried[23] have also obtained the MTF for a point source (spherical wave). The essential change caused by a spherical wave is that D(r) of Eq. (2b) must be multiplied by a factor of 3/8. The MTF for laser beam propagation has not been obtained.

The result for the MTF [Eq. (2a)] implies a "coherence area" of radius r_0 given by[21]

$$r_0 \doteq \left[6.88/A\right]^{3/5} \tag{3a}$$

where A is defined by

$$D(r) = A\, r^{5/3} \tag{3b}$$

in either the spherical or plane wave case. This parameter r_0 has great significance, since it is obtained from a theoretical development which does not require the Rytov approximation. In particular, r_0 describes the maximum useful aperture for an optical heterodyne receiver,[4] and may have other implications as described later.

---

(19) D. M. Chase, "Coherence Function for Waves in a Random Media," J. Opt. Soc. Am., vol. 55, November 1965, pp. 1559-1560.

(20) E. A. Trabka, "Average Transfer Function from Statistics of Wavefront Distortion," J. Opt. Soc. Am., vol. 56, January 1966, pp. 128-129.

(21) D. L. Fried, "Optical Resolution Through a Randomly Inhomogeneous Medium for Very Long and Very Short Exposures," J. Opt. Soc. Am., vol. 56, October 1966, pp. 1372-1379.

(22) M. J. Beran, "Propagation of a Spherically Symmetric Mutual Coherence Function Through a Random Medium," IEEE Trans. on Antennas and Propagation, vol. AP-15, January 1967, pp. 66-69.

(23) D. L. Fried, "Limiting Resolution Looking Down Through Atmosphere," J. Opt. Soc. Am., vol. 56, October 1966, pp. 1380-1384.

In order to obtain more detailed information concerning separate phase and scintillation effects, we must use the wave equation and geometric optics (near field of ℓ_o), or the Rytov approximation (far field of ℓ_o). The near-field results for the phase structure function, $D_\phi(r)$, and log-amplitude variance, $C_a(0)$, are [12]

$$D_\phi(r) = 2.91\, k^2\, L\, C_n^2\, r^{5/3} \tag{4}$$

$$C_a(0) = 2.46\, C_n^2\, L^3\, \ell_o^{-7/3} \tag{5}$$

Now, it may readily be shown[20] that the wave structure function and phase and log-amplitude structure functions are related at any range by

$$D(r) = D_\phi(r) + D_a(r) \tag{6}$$

Comparing Eq. (4) with Eq. (2b), we conclude that the log-amplitude structure function must be zero in the near field of the inner scale; that is, the amplitude fluctuations across the beam are perfectly correlated at short ranges (beam "breathing").

The far-field results as obtained from the Rytov approximation are not so easily expressed. The log-amplitude variance for the horizontal plane wave case is[12]

$$C_a(0) = 0.31\, C_n^2\, k^{7/6}\, L^{11/6} \tag{7a}$$

and for the spherical wave case is[24]

$$C_a(0) = 0.124\, C_n^2\, k^{7/6}\, L^{11/6} \tag{7b}$$

For a plane wave the phase structure functions in the limits of small and large (r) are given by[12]

$$D_\phi(r) = 1.46\, k^2\, L\, C_n^2\, r^{5/3}, \quad r \ll (\lambda L)^{1/2} \tag{8a}$$

$$D_\phi(r) = 2.91\, k^2\, L\, C_n^2\, r^{5/3}, \quad r \gg (\lambda L)^{1/2} \tag{8b}$$

The exact curves for $C_a(r)$ and $D_\phi(r)$ are given in Reference (25) for plane waves and in Reference (24) for spherical waves.

---

(24) D. L. Fried, "Propagation of a Spherical Wave in a Turbulent Medium, J. Opt. Soc. Am., vol. 57, February 1967, pp. 175-180.

(25) D.L. Fried and J.D. Cloud, "Propagation of an Infinite Plane Wave in a Randomly Inhomogeneous Medium," J. Opt. Soc. Am., vol. 56, December 1966, pp. 1667-1676.

In particular, for large (r), $D_a(r)$ approaches the asymptote

$$D_a(\infty) = 2\, C_a(0)\ [1 + C_a(0)] \tag{9}$$

Since $D_\phi(r)$ does not approach a constant for large (r), $D_\phi(\infty) = D(\infty)$ as may be seen from a comparison of Eq. (8b) and Eq. (2b). It should be pointed out that there are mathematical problems with the existence of the variance or covariance of phase, so that only the structure function of (ϕ) is used. Also, it may be shown that the mean value of log-amplitude is not zero and is, in fact, given by

$$\bar{a} = -C_a(0) \tag{10}$$

This very important point is central in the answer of Brown's objection to the Rytov method.(16,17)

In the results for $C_a(r)$ given in References (24) and (25), the log-amplitude covariance falls to zero when $r \approx (\lambda L)^{1/2}$. That is, the theory predicts a log-amplitude correlation area with radius = $(\lambda L)^{1/2}$. This predicts that the amplitude correlation area will increase indefinitely with increasing range L. Also, Eq. (7) predicts that the log-amplitude variance also increases indefinitely with L. Both predictions are physically impossible, and prove that the Rytov approximation must still have a limit on the range of validity. Tatarski has recently made this point(27), but his alternate arguments are also disputed.(38)

At any rate, there must be a range wherein scintillation "saturation" sets in so that the variance and correlation area of the log-amplitude can no longer increase with L. This has been experimentally observed. Fried (17,38) speculates that the limit of validity of the Rytov approximation is reached at a range for which r_o (obtained independently of the Rytov approach) equals $(\lambda L)^{1/2}$. Equivalently, this is the range for which $C_a(0)$ equals approximately 1/2. For conditions of fairly strong turbulence this critical range can be on the order of 5 km, and for longer ranges there are no analytic solutions other than for the modulation transfer function. Furthermore, we speculate here that this is the critical range for which beam-boiling is observed to change in character to gross beam-tearing, with characteristic spots whose size is more or less independent of further increases in range.(28)

---

(26) D. D. Fried, "Aperture Averaging of Scintillation," J. Opt. Soc. Am., vol. 57, February 1967, pp. 169-174.

(27) V. I. Tatarski "On Strong Fluctuations of Light Wave Parameters in a Turbulent Medium," Soviet Physics JETP, vol. 22, May 1966, pp. 1083-1088.

(28) Conference on Atmospheric Limitations to Optical Propagation, Boulder, Colo., March 1965.

The results given above for the infinite plane and spherical wave cases cannot be applied too closely to the case of a laser beam. The laser beam case itself has been analyzed by Schmeltzer,[29] and he has obtained unevaluated integrals for the structure functions of phase and log-amplitude. Although the Rytov approximation was not used per se, Fried has pointed out that the effect was the same.[30] The results are thus subject to the above range limitation.

Fried has used Schmeltzer's analysis to calculate the variance of the log-amplitude for vertical and horizontal propagation.[31,32] For horizontal propagation, he has normalized the variance with that for spherical propagation [Eq. (7b)], and plotted it against the normalized transmitter size (Ω):

$$\Omega = k\alpha^2/L \tag{11}$$

where α is the standard deviation of the amplitude distribution across the transmitter aperture. He has plotted separate curves for a collimated and a focused beam, and noted that the variance approaches that for the spherical wave case when L is large, as might be expected. An inflection takes place near the critical value $\Omega = 1$, and Fried argues that the critical role of such quantities as $(\lambda L)^{1/2}$ and Ω should be self-evident from dimensional analyses. The laser beam result for log-amplitude variance is one theoretical prediction that can be directly compared with experiment.

Although Schmeltzer's results for the log-amplitude structure function or covariance of a laser beam have not been evaluated, Fried uses some recent experiment and dimensional analyses to argue that the covariance is in the form[33,38]

$$C_a(r) = C_a(0) \cdot f\left[r/(\lambda L)^{1/2},\ r/(L/k\alpha)\right] \tag{12}$$

where f is some undetermined function whose general nature is known.[33] The experiments will be further discussed in paragraph 9.1.2.

---

(29) R. A. Schmeltzer, "Means, Variances, and Covariances for Laser Beam Propagation Through a Random Medium," Quarterly of Appl. Math., vol. XXIV, January 1967, pp. 339-354.

(30) D. L. Fried, "Test of the Rytov Approximation," J. Opt. Soc. Am., vol. 57, February 1967, pp. 268-269.

(31) D. L. Fried and J. B. Seidman, "Laser-Beam Scintillation in the Atmosphere," J. Opt. Soc. Am., vol. 57, February 1967, pp. 181-185.

(32) D. L. Fried, "Scintillation of a Ground-to-Space Laser Illuminator," (to be published).

(33) D. L. Fried, G. E. Mevers and M. P. Keister, Jr., "Measurements of Laser Beam Scintillation in the Atmosphere," (to be published).

It should also be pointed out that a new attempt to consider multiple scattering, and terms of higher order than allowed by the Rytov approximation, has been reported by Livingston.(34) Also, Brown(35) has borrowed techniques such as Feynmann diagrams from quantum electrodynamics to study the multiple scattering of light by weak random inhomogeneities in the atmosphere. Brown's method agrees with the single scattering results for short ranges but must be altered to include the Gaussian shape of the actual laser wavefront before its longer range predictions can be experimentally tested. Finally, Taylor(36) has reconsidered the validity of the Rytov approximation from the point of view of Keller's(37) theory of linear stochastic operators and perturbations. He finds the Rytov solution cannot apply beyond the single scattering domain covered with equal felicity by the Born approximation. However, since Taylor considers the solutions themselves instead of their variances, it is not clear whether his objections have not already been answered by Fried.(38)

9.1.1.2 Use of the "Incorrect" Turbulence Theory

The use of a Gaussian structure function for the index-of-refraction, in place of the Obukhov-Kolomogorov function of Eq. (1), is worth additional comment, since it is the basis of one text on the topic(14), as well as the detailed geometric-optics calculations of Beckmann(1) and Hodara.(10)

The argument is basically that the structure of the index of refraction may be (at least to good approximation) described by a single characteristic correlation length, R, rather than by an inner and outer scale. This leads to two serious errors. First, since R in this context has a large value (meters), it is erroneously concluded by Beckmann (and, essentially, by Hodara) that the receiver will always be in the near field of R over any atmospheric path, and hence that geometric optics will suffice for any range L. Second, even in the range where geometric optics are accepted by the rigorous theory (the near field of ℓ_0), the use of the incorrect

---

(34) P.M. Livingston, "Multiple Scattering of Light in a Turbulent Atmosphere," J. Opt. Soc. Am., vol. 56, December 1966, pp. 1660-1667.

(35) W.P. Brown, Jr., "Propagation in Random Media - Cumulative Effect of Weak Inhomogeneities," IEEE Trans. on Antennas and Propagation, vol. AP-15, January 1967, pp. 81-89.

(36) L.S. Taylor, "On Rytov's Method," Radio Science, vol. 2, April 1967, pp. 437-441.

(37) J.B. Keller, F.C. Karal, Jr., "Elastic, Electromagnetic and Other Waves in a Random Medium," J. Math. Phys., vol. 5, April 1964, pp. 537-547.

(38) Seminar on Atmospheric Effects on Optical Propagation, given by D.L. Fried, University of Alabama Research Institute, Huntsville, Ala., April 3-6, 1967.

index-of-refraction structure leads to serious errors in the functional dependence of the results. For instance, the phase structure function implicit in Beckmann's analysis is

$$D_\phi(r) = \frac{\langle \mu^2 \rangle k^2 L \pi^{1/2} r^2}{R} \tag{13}$$

which is proportional to 1/R. On the other hand, the true structure function [Eq. (4)] is independent of ℓ_0 or the turbulent scale. Also, the coherence radius, r_0, as deduced from Beckmann depends on $R^{1/2}$, whereas the true r_0 is independent of ℓ_0. Beckmann's detailed results for beam steering, etc., and his argument that "large blobs cause the effects," is apparently incorrect.

As a further criticism of the incorrect turbulence representation, we note that Chernoff's result in the far field of R for $C_a(0)$ is proportional to (RL), while the true result [Eq. (7)] is proportional to $L^{11/16}$ and independent of ℓ_0.

One justification Beckmann gives for his use of the incorrect turbulence representation is that it enables him to include anisotropies in his calculations. However, observed anisotropies are generally small and primarily involve slow beam steering.

Finally, we note that the only analysis of depolarization effects due to turbulence is that of Hodara, which, on the above grounds, must be taken with caution.

9.1.1.3 Other Considerations

There are several other considerations of interest in any discussion of turbulent propagation theory:

a. Refractive Index Structure Constant

It must be pointed out that the quantity C_n, which is a measure of the strength of the turbulence at any given place and time, plays a central role in the quantitative predictions of turbulent effects given above. Unfortunately this parameter is difficult to calculate or measure nonoptically. General data on average C_n vs. altitude have been given by Hufnagel and Stanley,(11) and there has been good experimental verification by other investigators. Coulman(39) has reviewed a method of calculation of C_n based on such

(39) C.E. Coulman, "Optical Image Quality in a Turbulent Atmosphere," J. Opt. Soc. Am., vol. 55, July 1965, pp. 806-812.

C.E. Coulman, "Dependence of Image Quality on Horizontal Range in a Turbulent Atmosphere," J. Opt. Soc. Am., vol. 56, September 1966, pp. 1232-1238.

C.E. Coulman and D.N.B. Hall, "Optical Effects of Thermal Structure in the Lower Atmosphere," Applied Optics, vol. 6, March 1967, pp. 497-503.

meteorological measurements as temperature lapse rate (vertical gradient), wind speed and gradient, and surface roughness. The calculations are only valid below a certain rather low altitude (e.g., 60 meters) known as the "Obukhov length". On the other hand, it is well known that turbulence is much higher near the ground than at a reasonable distance from it. C_n, which is directly related to the temperature structure constant, C_T, may also be determined from the measurement of the instantaneous temperature distribution throughout the region of interest. This requires the use of a high-speed thermometer.

b. Spectrum of Scintillations

The spectrum of the signal fluctuations in a photodetector is of interest. Based on the hypothesis of a turbulent pattern which is "frozen-in" and blowing laterally through the path of propagation, the spectrum has been calculated for the case of infinite plane wave propagation.[12, 40, 41] The frequency content of the scintillations is predicted to drop rapidly, above some frequency which is given by the ratio of the transverse wind velocity and the log-amplitude correlation length $(\lambda L)^{1/2}$. The experimental results will be discussed in paragraph 9.1.2. We note that the scintillation contains only negligible components above a few hundred hertz.

c. Angular and Spectral Covariance

Fried[38] has also generalized the calculation of structure functions to include two different wavelengths at points 1 and 2 in the receiver plane, or alternatively, two different angles of arrival. His results indicate that spatial diversity may be desirable--i.e., two nearby source points may scintillate independently--and that spectral spread of a modulated signal should be negligible.

d. Performance of an Optical Heterodyne in the Presence of Turbulence

Atmospheric turbulence degrades the performance of an optical heterodyne system to the point where much of the original enthusiasm for these systems has subsided, at least at visible and near-infrared wavelengths.[6] In particular, a simple heterodyne cannot obtain an increase in signal for

---

(40) E. Ryznar, "Dependency of Optical Scintillation Frequency on Wind Speed," Applied Optics, vol. 4, November 1965, pp. 1416-1418.

(41) J. I. Davis, "Consideration of Atmospheric Turbulence in Laser Systems Design," Applied Optics, vol. 5, January 1966, pp. 139-147.

an increase in aperture radius[4] above r_0. A number of suggestions have been made to the effect that a heterodyne receiver which electronically tracks the instantaneous wavefront tilt (image dancing) may partially overcome this limitation.[42, 43, 44]

Fried[21] has used the wave structure function for infinite plane and spherical waves to calculate the optical resolution or MTF for long and short exposures in a photographic system operating through the atmosphere. He then relates these results to the case of a tracking heterodyne receiver,[45] and shows that the short-exposure case is analogous to the tracking-heterodyne case. He further shows, in contrast to previous papers, that the improvement to be obtained through heterodyne tracking is not substantial except in the near field of the transmitter.

Heterodyne tracking of the wavefront tilt is difficult to implement, and in view of the above considerations, is of questionable value. Fried recommends the use of an array of heterodyne receivers with phase-locking of their IF outputs[38], but this may also be very difficult.

Performance of Direct-Detection Receivers in the Presence of Turbulence

Fried has shown[33] that the log-amplitude (point detector) and phase hav Gaussian probability distributions. Phase coherence is not of importance in a direct-detection optical receiver, providing that the detector area is

(42) D. M. Chase, "Power Loss in Propagation Through a Turbulent Medium for an Optical-Heterodyne System with Angle Tracking," J. Opt. Soc. Am., vol. 56, January 1966, pp. 33-44.

(43) W. S. Read and R. G. Turner, "Tracking Heterodyne Detection," Applied Optics, vol. 4, December 1965, pp. 1570-1573.

(44) G. R. Heidbreder, "Aperture-Gain Loss Due to Atmospheric Turbulence," J. Opt. Soc. Am., vol. 56, November 1966, pp. 1634-1635.

G. R. Heidbreder and R. L. Mitchell, "Effect of a Turbulent Medium on the Power Pattern of a Wavefront-Tracking Circular Aperture," J. Opt. Soc. Am., vol. 56, December 1966, pp. 1677-1684.

G. R. Heidbreder, "Image Degradation with Random Wavefront Tilt Compensation," IEEE Trans. on Antennas and Propagation, vol. AP-15, January 1967, pp. 90-98.

G. R. Heidbreder and R. L. Mitchell, "Power Pattern Degradation for Weighted Circular Apertures in a Turbulent Atmosphere," IEEE Trans. on Antennas and Propagation, vol. AP-15, January 1967, pp. 191-192.

(45) D. L. Fried, "Optical Heterodyne Detection of an Atmospherically Distorted Signal Wavefront," Proc. IEEE, vol. 55, January 1967, pp. 57-67.

not too small. Also, the effects of scintillation, as expressed by $C_a(r)$, may be averaged-out through the use of a large receiving aperture, which need not be diffraction-limited. The fluctuations in the total received signal or photocurrent with a large aperture have been predicted by Tatarski [12, 27] to have a Gaussian probability distribution. This result can also be obtained by applying the central limit thereon. However, Fried has stated that this is generally not the case [26, 33] and, in fact, it appears that the total received power will also undergo log-normal fluctuations, albeit with a smaller variance. Unfortunately, the utility of Fried's detailed predictions for the aperture-averaging of scintillation (Reference 26) is somewhat limited, since the solution is for the infinite plane wave case. His conclusion regarding log-normal statistics, however, is general. [33]

9.1.2 Experimental Observations of Turbulence Effects

The effect of the atmosphere on astronomical seeing has been reviewed by Ellison. [46] The observations of laser beam degradation that have been carried out have, in general, given sketchy results and do not serve to verify or disprove the theory.

Hinchman and Buck have reported measurements on a He-Ne laser beam propagated horizontally over distances of 9 and 90 miles. [2, 47] The beam divergence was effectively 8.7 and 13 arc-seconds, respectively, while the diffraction spread in an ideal medium would have been 1 second of arc. The beam diameter increased as the 1.27 power of range, and increases in beam spread were noted in the presence of significant aerosol concentrations. The light was collected using 3-inch optics and a photomultiplier. The detected level was little above the background, except for short bursts 10-dB higher, indicating severe beam tearing. The beam was observed to wander over an area several times its diameter, and long-term angular drifts were noted. The detected signals from a horizontal array of six photomultipliers each spaced by six inches were uncorrelated. It seems clear that the Rytov theory must not apply over these long ranges.

Theoretical predictions of beam spread due to turbulence have not been directly obtained. However, as mentioned in paragraph 9.1.1.3, there is reason to believe that the minimum spread for a large, diffraction-limited transmitter will be determined by r_o.

---

(46) M. A. Ellison, "The Effects of Scintillations on Telescope Images," Proceedings of a Symposium on Astronomical Optics and Related Subjects, Z. Kopal, Ed., John Wiley and Sons (Interscience), N. Y., 1956.

(47) A. L. Buck, "Laser Propagation in the Atmosphere," Proceedings of the Conference on Atmospheric Limitations to Optical Propagation, Boulder, Colo., March 1965.

Photographs which graphically depict beam tearing have been published by Whitten, et al. [3] Ruby laser pulses of 40-nanosecond duration were propagated over a 10-mile path and photographed on a 28-inch screen. Small bright spots were observed, from 1/2 to 5/4 inch in diameter, in clusters of 1 foot across. The instantaneous range of brightness within the average beam diameter was 40 dB, and the illumination was never uniform over any appreciable area.

It is interesting to note that a truism has grown among laser experimenters that the size of the bright spots in a "torn" beam is more or less independent of range, beyond some critical distance. [28] The conjecture that this critical distance is that at which the Rytov approximation breaks down ($r_0 = \lambda^{1/2}L^{1/2}$) suggests that the amplitude correlation radius probably becomes r_0, which is proportional to $L^{-3/5}$, and hence shows a weak inverse dependence on range.

In measurements over a 3.2-km path, Straub [48] has found peak-to-peak beam pointing of 6 meters in the vertical direction and 30 cm in the horizontal direction. Two side-by-side beams were observed to bend in opposite directions.

9.1.2.1 Quantitative Measurements of Scintillation

Quantitative measurements have been made of scintillation (photocurrent) spectra, scintillation statistics and aperture averaging, beam diameter, transmitter aperture effects, and range dependence.

The spectrum of the photocurrent or total received signal in the presence of scintillation has been found by a number of workers [40, 49, 50, 51], to correlate with the transverse wind speed, as discussed in paragraph 9.1.1.3. However, the spectral width has not been found [50, 52] to be proportional to $L^{-1/2}$. In fact,

---

(48) H. W. Straub, "Coherence in Long Range Laser Beams," Applied Optics, vol. 4, July 1965, p. 875.

(49) M. Subramanian and J. A. Collinson, "Modulation of Laser Beams by Atmospheric Turbulence--Depth of Modulation," Bell Sys. Tech. J., vol. XLVI, March 1967, pp. 623-648.

(50) D. H. Höhn, "Effects of Atmospheric Turbulence on the Transmission of a Laser Beam at 6328 Å," Applied Optics, vol. 5, September 1966, pp. 1427-1436.

(51) G. E. Axtelle, Jr., "Optical Propagation Studies," Proceedings of the Conference on Atmospheric Limitations to Optical Propagation, Boulder Colo., March 1965, pp. 8-12.

(52) A. L. Buck, "Effects of the Atmosphere on Laser Beam Propagation," Applied Optics, vol. 6, April 1967, pp. 703-708.

Hinchman and Buck have reported that the spectrum was the same at 9 and 90 miles. (2) Again, many of these experiments may have been outside of the range of validity of the Rytov approximation. Also, at least one set of measurements (5) can be criticized on the grounds that a free-running, multimode laser was used, which probably resulted in the presence in a large amount of low frequency laser noise. The spectra have been found to be independent of the receiver diameter, (52) or to have a steep slope at large apertures. (52) The theoretical $\lambda^{-1/2}$ dependence of the spectral width has been tested by Chu, (53) and it was found that the (negative) exponent is actually smaller than 1/2.

Measurements of total signal fluctuations vs. aperture size at ranges of 4.5 km and 14.5 km by Höhn (50) have shown that the log-normal statistics are not too good over a long path with large amounts of scintillation. Under these conditions it was also found that the dependence of fluctuations on aperture size was small. Using distances up to 145 km, Buck (52) has found no systematic variation of signal fluctuation with range. The amount of fluctuation was found to approach zero for apertures on the order of 40 cm.

On the other hand, Subramanian and Collinson, (49) using a folded range of up to 2400 feet in length and a very-low-noise laser, have found that the fluctuations do not go to zero for an aperture larger than the beam diameter. They measured a depth of modulation proportional to L^3 as predicted by Eq. (5). Hence, it was concluded that their operation was in the near field of the turbulence scale, which was deduced to be on the order of 5 cm. This is a surprising result. They also observed the scintillation changing by an order of magnitude in a matter of seconds.

The most sophisticated scintillation measurements have recently been made by Fried. (33) Using an 8-km path, he and his co-workers have found the signal fluctuations to be log-normal for apertures up to 100 cm. Also, he has found that the covariance of scintillation falls rapidly until $r = (\lambda L)^{1/2}$, and then remains nearly constant until $r = L/k\alpha$. (It then presumably falls slowly to zero with further increases in r.) This has lead to speculations involving the form of Eq. (12). It appears that these results can be explained through the predictions of the Rytov-based theory with approximate corrections for the finite laser aperture.

There are thus two critical separations (r) in the transverse plane, from the standpoint of amplitude correlations: the Fresnel distance, $(\lambda L)^{1/2}$, and the transmitter diffraction distance, $L/k\alpha$. This can be argued strictly from dimensional analysis.

---

(53) T. S. Chu, "On the Wavelength-Dependence of the Spectrum of Laser Beams Traversing the Atmosphere," Applied Optics, vol. 6, January 1967, pp. 163-164.

Thus, one cannot substantially reduce signal fluctuations with a receiver larger than the Fresnel distance but smaller than the transmitter diffraction distance. Furthermore, in attempting to reduce fluctuations by using a large transmitter (α), there may be no point in going beyond $\alpha = (L/k)^{1/2}$. Using the parameters from Fried's experiments, this would represent a maximum useful transmitter diameter of 10 cm. Similarly, Buck[52], has determined the maximum useful transmitter aperture for a range of 2 km to be 11 cm.

9.1.2.2 Measurements of Phase Distortion

The measurement of phase or wavefront distortion has generally been accomplished indirectly using image-quality or optical heterodyne receiver performance. These are really a measure of the MTF or r_0, rather than the phase covariance.

Rogers has measured the dependence of the image blur circle on range up to 3000 yards.[54] He concluded that the rms angular size of the image increased as the 0.44 power of the range, rather than the theoretical prediction of 0.6. However, this result was taken from short exposures, in which full time-averaging of the turbulent image distortion did not take place.

Buck[47] has performed measurements which indicate that the incident wave is best represented in terms of infinite plane waves arriving at discrete angles. In these measurements, the image was photographed as the receiver aperture was varied from 1.3 cm to 27.7 cm, with a propagation range of 13 km. In all cases, the image appeared as separate clusters of spots, the overall cluster size being roughly 150 microradians in extent, independent of aperture. However, the clusters were made up of individual spots which were diffraction limited by the (variable) aperture. This is a different qualitative picture than one might expect, if one thinks of each phase correlation area as probably resulting in an amorphous image.

Experimental work performed by Goldstein, et al.[4] on heterodyne performance vs. receiver aperture has shown a rough agreement with the coherence area predicted by r_0. The experiments clearly show the existence of a maximum effective aperture which varies with turbulence conditions.

Sophisticated experiments have been performed by Coulman, in which he determined the Modulation Transfer Function (MTF) for a point source.[39] He did not have the results of the spherical wave theory,[23] and his integration time was

---

(54) C. B. Rogers, "Variation of Atmospheric 'Seeing' Blur with Object-to-Observer Distance," J. Opt. Soc. Am., vol. 55, September 1965, pp. 1151-1153.

perhaps too short for full averaging. Referring to Eq. (2b), with the coefficient multiplied by 3/8 to correct for spherical propagation, it is possible to compare his results with theory. The dependence on $r^{5/3}$ was supported. The dependence of the "blur circle" or (r_o) on range was in agreement with Rogers and, hence, not in agreement with theory. However, Fried (30) has used these data to show an excellent fit of the MTF vs. C_T^2 (or C_n^2), thus correborating the numerical coefficient (2.91 x 3/8) and the validity of the theory beyond the realm of geometric optics.

9.1.2.3 Transit-Time Dispersion of the Beam

There are a number of mechanisms for which transit-time dispersion of the beam can be predicted and estimated. These will not be reviewed here. However, this effect would result in a limitation on modulation bandwidth or pulse shortness. Kerr is currently in the process of measuring the transmission of short optical pulses over a long path.

Related measurements of absolute phase variations have been attempted by Goodwin (8) and Buck. (52) Goodwin succeeded only in setting a lower bound on the effect, since his measurements were limited by laser stability. Buck has set up an interferometer with a 48.8-meter path length and one leg in a nonturbulent tunnel. He has measured a mean phase deviation of 0.25 microns, which is quite substantial. Much further work is needed here.

It is important to note here that if $2r_o$ is the phase correlation diameter at the receiver, and the transverse wind speed is v_T, then the ratio $v_T/2r_o$ is the <u>rate</u> of phase variation, not the amount. This is contrary to many statements in the literature.

9.1.2.4 Other Measurements

The nonoptical determination of the strength of the turbulence, i.e., the structure constant C_n, is desirable for an independent check of the theory. This is a difficult problem, and can only be attempted over highly artificial, uniform propagation paths. The measurement of micrometerological parameters (39) has in at least one instance led to values of C_n which agree well with optical experiments. However, other investigators have found very poor correlations. (49)

Fried and Mevers (9) have inferred the surprising experimental conclusion that the optical polarization can vary significantly after traversing a turbulent medium. It is hypothesized that this is caused by light scattering out of the beam (large-angle scattering), for which there is very little theoretical description. (34) However, scintillation is not considered. More recently Saleh[55] has reported measuring no depolarization effect at 0.6328 microns over a 2.6-km path with a measurements sensitivity of 45 dB.

The above experiments on optical propagation through the atmosphere can be classified into two basic categories: 1) electronic observations and 2) photographic observations. The use of moving or still pictures, either of the direct beam or of the image, is attractive in that data processing need not be done in real time. However, the accurate densitometric evaluation of the results requires extreme skill and caution. The most advanced work in this area is probably that by Deitz.[56]

9.1.3 Needed Measurements

9.1.3.1 Scintillation of a Ground-to-Space Laser

The scintillation of a laser beam propagating through a turbulent atmosphere from a ground transmitter to a spacecraft receiver, measured in terms of the log-amplitude variance, $C_a(o)$, has been examined theoretically by Fried.[32] The analysis, which assumes a collimated Gaussian shaped laser beam, shows that $C_a(o)$ can be expressed in terms of a transmitter size independent term $C_a^S(o)$ and a size dependent factor which is a function of the ratio $k\alpha_o^2/Z$ where k is the wave number ($k = 2\pi/\lambda$); Z is the propagation path length, and α_o is the standard deviation of the beam amplitude pattern. $C_a^S(o)$, which is essentially a normalization factor, is the value of $C_a(o)$ associated with a point source transmitter ($\alpha_o = o$), i.e., propagation of a spherical wave. The spherical wave log-amplitude variance is given by[32]

$$C_a^S(o) = 0.727 \sec^{11/6} \theta \, (5 \times 10^{-7}/\lambda)^{7/6}$$

where λ is the wavelength in meters and θ is the angle away from the Zenith direction.

Figure 9.1.3.1-1, from Reference (32), shows the dependence of the normalized log-amplitude variance upon the normalized source size Ω. The interesting feature of this result is that the Gaussian plane wave scintillation can be substantially lower than the spherical wave case for large transmitting optics or wavelengths.

---

(55) A. A. M. Saleh, "An Investigation of Laser Wave Depolarization by Atmospheric Transmission," presented at 1967 IEEE Conference on Laser Engineering and Applications, Washington, D. C.

(56) P. H. Deitz, "Optical Method for Analysis of Atmospheric Effects on Laser Beams," (to be published).

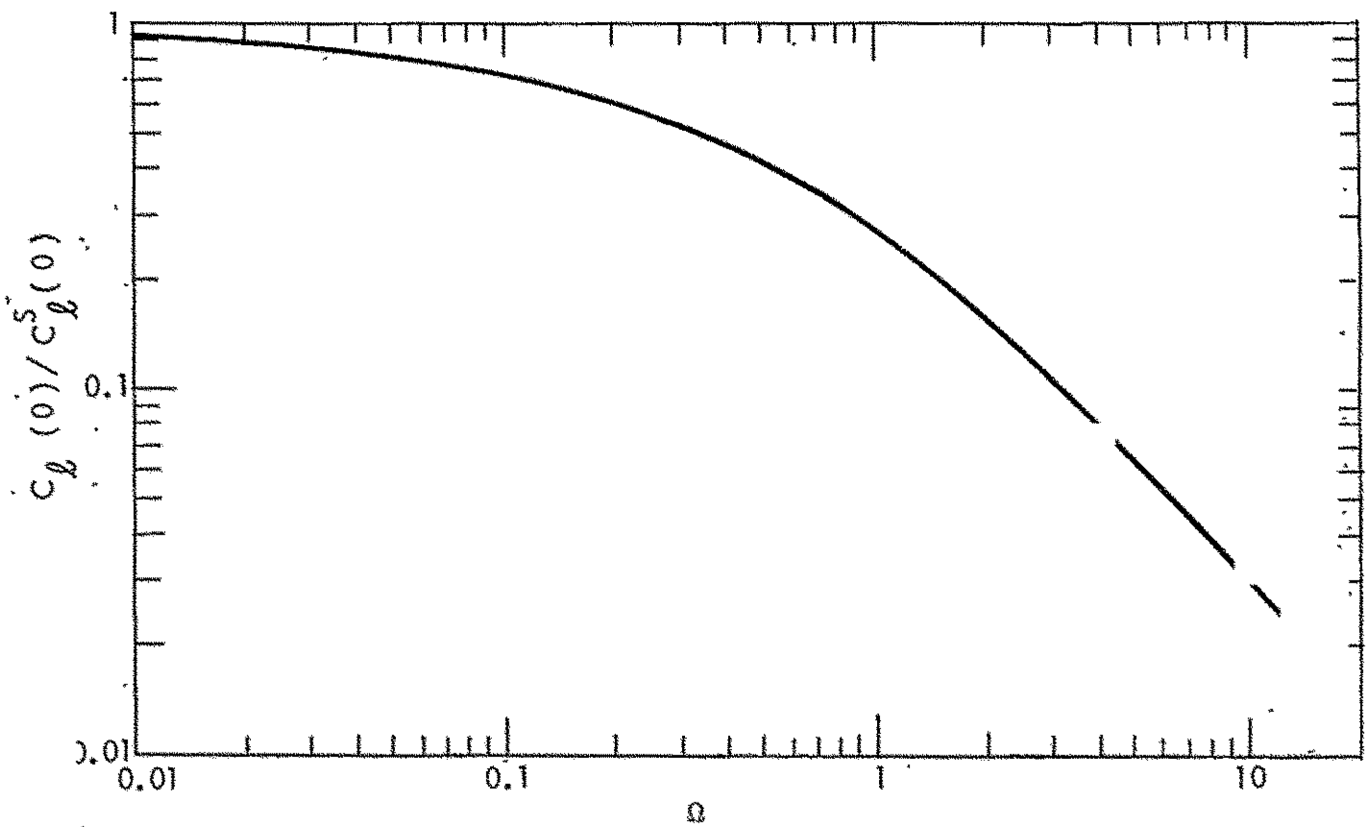

Figure 9.1.3.1-1. Dependence of the Normalized Log Variance, $C_a(o)/C_a^S(o)$, on Normalized Source Size Ω Observations from Space of a Ground Transmitter. ($C_a(o)$ is the log-amplitude variance served for transmission of radiation with wave number k (wavelength $\lambda = 2\pi/k$) at an gle θ off of the zenith. The transmitter optics are illuminated with a Gaussian spread of tensity, the standard deviation of the amplitude is α_o. The normalized source size, $\Omega = k\alpha_o^2/k_o \sec\theta$, where k_o=3200 meters is the "scale height" of refractive index turbulence n the atmosphere.)

In order to use these results to estimate the effects of laser scintillation on OTAES experiments, the additional relationship between log-amplitude variance and rms intensity fluctuation is required. For the case where scintillation statistics follow a log-normal distribution, the fractional intensity variance $C_I(o)$ is given by[26]

$$C_I(o) = \exp \left[4C_a(o)\right] - 1$$

and the rms intensity fluctuation is then $\left[C_I(o)\right]^{1/2}$.

Table 9.1.3.1-1 shows the rms intensity fluctuation in the zenith direction for the OTAES laser wavelengths vs. typical ground transmitter sizes. It has been assumed in these calculations that a transmitter of diameter $2\alpha_0$ can collect all of the energy of a beam of Gaussian spread α_0. Also, an average wavelength of 0.5 microns has been assumed for the Argon ground beacon since approximately two-thirds of the total energy is in the 0.488 and 0.545 micron emission lines.

TABLE 9.1.3.1-1

RMS INTENSITY FLUCTUATION FOR VARIOUS GROUND TRANSMITTERS

Wavelength (Microns)	Percent Intensity Fluctuation*		
	5 cm. Dia.	10 cm. Dia.	50 cm. Dia.
0.488-0.515	74%	30%	<5%
0.63	72%	28%	<5%
10.6	22%	20%	≤5%

* The intensity variance $C_I(o)$ is defined by $\langle [I(\lambda) - I_o]^2 \rangle$ where I_o is the average value of $I(\lambda)$. The standard deviation or rms intensity fluctuation is then $\langle [I(\lambda) - I_o]^2 \rangle^{1/2}$. An rms intensity fluctuation of 200 percent, for example, corresponds to instantaneous values of intensity of two times the average intensity value.

The results of table 9.1.3.1-1 indicate severe scintillation of the received signals aboard the spacecraft unless the transmitting telescope diameter is 50 cm or greater. This is not a particularly stringent requirement since other considerations (small beam divergence) also require large diameter ground transmitting telescopes. The effects of signal fluctuation on direct detection experiments will be discussed in paragraph 9.1.3.3. However, two comments concerning the calculations above should be made. First, the theoretical values have not been experimentally verified. Fried (32) has attempted to compare the theory with pulsed ruby laser experimental results for signals retroreflected from the S-66 satellite, but the tracking errors and interference between corner reflectors pre vented a meaningful comparison. Secondly, the calculations given do not have th strength of atmospheric turbulence included. Since the atmosphere's refractive index structure constant C_N^2 can vary over a wide range, the intensity fluctuations calculated are to be considered as average values.

9.1.3.2 Scintillation of a Space-to-Ground Laser

The scintillation of spaceborne laser light observed at a ground receiver can be calculated by assuming the laser beam to be an infinite plane wave incident on a randomly inhomogeneous medium. Following the original work of Tatarski, (12) and using a model of the vertical distribution of the strength of atmosphere turbulence, (11) Fried and Cloud (25) have calculated the intensity fluctuations in terms of the log-amplitude variance, $C_a(o)$. The expression derived,

$$C_a(o) = 0.727 \sec^{11/6} \theta \, (5 \times 10^{-7}/\lambda)^{7/6}$$

is identical to the calculated log-amplitude variance for a spherical wave given in the previous section. This suggests an atmospheric reciprocity relationship. In fact, Fried, (38) has conjectured that scintillation effects are independent of the location of the atmospheric "slab" between ground and space for small transmitting apertures.

Table 9.1.3.2-1 shows the rms intensity fluctuation for the two OTAES spacecraft laser wavelengths vs. Zenith angle for a very small aperture ground collector. For the calculations shown a log-normal distribution of scintillation statistics has been assumed and the rms intensity fluctuation calculated from the intensity variance $C_I(o)$ as in the ground-to-space case.

TABLE 9.1.3.2-1

RMS INTENSITY FLUCTUATION AT POINT GROUND RECEIVER

Wavelength (Microns)	Percent Intensity Fluctuation		
	0=0° (Through Zenith)	0=30°	0=45°
0.63	280%	405%	775%
10.6	28%	32%	40%

Assuming the propagation theory to be correct, some rather obvious remarks can be made concerning the scintillations calculated. First, the extremely large signal fluctuation particularly for the 0.6328-micron He-Ne laser, would present severe problems for an optical communications link. It would be subject to deep fades of the information carrier and excessive bit error rates. Although the 10.6-micron CO_2 laser link would be considerably quieter, the fluctuation level is still objectionably high. Also, it can be seen that the angle offset from the zenith would increase the scintillation.

The large scintillation effects shown in table 9.1.3.2-1 can be averaged-out through the use of a large receiving aperture. The smoothing or aperture averaging of an infinite plane wave propagated from space-to-ground has been analyzed by Fried,(26) and the results presented in the form of an aperture-averaging factor Ⓗ which is a function of the log-amplitude variance $C_a(o)$ and a normalized collector diameter $D/(4h_o \sec \theta/k)^{1/2}$, where D is the telescope diameter in meters. Since the rms signal intensity fluctuation decreases(26) as Ⓗ $^{1/2}$, this factor should be made small as possible in the OTAES experiments by using large ground collectors.

Figure 9.1.3.2-1, from Reference (26), shows the dependence of the aperture averaging factor upon the normalized collector diameter for various log-amplitude variance values. It can be seen that the aperture averaging factor Ⓗ varies as the inverse square of the aperture diameter over most of the curves.

Table 9.1.3.2-2 shows the rms intensity fluctuation in the zenith direction for the OTAES spacecraft lasers vs. various size ground apertures.

Although zenith angle dependence is not shown in table 9.1.3.2-2, the aperture averaging factor for the one-meter aperture is almost constant for angles between zero and 45 degrees for the log-amplitude variances calculated. The angle dependence for table 9.1.3.2-2 can be approximately obtained by scaling the rms intensity fluctuation values of table 9.1.3.2-1. Comparing these values with those of table 9.1.3.2-1 for a small receiver $(D \leq (4h_o \sec \theta/k)^{1/2}$, it can be seen that a one-meter ground collector can reduce the signal ripple for the He-Ne laser direct detection link from over 200 percent to about 10 percent. Since signal ripple on an optical communication channel may result in drastically reduced link performance (discussed in a following section), the ground station direct detection optical receiver diameter may be required to be considerably larger than that necessary for light collection, in order to suppress scintillations.

TABLE 9.1.3.2-2

RMS INTENSITY FLUCTUATIONS FOR VARIOUS GROUND RECEIVERS

Wavelength (Microns)	Percent Intensity Fluctuation		
	5 cm. Dia.	1 Meter Dia.	5 Meter Dia.
0.63	155%	9%	<1%
10.6	28%	4%	<1%

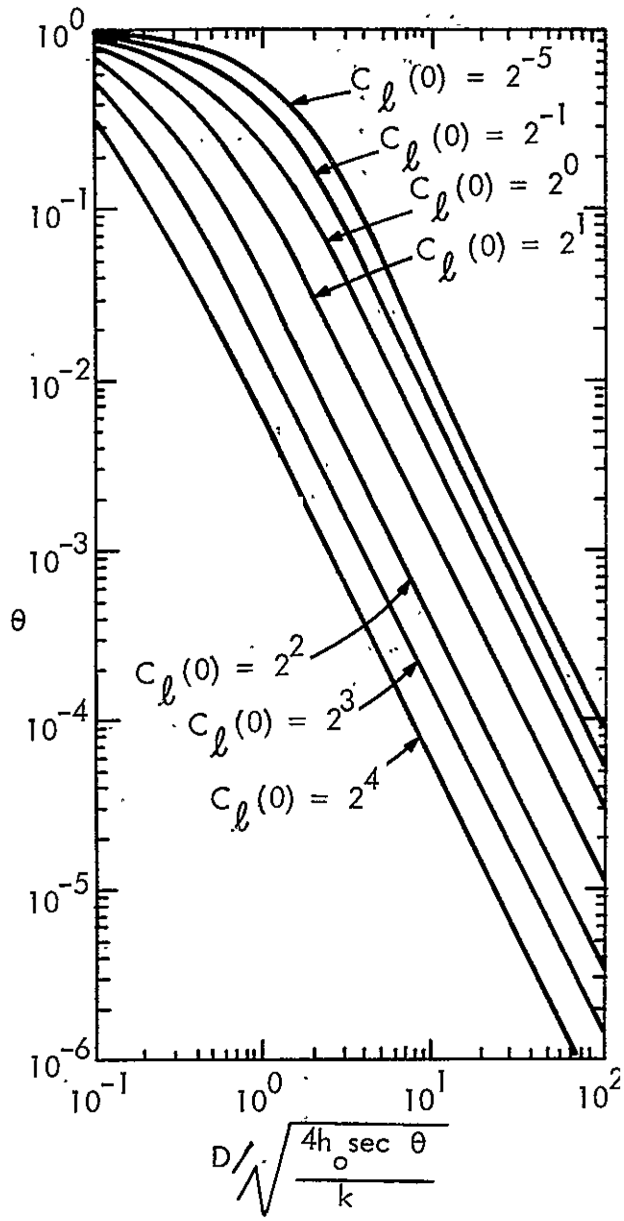

Figure 9.1.3.2-1. Dependence of the Aperture-Averaging Factor, θ, upon the Normalized Aperture diameter, $D/(4h_o \sec\theta/k)$. The calculated curves are shown for various values of $C_\ell(O)$, the log amplitude variance, are based upon the statistics of propagation of an infinite plane wave of wave number, k, traveling from space to the ground and arriving with a zenith angle θ (h_o = 3200 m.)

9.1.3.3 Atmospheric Scintillation Effects on Optical Communication Channels

Atmospherically induced scintillation of space-to-ground laser links has been previously discussed, and estimates of the rms intensity fluctuation calculated for both the up and down link. In this section, effects of the signal fluctuation on the performance of a direct binary communication channel will be discussed.

Fried and Schmeltzer (57) have used the assumption of log-normal scintillation to calculate the increase in signal necessary to preserve the bit error rate in a binary system in the presence of turbulence. The analytical results are expressed in terms of a loss factor, L_f, which is the extra number of decibel signal-to-noise ratio necessary to keep the bit error probability in a turbulent atmosphere up to the level achievable in a nonturbulent atmosphere. The analysis assumes a Gaussian distribution of the intrinsic channel noise with a constant noise variance. This corresponds to a detector- or background-noise-limited case, as opposed to a quantum- or signal-noise-limited case when the variance varies as the square root of the signal strength.

Figure 9.1.3.3-1, from Reference (57), is a graph of the loss factor, L, vs. binary error probability, P_E, for various values of the log-amplitude variance $C_a(0)$. The significance of these curves can be demonstrated by considering the rms intensity fluctuation of a He-Ne 0.63-micron direct detection uplink. From table 9.1.3.1-1 a 28 percent rms intensity fluctuation, corresponding to a log-amplitude variance $C_a(0)$ of about 0.02, is tabulated for a 10-centimeter diameter transmitter. Using this $C_a(0)$ and referring to the curves of figure 9.1.3.3-1, an additional 8 dB in photodetector signal-to-noise ratio is required in order to retain a 10^{-6} bit error probability.

There is considerable doubt as to the applicability of these curves to large values of log-amplitude variance. Experimental results of Gracheva and Gurvich, as reported by Tatarski, (27) followed the Rytov theory to a maximum log-amplitude variance value of 0.6. Even so, a loss factor in excess of 50 dB is predicted for a 10^{-6} error rate binary communication channel. Unless large ground transmitting and collecting optics are used to aperture average the scintillation effects, a direct detection link will be subject to deep fades in signal strength and periods of unusually high error rate if log-normal scintillations exist.

---

(57) D. L. Fried and R. A. Schmeltzer, "The Effect of Atmospheric Scintillation on an Optical Data Channel -- Laser Radar and Binary Communications," (to be published).

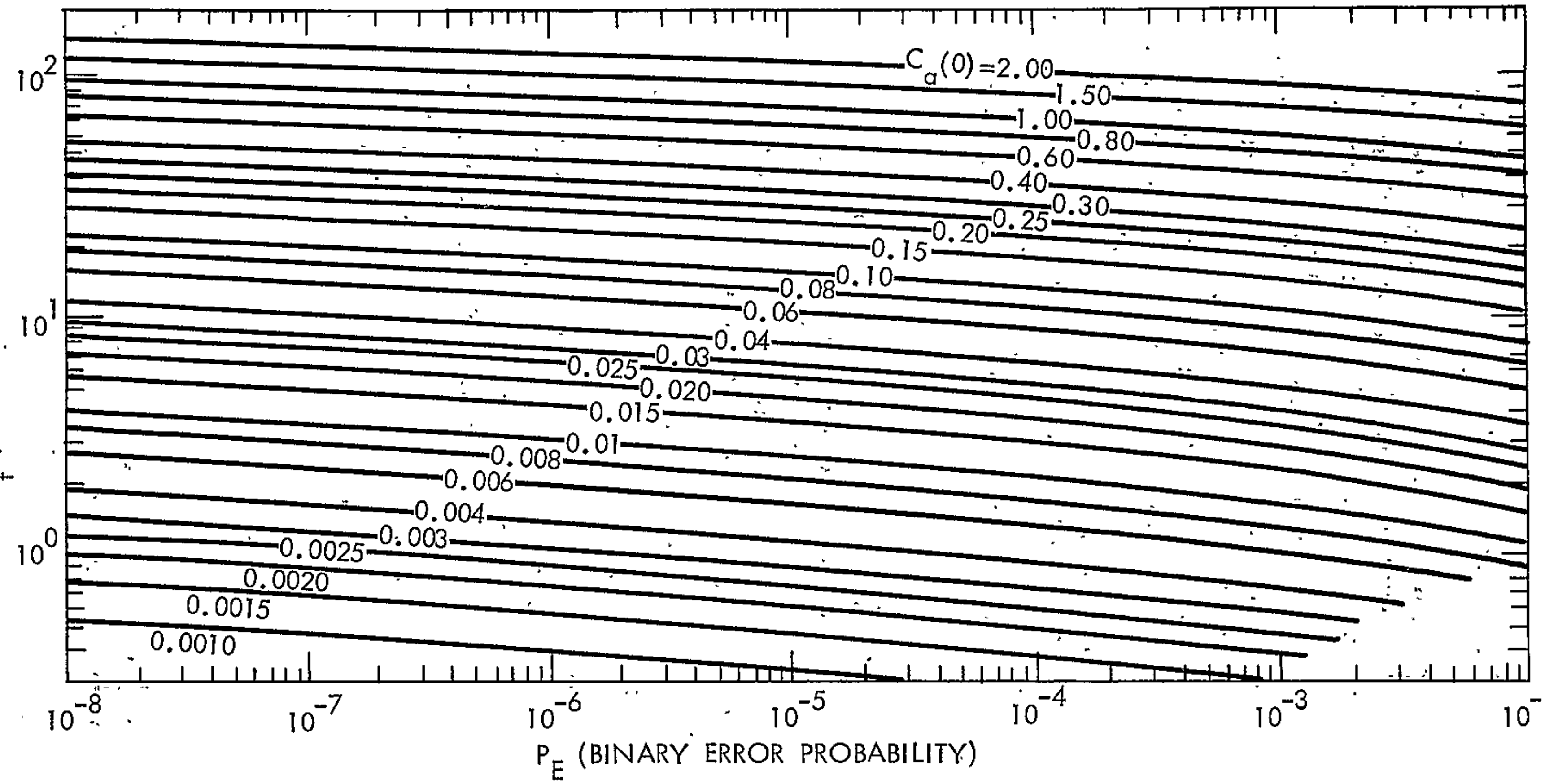

Figure 9.1.3.3-1. The Loss Factor, L_f, as a Function of the Probability of Error, P_E, for an Optical Binary Communications Link in the Presence of Log-Normal Scintillation. (The loss factor is the extra number of decibel signal-to-noise ratio required above that needed because of the regular noise of the system, to compensate for the adverse effect of scintillation. The calculations are carried out for a range of values of the log-amplitude variance, C_a (O).)

Although there is no experimental measurement data available, it has been conjectured[57] that space-to-ground signal fluctuations will follow a normal distribution rather than a log-normal distribution, particularly where large collectors are used. In this case, the loss factor, L_f, for binary communications is simply[57]

$$L_f = 20 \log_{10} \frac{(\sigma_N^2 + \sigma_S^2)^{1/2}}{\sigma_N}$$

where σ_S^2 and σ_N^2 are the variances of the signal and system noise, respectively.

9.1.3.4 Optical Heterodyne Detection from Space-to-Ground

As indicated previously, an optical heterodyne system requires complete spatial coherence across the signal wavefront for maximum detection efficiency. Heterodyne experiments will not only be degraded by scintillation or intensity variation effects, but also, any optical wavefront distortion over the collecting aperture.

Following the work of Tatarski, the interesting case of a space-to-ground heterodyne link has been theoretically examined by Fried. [45] The statistical treatment, based upon an infinite plane wave incident on an inhomogeneously random medium, includes intensity variations across the wavefront as well as warping of the isophase surface. The results show that atmospheric turbulence limits the useful size of the telescope aperture that can be used with a heterodyne system. Figure 9.1.3.4-1, from Reference (45), shows the normalized heterodyne signal-to-noise ratio vs. the normalized telescope aperture, D/γ_0. (D is the actual telescope diameter.) The normalization factor, γ_0, (called the "efficiency saturation diameter" by Fried) is essentially the minimum diameter aperture that could be used to achieve good heterodyne efficiency. The normalized signal-to-noise ratio is essentially the heterodyne efficiency (ratio of actual signal to maximum signal). The curve shows that if the collector aperture is much less than γ_0, the average signal power is nearly equal to that which would be expected in the absence of wavefront distortion. For receiver apertures much larger than γ_0, the average signal power is so severely limited by turbulence effects that it can never approach the value obtained for an equal-sized aperture in a turbulence-free atmosphere. In fact, as discussed later in this section, it has been predicted that the "excess" aperture may actually degrade the system signal-to-noise ratio.

The actual value of γ_0 depends upon the strength of atmospheric turbulence which is described in the Tatarski approach by the magnitude of the structure constant C_N^2. For the case of a space-to-ground link, C_N^2 is a function of the local ground roughness, as well as having an altitude dependent refractive index

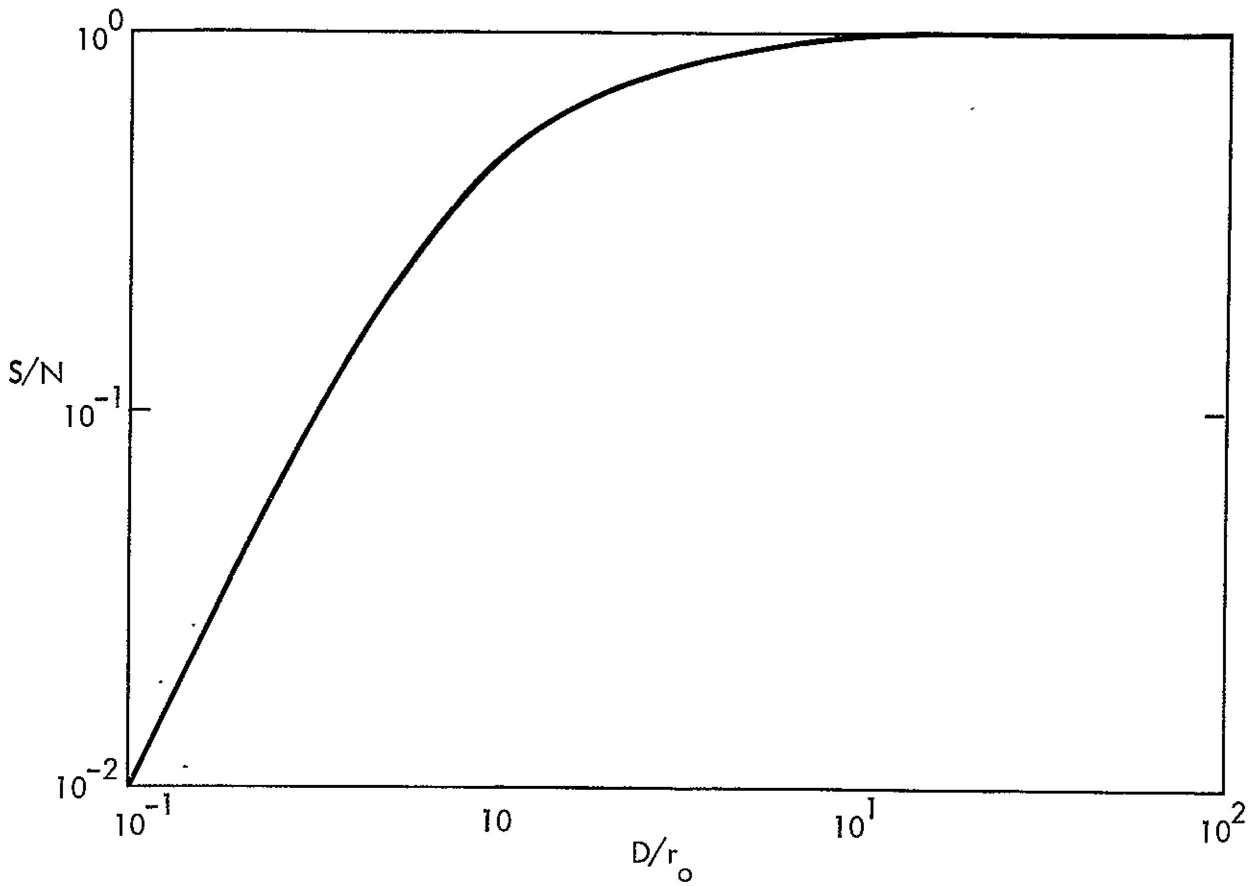

Figure 9.1.3.4-1. Dependence of the Normalized Signal-to-Noise Power Ratio, S/N, Achievable by an Optical Heterodyne Receiver Operating in the Atmosphere, as a Function of Collector Diameter D. (r_o is a parameter set by the strength of atmospheric turbulence.)

fluctuation. Fried has based his γ_0 calculations upon typical $C_N{}^2$ values for the variance of the atmosphere's turbulent refractive index variation with altitude. Figure 9.1.3.4-2, from Reference (45), shows γ_0 for a signal source located above the atmosphere at the zenith angle, θ, for an earth collector altitude of H. Based upon day and night time measurements of stellar images, Fried has introduced a factor of two difference in the γ_0 value.

As can be seen, the predicted useful heterodyne collector diameter may be quite small for a 0.6328-micron He-Ne laser link. Assuming a ground station altitude of 3 kilometers, a maximum efficient receiver diameter between 5 cm and 10 cm is indicated. The advantages of going to longer wavelengths are obvious. Since the analytical expression for $\gamma_0 \sim \lambda^{6/5}$, a 10.6-micron CO_2 link would have a useful diameter about thirty times as large ($\gamma_0 \approx 1.5$ to 3 meters).

Quite obviously, the space-to-ground γ_0 values in figure 9.1.3.4-2 have not been experimentally verified. However, measurements (4) taken with a 0.6328-micron He-Ne laser over horizontal paths have demonstrated the heterodyne limited aperture effect; perturbation-free apertures up to 10 cm were observed in good seeing conditions and as low as 1 mm under poor conditions.

Two rather interesting speculations have been made by Fried (45, 58) concerning the efficiency saturation dimension, γ_0. The first involves a reciprocity relationship. It is conjectured that if the conventional reciprocity between transmitter and receiver antenna gain still applies in a turbulent atmosphere, the quantity γ_0 also represents the largest diameter which could be used effectively for the collimating optics of an optical heterodyne transmitter located in the atmosphere. The relationship, if valid, would mean that large transmitting optics, although effective in reducing scintillations, would not require correction to the diffraction limit. The second phenomenon predicted is the presence of an aperture size dependent "modulation" noise. Analysis by Fried (58) on the statistics of optical propagation using the wave-structure function shows that to avoid a large signal-power variance the receiver collector diameter should be no larger than γ_0. The modulation noise is attributed to the reception of uncorrelated wavefronts out of phase with the local oscillator wavefront. This indicates that in order to optimize the heterodyne signal-to-noise ratio, an adjustable iris over the aperture is necessary to set the diameter for various turbulence conditions.

---

(58) D. L. Fried, "Atmospheric Modulation Noise in an Optical Heterodyne Receiver," (to be published).

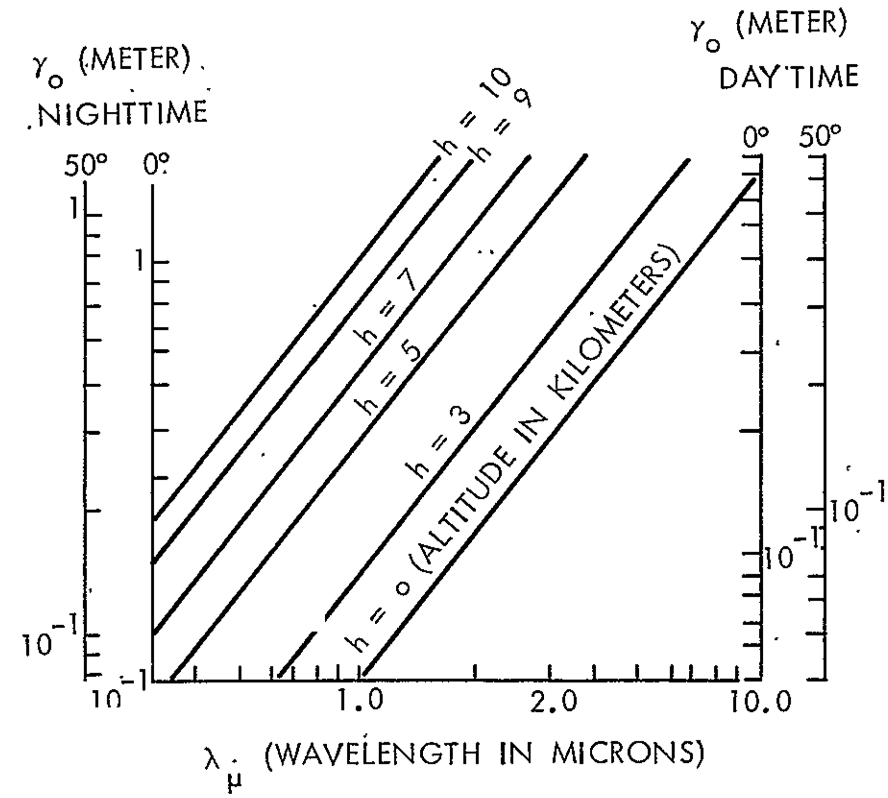

Figure 9.1.3.4-2. Dependence of γ_o Upon Wavelength, λ, Zenith Angle θ, and Altitude h for Optical Heterodyne Reception of a Space-to-Earth Signal.

9.1.3.5 Optical Heterodyne Detection from Ground-to-Space

The effect of atmospherically distorted wavefronts on a ground-to-space heterodyne link has not been examined theoretically. The differences of the up and down links from an analytical point of view are briefly as follows. A spacecraft transmitted beam, being well above the atmosphere, can be treated as a plane wave incident on an inhomogeneously random medium; expressions for an arbitrary source size and source wavefront radius of curvature are not required. For the case of the laser transmitter beam immersed in the atmosphere (ground-to-space), the propagation theory is dependent upon the finite transmitting aperture and wavefront curvature. As indicated in the earlier discussion of propagation theory, evaluation of Schmeltzer's [29] integrals for the phase and log-amplitude structure functions of laser beams is necessary before the heterodyne case can be formally analyzed.

However, on the basis of a purely intuitive argument, we can speculate about the ground-to-space heterodyne link performance since the turbulence effects are dependent upon the relative position of receiver and atmosphere. We can imagine the ground transmitted laser beam wavefront as being distorted by refractive-index inhomogeneities when it traverses the atmosphere. At the top of the atmosphere, it would propagate as a distorted plane wave of varying intensity and phase across the wavefront. A spacecraft telescope intercepting a small portion of the wavefront would not be subjected to drastic angle of arrival jitter and near-field wavefront distortion. Consequently, we might expect the equivalent spacecraft γ_0 to be larger than the ground receiver maximum efficiency diameter, γ_0. Simultaneous heterodyne measurements over both ends of the link coupled with γ_0 determination on the ground will, of course, give the equivalent spacecraft γ_0 value.

9.1.4 Experiment Design

The rigorous Obukhov-Kolmogorov (O-K) theory of turbulence is generally accepted as the correct treatment of atmospheric phenomena. Although the optical propagation descriptions are incomplete, particularly for laser or finite aperture transmitters, some theoretical predictions have been verified by experiment. Careful atmospheric measurements over uniform turbulence paths, as described later in this section, are necessary to fully evaluate the theory and establish the validity range of the Rytov approximation. The less complicated geometrical optics formulation of turbulence has some serious errors which limit its utility to near field phenomena. Even then, the theory predicts incorrect functional dependences of important parameters and must be viewed with caution.

One of the unfortunate features of atmospheric laser propagation work is the almost chaotic manner in which many of the experiments have been performed. Much of the work has been of a purely qualitative nature, and little effort has been made to correlate experimental results with theory. Perhaps more distressing is the fact that, except for rare instances, the measurements were small samples taken over nonuniform turbulence paths so that the correlations with theory would be meaningless.

Some rather obvious conclusions are in order at this point. First, a well designed set of ground-to-ground atmospheric propagation experiments must be conducted over a uniform turbulence path with an independent measurement of the refractive index structure constant, C_n. The technique developed by Coulman (39) and described in paragraph 9.1.1.3 would accomplish the C_n measurement. All propagation measurements should be conducted below the "Obukhov altitude." The following laser propagation properties should be measured as a function of the strength of turbulence:

a. Intensity fluctuations and probability distribution

b. Phase fluctuations

c. Polarization effects

d. Transit-time dispersion

e. Synoptic conditions (temperature, humidity, pressure, wind, temperature lapse rate).

These measurements are to be made with laser wavelength, range, and receiver aperture as variables over a wide variety of turbulence conditions. Also, a large number of samples should be taken to improve the statistics. A description of the method of meteorological data collection to compare the experimental results to the O-K theory is outlined in section 19.

The calculations made in paragraph 9.1.3.2 have indicated severe scintillation is possible in space-to-ground direct-detection laser links unless sufficiently large transmitting and receiving telescope apertures are used. Based upon these figures, the ground transmitter for a 10.6-micron OTAES direct detection uplink should be tentatively set at 30 cm. Also cited in this section are Fried's calculation of the effect of scintillation on a PCM direct detection trial communication channel. Quite obviously, the distribution of amplitude fluctuations must be determined before the bit error rate dependence on signal fluctuation is known. The heterodyne detection results of paragraph 9.1.2.4 indicate that 1.0-meter apertures used in the OTAES spacecraft and ground station would certainly be large enough to insure optimum aperture sizes for the He-Ne link in best seeing conditions. One-meter apertures are probably large enough to optimize the 10-micron heterodyne link most of the time. However, optical propagation measurements, preferably from balloon platforms, are necessary before the altitude dependence in the O-K theory used for these predictions can be verified.

Balloon platforms, as opposed to aircraft, are attractive because they do not induce significant local turbulence which may mask the effects to be measured. Other factors such as low cost, small tracking rates, and overall cost effectiveness are also important considerations.

9.2 SECOND JUSTIFICATION-OPTICAL COMMUNICATION DIAGNOSTICS

The information rate of any communications system is limited by the noise characteristics of the communications channel. Sources of noise which can often be neglected in conventional radio frequency systems frequently become of importance in an optical communications system. Fortunately, in certain optical channels the limiting noise sources can be treated as white Gaussian noise with the result that a large part of communications theory and design information is directly applicable to the problem of optimizing communications systems design. Quantum effects on communications have also been studied,(1) and a comparison of the communications efficiency of various techniques has been made over a wide range of signal-to-noise ratios where the noise is considered as having the statistical properties of additive white noise. The inherent quantum noise, receiver-generated noise, and most background noise usually fall in this category for practical communications bandwidths.

When the transmission path is not in free space, however, other noise effects appear which cannot be considered as additive, white Gaussian noise. Multipath effects and perturbations of the phase front are two such sources of noise which can have a marked effect on communications. At radio frequencies in the two important communications techniques of tropospheric scatter as well as ionospheric reflection, considerable work has been done in the investigation and reduction of the effects of multipath transmission. For a review of the analytical tools required, as well as a description of the physical phenomena involved, the reader is referred to Schwartz et al.(2) In addition to knowledge of the physical nature of the noise source, the statistical parameters which describe the noise in the communication terms are required before communication system design can proceed. At optical frequencies, data relative to propagation through the entire atmosphere has been collected by astronomers. The astronomer has been particularly interested in minimizing these effects, e.g., moving to the top of a mountain, and hence has usually measured average values of statistical parameters rather than the distribution functions and temporal variations which are of interest to the communications systems designer. In some cases, effects disturbing to an image can be ignored or compensated for in a communication system. With the possible application of the laser in communications, there have been a few measurements made over particular communication links. These measurements have limited applicability because of the small amount of data collected. For example, the heterodyne mixing efficiency as a function of aperture diameter is often measured. The mixing efficiency is a function of local oscillator stability and alignment as well as the phase variations over the aperture, however, so that unless

---

(1) J. P. Gordon, "Quantum Effects in Communications Systems," Proc. IRE, vol. 50, September 1962.

(2) M. Schwartz, W.R. Bennett, and S. Stein, Communications Systems and Techniques, McGraw-Hill, New York, 1966.

these effects are separated the measurements are only applicable to the particular path measured. Again, measurements of coherence diameter have failed to account for anisotropies in phase variations over the aperture. If measurements could be made on two axes in the aperture plane, these anisotropies would be revealed. Such variations in the optical wave must be considered by the communicator in the design of his equipment.

Variations in received amplitude, regardless of the cause, will affect both coherent and incoherent systems. These variations arise through beam bending, beam break-up, or extinction phenomena. When the source is highly monochromatic, multipath effects will cause variations in amplitude because the phase relationship of the portions of the signal arriving over different paths will change in time. For a given path, the statistics of the amplitude variations are required for optimum system design. For example, consider a direct detection system which must be operated at a given bandwidth and information rate. Increasing the size of the collector will increase the signal energy; but at the same time the angle of view (and, hence, background noise) will also be increased because of the difficulty of maintaining optical tolerance for large collectors. With accurate knowledge of the path fading statistics and spatial correlation, the designer may be able to devise a diversity system using a number of smaller collectors which can be built to closer tolerances and, hence, can be used with a smaller angle of view. Over a given path, both amplitude variations and the spatial correlation of these variations should be measured prior to system design.

Coherent systems will respond to amplitude variations as well as variations in phase and phase front alignment. The phase variations over the collecting aperture cause a reduction in heterodyne detection efficiency. (In recent years, microwave antennas have been built so large that phase variations over the aperture have reduced the effective antenna gain which affects communications in the same manner.) Temporal variations in phase will introduce an undesired phase modulation which may interfere with communication modulations. Some measurements have been reported in which aperture coherence diameters have been determined. These measurements are not always independent of the equipment used, and, hence, are not always meaningful when applied to other systems. For example, when using the homodyne technique where the laser is used as its own local oscillator, the local oscillator path is often very short compared to the transmission path measured. Unless the laser is very stable, it is possible for the length of the transmission path to approach or exceed the coherence length of the laser transmission. When this occurs, the laser will become incoherent with itself and homodyne detection efficiency will be reduced even in free space.

9.2.1 Parameters

Although the astronomer has a number of terms to describe the optical effects of transmission through a turbulent medium, the communicator is interested only in the amplitude and phase variations of the electromagnetic wave as it strikes the surface of his detector. The two-dimensional image transmission problem (which may be of interest in certain types of communications), as well as the low signal-to-noise situation requiring the use of quantum counters, are not under discussion in this context. Fortunately, a large body of theoretical knowledge is available on the effects of a turbulent medium on the transmitted wave (section 9.1) and work is continuing in many areas. The major lack is a collection of good data on the fundamental quantities on which the theory is based... the statistical parameters of the atmosphere from which both optical image transmission and communication transmission properties could be derived. It is necessary then, for any particular path, that measurements be made of the following quantities in order to determine the statistical parameters.

a. Variations in phase and amplitude (using as small an aperture as possible) as a function of time and space, preferably in three dimensions.

b. Variations in angle of arrival which will assist in the interpretation of the data collected in (a). As long as a clean image is recorded, one can be assured that the collecting aperture is not averaging out small scale variations over the aperture.

If these data can be collected over a sufficiently long period of time, suitable processing of the data should reveal:

a. Duration of the period of stationary random processes

b. Nature of such random process (whether Rayleigh, Gaussian or some other)

c Values of pertinent descriptive parameters, moments, correlation functions, spectra

d. Diurnal or other temporal variations of the parameters.

9.2.2 Measurements

Although the instrumentation problems in making some of these measurements are formidable, they are within the state-of-the-art given the transmission of highly monochromatic signals from space. (Although amplitude scintillations could be observed with a noncoherent source, such a source would be too broadband to have amplitude fluctuations due to changing phase paths.) Two or more widely separated optical frequencies should be received by a number of receivers simultaneously.

a. A direct (energy) detection receiver which uses as small an aperture as is necessary to get a satisfactory signal-to-noise ratio. Such a receiver would measure the amplitude of the received signal, and statistics could be gathered on the variations in amplitude caused by having the beam bend out of the receivers view, and beam break-up, as well as those amplitude variations due to multipath effects.

b. A superhetrodyne or homodyne receiver with a stable local oscillator which could measure the phase perturbations on the received signal. Such phase perturbations could be ascribed to multipath effects, and correlation with the record provided by the direct detection receiver would serve to identify "fades" due to multipath as distinguished from those due to strictly, say, beam bending which would not be expected to affect the phase of the receive signal.

c. A phase correlation measurement as described in the OTAES final report which would provide information on the spatial correlation of the observed phase changes.

d. An angle of arrival measurement relative to two orthogonal axes which combined with the phase spatial correlation measurements would provide data for choice of aperture size for heterodyne detection.

In addition to the measurements described above which measure the spatial and narrow-band characteristics of the optical transmission, it would be desirable to transmit a very wideband signal to observe if conditions for selective fading exist which can impair wideband transmission.

A signal could be generated by a series of tones over a wideband with a receiver capable of monitoring the phase relationship between the various tones. Frequencies should be selected which would have a periodic in-phase relationship to serve as a reference. Variations in the phase relationship or differential variations in the amplitude of the various tones would reveal the existence of conditions which would give rise to selective fading over the bandwidth used.

A second method of generating a wideband transmission would be the use of a very narrow pulse such as that attainable with a mode-locked laser.

Although these two techniques make essentially the same measurement, the spaced tones and the pulsed techniques will provide more accurate information at different fluxuation frequency bands, depending upon the instrumentation. The rapid sampling of the atmosphere available with the mode-locked laser will reveal variations at kilohertz rates which might be masked by the integrating effect of the tone filters. Needless to say, both techniques have instrumentation problems.

9.2.3 Experiment Design

The diagnostic instrumentation described in the preceding section implies, in essence, the establishment of communication links. Hence, there is a temptation to enlarge upon such measurements to incorporate specific communication system postulates. Of the two fundamental techniques, heterodyne and direct detection, the latter is most readily lent for such specific system testing. Those measurements predicated upon amplitude and polarization sensing can be accomplished with a space-to-ground direct detection communication system scaled to simulate planetary requirements. Such experimentation is valid in the joint context of communication diagnostics and solution-oriented testing.

It should be noted, however, that without its diagnostic content, such a direct detection space-to-ground experiment would reduce to a simple equipment demonstration. The direct detection system technique permits straightforward overdesign to compensate for transmission medium unknowns. Trade-offs include increased receiving aperture size, narrower filter bandwidth, and improved pointing. The technology here is in an advanced stage of ground-based development. Except for space qualification of specific equipment designs, high altitude airborne tests would be adequate to verify this potential form of planetary optical communication. For this reason, an alternative sequence of ground and airborne experiments has been described which can provide a degree of confidence equivalent to that attainable by tests using earth-orbiting transmitters. Once a thorough air-to-ground test sequence has been accomplished, various combinations of modulation (intensity or polarizatio carrier (direct, FM, or PCM), and signal source (voice, TV, or digital words) can be examined. However, true value of the diagnostic approach applies to the relative assessment of heterodyne and direct detection planetary communication alternatives Although there is much evidence to suggest that a major portion of the amplitude and angle-of-arrival perturbations may be introduced in the lower atmosphere, this conclusion should be verified. Moveover, a similar conclusion with respect to phase perturbations cannot be drawn with equal confidence. It is necessary to propagate optical frequencies through the whole atmosphere along near-zenith and slant paths before firm conclusions can be drawn. This necessity derives from two main considerations:

a. Since phase perturbations may arise from multipath effects, the atmo sphere should be illuminated from above.

b. Care should be taken that the atmospheric disturbance is introduce the far field ($R > 2 D^2 \lambda^{-1}$) since this would be the case for planetary communication. Except for the longer wavelength, higher power lasers, this requirement translates directly to orbital altitudes.

This consideration also raises the question of coherent light behavior when identical disturbances are introduced in the near field and in the far field. If an optical ground-to-space link and an identical space-to-ground link are juxtaposed, the atmosphere then serves as such an identical and realistic disturbance.

Collectively, the space-to-ground communication experiments provide a comparison of the fundamental communication techniques: direct detection and heterodyne detection. The heterodyne experiment is formulated on a scale sufficient to allow comparison between laser and radio frequency communication. Direct detection, which has the advantages of system simplicity, lenient pointing tolerances, and an advanced state of ground-based development, is also the subject of a proposed experiment. Two experiments of the optical propagation group are designed to explore important properties of the atmosphere in order to first test a technique for measuring phase variations as a function of time with a highly monochromatic laser source and, second, to study phase and amplitude characteristics of the atmosphere as a transmission medium.

Three experiments of the optical propagation group are concerned with the development of the technology required for eventual optical communication from deep space. To utilize the narrow beams in which the laser power may be concentrated requires a pointing capability commensurate with the beam divergence (e.g., 0.1 arc second). Achieving this accuracy requires a precise reference from the ground station to the spacecraft. This reference is established by precise tracking of an upcoming laser beam. Such tracking is the subject of one experiment.

An important element of the communication experiments is to simulate, as nearly as is practical, communication conditions from deep space. For tests having alternate objectives, such as the development of operational techniques, it is important that the technology be exercised under realistic conditions since communication from the planets will require, among other things, the transfer of tracking from one ground station to another. The objective of one of the proposed experiments is to develop this capability. Another particularly difficult problem for a two-way communication link with deep space is the lead angle which must be incorporated into the transmitter beam. Caused by the relative velocities between the spacecraft and the ground station and the relatively long transit times, the lead angle requirement may typically be as great as 40 arc seconds for a Mars flyby.

Accordingly, the following nine experiments, taken together, comprise the Optical Propagation Experiment group. Each is described in detail in section 9.6.

a. Optical Heterodyne Detection on Earth

b. Optical Heterodyne Detection in the Spacecraft

c. Direct Detection on Earth

d. Megahertz Optical Communication

e. Precision Tracking of a Ground Beacon

f. Point Ahead and Space-to-Ground-to-Space Loop Closure

g. Transfer Tracking from One Ground Station to Another

h. 10 Micron Phase and Amplitude Correlation

i. Pulse Distortion Measurements

9.3 THIRD JUSTIFICATION - NEED FOR SPACE TESTING

The Optical Propagation Experiment group has a triple objective: increased physical knowledge of the atmosphere, communication diagnostics, and assessment of precision pointing and tracking forms. For each of the nine propagation experiments, there are specific reasons why space testing is important. These reasons all relate to the group objectives and can be classified further in terms of the mathematical subdivisions adopted in theoretical analysis.

For instance, mathematical solutions have been limited until recently to the case of an infinite plane wave incident upon the medium. To correlate theory with experiment rigorously, then, requires far field measurements.

Second, although major upper air turbulent disturbances seem to be concentrated between the 20,000- and 60,000-foot altitudes, there is no conclusive proof that the total effect is introduced at these altitudes. For many of the propagation experiments, the total atmospheric effect is important to future engineering utility of the data to be gathered.

Again, realism in terms of future uses of the data to be obtained and engineering conclusions to be drawn will impose scaling laws. Thus, the need to minimize the angular subtense of certain disturbances or to reduce the effect of angular excursions results in geometrical arguments for Earth-orbit testing. Furthermore, the special cases in orbital mechanics which obtain at the 24-hour orbit altitude offer enhanced measurement value through statistical opportunity or instrument simplification.

9.3.1 Far Field

As noted in paragraph 9.1.1, optical propagation descriptions by the rigorous Kolmogorov turbulence theory are incomplete. Recent solutions for a point source and (in terms of unevaluated integrals) for the actual case of a laser leave unresolved questions. The main body of existing solutions, however, take the far-field assumption. This assumption is valid at a distance:

$$R_f = \frac{2D^2}{\lambda}$$

where D is the optical aperture diameter and λ is the wavelength. Since the visible frequency communication diagnostic experiments require a one-meter aperture, this distance (hundreds of kilometers) exceeds the altitude capabilities of air-supported vehicles.

9.3.2 Total Atmospheric Effect

The effects of the atmosphere in a long slant propagation path cannot be adequately predicted by the results of laser propagation tests on long horizontal paths. The structure and scale of the turbulence is very different. Yet, to date, no laser space-to-ground experiment has explored this question. Although stellar scintillation is largely traceable to the winds at 20,000-foot to 60,000-foot altitudes, it is not known that these produce the total effect. It is therefore, important to the atmospheric physics of the OTAES propagation experiments that these effects be included if, indeed, they are introduced by the upper stratosphere.

From the viewpoint of the communication engineer, transmission through the whole atmosphere is also important. Component performance and some system parameters can be evaluated through ground-based test programs. However, because the atmospheric transmission medium is neither homogeneous nor isotropic, it must be evaluated in its totality to obtain valid statistical properties for engineering application. Extrapolation from data taken at other frequencies is possible when the statistical properties of additive white noise can be assumed. This is not the case, however, for multipath, phase-front perturbations and the effects of water vapor.

Narrow beam, coherent laser light can be expected to have more pronounced scintillation effects than starlight. The narrow beam illuminates a small volume as it passes through the atmosphere. Light scattered or refracted out of the beam effectively increases the illuminated area with attendant reduction of intensity.

A distorted wavefront will have random displacements which will appear as a phase perturbation to any receiving aperture parallel to the "average" phase-front. For a sufficiently small aperture, the entire wavefront will arrive at an angle θ which will cause motion of the entire image in the focal plane of the lens. When the magnitude of this angle subtends a significant fraction of a wavelength across the receiving aperture, the advantages of the heterodyne technique are compromised. From measurements made by astronomers, θ has been found to be up to 3 arc seconds ($\approx 15 \times 10^{-6}$ radians) with the wavefront correlated up to a distance of $\rho = 6$ inches (15 cm), or more, under conditions of great image motion. An extreme of 10 arc seconds has been reported.

With these numbers assumed, a short calculation shows that the phase perturbation at any point:

$$\frac{2\pi\rho\theta}{\lambda} \doteq \frac{2\pi(.15)15 \times 10^{-6}}{.6328 \times 10^{-6}} = 2\pi\ (3.5) \text{ radians}$$

which is greater than an optical wavelength. Because these phase jumps can occur in 1/10-second intervals or less, frequency shifts of greater than 30 hertz can be expected under rather ordinary conditions.

9.3.3 Measurement Geometry

For certain precision measurements to be made with the OTAES, angular errors and tracking noise set a minimum allowable distance between atmospheric perturbations and instrumentation. For example, the effective motion of a "turbulon" (gas lens), $h\theta$, may be inferred from the angular fluctuation it imparts to a stellar image (figure 9.3.3-1) by taking the turbulon altitude as 10^4 feet and a ±10 arc second image dancing. The Airy-Disk in a 1.0-meter telescope is of the order of 0.1 arc second, and lateral shifts of 1/10 in the Airy-Disk (0.01 arc second) are observable. It follows that the telescope must be at least 2000 miles above the turbulence layers to separate such tracking noise from true tracking system performance measurements.

9.3.4 24-Hour Orbit Altitudes

From the viewpoint of experimental technique, the synchronous altitude is preferred. For ground-based measurements of phase-front perturbations, it would be desirable to reduce angle tracking noise to say, 1/10 of the expected phase deviation. For a one-meter aperture, the phase perturbation calculated in paragraph 9.3.2 suggests a tracking accuracy of 0.05 arc seconds, an unreasonable objective for ground-based instrumentation. The nearly stationary line-of-sight subtended by a 24-hour altitude satellite would obviate the need for tracking (i.e., permit time-limited use of a stationary aperture).

Again, this property of the 24-hour orbit altitude will allow measurements to be made over a sufficiently long time to obtain statistically meaningful data as well as to monitor minute-by-minute changes in atmospheric conditions with a fixed line-of-sight. Measurement from lower altitude vehicles would be complicated by their limited time-in-view of the ground station.

9.3.5 Alternatives to Space Flight

Our present knowledge of atmospheric effects on optical propagation has been largely drawn from horizontal observations and from measurements made with starlight and satellite-borne retroreflectors. The application of such conventional techniques to the OTAES experiment objectives was reviewed to assure that an optical technology satellite is essential to these objectives. In addition, other potential instrumentation platforms such as rockets, aircraft, and balloons were examined. The results of these evaluations are summarized in the following paragraphs.

In principle, the amount of scintillation at a given optical frequency could be obtained by measuring starlight through very narrow-band filters. Optical filters are not yet available which provide the narrow line width of a gas laser transmission.

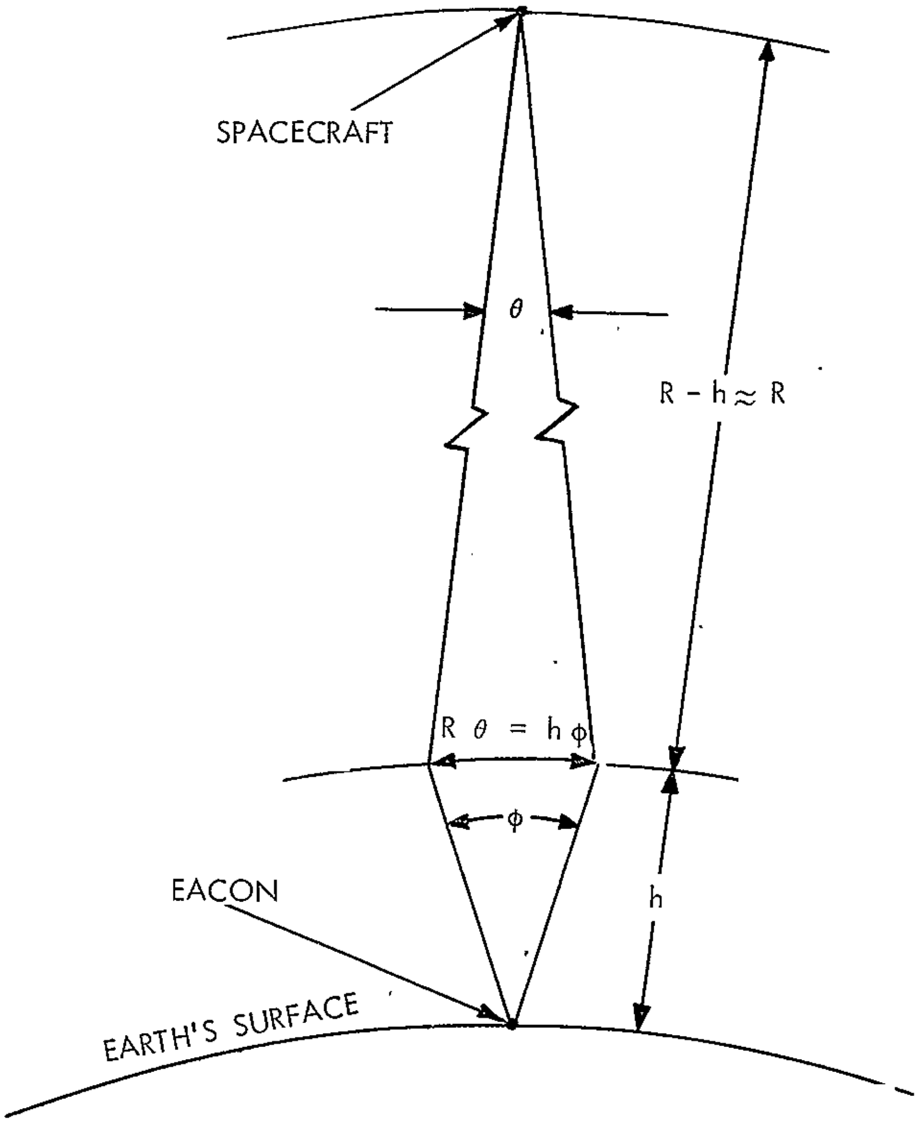

GIVEN: $h \leq 10{,}000$ FT.

ϕ BETWEEN ± 5 TO ± 10 ARC SEC.

SPECIFIED: $\theta \leq 0.01$ ARC SEC.

THEREFORE, $R = \frac{h\phi}{\theta} \approx 2000$ STATUTE MILES
(FOR $\phi = 10$ ARC SEC.)

Figure 9.3.3.-1. Image Dancing.

However, even if they were, the received spectral intensity of starlight would be orders of magnitude less than that of laser light. For example, the spectral irradiance outside the Earth's atmosphere of one of the brightest stars in the sky, Sirius A, has been computed[1] to be approximately 10^{-11} watts cm^{-2} μ^{-1} at 0.63 micron. If it is assumed that a nonattenuating filter with a bandwidth of 2A could be used, the irradiance would be reduced by a factor of 2×10^{-4} to 2×10^{-15} w/cm^2. Using a 10-milliwatt laser with a diffraction-limited beam from a one-meter aperture at synchronous altitudes as a transmitter, the computed radiance is 1.49×10^{-9} $watt/cm^2$, all of which would pass through a 2A filter.

Under these conditions, the laser source is 10^6 times as bright as the star. Even with a much smaller transmitting aperture, the laser is still orders of magnitude greater than starlight. Measurements of scintillation made with the more intense laser light will be made more accurately because the "signal-to-noise" ratio will be better. The use of the more intense light will also permit measurements at much smaller apertures than would be possible with starlight. In addition, if stars were relied on for daytime measurements, then the measurements would be very restricted.

Measurements on starlight as well as ground-based measurements of laser light have shown the aforementioned dependency on the distance to the receiver, as well as to the transmitter of the disturbing elements of the atmosphere. It seems, therefore, that the use of a satellite-borne retroreflector would introduce up-link effects that would be difficult, if not impossible, to separate from the down-link effects.

For statistical purposes, within both the communication and atmospheric physics objectives, repeated long data intervals are desired over periods of months. Thus, free rockets, with their short payload dwell times, imply many launchings.

Aircraft, although convenient to use, are not attractive instrumentation platforms for precision optical experiments. Since the turbulence region of interest extends above 10 kilos, high performance aircraft would be required; but coherent light experiments cannot be performed from a high performance airplane. The turbulence local to such a lifting body would sheath the instrument aperture in a turbulent flow characterized by severe temperature discontinuities. These would tend to mask the effects to be measured. Furthermore, the high vibration environment aboard an aircraft poses laser stability problems.

Upper air balloon tests offer the most benign airborne environment for propagation measurements and, for float altitudes below 25 kilos, are relatively inexpensive. At this altitude, however, a significant percentage of the stratosphere is

---

[1] Investigation of Optical Spectral Regions for Space Communications, ASD-TDR-63-185 (AD 410 537) Air Force Systems Command, Wright-Patterson Air Force Base, Ohio, p. 160.

still eliminated from the transmission path. Furthermore, balloons cannot satisfy the geometric requirements described in paragraph 9. 3. 3 and are restrained in operation to essentially fair weather (launch conditions) and, for long float durations, to summertime testing.

9.3.6 Summary of Space Test Justifications

The need to perform certain of the OTAES optical propagation experiments in space rests with the need to perform them as a group. This is particularly true of the Direct Detection and 10-MHz Bandwidth tests. These experiments are included for correlation with the Heterodyne Detection experiment results. However, it is also true that, with one minor exception, they impose no additional spaceborne equipment burden. The satellite heterodyne transmitters and receivers are used; only an uncooled, narrowband infrared detector has been added. On the ground, the equipment required is no different than would be required to accomplish the same objectives by, say, balloon testing.

Thus, for certain of the experiments, space testing is essential. Their experiment objectives could be achieved in no other way. For others, the justification for space performance lies with a correlate experiment. These more subtle factors are noted later in the individual experiment descriptions. Table 9. 3. 6-1 associates the critical need for space testing with the three Optical Propagation Experiment group objectives.

TABLE 9.3.6-1

NEED FOR SPACE TESTING - OPTICAL PROPAGATION GROUP

Experiment \ Reason	Far Field	Total Atmosphere	Geometrical
1. Optical Heterodyne Detection on Earth	Atmos. Phys.	Communic.	
2. Optical Heterodyne Detection on the Spacecraft	Atmos. Phys.		
3. Direct Detection on Earth		Atmos. Phys. Communic.	
4. Megahertz Optical Communication		Communic.	
5. Precision Tracking of a Ground Beacon		Atmos. Phys.	Pointing
6. Point Ahead and Space-to-Ground-to-Space Loop Closure			Pointing
7. Transfer Tracking from One Ground Station to Another		Communic.	Pointing
8. 10-Micron Phase and Amplitude Correlation	Atmos. Phys.	Communic.	Pointing
9. Pulse Distortion Measurements	Atmos. Phys.	Communic.	

Atmos. Phys. = Atmospheric Physics.

Communic. = Communication

9.4 SPACEBORNE REQUIREMENTS

During the development of the optical propagation experiments, certain factors developed that determined the requirements that must be established for spaceborne telescopes. Experiment design studies led to the selection of 0.6328-micron and 10.6-micron downlinks and 0.488-micron and 0.6328-micron uplinks. In the following paragraphs, those conditions which prescribed the need for the selected apertures are discussed.

9.4.1 Mirror Diameter and Pointing

Certain of the laser experiments are predicated on phase coherence measurements. A diffraction-limited aperture will preserve the spatial coherence of the source and conserve the transmitted energy. Size and mass are secondary, but important, considerations. Acceptance of the diffraction limit leads to the smallest possible aperture requirement with attendant easing of spacecraft packaging and of pointing actuator drive power problems.

Taking the ratio of the well-known Friis transmission expressions for optical and microwave communication and equating prime power and bandwidth, gives:

$$\frac{\left(\frac{S}{N}\right)_0}{\left(\frac{S}{N}\right)_m} = \frac{\epsilon_{to} A_{to} \lambda_m^2 A_{ro} kT}{\epsilon_m A_{tm} \lambda_o^2 A_{rm} h\nu/q}$$

which relates transmitter efficiencies, ϵ; aperture areas, A; wavelengths, λ; detector quantum efficiency, q; noise temperature, T; frequency, ν; and the familiar constants of Planck, h, and Boltzmann, k. The subscripts t, r, m, and o denote transmitter, receiver, microwave, and optical, respectively.

In table 9.4.1-1, the various terms of this relation are evaluated from the viewpoint of microwave optimism (e.g., a 100-meter diameter, X-band receiving aperture on the Earth; a 30-meter diameter X-band transmitter on the spacecraft; a 100°K receiver noise temperature; a 50 per cent, X-band transmitter efficiency, etc.). For the 0.6328 micron laser it is not reasonable to expect future performance to exceed $\epsilon_o < 0.0045$. Thus, the noise, receiving aperture, and transmitter efficiency ratios (23.5 + 20.0 + 20.5 = 64.0 dB) are inherently advantageous to the microwave technology. Only the wavelength (93.5 dB) term favors the optical technique. For equivalence between the microwave and optical techniques, the ratio of transmitting apertures on the spacecraft must give no more than a 29.5 dB advantage to the microwave technique. Thus, a favorable comparison of optical communication with microwave communication cannot be made with apertures less than one meter; and this choice results in a 0.14 arc second beamwidth, imposing a 0.1 arc second pointing requirement. This one-meter aperture gives adequate signal strength for the pulse distortion experiment and permits the use of 2-cm apertures on Earth for the phase correlation experiment.

The helium-neon, single frequency laser, the one-meter diffraction-limited aperture, and the 0.1 arc second pointing system combined in a single Earth orbital test, will make a significant comparison of wideband planetary communication capability at optical frequencies.

TABLE 9.4.1-1

MARS MISSION COMMUNICATION COMPARISON PARAMETERS

$\frac{kT}{h\nu/q}$	$\frac{A_{ro}}{A_{rm}}$	$\frac{\epsilon_o}{\epsilon_m}$	$\frac{\lambda_m^2}{\lambda_o^2}$	$\frac{A_{to}}{A_{tm}}$
At 6328° A OPTICAL $h\nu = 3.12 \times 10^{-19}$ Joules $q = 0.05$	D=10 Meter $A_{ro} = 78.5 m^2$	0.0045	$\lambda_o^2 = 4 \times 10^{-13}$ m^2	D=1 Meter 0.785 m^2
AT 100°K MICRO- $kT = 1.38 \times 10^{-21}$ WAVE Joules	D=100m $A_{rm} = 7850 m^2$	0.5	$\lambda_m^2 = 9 \times 10^{-4} m^2$	D=30 Meters $A_{rm} = 706 m^2$
dB: - 23.5	-20	-20.5	+93.5	-29.5

9.4.2 Auxiliary Apertures

The 0.6328-micron link offers reliability and can be used in a simulated planetary mission context to generate system engineering data. However, the HeNe laser is not the ultimate device for operational applications. Its efficiency appears limited to a maximum in the order of 0.004, and there is little hope of increasing its maximum output power beyond 200 milliwatts. It was selected here for its advanced state of development, proven operation, and flexibility (e.g., its adaptability for single frequency, super-mode, and mode-locked operation). There are other lasers which exhibit better operational potential.

Furthermore, the atmospheric physics experiments would be better served by including at least two transmitter wavelengths on the spacecraft. In fact, the phase correlation experiment is predicated on the use of widely separated wavelengths to establish coherence scaling laws. Thus, a second transmitter frequency is not only desirable in all of the propagation experiments, it is essential in some.

The nitrogen carbon-dioxide (CO_2-N_2) laser is a new form showing great promise because of its high power and efficiency and favorable wavelength for operation in the atmosphere. Significant advances in detection and modulation devices will be required before this laser can be applied in operational wideband systems. However, its threshold of oscillation is about one tenth that of argon lasers of comparable power.

The laser will not be massive since a solenoid is not required, but additional space may be needed to carry reservoirs of the N_2 and CO_2 gases. For the proposed optical heterodyne detection experiment at a long optical wavelength, the transmitter is aboard the spacecraft and the receiver is at the ground station, where it is practical to use cryogenically cooled detectors for wide bandwidth performance. Because of the longer wavelength, the tuning and alignment problems are less severe than for the helium-neon local oscillator. However, the output will have to be maintained at specified frequency in a single TEM_{00} mode.

Such a wide separation in frequency (0.488 micron to 10.6 microns) imposes very stringent requirements on the laser telescope design. Conventional materials which transmit at one of the wavelength extremes are opaque at the opposite extreme. Three avenues of solution are evident: (a) develop a new refracting material, (b) restrict the laser telescope to an all-reflecting configuration, or (c) use a separate telescope for the 10.6-micron transmitter. The latter solution is the simplest and the lowest-risk alternative.

To compare a 10.6-micron link with a 0.6328-micron link, consider the transmission equations once again. Equating signal-to-noise ratio, prime power, receiving aperture, and bandwidth:

$$\left(\frac{D_{t_1}}{D_{t_2}}\right)^2 = \left(\frac{q_2}{q_1}\right)\left(\frac{\epsilon_2}{\epsilon_1}\right)\left(\frac{\lambda_1}{\lambda_2}\right)$$

Comparison of 0.6328-micron and 10.6-micron links on a detector quantum efficiency basis is not rigorous. In the visible region, photoemissive detectors apply. These are customarily compared on a quantum efficiency basis. Infrared detectors are photoconductive, hence should be compared on a detectivity basis. However, for a gross comparison, the equivalent infrared detector quantum efficiency can be postulated as approximately twice that of visible light detectors. Thus, an order of magnitude comparison of the spacecraft transmitting aperture requirement can be made as:

$$\left(\frac{D_{t_1}}{D_{t_2}}\right)^2 < \frac{1}{2}\,\frac{\epsilon_2}{\epsilon_1}\,\frac{\lambda_1}{\lambda_2} = 0.067$$

since at $\lambda_2 = 0.6328$ micron, $\epsilon_2 < 0.0008$; and at $\lambda_1 = 10.6$ microns, $\epsilon_1 > 0.1$. It follows that a 10.6-micron link with a 0.3-meter aperture should give equivalent, or slightly superior, received signal characteristics.

For a 0.3-meter aperture, 10.6-micron transmitter, the diffraction-limited half power beamwidth is 7 arc seconds, allowing an absolute alignment error of ±3 arc seconds. Using the 3 σ probability criterion for circular errors, this translates into an error budget of $\sigma_\theta = 1$ arc second. Such a tolerance is large enough to consider slaving the 0.3-meter telescope to the 1.0-meter telescope, thereby eliminating the need for a second precision tracking system in the smaller telescope. Preliminary structural analysis of a strap-together 1.0-meter/0.3-meter telescope configuration indicates that angular deflections will be less than 1 arc second for typical spacecraft attitude disturbances. It follows that, if 0.1 arc second error tolerances are assigned to boresight parallelism, the 1.0-meter telescope tracking error, and the 0.3-meter telescope point-ahead device, respectively, adequate pointing accuracy can be assured for the slaved, strap-together telescope.

Narrow bandwidth detectors at 10.6 microns do not need cryogenic cooling for satisfactory performance and can be used in a spaceborne receiver. The spaceborne receiver at 10.6 microns will be used to measure the low frequency (< 1000 Hz) scintillation of the atmosphere on the uplink. Polarization modulation of the transmitter beam provides an outgoing beam of constant intensity. Isolation between receiver and transmitter is not critical because the constant intensity transmitter beam will only appear as a bias in the receiver if cross talk appears. Therefore, the transmitter and receiver may be operated simultaneously.

9.4.3 Separately Gimbaled Apertures

It is desirable, from the viewpoint of atmospheric physics experiment design, to provide another Earth-to-space propagation link at one of the shorter wavelengths. This strategem serves to correlate observed effects and, in some instances, to isolate test variables. Thus far, the logic for including a 0.488-micron uplink and a 0.6328-micron downlink has been developed. The needed coincidence of uplink and downlink frequency can be obtained by adding a reverse direction link at one of these frequencies. The simplest solution might be to use a corner reflector—but this approach violates the desire to correlate observed effects.

To add a 0.488-micron downlink imposes the same threshold power penalty which was avoided in the initial choice of spaceborne transmitter. A 0.6328-micron uplink would use proven components, many of them previously tested in space, making the 0.6328-micron uplink a desirable choice.

However, to incorporate both transmitter and receiver of the same frequency for simultaneous operation in the same telescope would result in obvious isolation problems. If such problems are solvable, the solution would surely add complexity with attendant reliability implications and would probably degrade experiments (such as Phase Correlation) to which signal power is critical. Installation in a different telescope is clearly indicated.

A ground-based helium-neon transmitter need not be constrained in size, power consumption, and environmental qualification as a spaceborne transmitter. Existing designs now operate with 100-milliwatt output power — in contrast with the 10-milliwatt output contemplated for the 1-meter aperture, helium-neon spaceborne transmitter (i.e., $P_2/P_1 = 10$). Once again returning to the transmission equation, recall that

$$\left(\frac{D_{t_1}}{D_{t_2}}\right)^2 = \left(\frac{D_{r_2}}{D_{r_1}}\right)^2 \left(\frac{P_2}{P_1}\right)$$

For the coherent light experiments, the same diameter limitations apply to an Earth-based transmitting aperture as to an Earth-based receiving aperture: $D_{t_2} \doteq D_{r_1}$. Then,

$$D_{r_2} \doteq \frac{D_{t_1}}{\sqrt{10}} = 0.3 \text{ meter}$$

Again, a 0.3-meter auxiliary telescope aperture would be adequate. But, in this case, the reasons previously given for optically dissociating the 0.6328-micron and 10.6-micron energy processing still hold. Combination in the 0.3-meter, 10.6-micron telescope is undesirable. Furthermore, the corresponding diffraction-limited beamwidth is less than half of an arc second—an order of magnitude smaller error budget for a 0.3-meter, 0.6328-micron strap-on configuration than for the 10.6-micron, 0.3-meter telescope. It follows that the 0.3-meter, 0.6328-micron receiving telescope should contain a separate fine tracking device.

There are secondary bonuses to a separately gimbaled, 0.3-meter telescope. In transferring tracking from one ground station to another, a separation of at least 30 arc seconds is contemplated. If handled within the 1.0-meter telescope, the tracking transfer experiment would impose additional field-of-view and defocusing requirements. These requirements are relaxed when two separately gimbaled telescopes are used.

Finally, there can be space behind the separately gimbaled 0.3-meter telescope to install a back-up 0.6328-micron laser transmitter. This back-up laser is redundant. It will not be operated under normal experiment conditions. It is included to assure qualified success in the event of a debilitating or catastrophic failure of key elements housed in the 1.0-meter telescope well. Each of the space-to-Earth propagation experiments can be conducted with the back-up laser transmitter on the 0.3-meter telescope—compromised by reduction in signal strength and pointing accuracy as compared to the 1.0-meter telescope.

9.5 LASER TELESCOPE DESCRIPTIONS

9.5.1 One Meter Telescope

The one meter telescope system is an optical frequency transmitter-receiver with tracking capability, operating through a common Cassegrainian telescope which serves as a highly directional collector and collimator of light energy. The transmitter and principal receiver operate at a wavelength of 6328Å and the tracking subsystems and the auxiliary receiver operate at 4880Å. The telescope system contains provisions for modulating the transmitter carrier, detecting the modulation on the receiver carrier, centering its beam on the ground station, compensating for transit time differences and making certain alignment adjustments. (See block diagram in figure 9.5.1-1.)

Rigidly mounted to the one meter telescope is a 0.3 meter transmitter telescope which will be described in subsection 9.5.2. These telescopes are illustrated in figure 9.5.1-2.

9.5.1.1 Transmitter

The transmitter of the one meter telescope is illustrated in figures 9.5.1-3 and 9.5.1-4a. It consists of a transmitting laser package, a complex of processing optics and the Cassegrainian telescope. The laser package is an integrated unit including two helium-neon laser tubes with associated cavities and controls, electro-optical modulator and optical switch for laser selection. The energy emerging from the laser package is plane polarized, amplitude modulated and in a beam 1.5 mm in diameter and diverging at an angle of one milliradian.

On emerging from the laser package the beam is passed through a beam expanding telescope which serves four functions: (1) it matches the laser output beam to the aperture of the succeeding processing optics and eventually the input aperture of the telescope; (2) it collimates the output for diffraction limited performance; and (3) it provides a means for calibrated decollimation for controlling beam spread. The fourth function is to redistribute the energy to provide a more efficient match between the Gaussian laser output and the centrally obscured Cassegrainian telescope. This is discussed in further detail in subsection 9.5.1.1.1.

Following the beam spread control telescope is a quarter wave plate to convert the plane polarized laser output to circularly polarized light. A polarization compensator then corrects for the polarizing effect of the optical elements in the system by introducing a calculated polarization bias into the light beam. The compensator is installed and checked out during assembly. A variable density filter in the transmitter light path is used to attenuate the beam by a calibrated amount to simulate the deep space conditions. A filter wheel containing a suitable selection of filters is provided for this function. Additional attenuation is available through the beam spread control.

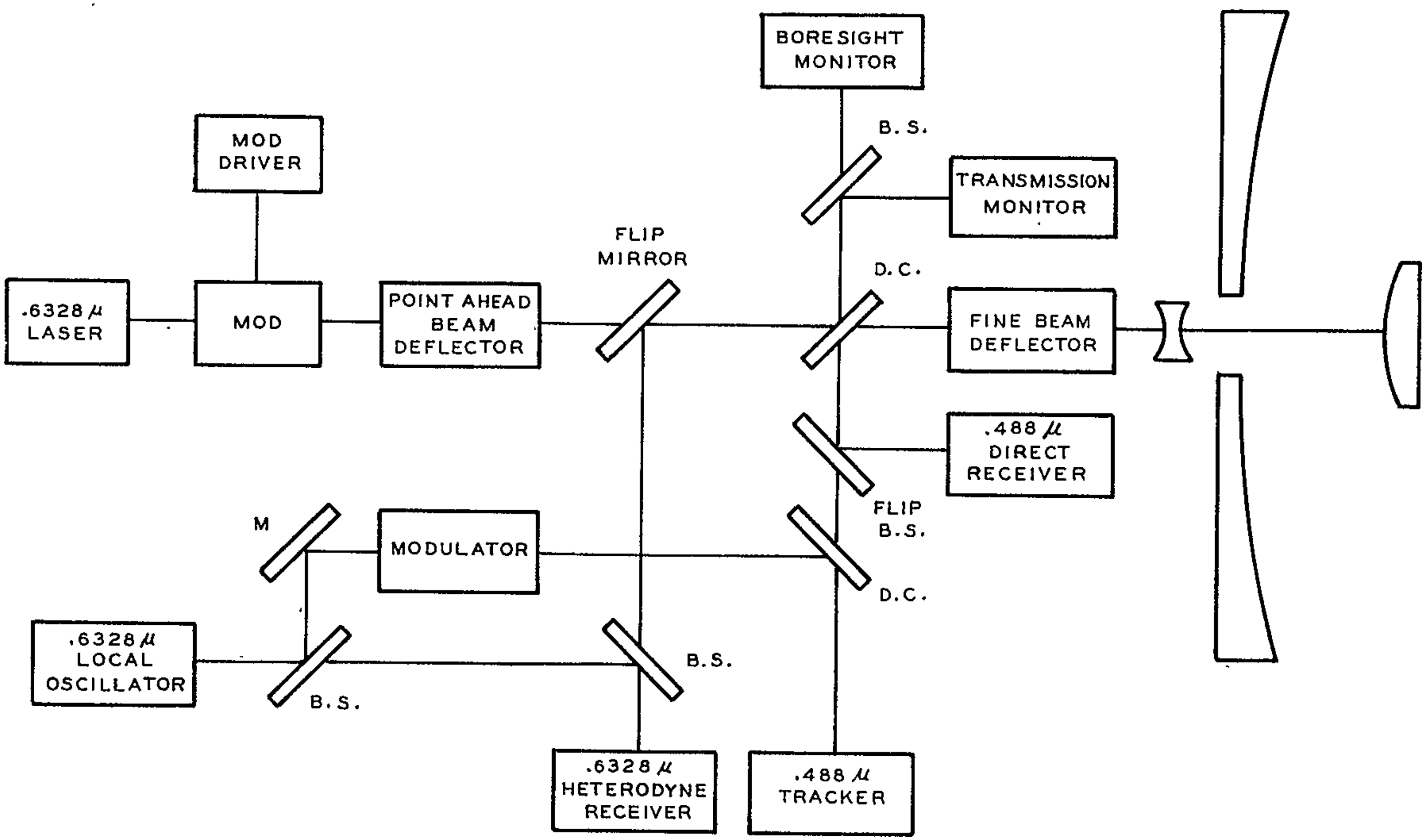

Figure 9.5.1-1. 1-Meter Gimbaled Telescope

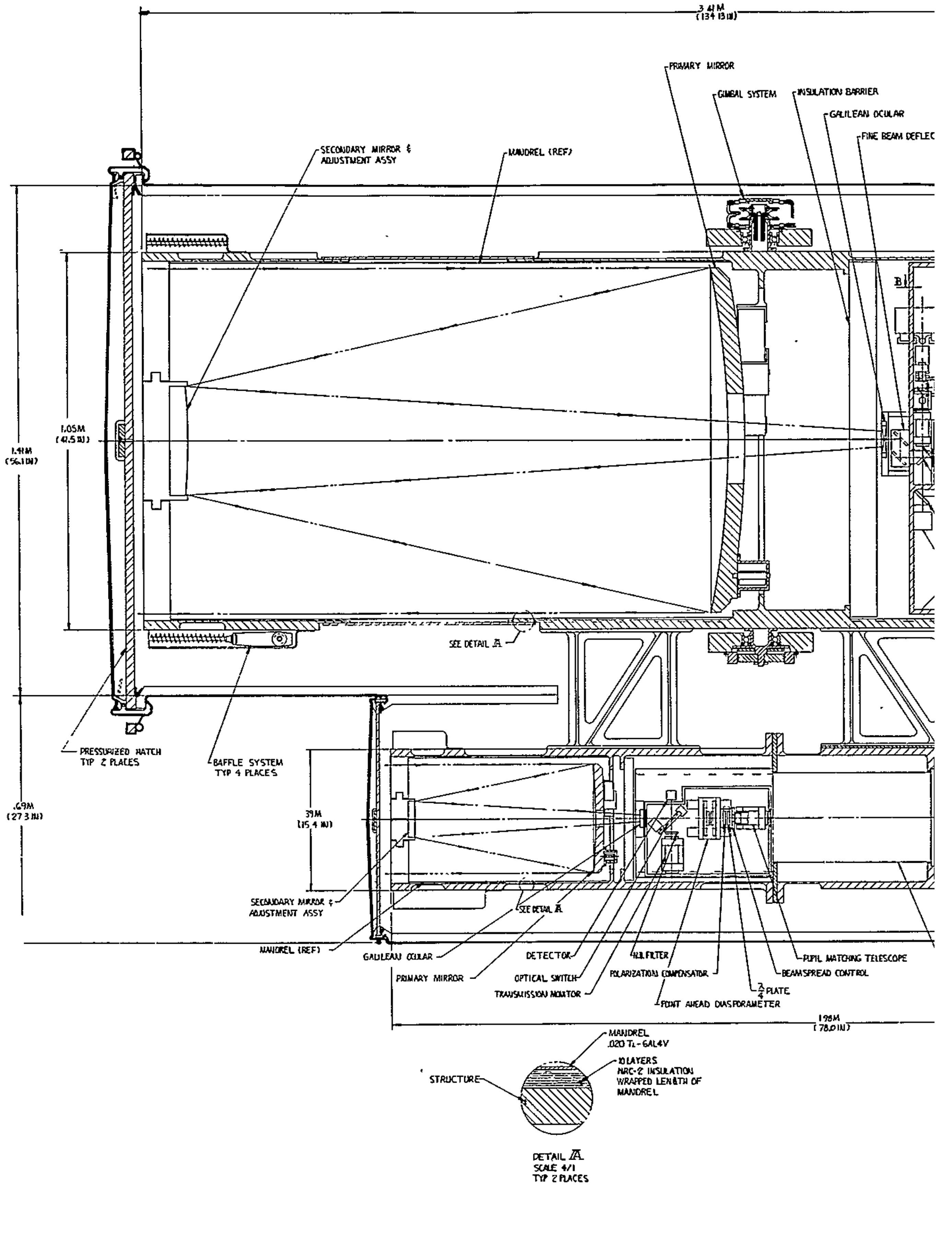

3.41M (134.13 IN)
PRIMARY MIRROR
GIMBAL SYSTEM
INSULATION BARRIER
GALILEAN OCULAR
FINE BEAM DEFLEC
SECONDARY MIRROR & ADJUSTMENT ASSY
MANDREL (REF)
B
1.05M (42.5 IN)
1.41M (56.1 IN)
SEE DETAIL A
PRESSURIZED HATCH TYP 2 PLACES
BAFFLE SYSTEM TYP 4 PLACES
.69M (27.3 IN)
.39M (15.4 IN)
SECONDARY MIRROR & ADJUSTMENT ASSY
SEE DETAIL A
MANDREL (REF)
GALILEAN OCULAR
PRIMARY MIRROR
DETECTOR
OPTICAL SWITCH
TRANSMISSION MONITOR
N.B. FILTER
POLARIZATION COMPENSATOR
λ/4 PLATE
POINT AHEAD DIASPORAMETER
BEAMSPREAD CONTROL
PUPIL MATCHING TELESCOPE
1.98M (78.0 IN)
MANDREL .020 Ti-6AL4V
10 LAYERS NRC-2 INSULATION WRAPPED LENGTH OF MANDREL
STRUCTURE
DETAIL A SCALE 4/1 TYP 2 PLACES

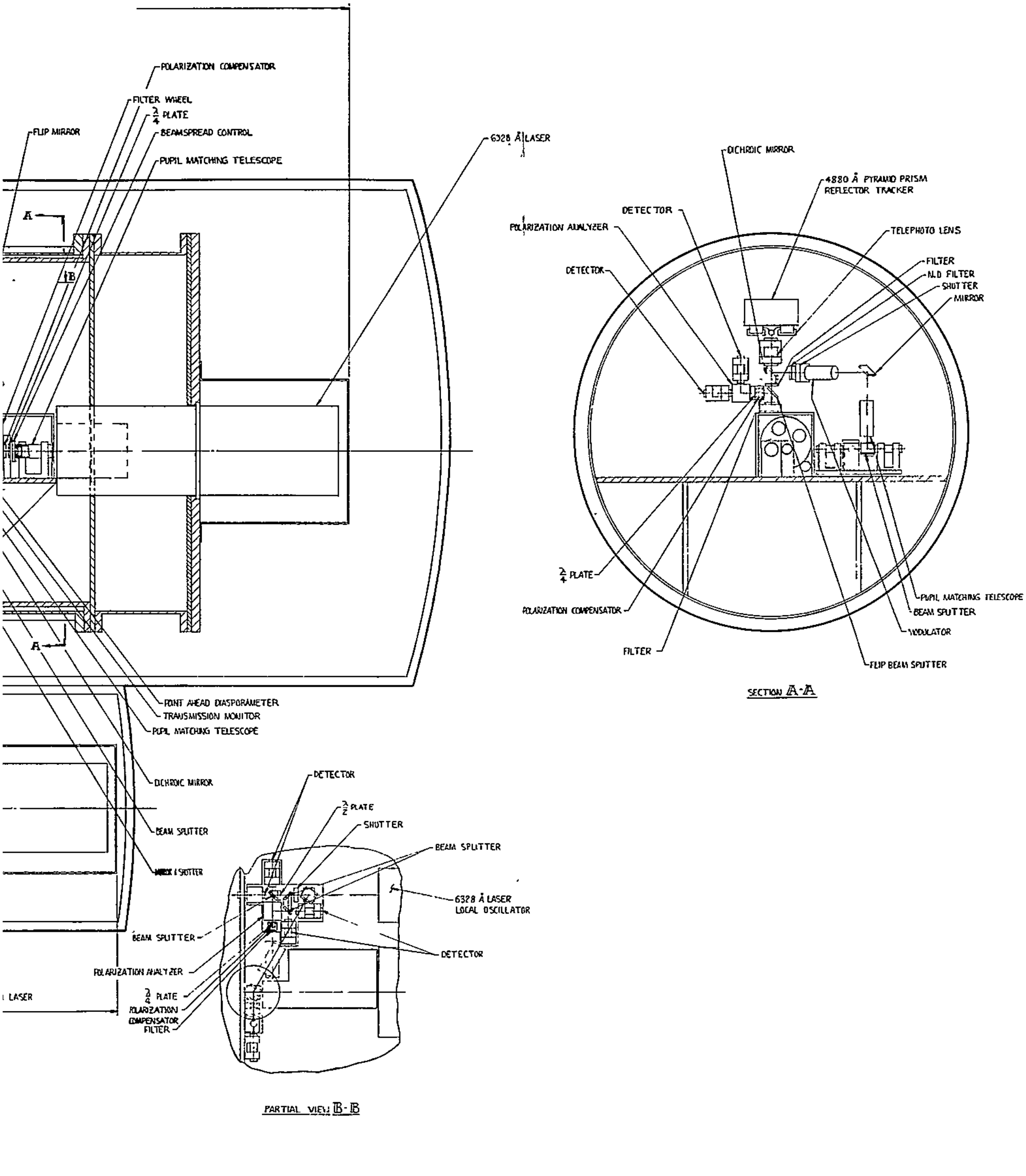

Figure 9.5.1-2. 1.0-Meter and 0.3-Meter Laser Telescope

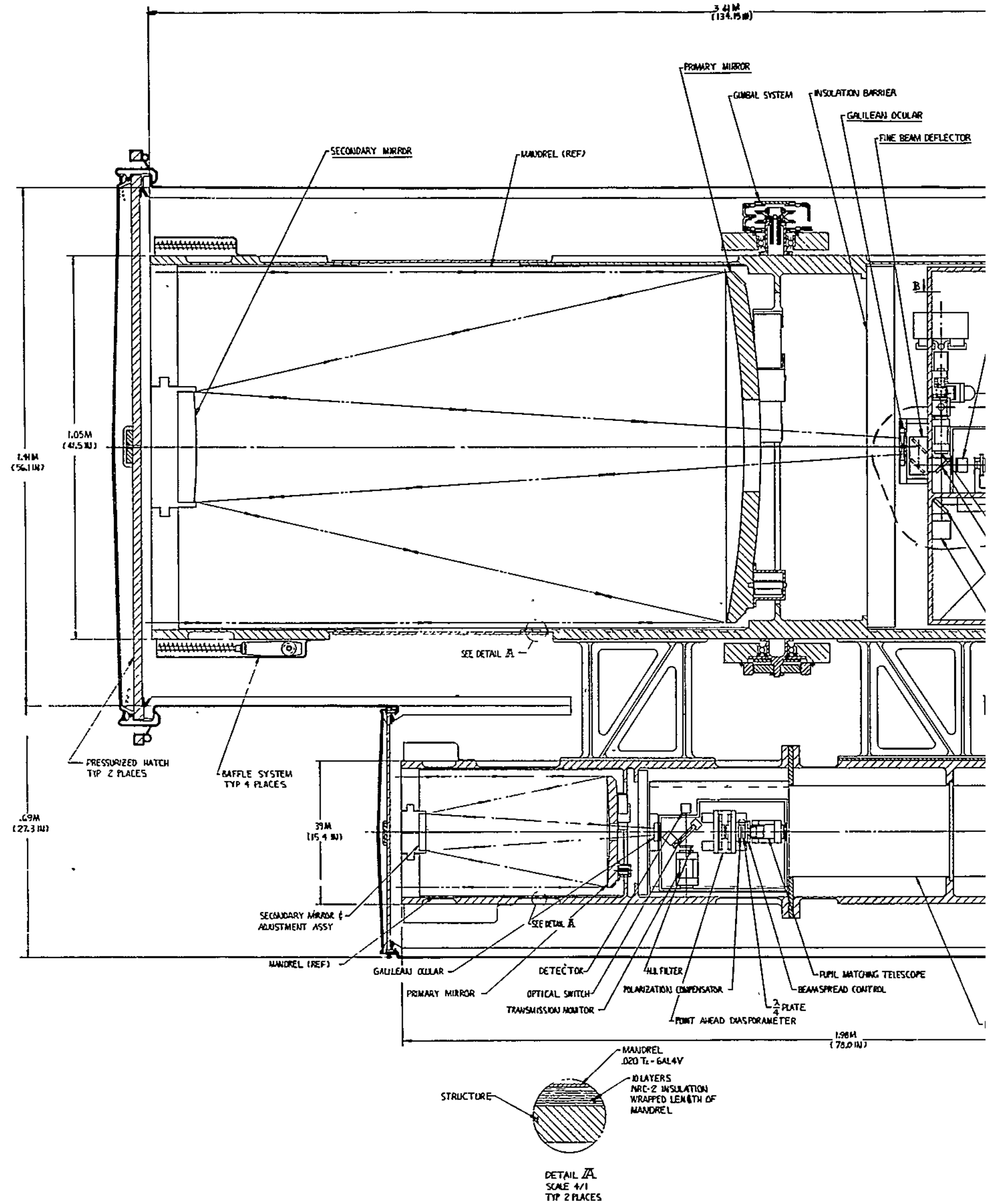

3.41M (134.15 IN)
PRIMARY MIRROR
GIMBAL SYSTEM
INSULATION BARRIER
GALILEAN OCULAR
FINE BEAM DEFLECTOR
SECONDARY MIRROR
MANDREL (REF)
1.05M (41.5 IN)
1.41M (56.1 IN)
SEE DETAIL A
PRESSURIZED HATCH TYP 2 PLACES
BAFFLE SYSTEM TYP 4 PLACES
.69M (27.3 IN)
.39M (15.4 IN)
SECONDARY MIRROR & ADJUSTMENT ASSY
SEE DETAIL A
MANDREL (REF)
GALILEAN OCULAR
PRIMARY MIRROR
DETECTOR
OPTICAL SWITCH
TRANSMISSION MONITOR
NULL FILTER
POLARIZATION COMPENSATOR
POINT AHEAD DIASPORAMETER
$\frac{\lambda}{4}$ PLATE
BEAMSPREAD CONTROL
PUPIL MATCHING TELESCOPE
1.98M (78.0 IN)
MANDREL .020 Ti - 6AL4V
10 LAYERS NRC-2 INSULATION WRAPPED LENGTH OF MANDREL
STRUCTURE
DETAIL A
SCALE 4/1
TYP 2 PLACES

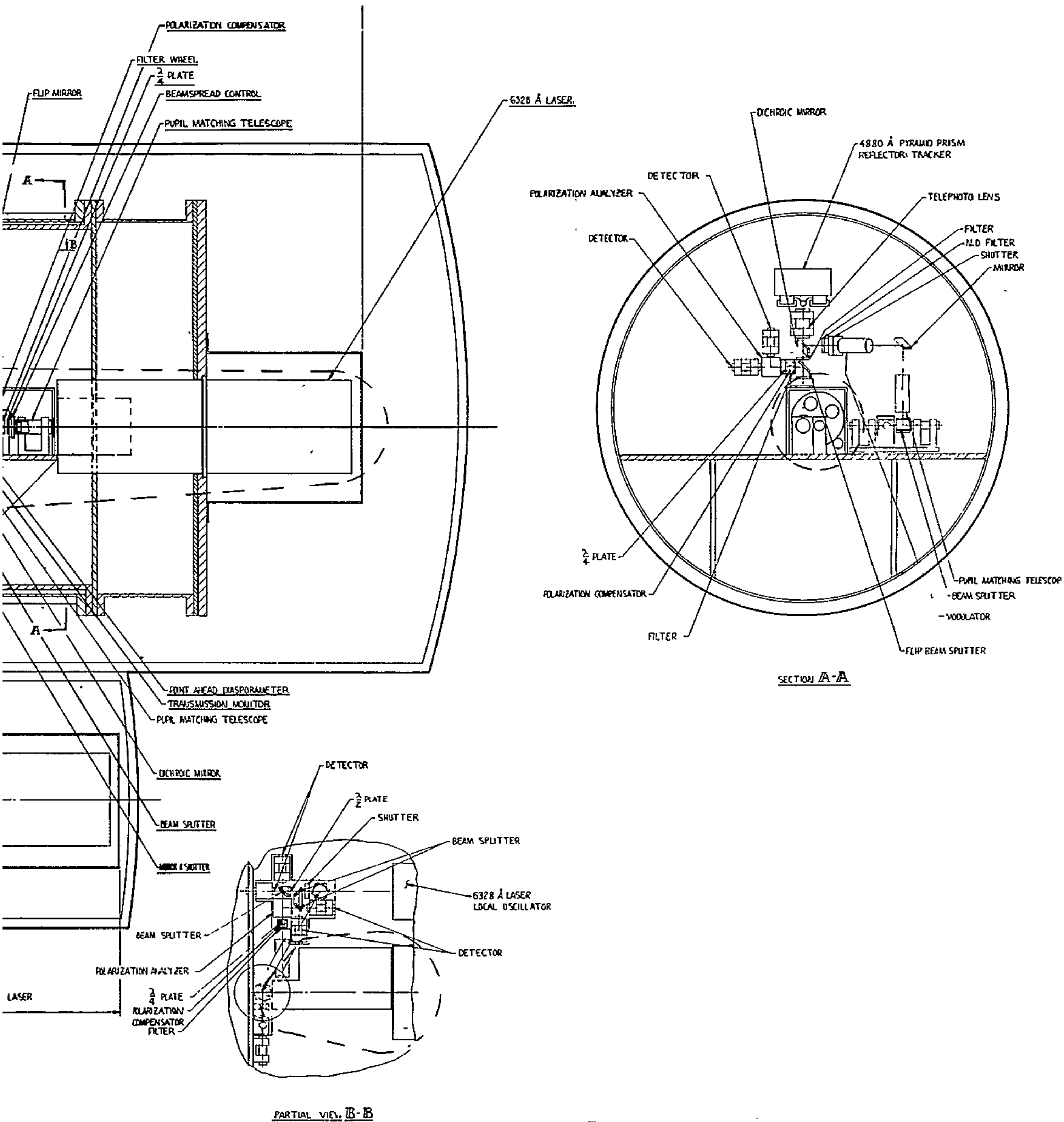

NOTE:
TRANSMITTER CALLOUTS UNDERLINED

Figure 9.5.1-3. 1-Meter Telescope-Transmitter Section

Following the filter wheel is the point ahead diasporameter which introduces a calibrated angular separation between the received and transmitted beams. This is to compensate for the relative velocity difference between the ground station and space station. A general discussion of diasporameters can be found in subsection 9.5.1.1.2.1. In the final report of OTAES Part I (1) it was stated that the point ahead diasporameter could generate vignetting of the transmitted beam up to a maximum of 25%. Refinements of design, chiefly in enlarging the aperture of the beam at the diasporameter with an accompanying decrease in magnification of the antenna telescope, and the shortening of the optical path through the fine beam deflector, have reduced the vignetting to a maximum of about 7%. It is felt that this amount of vignetting is acceptable and no positive steps need be taken to reduce it further.

The diasporameter wedges must be driven in counterrotation to provide the deflection for point ahead, and in unison to provide orientation. This can be accomplished with two motors, a differential and two rotation sensors. The sensor for deflection angle should be a resolver or a similar sinusoidal transducer and the sensor for the azimuth angle should be linear with angle. An alternate method for point-ahead generation is the use of four wedges arranged in two pairs with orthogonal axes, the two members of each pair being driven in counterrotation. This has the advantage of isolation of two axes and elimination of the differential from the drive. At the same time it is burdened by the requirement of added optical surfaces and additional length of optical path, involving an increase in volume. Either technique could serve the required function and a trade-off analysis is indicated before a choice can be made.

After the point ahead diasporameter, which is required to deflect the transmitted beam only, and before the fine beam deflection device which operates on both the transmitted and received beam is a dichroic beam splitter which passes the 6328Å energy and reflects 4880Å energy. Its function is to separate out the received 4880Å energy and direct it toward the direct detection receiver and tracker while not materially diminishing the transmitted energy. Less than one percent of transmitter energy is reflected and utilized for monitoring and boresight adjustment as described in a later paragraph.

Between the last two mentioned elements, namely the point ahead diasporameter and the dichroic beam splitter there is space for an optical switch or flip mirror "B" which is out of the circuit when the transmitter is in operation. It is switched into position when the heterodyne detection receiver is in use, making it impossible to use the heterodyne receiver and transmitter simultaneously in this instrument. The last element of

---

(1) (OATES Part I section 8.2.1.2.2)

processing optics in the transmitter chain is the fine beam deflector. Advances in technology (1) since the final report of OTAES Part I have permitted the inclusion of a much improved concept of fine beam deflector in the current telescope design. This is described in subsection 9.5.1.1.3.2. Because of its wider aperture and the larger amplitude of motion of the individual mirrors this deflector has significant improvement over the one previously described. (See subsection 9.5.1.1.3.1.) Since it uses only two reflecting surfaces instead of a minimum of 16, it needs no aperture transfer optics, and its geometry reduces vignetting to an acceptable level. What is sacrificed in order to gain these advantages is the kilohertz frequency response. This, however, is no serious disadvantage as the 0.1 kilohertz response remaining is adequate for the current application.

The antenna function of the transmitter is accomplished by a 38 power telescope consisting of a Cassegrainian objective of 0.965 meter aperture and 6.705 meter effective focal length, and a Galilean ocular of -176 mm focal length and a clear aperture of 30 mm. The eyepiece is achromatized for the two wave-lengths of interest, namely 6328Å and 4880Å, and corrected for reasonable image quality over a field of ± one minute. The objective consists of a primary mirror with a focal length of 2.235 meters and an aperture of 0.965 meter. The secondary is separated from the primary by 1.524 meters and has an aperture of 0.318 meter and a focal length of -1.067 meter. With the extremely small field of view requirements these can be a classical Cassegrain, with a paraboloidal primary and a hyperboloidal secondary. The principal telescope has two functions: it matches the 25.4 mm pupil of the transmitted beam at the fine beam deflector to a one meter pupil for transmission to earth in a highly directional beam; at the same time it collects the received energy from earth and collimates it into a one inch pencil for transmission to the receiver.

The transmitter energy which is reflected by the dichroic mirror, amounting to less than one percent of the total, is directed towards a beamsplitter where it is divided between the transmission monitor and the boresight shutter and mirror. The transmission monitor is a photomultiplier which detects the transmitter energy received and continuously checks the transmitter output level and modulation. The remaining energy is used for the transmitter boresight adjustment which is described in subsection 9.5.1.4.2.

9.5.1.1.1 Effect of Central Obscuration on Transmitter Beam

The combination of a laser transmitter and a collimating telescope of Cassegrainian configuration has an inconsistency which can cause a serious loss in efficiency. This is due to the fact that the aperture of the Cassegrainian telescope has a central obscuration through which nothing

---

(1) Investigation of Electro Optical Techniques for Control of The Direction of a Laser Beam, Contract NAS 8-11459 - May 12, 1967 AT&E Bayside, New York.

can be transmitted, while the output of the laser is Gaussian in distribution, which makes the central part of the beam carry the densest concentration of energy. Therefore, the richest part of the beam is blocked by the central obscuration.

There are several approaches to the solution of this problem which will be discussed in order. They include refractive optics, Herschelian telescope, refractive compensation and reflective redistribution of energy.

9.5.1.1.1.1 Refractive Optics

The first and most obvious method of correcting the inconsistency is to eliminate the central obscuration. One way in which this can be accomplished is by the use of refractive optics. While this is quite feasible for small optics, the likelihood of success decreases rapidly as the aperture increases. In fact, the optical design described in this report uses refractive optics for all elements whose apertures are less than one inch; however, the use of refractive elements for the main objectives of the telescopes is out of the question for several reasons including the weight penalty of such a large piece of optical glass, the difficulty and expense of manufacturing such a large lens and the difficulty of supporting it adequately to survive the launch environment. Any lingering suspicion that this is a practical solution should be dispelled by the fact that the largest refractive astronomical telescope in the world has an objective no larger than the one required for the 1.0 meter telescope.

9.5.1.1.1.2 Herschelian Telescope

There is a type of reflecting telescope which also avoids the central obscuration. This is the Herschelian telescope, shown in figure 9.5.1-5a whose objective is a portion of an off-axis paraboloid and whose secondary mirror is outside of the field of the primary. This configuration not only eliminates the central obscuration but it also eliminates the diffraction effects of the support structure for the secondary. The disadvantages of the Herschelian telescope are three:

a. It is non-symmetrical, thus eliminating any balancing of aberrations that can be derived from a symmetrical telescope.

b. The extreme rays are twice as far off-axis in a Herschelian telescope as in a Cassegrainian; and, in the case of the 1.0 meter telescope approach a focal ratio of 1.16 rather than 2.32, thus making correction to a diffraction limit more difficult.

c. The manufacture of an off-axis mirror frequently requires finishing one twice the required size, cutting out the part desired and discarding the remainder. Making a two meter mirror is many times more difficult than making a one meter mirror.

Therefore, the Herschelian telescope is not recommended as the answer.

II 65-66 PRECEDING PAGESBLANK NOT FILMED.

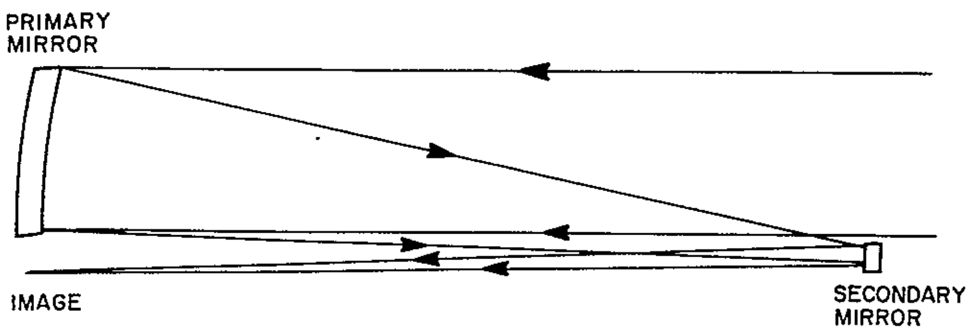

(a) Herschelian Telescope

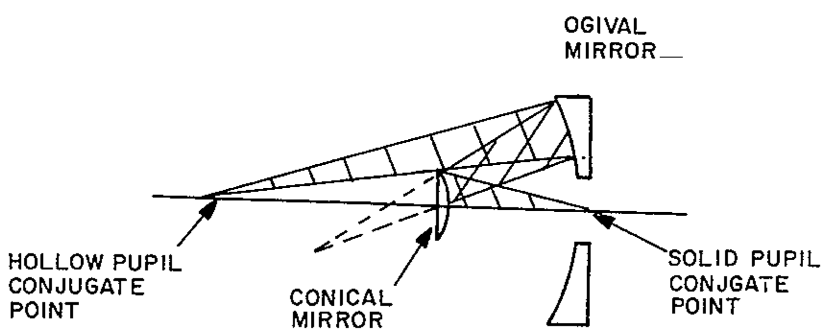

(b) Reflective Redistribution of Energy (1)

---

(1) Journal of the Optical Society of America,
Vol. 45, p. 398

Figure 9.5.1-5 Central Obscuration Correction

9.5.1.1.1.3 Refractive Compensation

9.5.1.1.1.3.1 Aspherics

Another approach is to redistribute the energy in the laser output beam to change the Gaussian distribution of the output to uniform distribution, or even to over-compensate and put the bulk of the energy into an annular zone where it will be free of central obscuration. Two media present themselves whereby this might be accomplished within the pupil matching telescope at the modulator output. One mechanism is the use of aspheric surfaces on the telescope lenses designed to deviate the central rays more sharply at the center of the field than at the edge. A corresponding aspheric in the recollimating lens is required to maintain a collimated beam.

9.5.1.1.1.3.2 Elements with Coma

A method not using aspherics is also available. Coma is an aberration which is characterized by differential magnification as a function of displacement from axis. If the lens has higher magnification in the outer zones, the coma is said to be positive; if the magnification is greater in the center, the coma is negative. Using the above definitions, consider the short focal length lens to possess negative coma, and the long focal length lens to possess positive coma; some of the energy should be redistributed out of the central zone and into the outer zones, producing effects similar to those described for the aspheric lenses. To determine the actual effectiveness of these schemes, a ray trace program must be conducted.

9.5.1.1.1.3.3 Double Cone Inverter

A different and promising means of refractive correction is the addition of a separate element placed in collimated space between the beam spread control telescope and the point-ahead diasporameter. This element effectively turns the beam inside out. If the input beam is expanded to a diameter 50% greater than optimum without this device and then inverted, the centrally obscured portion of the exit beam would contain energy to have been rejected in any case, and the energy which would have been sacrificed to the central obscuration is shifted to an outer zone and preserved.

The element which performs this function is a proprietary device for which patent protection is being considered. It consists of a double ended right circular cone (a number of alternate configurations are feasible), which is made coaxial with the beam. Figure 9.5.1-6 illustrates the geometry of the device and its effect on the energy distribution. The incident rays on striking the entrance surface of the cone are refracted toward the optical axis. After they cross the axis by the appropriate amount they are refracted by the exit face. Because of the symmetry of the device, the two faces as seen by any ray are parallel to each other so that the emerging ray is parallel to the entering ray but displaced by the desired amount. By manipulating the cone angle and the length of the double cone

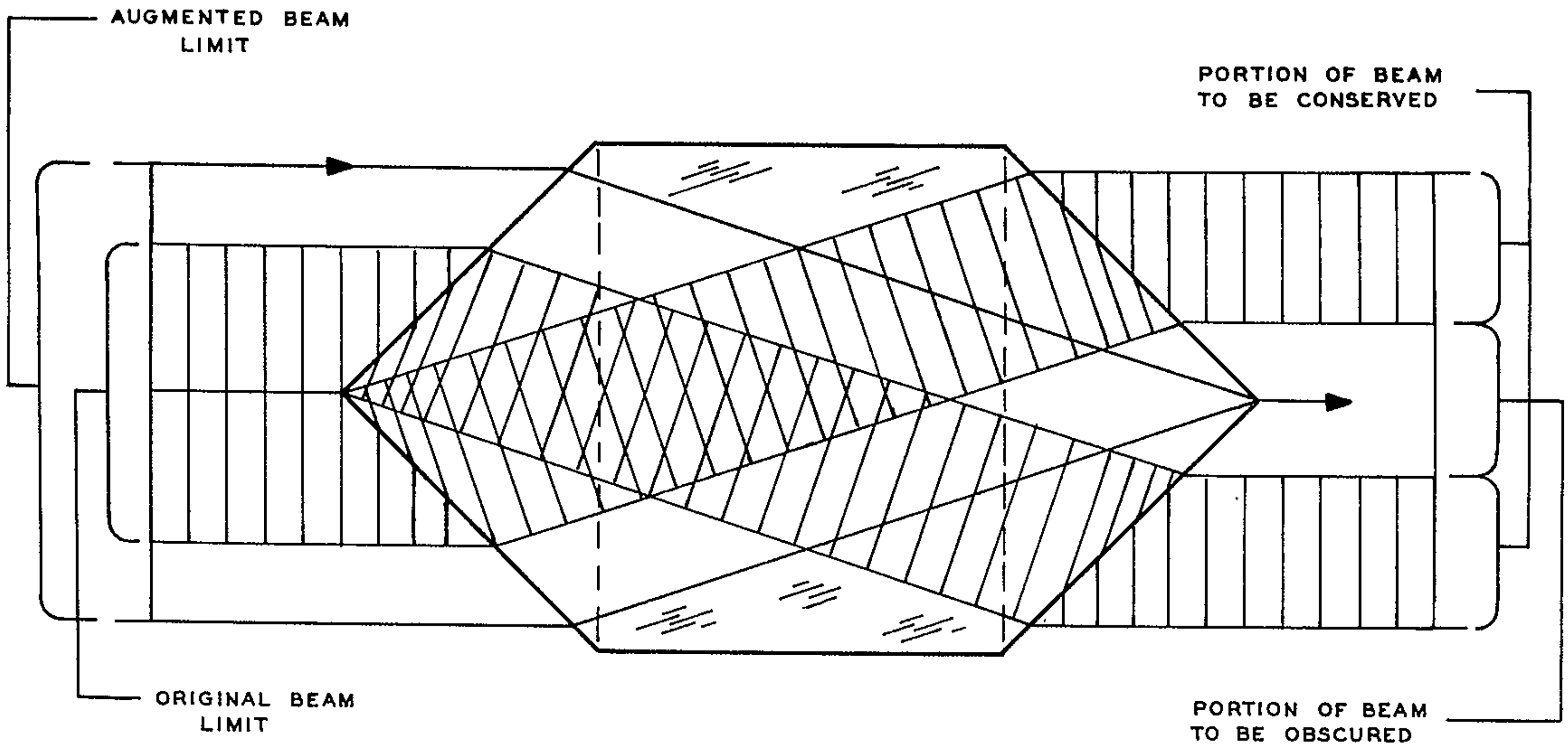

Figure 9.5.1-6. Principle of Double Cone Inverter

a wide range of output patterns can be achieved. The cone angle and overall length are balanced for the best compromise of size and polarization effects. Antireflection coatings reduce reflection and resulting polarization, and residual polarization is handled by the polarization compensator.

9.5.1.1.1.3.4 Reflective Redistribution of Energy

A mechanism has been described (1) whose function is "to create or eliminate holes in the pupil of a beam of light". It consists of a conical mirror and an ogival mirror. See figure 9.5.1-5b. When used to create the hole as in the present requirement, the incoming light strikes the conical mirror and is diverged in a hollow cone. The light is recollected and reimaged or recollimated in a beam of annular cross section. While the device illustrated shows finite conjugates, the text of the reference indicates that it can also be corrected for collimated light. Such a device has been constructed and used, but as in the prior case, further investigation in the form of a ray trace analysis is recommended.

In summary, although a laser and a Cassegrainian telescope make poor companions, it may be possible to reduce and, perhaps, even eliminate the incompatibility so that they can perform quite efficiently when used together.

9.5.1.1.2 Point-Ahead Deflector

Several mechanisms have been studied as the preferable way of achieving the point-ahead correction for transit time to the ground station. Since the magnitude of deflection required for point-ahead is comparable with that of the fine beam deflection, the use of the same type of mechanism for both deflections was considered. However, the bandwidth requirements are vastly different and it became evident that the sophisticated approach required to get the high speed of response in the fine beam deflector is entirely unnecessary in the point-ahead function. For the comparatively static correction required and the low speed of response the diasporameter is adequate, and its efficiency, stability and reliability highly recommend its use for point-ahead deflection.

9.5.1.1.2.1 Diasporameter

A diasporameter consists of a pair of optical wedges, each effecting a small angular deviation on an incident light ray. As generally applied, the deviation is the same in each wedge, although there are specific cases where they may not be equal. In this discussion, only matched pairs are considered.

(1) (Ref. Seymour Rosin - JOSA Volume 45 P398, "Mirror Condenser for Spectrographs")

An optical wedge, as shown in figure 9.5.1-7 deflects an incident ray by bending it toward the normal on entering the wedge and away from the normal on leaving the wedge. For small angles:

$$\rho = a(n-1)$$

where:

ρ is the angular deviation

a is the apex angle of the wedge

n is the refractive index of the wedge material

The deviation can be resolved into components as follows:

(Figure 9.5-7b)

$$\rho_x = \rho \cos\theta$$

$$\rho_y = \rho \sin\theta$$

where

ρ_x and ρ_y are the x and y components of ρ

θ is the angle between the thick end of the wedge and the positive x axis

When the wedges are used in a diasporameter, the effect of both wedges is summed. If Θ is the same in both wedges, as shown in figure 9.5.1-7c,

$$\rho_x = \rho \cos\Theta + \rho \cos\theta = 2\rho \cos\theta$$

$$\rho_y = \rho \sin\Theta + \rho \sin\theta = 2\rho \sin\theta$$

Hence, the net effect of two wedges with the same orientation is double the effect of a single wedge.

Next consider the effect when the angles are separated by 180°.

$$\rho_x = \rho \cos\theta + \rho \cos(180° + \theta) = 0$$

$$\rho_y = \rho \sin\theta + \rho \sin(180° + \theta) = 0$$

Hence the effect is a net cancellation.

The third case of special interest is the situation where the angles are equal but opposite. See figure 9.5.1-7d.

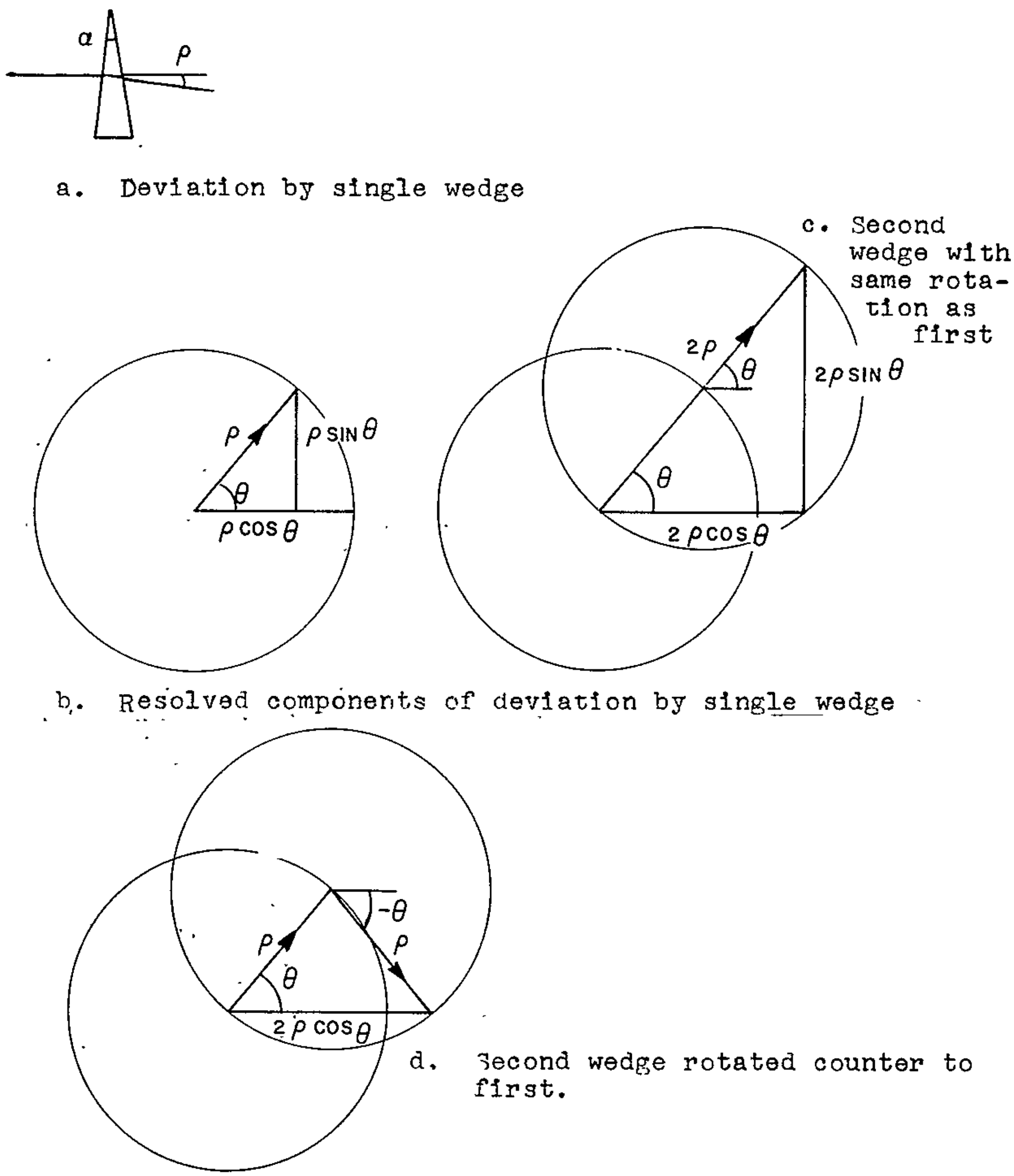

a. Deviation by single wedge

b. Resolved components of deviation by single wedge

c. Second wedge with same rotation as first

d. Second wedge rotated counter to first.

Figure 9.5.1-7 Beam Deviation by Diasporameter

$$\rho_x = \rho \cos \theta + \rho \cos(-\theta) = 2 \rho \cos \theta$$

$$\rho_y = \rho \sin \theta + \rho \sin(-\theta) = 0$$

Hence the x components are additive, the deviation bears a cosine relation to the wedge rotation, and the y components cancel.

From the foregoing, it can be concluded that any displacement between zero and 2θ can be achieved by counter-rotating the wedges by a specific amount between 0° and 90°, and that the orientation of the displacement angle can be adjusted by moving the two wedges in unison.

9.5.1.1.3 Fine Beam Deflectors

The choice of a beam deflector for an optical tracking system depends upon the requirements set for resolution, speed of response, optical attenuation and the optical configuration of the rest of the system. If it is to be launched the unit must also be rugged, and weight and power consumption become important considerations. Those beam steering devices which will be discussed herein will be limited to three reflection type devices, the shear-plate mirror, the bender-mode mirror, and the mirror galvanometer. Each of these is basically a transducer driven mirror. Other beam steering techniques are not being considered since they fail to meet the resolution requirement of ±300 spot diameters.

9.5.1.1.3.1 Shear Plate Deflector

Wideband reflection scanning may be achieved by using mirrors attached to piezoelectric shear transducers, as shown in figure 9.5.1-8. These transducers develop a shear strain in response to an electric field applied perpendicular to their poling direction. The induced shearing action causes the mirrors to tilt through an angle proportional to the applied field. Multiple mirror structures are employed to increase the scan angle, and hence the resolution of the device. With presently available piezoelectric materials, peak-to-peak angular mirror motions of 0.05° are possible. The relative sizes of the mechanical components govern the operating bandwidth by determining the mechanical resonance frequency of the mirror-driver combination. Units with half inch mirrors have been made to operate over a bandwidth of dc to 17 kHz; however, 18 mirrors are needed to obtain 400 spot resolution and optical attenuation becomes excessive. This same problem is present in designs for lower frequency, higher resolution operation due to the large number of reflections needed.

9.5.1.1.3.2 Bending Deflector

There is another type of piezoelectric transducer which can be designed to give much larger angular deflections, but which is more compliant than the shear transducer. This element is the piezoelectric bender and is illustrated in figure 9.5.1-9a. The bender construction and action is similar to that of a bimetallic thermometer. Two piezoelectric expanders are bonded together and energized so that one expands as the other contracts. This causes the entire unit to bend. If the bender is mounted as a cantilever beam with a mirror on the free end, the tilting of this end may be used to steer a light beam. Since the deflection and compliance of the bender are both proportional to its length, large scan angles in a single element are achieved only at the expense of bandwidth. Because of this, and the fact that the maximum deflection is not inherently limited, the bender seems more suited than the shear transducer to low frequency scanning up to a few hundred hertz.

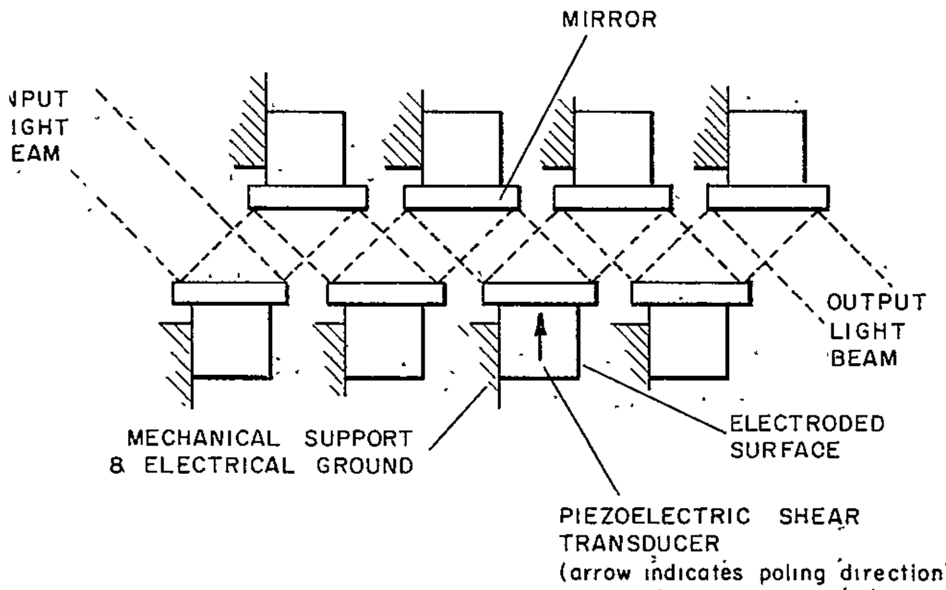

Figure 9.5.1-8 Shear Plate Mirror Deflector Uses Shear-Mode Transducers To Tilt The Mirrors

Recent advances in the technology of beam benders have developed this concept into the probable selection for the beam deviation function in the laser telescopes. The rudimentary unit shown in figure 9.5.1-9a has been improved, as shown in figure 9.5.1-9b, by making the mirror parallel to the rest position of the crystals. This brings the center of gravity closer to the center of rotation thus improving the resonance characteristics of the unit. The mirrors are large enough, 1.5 by 2.0 inches, to permit a one-inch diameter beam to be operated upon, and the maximum beam deflection amplitude of ±50 minutes permits the use of a 38 power antenna telescope with a resulting deviation capability of ±1.3 minutes in external space. This exceeds the required deviation by a factor of 4, thus permitting the use of relatively small excitation voltages on the crystals, on the order of 200 volts. Furthermore a single pair of deviators, one for each coordinate, is adequate for the telescope. The arrangement is shown in figure 9.5.1-9c. For further details the reader is referred to a report on the development of the device.(1)

9.5.1.1.3.3 Mirror-Coil Assembly

The mechanism of the traditional optical galvanometer consists of a mirror attached to a coil which is suspended in a steady magnetic field. Passing a current through the coil causes the mirror-coil assembly to twist on the suspension. The magnitude of the current governs the twist angle while the suspension provides the restoring force. Systems of this type may be constructed to give 400 spots resolution at a few kHz from a single mirror. Because of the need for a magnet to provide the dc field the weight of a one-dimensional scanner may reach 10 lbs. or more and require many times the volume of the previous devices. These factors will most likely limit its usefulness for spaceborn applications.

9.5.1.2 Receivers

The 1.0 meter telescope has two receivers; one is a 6328Å heterodyne receiver which can be operated at any time when the transmitter is not in operation, and the other is a 4880Å direct detection receiver which can be

---

(1) Investigation of Electro-Optical Techniques for controlling the Direction of a Laser Beam, Interim Report, Contract NAS 8-11459, Gen. Te. & Electronics Lab., Inc., Bayside, N. Y.

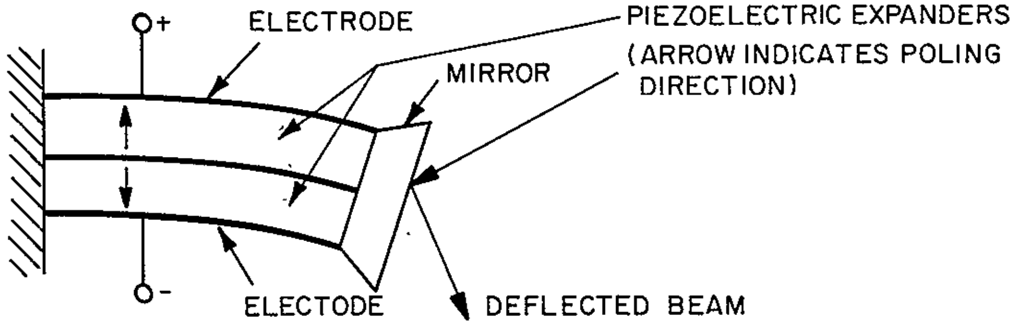

(a) Cantilever Mounted Piezoelectric Bender

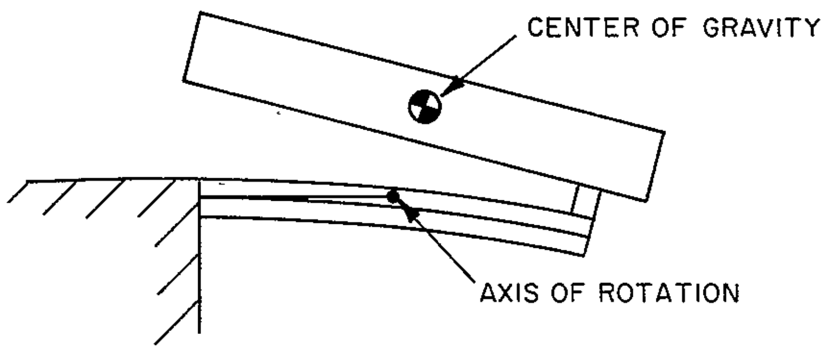

(b) Improved Bender Arrangement

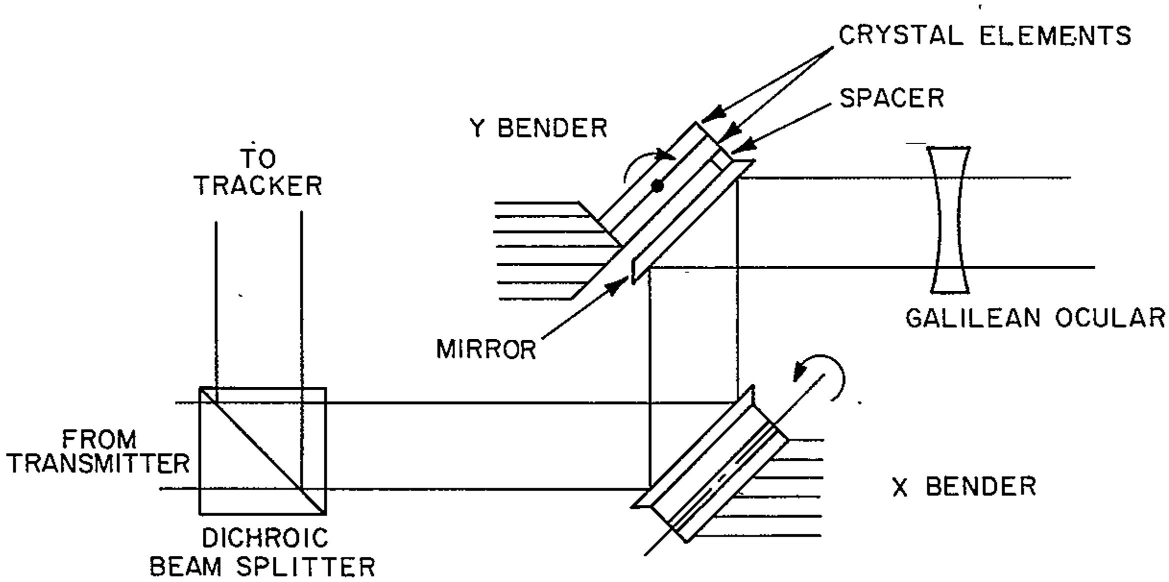

(c) Arrangement of Bender Mirrors

Figure 9.5.1-9 Piezoelectric Bender Configuration used at any time that the ground station is operating at full power. Both receivers as well as the tracker operate on energy collected by the telescope and collimated into a 25.4 mm beam by the Galilean ocular (see figure 9.5.1-10 and 9.5.1-4b). The line of sight is then stabilized by the fine beam deflector and separated by the dichroic beam splitter. The signal for the direct detection receiver and the tracker are directed away from the telescope axis and toward the tracker. This line of sight will be resumed in the discussion of the direct detection receiver.

9.5.1.2.1 Heterodyne Receiver

The 6328Å light for the heterodyne receiver passes through the dichroic mirror to the flip mirror optical switch. When this switch is in the receiver position the heterodyne receiver beam is reflected out of the transmitter line of sight toward the heterodyne receiver subassembly. Between the dichroic beam splitter and the heterodyne receiver subassembly is an aperture matching telescope which serves to narrow down the one inch beam produced by the antenna telescope to a two millimeter diameter suitable for the receiver subassembly.

The heterodyne receiver subassembly contains the local oscillator, four detectors and the appropriate processing optics for the signal and local oscillator beams and their combination. The signal beam, after being narrowed down by the aperture matching telescope mentioned above is passed through a narrow band interference filter centered at 6328Å for the purpose of reducing background noise from other parts of the spectrum. A polarization compensator then removes the polarization bias that may have been introduced by the preceding optical elements. This element returns the beam to its original circularly polarized state. A quarter-wave plate then transforms the circularly polarized input light to plane polarized light. The polarization analyzer, a Wollaston prism, separates the beam into two polarization components, which, with the aid of an auxiliary mirror are made mutually perpendicular. Each ray is directed toward a beam splitter which divides the energy equally between two multiplier phototubes. Thus the signal energy is divided among four photomultipliers through the instrumentality of the polarization analyzer and the two beam splitters.

Concurrently the same four tubes are illuminated by the local oscillator through its own processing optics consisting of an aperture matching telescope, two beam splitters, a shutter and a half wave plate in addition to the two beam splitters associated with the photomultipliers. The local oscillator is a single frequency helium-neon laser with automatic frequency control, producing a beam of 1 mm cross-section, 2 milliradian divergence and 0.1 milliwatt power output. The aperture matching telescope expands the beam from 1 to 2 millimeters to provide the required match for the detectors. The near beam splitter taps off the energy not required for the heterodyne receiver and shunts it into another line of sight where it is used for a tracker balance calibration which is discussed later. The shutter labeled Shutter "A" is closed when it is desired to operate the heterodyne receiver as a direct detection receiver and during the preliminary equipment checkout. This shutter, as are the other two shutters used in this telescope, is a simple electromechanically actuated device.

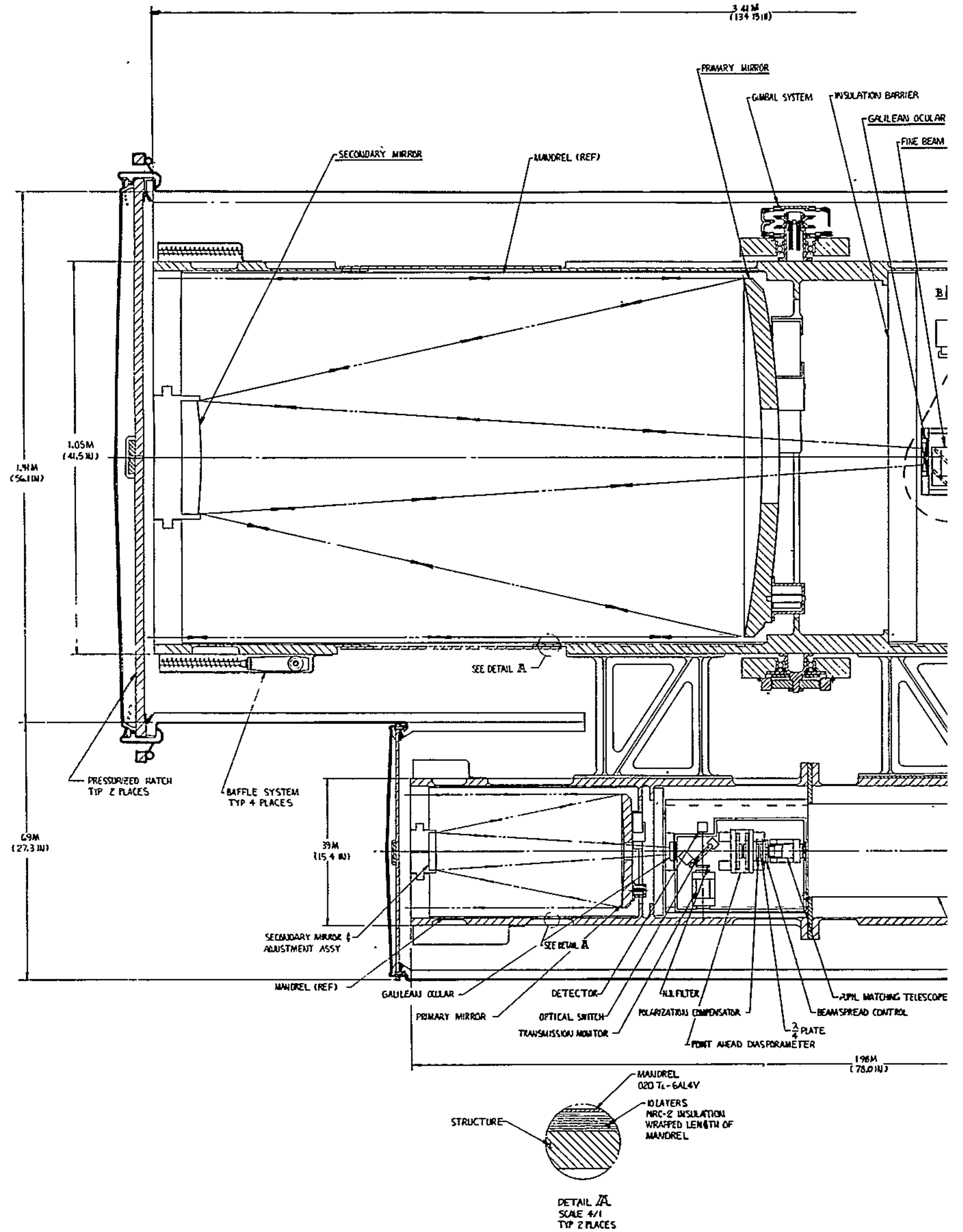
3.41M (134.15 IN)
PRIMARY MIRROR
GIMBAL SYSTEM
INSULATION BARRIER
GALILEAN OCULAR
FINE BEAM
SECONDARY MIRROR
MANDREL (REF)
1.05M (41.5 IN)
1.91M (56.1 IN)
SEE DETAIL A
PRESSURIZED HATCH TYP 2 PLACES
BAFFLE SYSTEM TYP 4 PLACES
.69M (27.3 IN)
.39M (15.4 IN)
SECONDARY MIRROR & ADJUSTMENT ASSY
SEE DETAIL A
MANDREL (REF)
GALILEAN OCULAR
PRIMARY MIRROR
DETECTOR
OPTICAL SWITCH
TRANSMISSION MONITOR
N.D. FILTER
POLARIZATION COMPENSATOR
POINT AHEAD DIASPORAMETER
λ/4 PLATE
BEAMSPREAD CONTROL
PUPIL MATCHING TELESCOPE
1.98M (78.0 IN)
MANDREL .020 Ti-6AL4V
10 LAYERS NRC-2 INSULATION WRAPPED LENGTH OF MANDREL
STRUCTURE
DETAIL A SCALE 4/1 TYP 2 PLACES

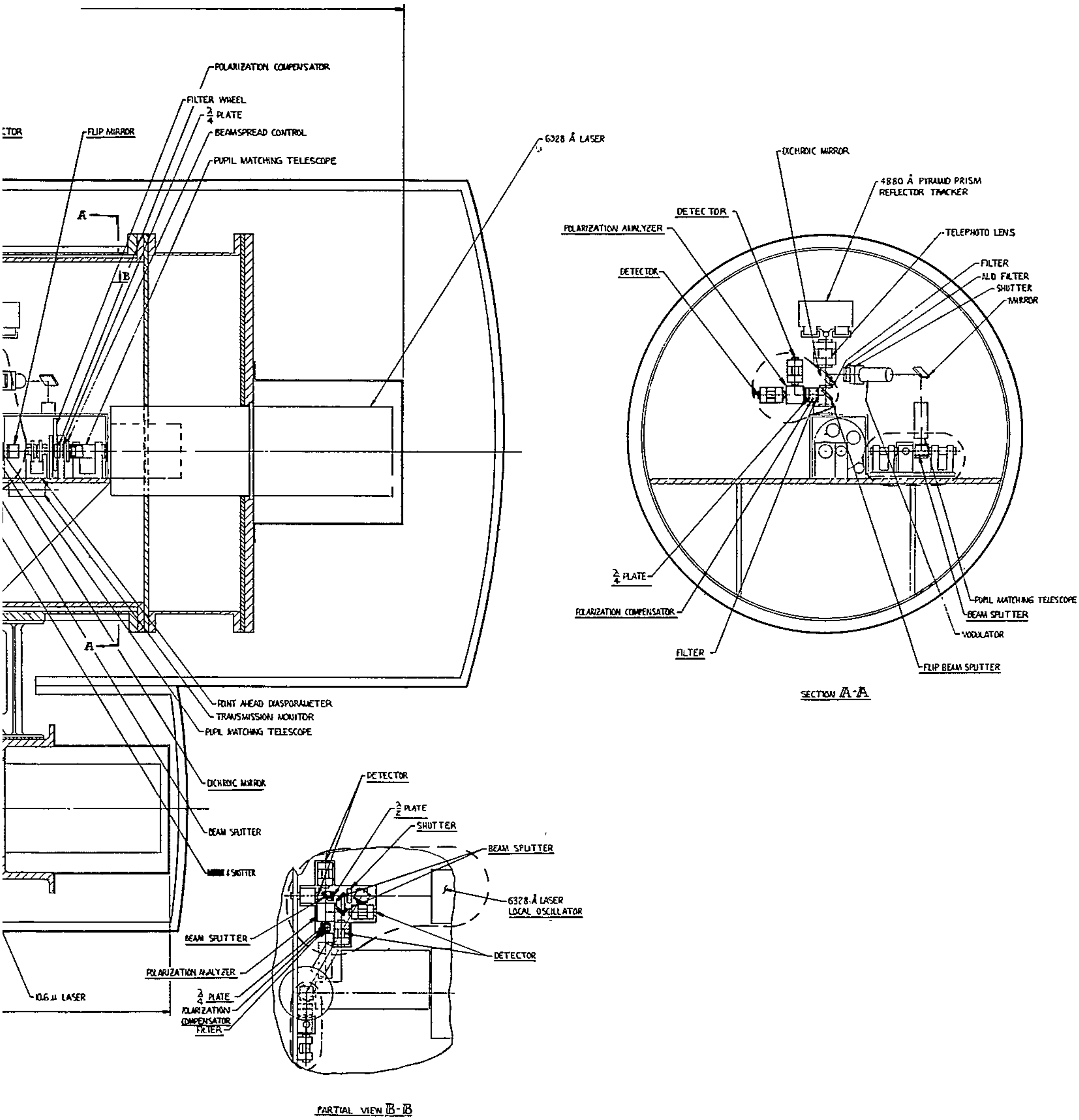

NOTE:

RECEIVER CALLOUTS UNDERLINED

Figure 9.5.1-10. 1-Meter Telescope-Receiver Section

The beam splitter between shutter "A" and the half-wave plate divides the beam into two equal parts, one for each pair of detectors. The local oscillator laser is oriented so that the polarization of the beam which does not pass through the half-wave plate is parallel to the polarization of the beam with which it mixes. Thus it is crossed relative to the polarization of beam incident on the other pair of detectors. To remedy this a half-wave plate is introduced in the appropriate path. This element produces a 90 degree plane change in the polarization of the beam with the effect that it too is coplanar with the beam with which it mixes. Thus each detector pair receives appropriately polarized light both from the ground station signal and from the local oscillator. The phototubes detect the temporal interference patterns between the mixing beams which emerges as an intermediate frequency signal. These in turn are processed by the necessary phase shifting and summing circuits and amplified for recording and display.

9.5.1.2.2 Direct Detection Receiver

The 4880Å received signal intended for the beacon tracker is diverted from the instrument optical axis and directed on a new line of sight toward the tracker. An aperture matching telescope, identical to the one used for the heterodyne receiver, narrows the 25.4 mm beam to 2 mm. At this point it encounters an optical switch in the form of a flip beam splitter. Normally this element is out of the circuit so the beacon signal passes unattenuated to the tracker. Under specified conditions, when it is desired to demodulate the 4880Å beam, the beam splitter is introduced. When in place it diverts about 15 to 20% of the beam toward the direct detection receiver. This receiver consists of a narrow band interference filter centered at 4880Å, a polarization compensator, a quarter wave plate and a polarization analyzer identical in function to those used in the heterodyne receiver subassembly. Both beams emerging from the analyzer are intercepted by multiplier phototubes where the signals are detected. The signals are then amplified and processed for display and recording.

9.5.1.3 Beacon Tracker

The last principal element of the 1.0 meter telescope is the beacon tracker shown in block diagram form in figure 9.5.1-11. Its function is to detect departures of the telescope axis from the ground station line of sight and to correct the departures by appropriate adjustment of the fine beam deflector and the gimbals. See also figures 9.5.1-12 and 9.5.1-4c. The input 4880Å signal is collected, as it is for the receivers, by the antenna telescope, collimated by the Galilean ocular, stabilized by the fine beam deflector, picked off the main axis by the dichroic beam splitter, compressed by the aperture matching telescope, and transmitted through with either 15% attenuation by the flip beam splitter for the direct receiver if to be used or by-passing it with no attenuation. At this point it passes through a very narrow band (1Å) interference filter centered at 4880Å to reduce background noise. It then passes through a dichroic beam combiner which serves to introduce a test signal originating at the local oscillator into

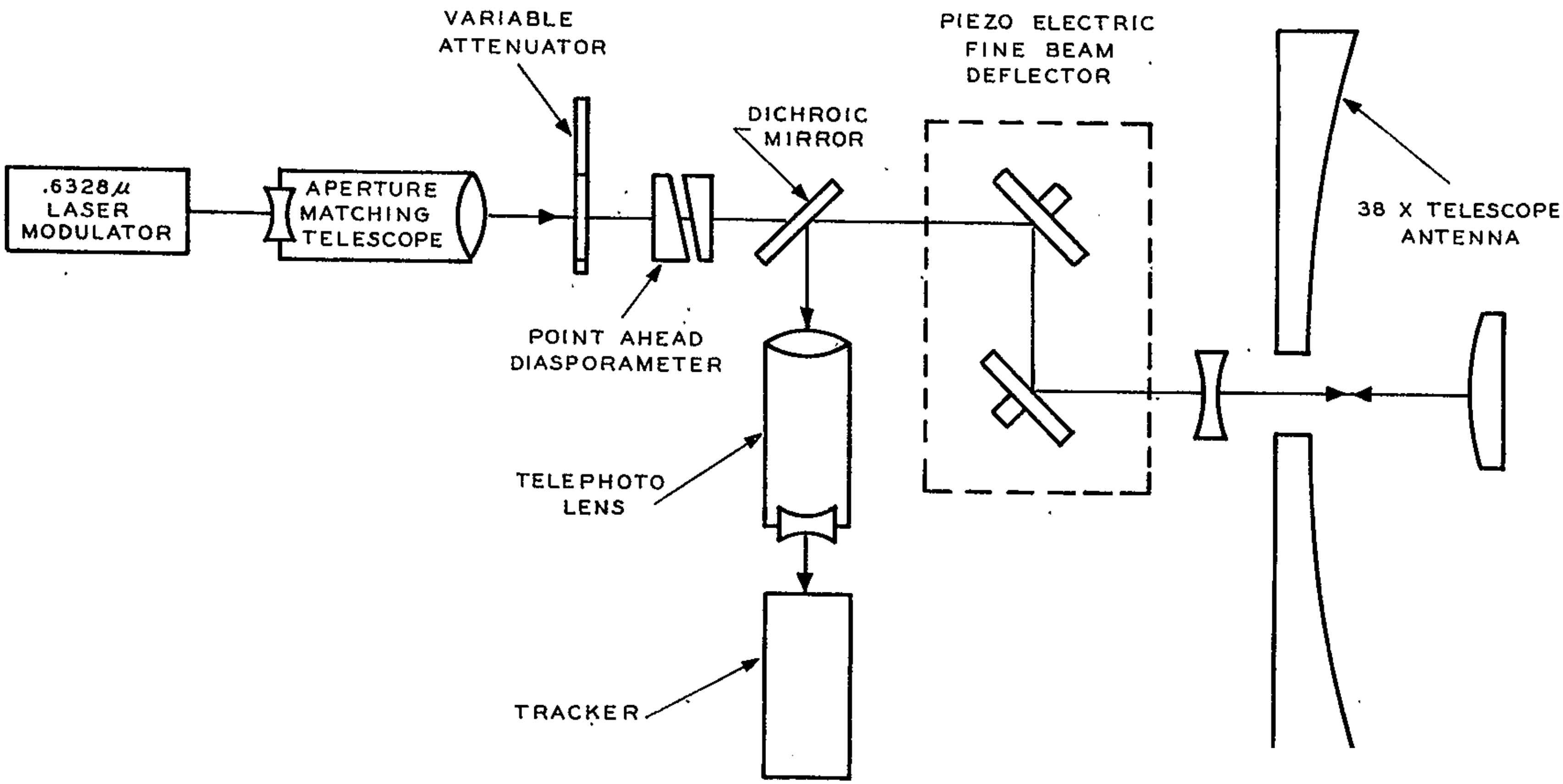

Figure 9.5.1-11. Tracker Beam Control Optical System

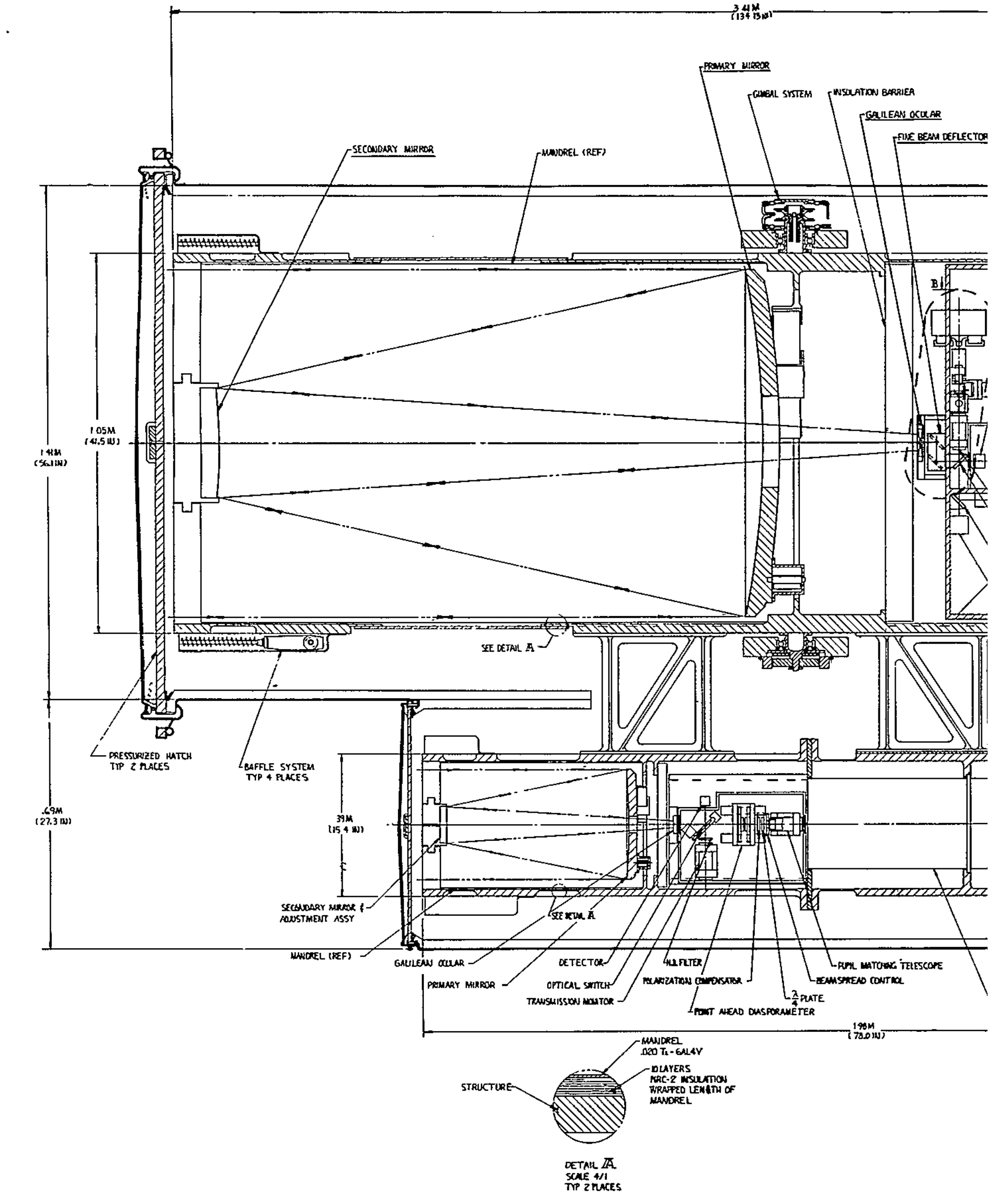
3.41M (134.15 IN)
PRIMARY MIRROR
GIMBAL SYSTEM
INSULATION BARRIER
GALILEAN OCULAR
FINE BEAM DEFLECTOR
SECONDARY MIRROR
MANDREL (REF)
1.05M (41.5 IN)
1.41M (56.1 IN)
SEE DETAIL A
PRESSURIZED HATCH TYP 2 PLACES
BAFFLE SYSTEM TYP 4 PLACES
.69M (27.3 IN)
.39M (15.4 IN)
SECONDARY MIRROR & ADJUSTMENT ASSY
SEE DETAIL A
MANDREL (REF)
GALILEAN OCULAR
PRIMARY MIRROR
DETECTOR
OPTICAL SWITCH
TRANSMISSION MONITOR
N.D. FILTER
POLARIZATION COMPENSATOR
POINT AHEAD DIASPORAMETER
3/4 PLATE
BEAM SPREAD CONTROL
PUPIL MATCHING TELESCOPE
1.98M (78.0 IN)
STRUCTURE
MANDREL .020 Ti-6AL4V
10 LAYERS NRC-2 INSULATION WRAPPED LENGTH OF MANDREL
DETAIL A SCALE 4/1 TYP 2 PLACES

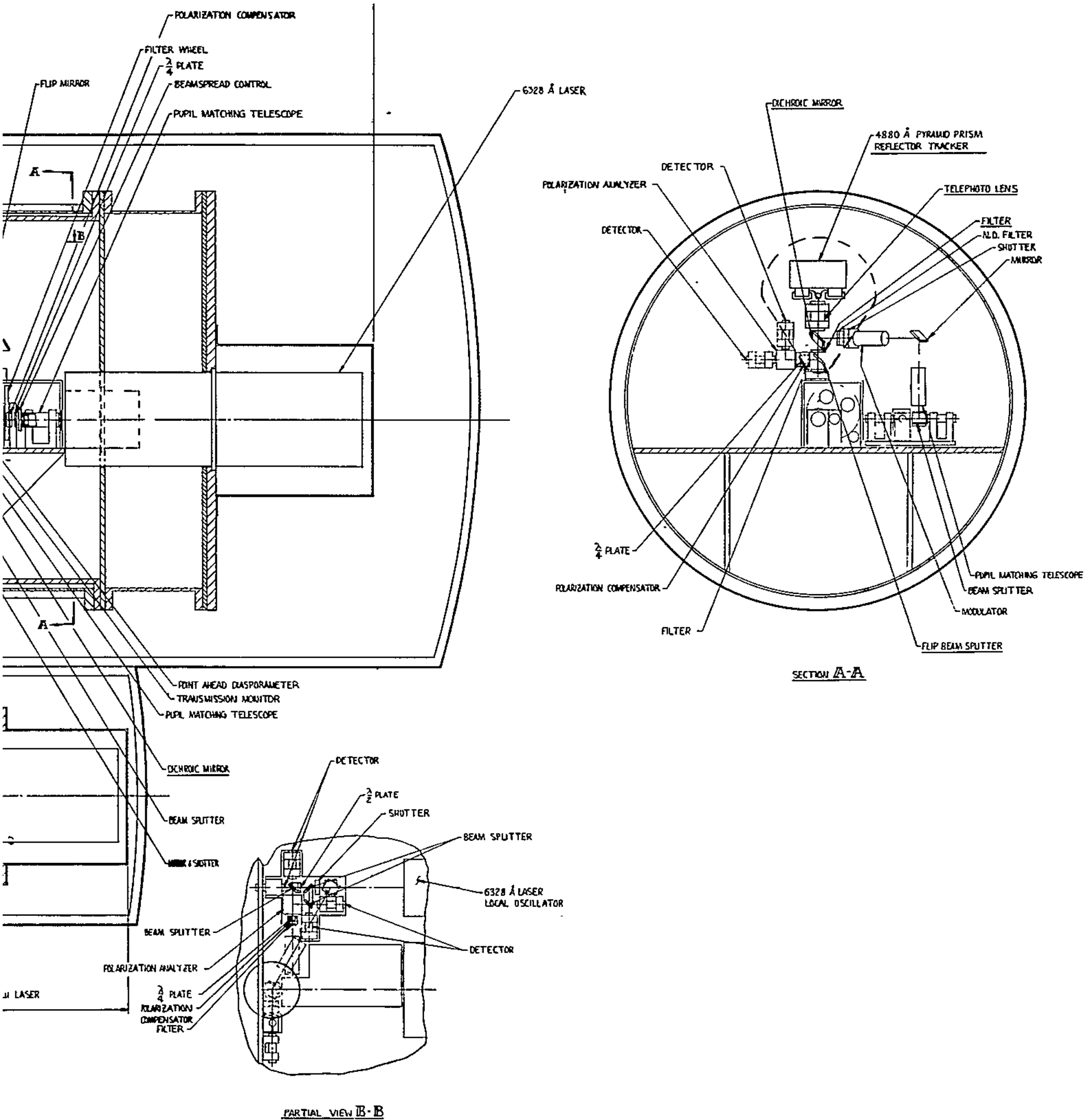

NOTE:
TRACKER CALLOUTS UNDERLINED

Figure 9.5.1-12. 1-Meter Telescope Tracking Section the tracker line of sight for tracker balance calibration. This will be discussed shortly. For reasons to be indicated this element passes the 4880Å energy with virtually no attenuation but acts as a beam splitter for 6328Å. The light is then brought to a focus by a telephoto lens subassembly. The focal length of this lens in combination with the antenna telescope and aperture matching telescope is calculated to provide a scale factor of 1 minute per inch. This comes to an effective focal length of 87.58 meters for the entire tracker system and 181 millimeters for the telephoto lens itself.

At or near the focus, at a precise position determined by an analysis of the tracker loop, is placed the apex of a field splitting pyramid prism reflector. This is the first element of the beacon tracker subassembly, and it divides the image of the tracker field of view into four quadrants precisely aligned to the axes of both the fine beam deflector and the point ahead diasporameter as well as the gimbal axes of the telescope. The light from each quadrant is collected by an eyepiece lens and a multiplier phototube is placed at each exit pupil. Processing electronics determine the position of the tracker axis with respect to the ground station line of sight and generate the required signal for the fine beam deflector to bring the two into register. Excessive bias on the fine beam deflectors is sensed and an appropriate correction signal is sent to the telescope gimbals.

9.5.1.4 Auxiliary Features

9.5.1.4.1 Tracker Balance Calibration

A beam splitter between the local oscillator aperture matching telescope and heterodyne receiver provides an additional optical path from the local oscillator to the tracker. The light is reflected by a dichroic beam combiner (which passes 4880Å light) and is directed to the tracker. The arrangement is shown briefly in figure 9.5.1-1 and 9.5.1-4 and in more detail in figure 9.5.1-13. This path is used as a means of detecting and compensating for any drift that may occur in the tracker detectors. The compensation is achieved by an automatic gain control action on the detector power supplies. This feature is required by the D.C. mode of operation of the detectors. The local oscillator energy which has been expanded by the aperture matching telescope is divided by the beam splitter mentioned above. The light not required for optimum performance of the heterodyne receivers is deflected into a new line of sight where it has a signal impressed on it by an electro optical modulator. A folding mirror then redirects the line of sight and a neutral filter reduces the intensity of the beam to a level suitable for the tracker. A shutter is used to isolate the local oscillator from the tracker when the balance calibration is not in use. This is referred to as Shutter "B" (figure 9.5.1-4). The beam is then merged with the tracker beam at the dichroic beam combiner, is imaged by the telephoto lens, split into quadrants by the pyramid and detected by the photomultipliers. A comparator amplifier, filtered to pass the modulator frequency determines the adjustment in the power supplies to balance the detectors.

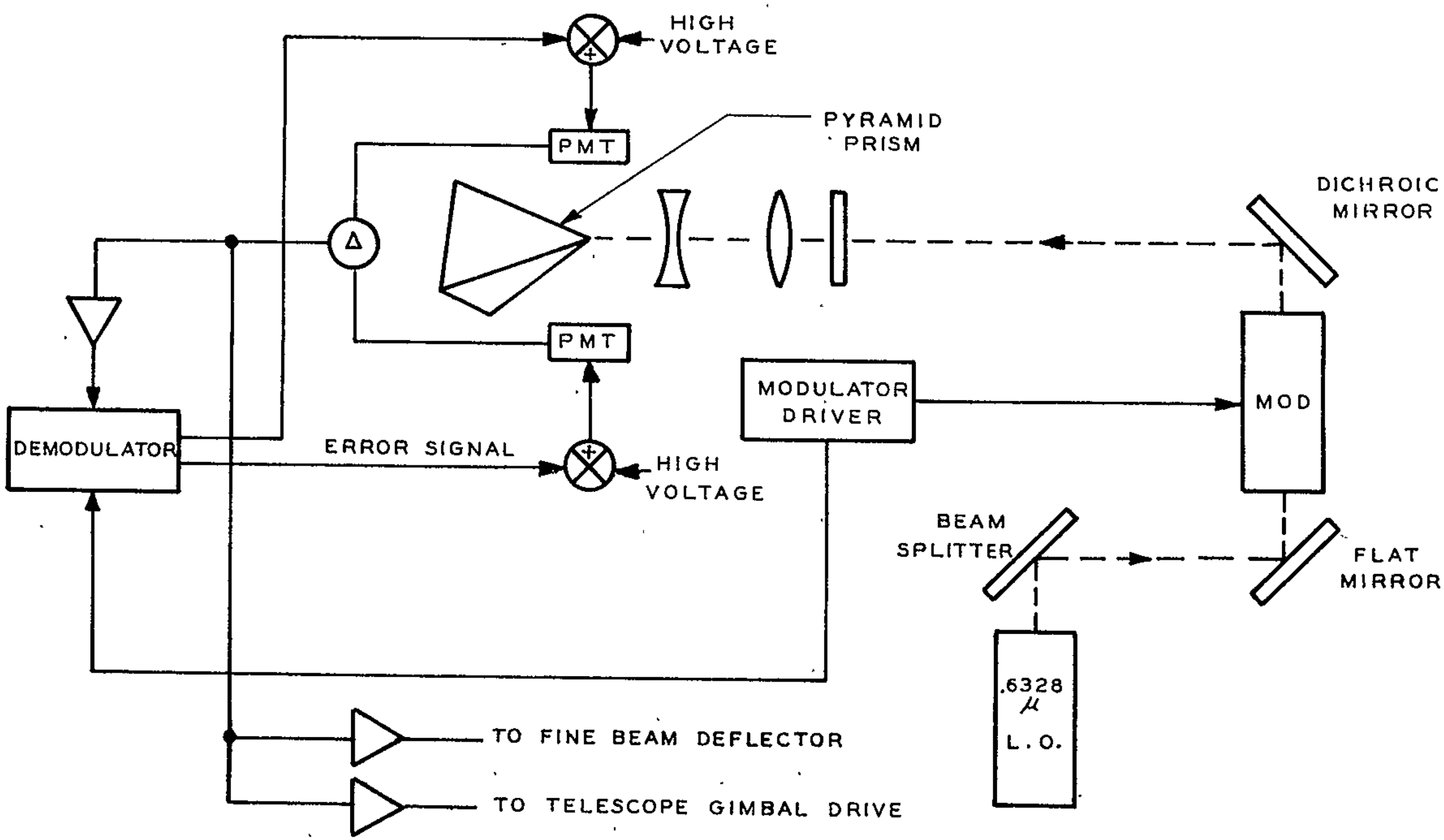

Figure 9.5.1-13. Differential Gain Control Loop for Photomultiplier Balance Calibration

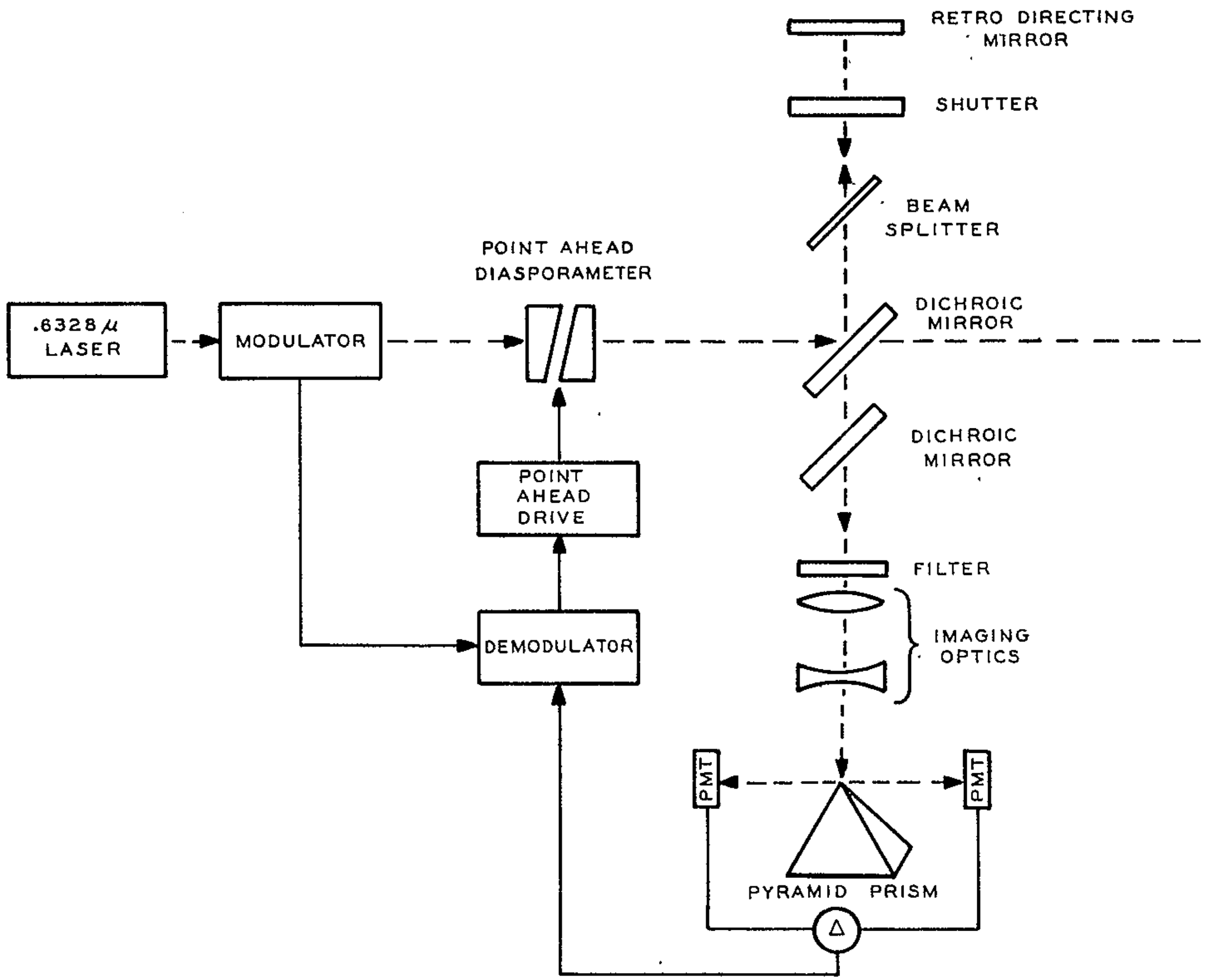

Figure 9.5.1-14. Transmitter Boresight Loop for Lead Angle Null Calibration

9.5.1.4.2 Transmitter Boresight

The dichroic beam splitter behind the fine beam deflector, although passing the great bulk of the transmitter power, nevertheless reflects a small portion (less than 1%). This energy is reclaimed to serve two useful functions, namely transmitter boresight calibration and transmission monitoring. The 1% or less of the transmitter power is reflected as stated before, and is divided into two beams by a beam splitter. The smaller amount is reflected and caused to fall on amultiplier phototube which measures the power level and modulation. The transmitted portion is directed through a normally closed shutter to a retroreflecting mirror (see figure 9.5.1-14 for additional details). When the boresight calibration is operative, the beam is caused to return on itself by the retroreflector, then passes through the dichroic beam splitter, is narrowed down by the aperture matching telescope, attenuated by the 4880Å filter and is passed through the dichroic beam combiner. with some additional attenuation. It is now focused by the telephoto lens and split by the pyramid apex, whence it is then detected by the photomultipliers. Any departure from null in the tracker output signifies a separation between the tracker and transmitter lines of sight. A corresponding error signal is developed which is used to drive the point ahead diasporameters until the tracker nulls. This null position is the calibrated boresight correction and becomes the zero position from which any point ahead offset is calculated.

9.5.2 0.3 Meter Strapped on Telescope

The 0.3 meter strapped on telescope illustrated in figure 9.5.2-1 is an infrared transmitter-receiver which has no tracking capability of its own, but relies on the tracker in the 1.0 meter telescope. It is shown schematically in figure 9.5.2-2. The transmitter, as with the 1.0 meter telescope, contains a transmitting laser package, processing optics and the antenna primary optics. The laser package includes a CO_2 laser tube with its cavity and stabilization circuits. It generates one to two watts of output power at 10.6 micron wavelength, in an output beam three millimeters in cross section and with a divergence of 2 milliradians. This beam is then expanded to 7.9 millimeters by an aperture matching telescope, transformed from plane to circular polarization by a quarter-wave plate and corrected for polarization bias by a polarization compensator.

A point-ahead diasporameter which can be slaved to the 1.0 meter telescope diasporameter or activated separately serves to provide the required transmitter lead angle. An optical switch consisting of a mirror for the receive position and an almost clear beam splitter for the transmit position permits the bulk of the transmitter power to pass through to the antenna telescope. The small fraction that is reflected is focused on a detector to monitor the transmitter power and modulation level. A neutral density filter between the beam splitter and the monitor reduces the power to an acceptable level for the monitor.

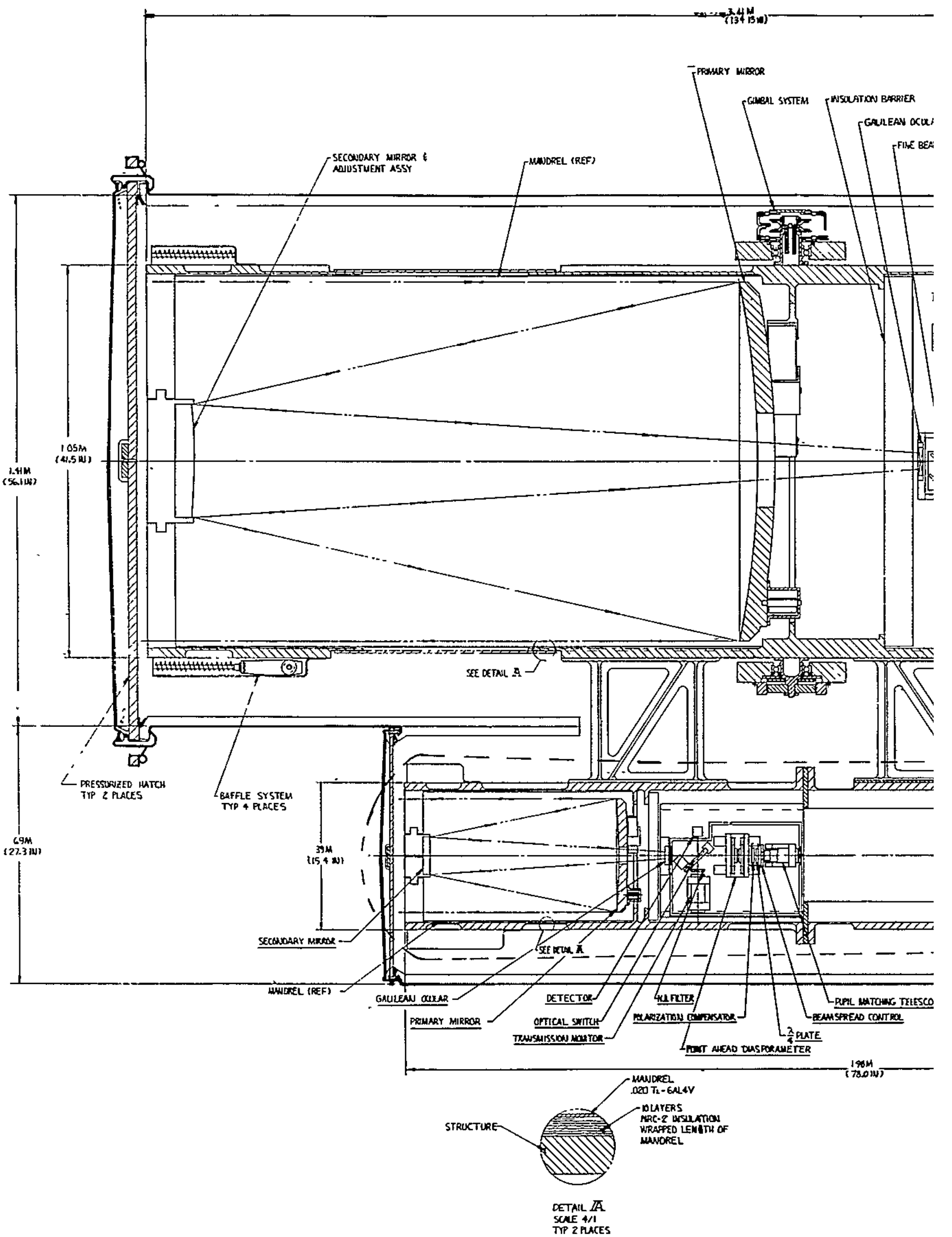
3.41 M
(134.15 IN)
PRIMARY MIRROR
GIMBAL SYSTEM
INSULATION BARRIER
GALILEAN OCUL
FINE BEA
SECONDARY MIRROR &
ADJUSTMENT ASSY
MANDREL (REF)
1.05M
(41.5 IN)
1.41M
(56.1 IN)
SEE DETAIL A
PRESSURIZED HATCH
TYP 2 PLACES
BAFFLE SYSTEM
TYP 4 PLACES
.69M
(27.3 IN)
.39M
(15.4 IN)
SECONDARY MIRROR
MANDREL (REF)
GALILEAN OCULAR
PRIMARY MIRROR
SEE DETAIL A
DETECTOR
OPTICAL SWITCH
TRANSMISSION MODULATOR
N.D. FILTER
POLARIZATION COMPENSATOR
POINT AHEAD DIASPORAMETER
λ/4 PLATE
BEAMSPREAD CONTROL
PUPIL MATCHING TELESCO
1.98M
(78.0 IN)
MANDREL
.020 Ti - 6AL4V
10 LAYERS
NRC-2 INSULATION
WRAPPED LENGTH OF
MANDREL
STRUCTURE
DETAIL A
SCALE 4/1
TYP 2 PLACES

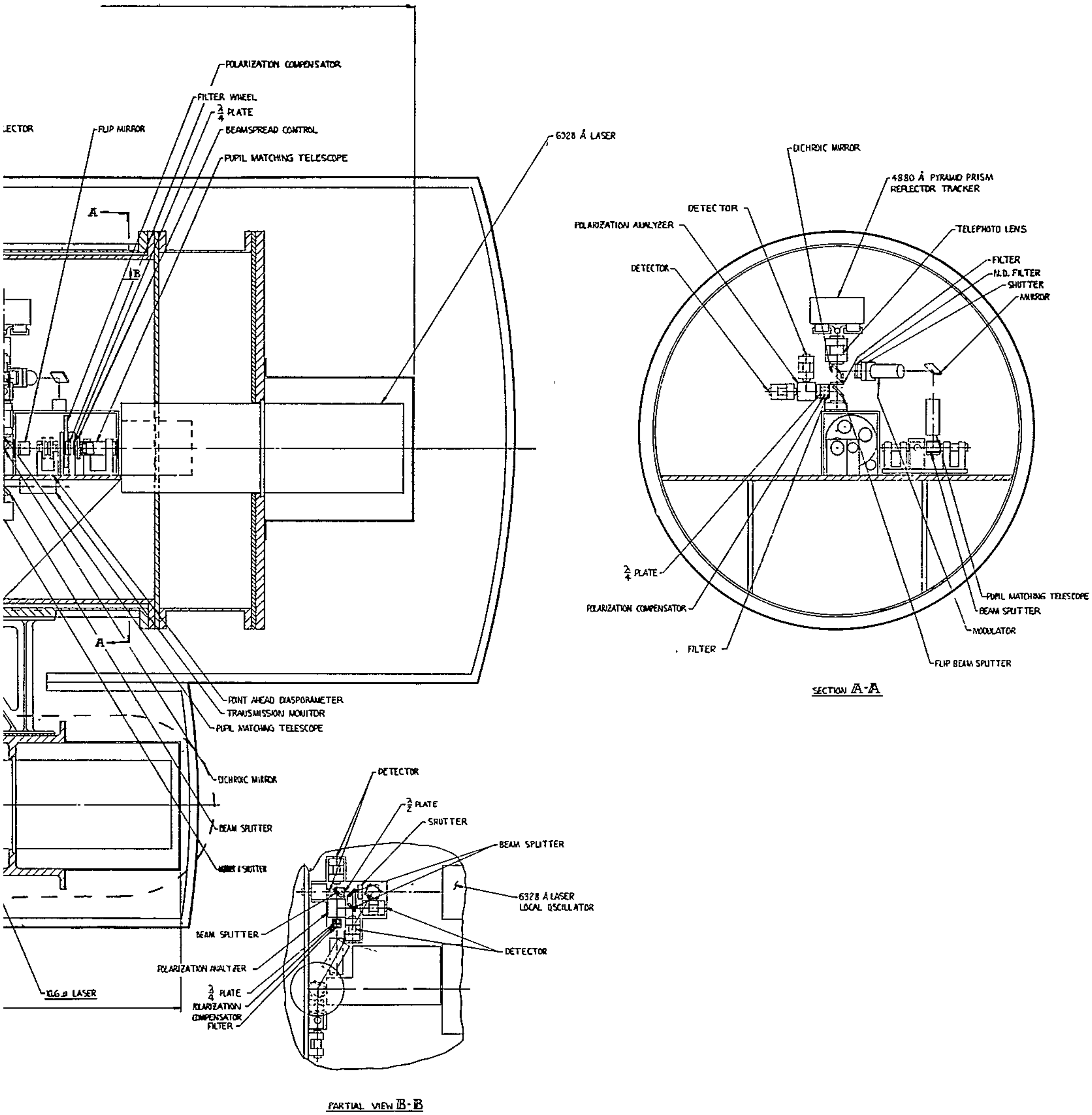

NOTE:

0.3M CALLOUTS UNDERLINED

Figure 9.5.2-1. 0.3-Meter Laser Telescope

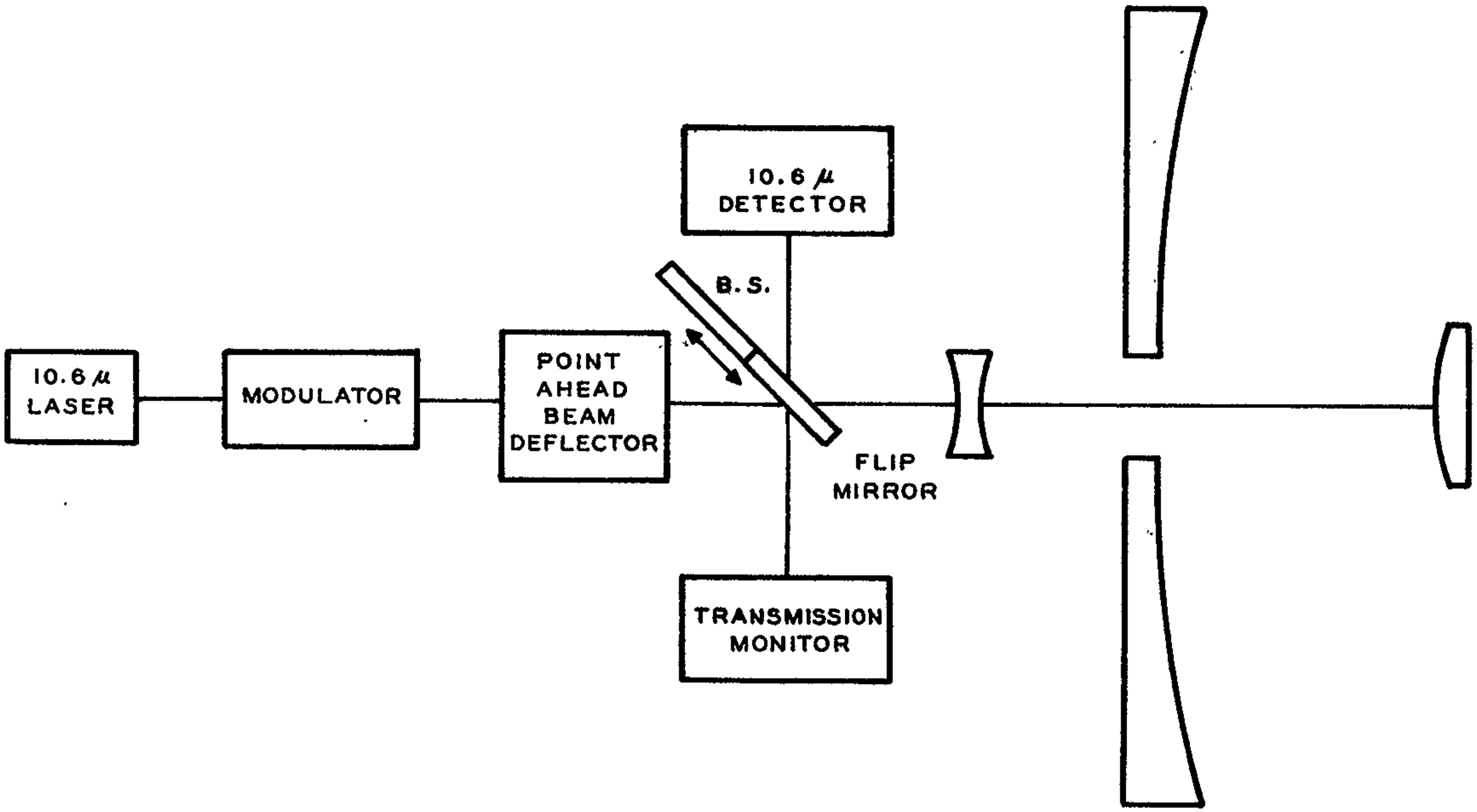

Figure 9.5.2-2. 10.6-Micron Telescope (0.3-Meter, Strapped Down)

The transmitted beam which passes through the beam splitter is again expanded by the antenna telescope from 7.9 millimeters to 300 millimeters. The telescope that performs this function is a Cassegrainian consisting of a parabolic primary mirror of 0.3 meter aperture and 0.762 meter focal length, a hyperboloidal secondary mirror of 0.1 meter aperture and -0.381 meter focal length separated from the primary by 0.508 meter, and a Galilean ocular of -60.16 millimeters focal length and 12 millimeter aperture. This provides an effective focal length of 2.286 meters for the Cassegrainian objective, and a magnification of 38 power. The diffraction limited beam spread for this telescope is approximately 9 seconds at 10.6 microns. To operate the 10.6 micron receiver the optical switch is moved so that the fully reflecting mirror section is in the line of sight. This condition assures that the incoming energy from the 10.6 micron ground station transmitter, after being collected and collimated into a 7.9 millimeter beam by the antenna telescope is reflected toward the receiver subassembly. The receiver subassembly consists of an aperture matching telescope to reduce the beam from 7.9 millimeters to the 1 millimeter size of the thermistor bolometer detector. The detector itself is placed at the exit pupil of the telescope. All refractive elements used in this telescope are selected for minimum absorption in the 10.6 micron region. Hygroscopic properties of materials used in these elements will be countered by suitable desiccation means in the telescope.

9.5.3 0.3 Meter Separately Gimbaled Telescope

The 0.3 meter telescope is primarily a backup device and contains all the essential features of the 1.0 meter telescope. The differences include the omission of the second laser in the transmitter laser subassembly, the omission of the direct detection 4880Å receiver and a few changes in parameters due to the difference in aperture of the antenna telescope. All other features are identical, including the tracker balance calibration and transmitter boresight function. A simplified block diagram is shown in figure 9.5.3-1. A more detailed block diagram is found in figure 9.5.3-2 and a conceptual design drawing in figure 9.5.3-3. The antenna telescope has an aperture of 0.300 meters and an effective focal length of 2.286 meters. It is composed of a parabolic primary mirror of 0.300 meters aperture and 0.762 meter focal length, and a hyperboloidal secondary mirror of 0.100 meter aperture and -0.381 meter focal length, separated by a distance of 0.508 meter. A negative collimating lens (Galilean ocular) of -60.16 millimeter focal length and 12 millimeter aperture provides a magnification of 38 diameters. Because of this magnification the intermediate beam diameter throughout this telescope is 7.9 millimeters instead of the 25.4 millimeter diameter used in the 1.0 meter telescope. Accordingly, the aperture matching telescopes for the tracker and receiver are both approximately 4 power instead of the 12 power of the 1.0 meter telescope, and the transmitter aperture matching telescope shows a reduction from approximately 17 power to 5.5. No change occurs in the telescope's local oscillator. One other difference is the tracker image plane scale factor. Instead of the 1 min. per inch specified for the 1.0 meter telescope it is desired to use a scale factor of 3 minutes per inch. This

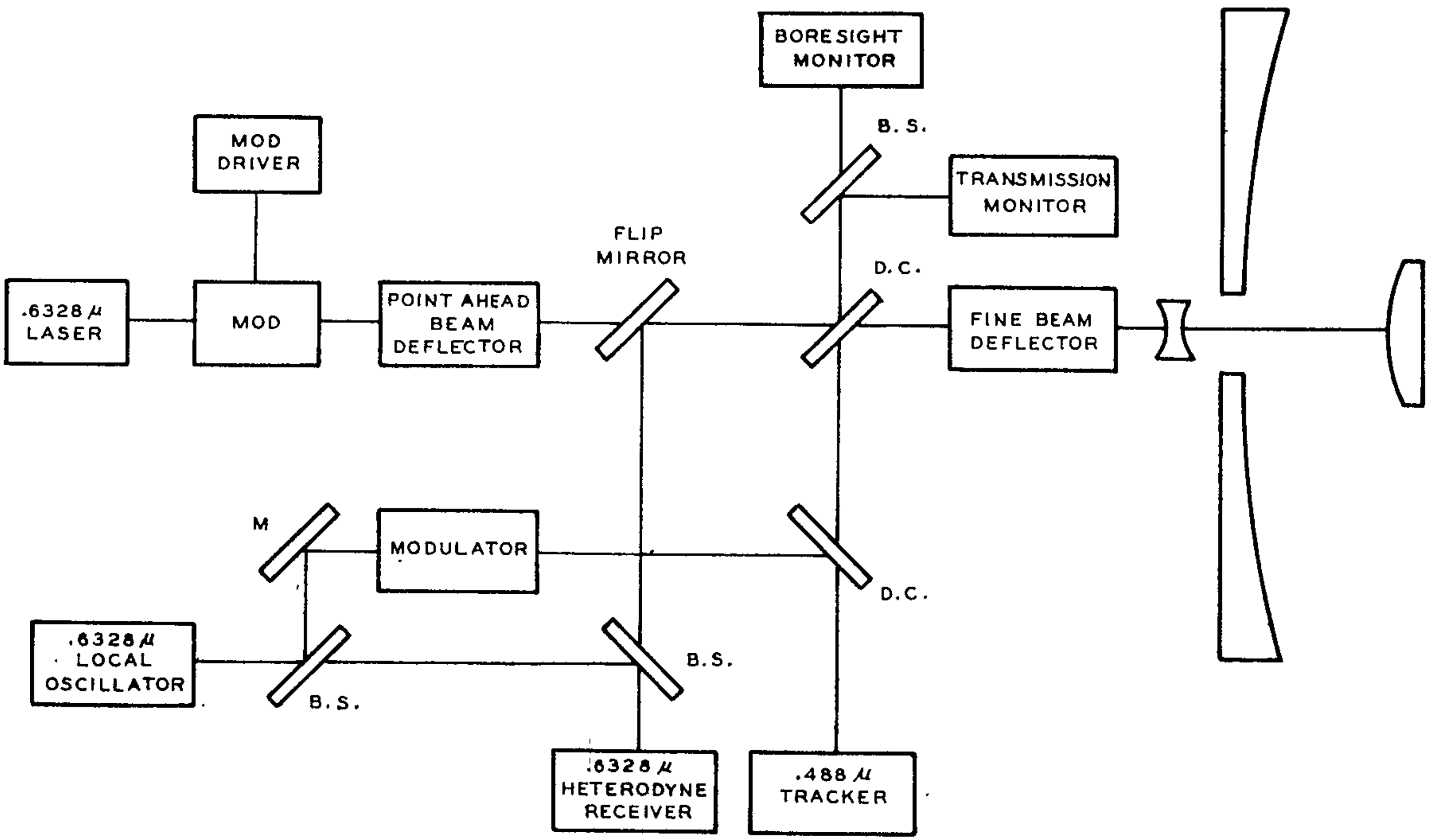

Figure 9.5.3-1. 0.3-Meter Gimbaled Telescope

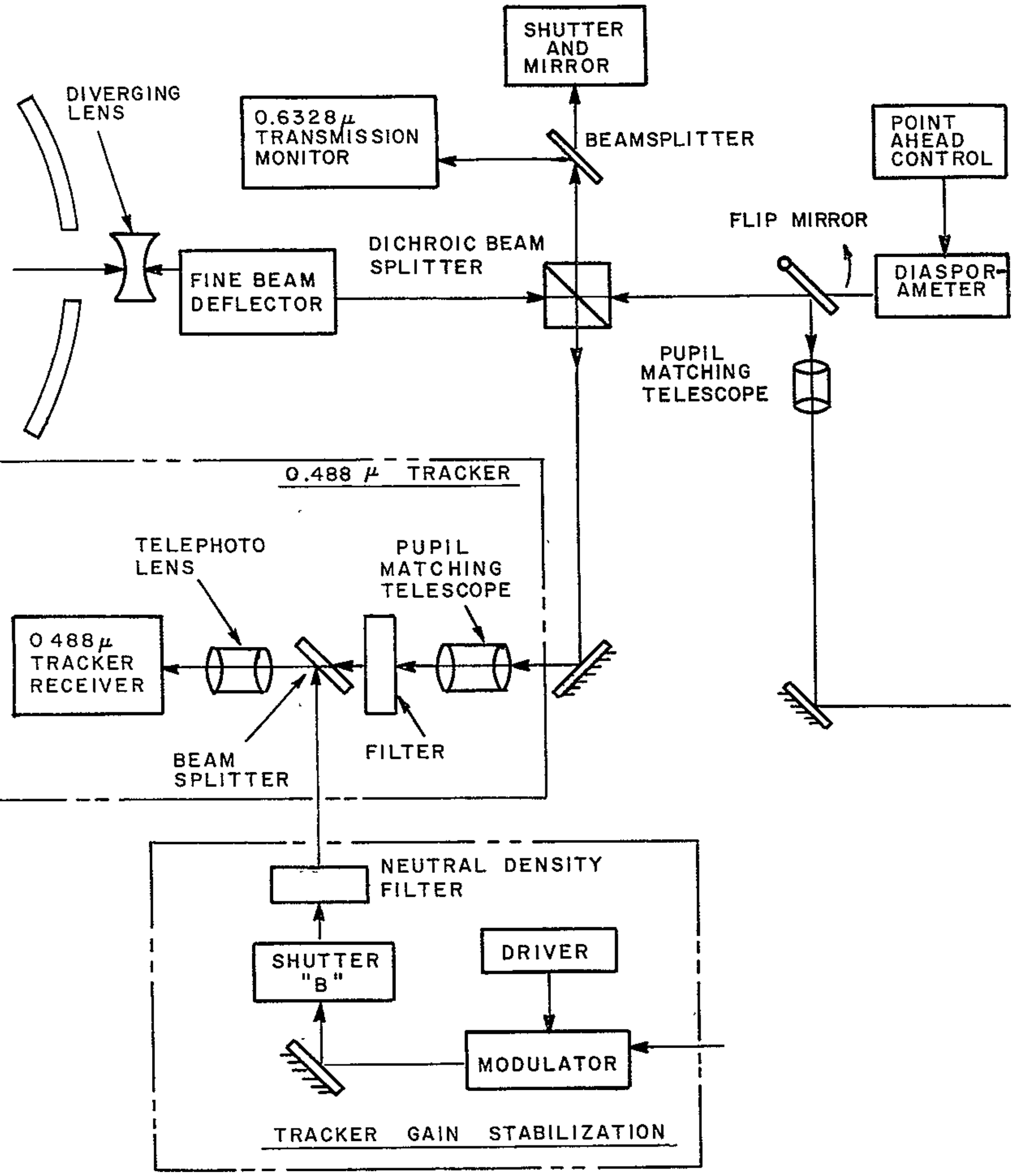

SHUTTER AND MIRROR
DIVERGING LENS
0.6328μ TRANSMISSION MONITOR
BEAMSPLITTER
POINT AHEAD CONTROL
FLIP MIRROR
DICHROIC BEAM SPLITTER
FINE BEAM DEFLECTOR
DIASPOR-AMETER
PUPIL MATCHING TELESCOPE
0.488 μ TRACKER
TELEPHOTO LENS
PUPIL MATCHING TELESCOPE
0.488μ TRACKER RECEIVER
BEAM SPLITTER
FILTER
NEUTRAL DENSITY FILTER
SHUTTER "B"
DRIVER
MODULATOR
TRACKER GAIN STABILIZATION

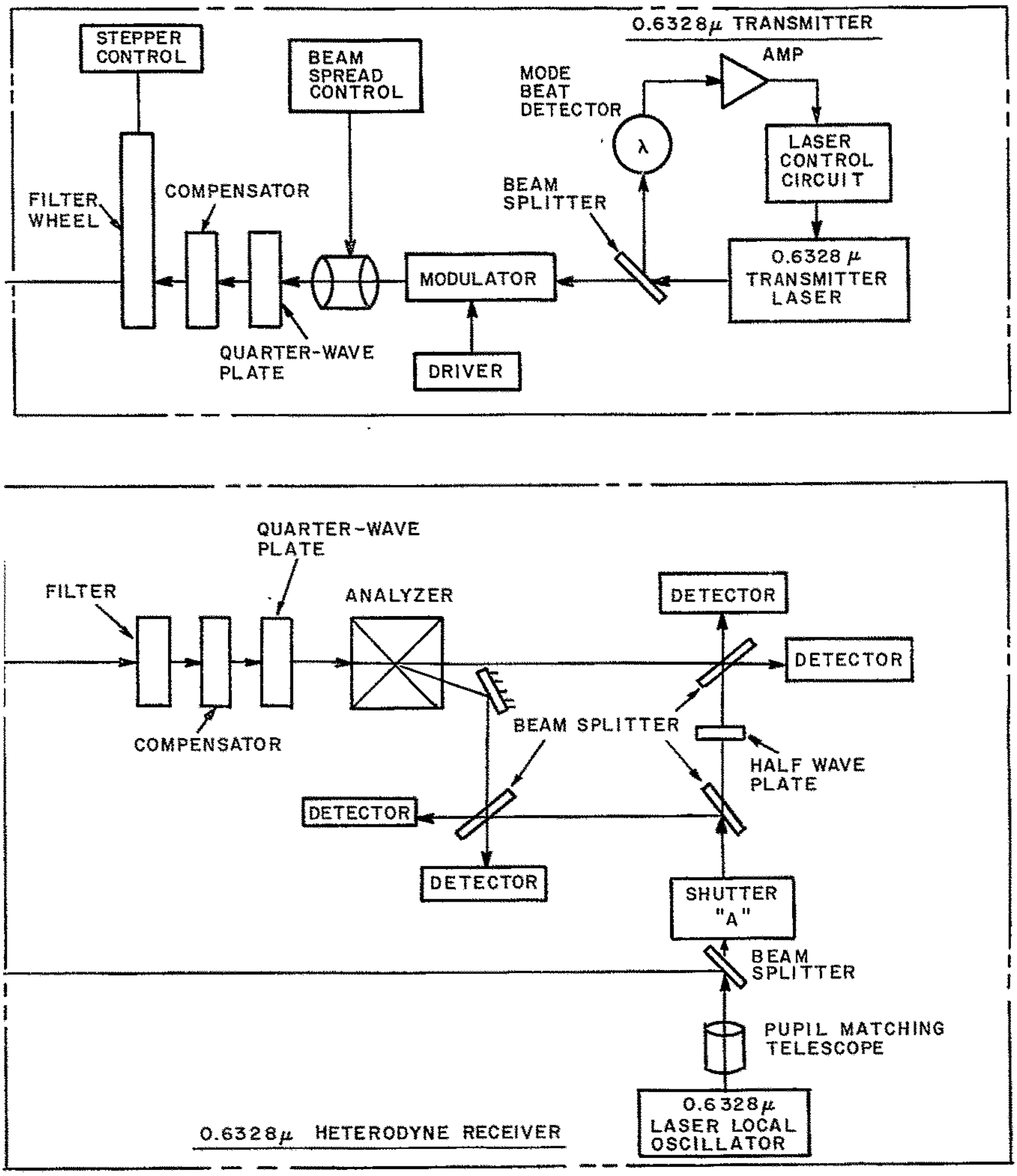

Figure 9.5.3-2. 0.3-Meter Separately Gimbaled Telescope, Block Diagram

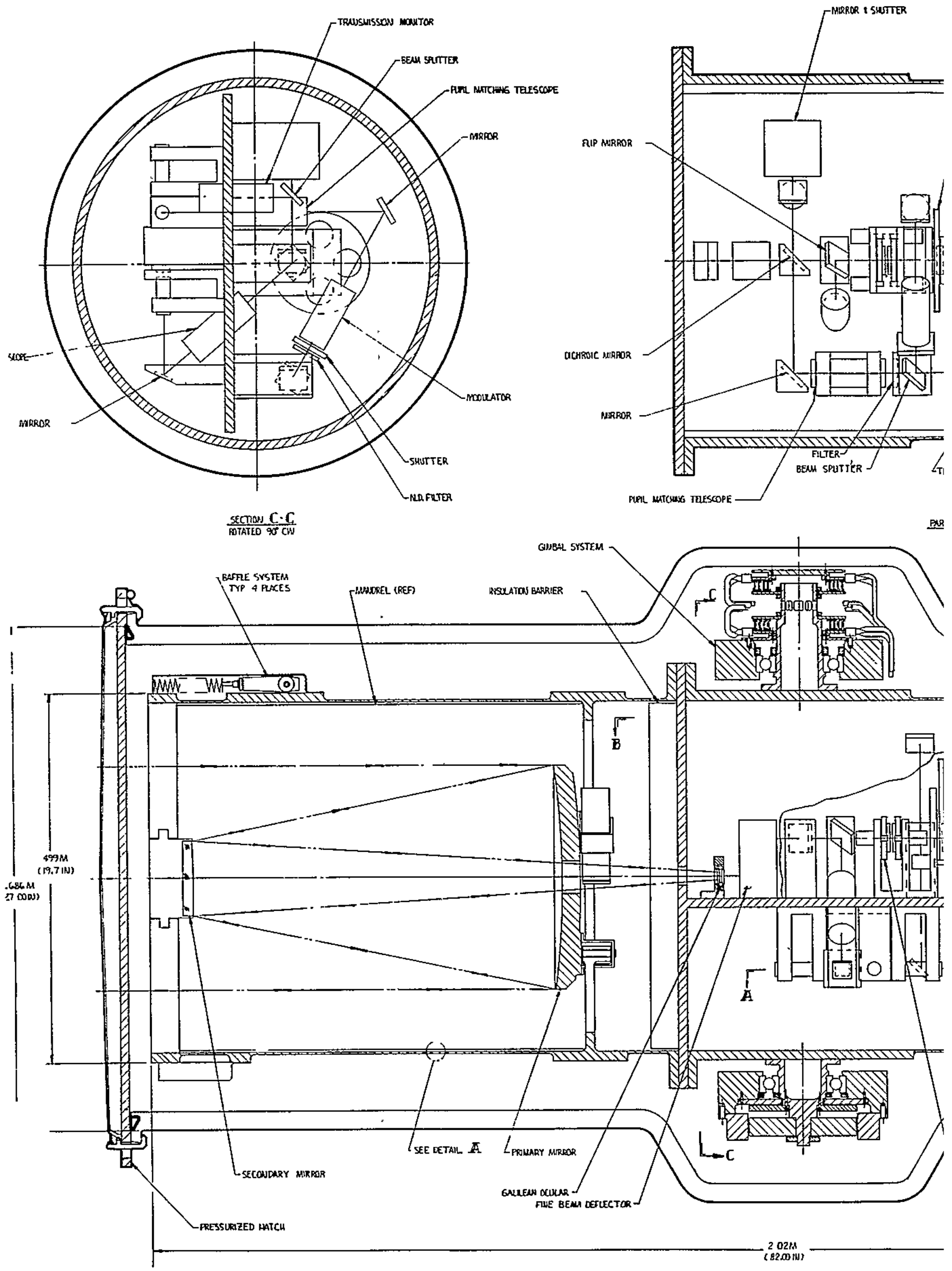
TRANSMISSION MONITOR
BEAM SPLITTER
PUPIL MATCHING TELESCOPE
MIRROR
SLOPE
MIRROR
MODULATOR
SHUTTER
N.D. FILTER
SECTION C-C
ROTATED 90° CW
MIRROR & SHUTTER
FLIP MIRROR
DICHROIC MIRROR
MIRROR
FILTER
BEAM SPLITTER
PUPIL MATCHING TELESCOPE
GIMBAL SYSTEM
BAFFLE SYSTEM
TYP 4 PLACES
MANDREL (REF)
INSULATION BARRIER
.499M
(19.7 IN)
.686 M
27 OD
SEE DETAIL A
PRIMARY MIRROR
SECONDARY MIRROR
GALILEAN OCULAR
FINE BEAM DEFLECTOR
PRESSURIZED HATCH
2.02M
(82.00 IN)

II-96

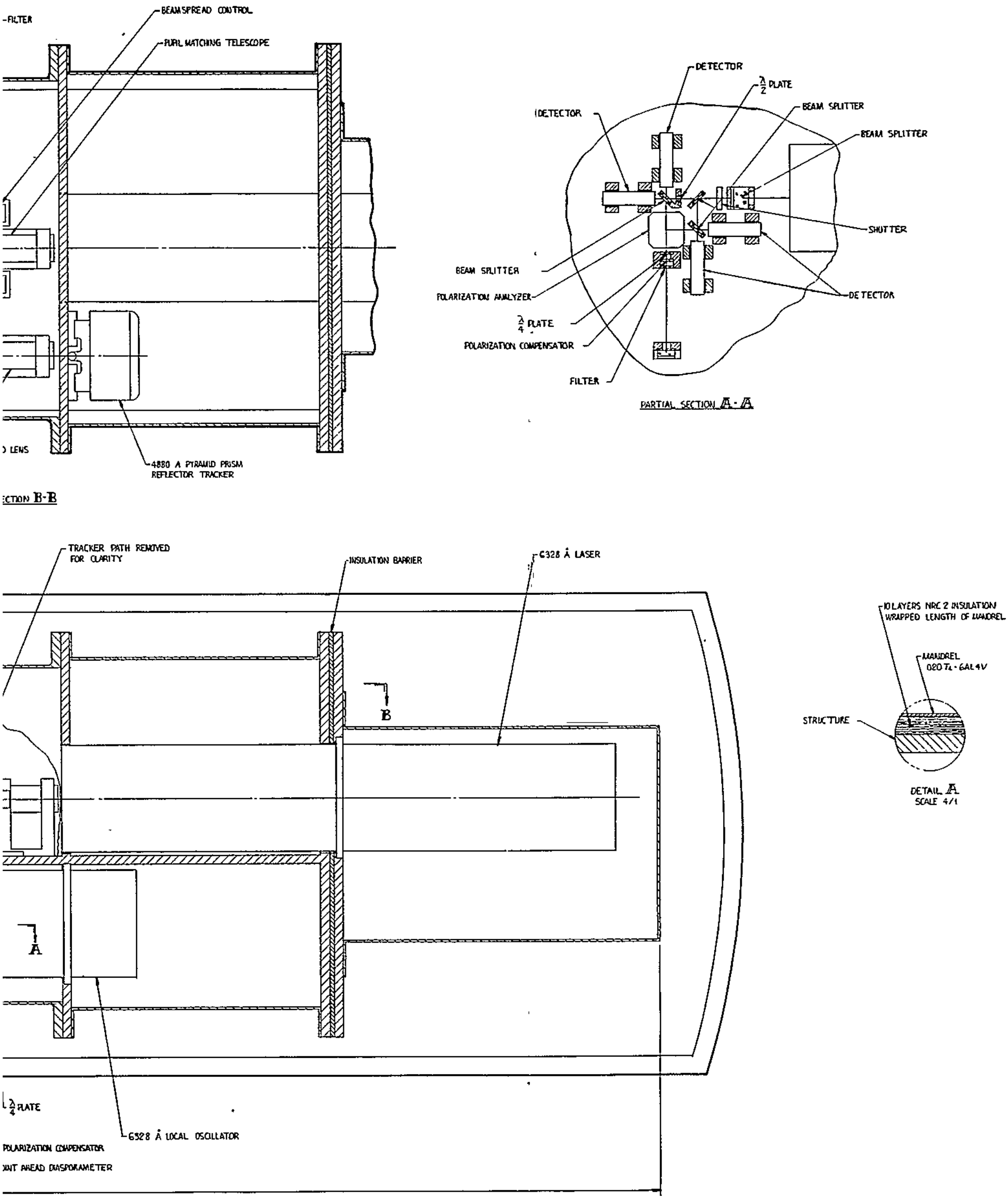

Figure 9.5.3-3. 0.3-Meter Laser Telescope Gimbaled

calls for an effective focal length of 29.21 meters instead of the 87.63 meters in the 1.0 meter telescope. But because the preliminary magnification (in the antenna telescope and aperture matching telescope) is reduced from 482.6 to 150 diameters the focal length of the tracker telephotolens becomes 195 millimeters as compared to the 181 millimeter focal length used in the 1.0 meter telescope.

9.5.4 Mirror Figure Tolerances

Because of the need to maintain the narrowest beam possible in the laser transmitters the laser telescope mirrors must be diffraction limited. To this end the tolerance must be within one quarter wavelength of a true parabola at 6328Å. The need for a diffraction limited beam is to provide adequate power density in the beam at the ground station receivers. Departures from the diffraction limit cause an increase in the size of the Airy disk in a receiving telescope, and by the same token, an increase in the beam-spread as measured in the far field of a transmitting telescope. Since the power is constant and the beam-spread is a two axis phenomenon the power density as seen by the ground station collectors is inversely proportional to the square of the beam-spread or airy disk diameter. Only in this fashion is the signal to noise ratio adequate for wide bandwidth communication.

For receiving purposes the mirror figure tolerance can be relaxed. At the current writing it is anticipated that it will be beneficial to spread the tracker image beyond the limits of the airy disk to reduce the tracking gradient and thereby soften the response of the system and increase its stability. The enlarging of the image spot will be accomplished by defocusing. The amount of image enlargement is to be determined on the basis of a simulation of the loop. The heterodyne receiver also has a requirement that is less severe than the transmitter, the main restriction being that the ground station image be contained within the area on the detector tubes that is illuminated by the local oscillator. The quality of the collector optics is however determined by the most critical function which is transmission and for this reason diffraction limited optics will be utilized in the system.

9.6 EXPERIMENTS

9.6.1 Optical Heterodyne Detection on Earth

The atmosphere has been studied for centuries from earth-bound observatories usin the noncoherent light from stars. Rockets and satellites now permit measurements of the atmosphere with controlled light sources in Earth orbit. As a tool to advance our knowledge in these areas, the laser possesses two highly useful properties: spatial coherence and temporal coherence. A laser transmitter can emit an extremely narrow, intense beam of monochromatic light. Furthermore, since it operates at frequencies sensitive to atmospheric absorption and scattering and variations in the index of refraction, the laser is the most promising instrument for obtaining a better understanding of the turbulent structure of the atmosphere.

However, uncertainties in the current state of atmospheric physical theory (paragraph 9.1.1) underline the need for empirical verification. They are crucial to arguments which suggest severe limitations on coherent reception; e.g., a diamete limitation to collimation (utility of correction to the diffraction limit), the presence of an aperture size-dependent modulation noise, a limit on the useful aperture size itself, etc. Space-to-earth experiment is particularly important since, even with the simplifying assumption of a plane wave incident on the turbulent medium, an uncertainty factor of two attaches to the coherence limit and the wavelength scaling exponent ($\lambda^{6/5}$) remains moot.

To study the physics of the atmosphere using a spaceborne light source is to study the character of the space-ground propagation path. The establishment of such a path is tantamount to establishing an optical communication link. Indeed, propagation experiments are the first step toward establishing the efficacy of lasers in their most promising operational application: wideband communication over extrem ly long distances. To achieve this goal, a foundation of spaceborne optical communication engineering data must be obtained. The propagation experiments, singly and as a group, are advanced as a means for studying the Earth's atmosphere as a prerequisite to the development of alternatives in the field of communication.

Collectively, the space-to-ground communication experiments provide a comparison of the fundamental communication techniques: direct detection and heterodyne detection. The heterodyne experiment is formulated on a scale sufficient to allow comparison between laser and radio frequency communication. Within this experiment (figure 9.6.1-1), provision is made for combining various signal forms, coding, and modulation methods for test under atmospheric constraints.

For the experiment, two laser wavelengths (0.6328 micron and 10.6 microns) will be transmitted from the spacecraft to an Optical Technology Test and Operations Station on Earth. Measurements will be made to determine: (a) phase and polarization perturbations introduced by the transmission medium, and (b) the degradation

Our present knowledge of optical propagation through a turbulent atmosphere is largely based upon stellar observations and ground-based laser tests along essentially horizontal paths. Yet, turbulence theory predicts that the scintillation and transit time fluctuations of space-to-Earth laser light will differ from those observed by starlight. Furthermore, a space-borne laser offers the means to study spatial coherence, beam steering, and depolarization. These effects have dual importance. They offer a better understanding of our atmosphere, and they bound the utility of optical communication from deep space. Measurements of heterodyne signal amplitude and phase, and direct signal intensity fluctuations, will be conducted in the visible (0.6328 μ) and infrared (10.6 μ) to obtain: (1) angle of arrival, phase and polarization fluctuations; (2) wavelength dependence of receiver diameter; and (3) heterodyne mixing efficiency. These measurements are to be made with a single frequency transmitter in the spacecraft and a duplex heterodyne receiver on Earth (capable of direct detection as well) and have been scaled to allow comparison between the various forms of laser and radio frequency communication.

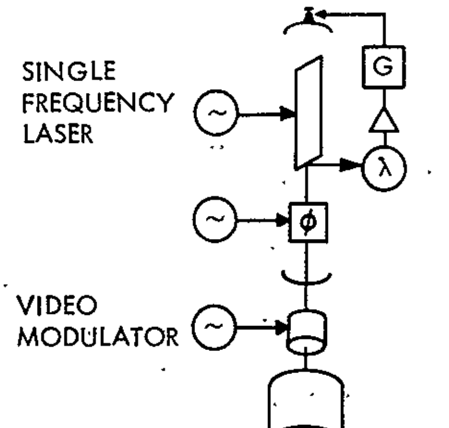

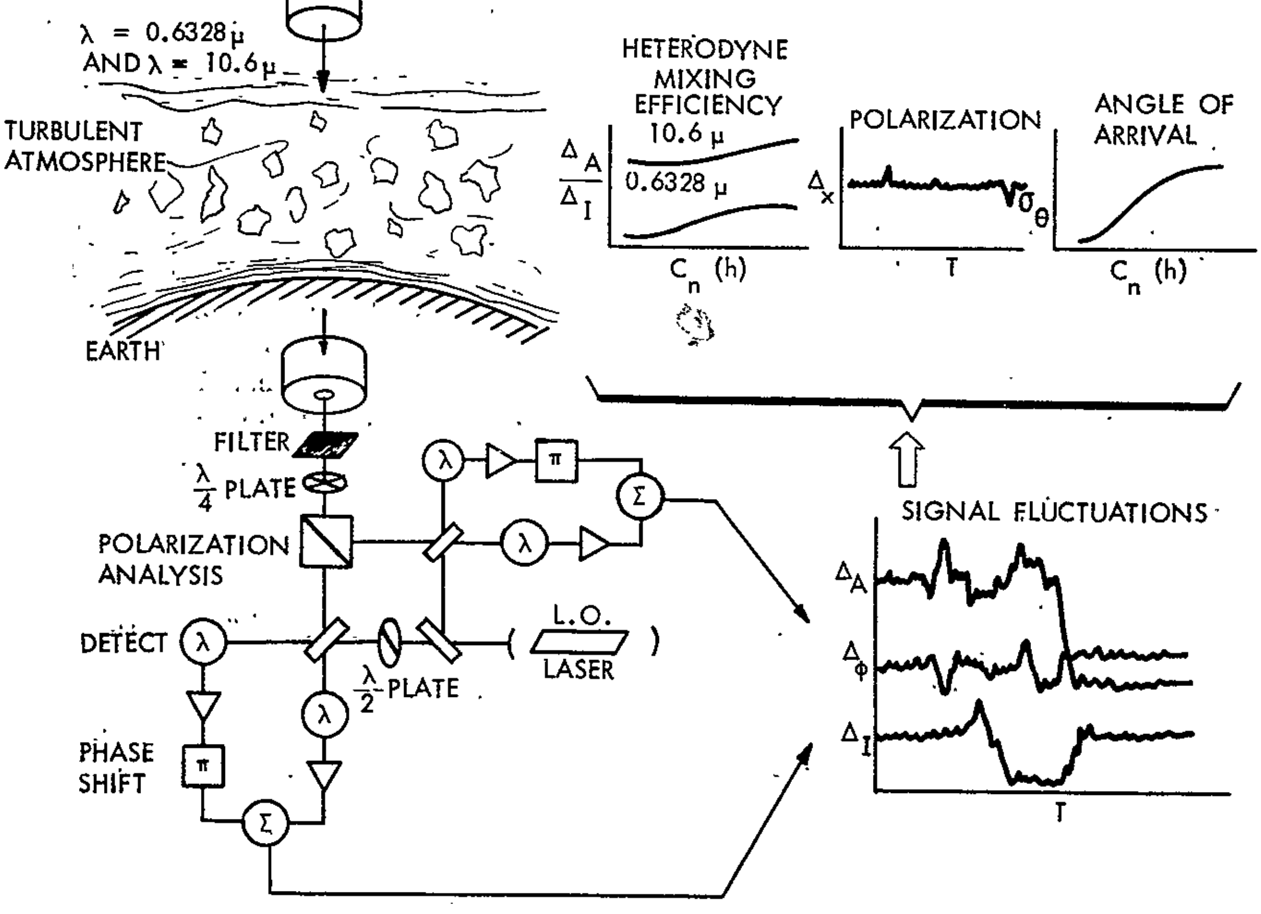

Figure 9.6.1-1. Optical Heterodyne Detection on Earth.

of heterodyne signal strength and bandwidth capability. Statistical data must be gathered over periods of many hours and repeated for many days under a variety of meteorological conditions. Signal distortion measurements must be made through the entire sensible atmosphere, and results must be correlated with observable meteorological parameters.

9.6.1.1 Justification

The laser offers an opportunity for scientific measurement which can lead to a better understanding of the turbulent structure of the atmosphere. The purpose of the optical heterodyne experiments is to provide good data to test the ranges of validity of the various turbulence theories. For example, a very interesting and potentially important point is that all the detailed theory applies to infinite plane-wave sources (1,2,5-17) and, recently, to spherical wave sources (1,18) (section 9.1). These are simple approximations to the Gaussian wavefronts of lasers. Therefore, an important result will be the comparison of the experimental data on laser propagation with the theoretical predictions based on geometric optics for the plane-wave theory(1,2,4,5-8,12,16) and on the Rytov approximation for both plane and spherical wave theories. (1,5,6,12-18,20) This comparison will determine to what extent these simpler, but detailed, approximate theories apply to the propagation of laser light.

The only theoretical work done on laser sources (3,19) i.e., sources with a collimated (or possibly focused) Gaussian wavefront, uses the Rytov approximation (paragraph 9.1.1). Although this work leaves the phase and amplitude fluctuations in terms of difficult integrals, some expressions for amplitude fluctuations have been evaluated in the cases of focusing the laser beam at infinity (collimated beam) and at the receiver. These results should presumably be better descriptions of the experimental situation than are the plane and spherical wave approximations. The proposed experiments will establish just how important the differences among these theories really are.

---

(1) V. I. Tatarski, Wave Propagation in a Turbulent Medium, McGraw Hill, N.Y., 1961, translated by R. A. Silverman.
(2) H. Hodara, Proc. IEEE, vol. 54, March 1966, p. 368.
(3) R. A. Schmeltzer, Quart. Appl. Math., vol. XXIV no. 4, 1967, p. 339.
(4) R. R. Horning, T. J. Gilmartin, and W. E. Adams, Paper FA14 presented at Spring Meeting, OSA, Columbus, Ohio, April 1967.
(5) R. E. Hufnagel and N. R. Stanley, J. Opt. Soc. Am., vol. 54, no. 1, 1964, p. 52.
(6) J. I. Davis, Applied Optics, vol. 5, no. 1, 1966, p. 139.
(7) P. Beckmann, Radio Science, vol. 69D, no. 4, 1965, p. 629.
(8) A. Consortini, L. Ronchi, Am. M. Scheggi, and G. Toraldo De Francis, Alta Frequenza, vol. 178E, 1963, p. 790.

It has frequently been stated that, to meet near future (1970-1980) interplanetary communication requirements, it would be necessary to develop information capacities greater than 10^7 bits per second.[21] Because of its high radiant intensity, laser communication system can achieve wide information bandwidths at great range. Since these ultimate advantages apply at extreme ranges, the potential of laser communication, and attendant developmental experiments, should be considered and evaluated in a planetary mission context. Clearly, it is desirable to conduct tests in Earth orbit which can be interpreted in the context of planetary mission applications.

---

(9) G. B. Parrent, Jr., R. A. Shore, and T. J. Skinner, J. Math. Phys., vol. 3, no. 4, 1962, p. 678.

(10) M. J. Beran, Stanford University Report SU-SEL-65-086, 1965.

(11) T. L. Ho and M. J. Beran, Paper FB 13, presented at the OSA Meeting, Columbus, Ohio, April 1967.

(12) D. M. Chase, J. Opt. Soc. Am., vol. 55, no. 11, 1965, p. 1559.

(13) W. P. Brown, J. Opt. Soc. Am., vol. 56, no. 8, 1966, p. 1045.

(14) D. L. Fried and J. D. Cloud, J. Opt. Soc. Am., vol. 56, no. 12, 1966, p. 1667.

(15) D. L. Fried, J. Opt. Soc. Am., vol. 56, no. 10, 1966, p. 1372

(16) D. A. DeWolf, J. Opt. Soc. Am., vol. 55, no. 7, 1965, p. 812.

(17) V. I. Tatarski, Soviet Physics JETP, vol. 22, no. 5, 1966, p. 1083.

(18) D. L. Fried, J. Opt. Soc. Am., vol. 57, no. 2, 1967, p. 175.

(19) D. L. Fried, J. Opt. Soc. Am., vol. 57, no. 2, 1967, p. 181.

(20) D. L. Fried, NASA Lectures, Huntsville, Ala., April 1967.

(21) M. C. Adams, Hearings before the Committee on Science and Astronautics, United States House of Representatives, Eighty-ninth Congress, February 23, 24, 25, and 28 through March 1, 2, 3, 7, and 8, 1966, Part 4, p. 97.

A. J. Kelley, "NASA's New Electronic Research Center," Astronautics and Aeronautics, vol. 3, no. 5, May 1965, pp. 58-63.

H. E. Newell, Hearings before the Committee on Aeronautical and Space Sciences, United States Eighty-ninth Congress, March 22, 23, 24, 25, and 30, 1965.

Space Research Directions for the Future, Space Science Board, National Academy of Sciences, National Research Council, Part I Planetary and Lunar Exploration, Dec. 1965, c.f., p. 6, Deep Space Information Transfer; p. 59 Laser Communication, ibid., Part II Optical Astronomy, January 1966, p. 9 Recommendation II of the Radio and Radar Astronomy Working Group.

Reference [22] derives the transmission equations for both heterodyne and direct detection optical communication shown in figure 9.6.1.1-1. For the ideal case of low background and diffraction-limited operation ($k = 1$), the heterodyne and the direct detection expressions only differ in performance by a factor of 4 (6 dB). Thus, if the arriving signal power is sufficiently larger than the total collected background power (upper right-hand portion of figure 9.6.1.1-1), the simplest, most reliable, and cheapest communication system will be the large aperture direct detection system.

A heterodyne detection receiver will outperform direct systems whenever the S/N x Δf requirement is low and background levels are not negligible (lower left portion of figure 9.6.1.1-1). Deterioration of the direct system (the change to steeper slope in figure 9.6.1.1-1) can be postponed through narrow-band, low-loss filters as indicated on curve B for a 2 Å filter. However, as a general conclusion, the heterodyne system seems inherently superior: (a) for beacon tracking in the presence of earthshine, or (b) for low data-rate, long-range communication links.

For comparable receiving apertures, heterodyne detection appears to offer certain advantages; namely, relaxation of the strict optical filter bandwidth since the signal-to-noise ratio is not a function of the background level. However, the effects of atmospheric turbulence serve to limit the effective receiving aperture for heterodyn detection. This compromises its expected advantages. Consequently, this experiment is needed to provide realistic experimental evidence for evaluation of the two detection techniques.

The curves also indicate that the performance of either kind of communication link depends very strongly on the choice of operating wavelength. Almost every paramet is wavelength dependent: quantum efficiency, η_q; transmitted solid angle, θ_t; and most especially the laser transmitter efficiency, η_t. Furthermore, for heterodyne systems, receiving aperture diameter, D_r, is wavelength dependent because the atmospheric transverse coherence length depends on wavelength. It is important to note that the transverse coherence length has not been determined for the 10.6-micron wavelength. For this comparison, it has been assumed to scale from the visible as $\lambda^{6/5}$. The promise of the highly efficient CO_2-N_2 laser (10.6 microns) is clear from this comparison. If large coherent collector apertures can be used at 10.6 microns, its efficacy will be clearly established. Fluctuations in angle of arrival can be measured and separated from scintillation in order to determine the effects of each. Measurements of pulse distortion and polarization fluctuation can be made. In addition, the optical phase noise over a long vertical path can be determined if sufficient frequency stability of transmitter and local oscillator lasers can be obtained. These effects will be established as functions of weather conditions and wavelength.

(22) Optical Technology Apollo Extension System, Part I, Final Technical Report, Volume I, Chrysler Corporation Space Division, October 21. 1966.

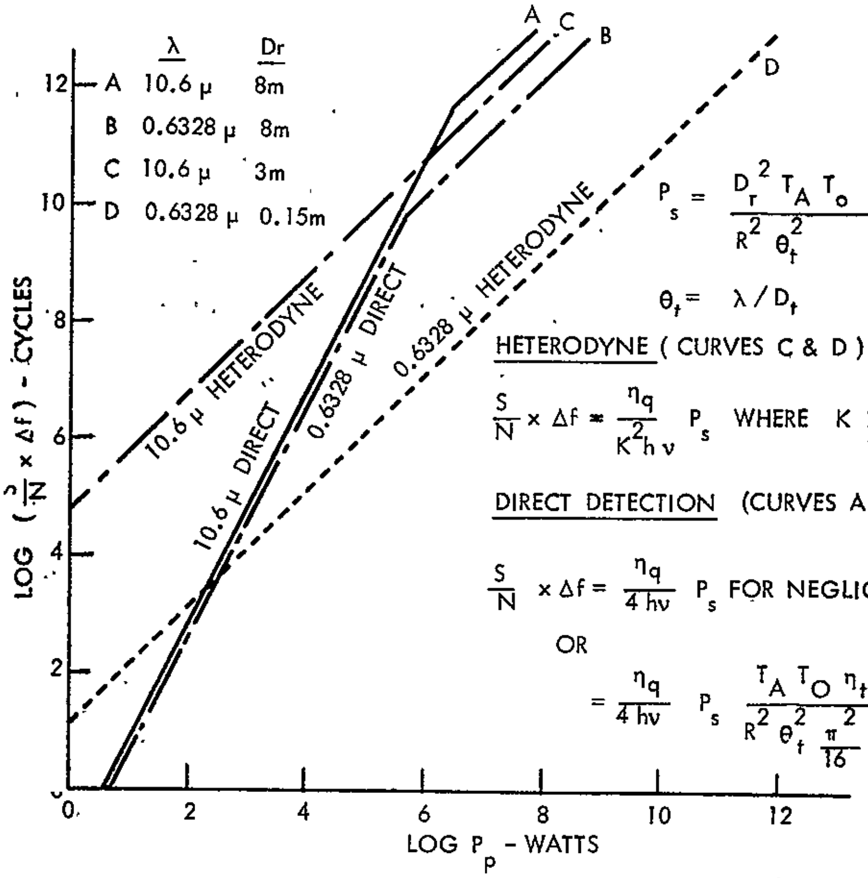

$$P_s = \frac{D_r^2 \, T_A \, T_o \, \eta_t}{R^2 \, \theta_t^2} \, P_p$$

$$\theta_t = \lambda / D_t$$

HETERODYNE (CURVES C & D)

$$\frac{S}{N} \times \Delta f = \frac{\eta_q}{K^2 h \nu} \, P_s \quad \text{WHERE} \quad K \geqq 1.0$$

DIRECT DETECTION (CURVES A & B)

$$\frac{S}{N} \times \Delta f = \frac{\eta_q}{4 h\nu} \, P_s \quad \text{FOR NEGLIGIBLE BACKGROUND}$$

OR

$$= \frac{\eta_q}{4 h\nu} \, P_s \, \frac{T_A \, T_O \, \eta_t \, P_p}{R^2 \, \theta_t^2 \, \frac{\pi^2}{16} \, \theta_r^2 \, N_\lambda \, \Delta\lambda}$$

PARAMETERS HELD CONSTANT

- TRANSMITTING APERTURE, D_t = 1.0 M
- MARS MAX. DISTANCE, $R = 3.8 \times 10^{11}$ M.
- OPTICS TRANSMISSIVITY, T_O = 0.3

WAVELENGTH DEPENDANT PARAMETERS

	0.6328 μ	10.6 μ
DETECTOR EFFICIENCY, η_q	5×10^{-2}	10^{-1}
FILTER BANDWIDTH, $\Delta\lambda$	2×10^{-4} μ	4×10^{-3} μ
ATMOSPHERE TRANSM, T_A	0.5	0.5
LASER EFFICIENCY, η_t	8×10^{-4}	8×10^{-2}
TRANSMITTED BEAM, θ_t	6.33×10^{-7}	1.06×10^{-5} RAD
BACKGROUND, N_λ	9.6	1.5 $\frac{W}{M^2\text{-STER}-\mu}$
PHOTON ENERGY, $h\nu$	3.1×10^{-19}	1.9×10^{-20} JOULES

Figure 9.6.1.1-1. Laser Communication

9.6.1.2 Experiment Design

Experiments to be conducted with the heterodyne system will include communication at wide bandwidths (paragraph 9.6.1.1) and measurements to determine the polarization, scintillation, and phase effects introduced by the atmosphere (section 9.1). To this end, statistical data will be gathered over long periods of time and correlated with atmospheric conditions. The system parameters to be recorded will include transmitted power, received power, bandwidth, and signal-to-noise ratio. These experiments will be made using several wavelengths of light energy to evaluate system performance over as much of the optical spectrum as is feasible.

The heterodyne technique provides a unique signal detection capability under conditions of high background illumination. Thus, a heterodyne detection optical communication system will be particularly valuable where the transmitter may be located in a high radiance background. The transmitter signal is modulated with the information to be communicated. In the receiver this composite signal is compared with a local oscillator operating at the transmitter frequency. The difference frequency is a reconstruction of the modulated information. For this reason the transmitter laser should operate at a stable frequency. Its output will be spatially and temporally coherent and linearly polarized.

The heterodyne detection system recommended for OTAES will be composed of two communication links: space-to-ground and ground-to-space. The spaceborne transmitter will have a single frequency laser, a wide bandwidth modulator, secondary optics, and a primary mirror to form the transmitted beam. The modulator must be capable of wide bandwidth performance and must not distort the spatial coherence of the beam. The output optics must be diffraction-limited in their performance to assure that the output energy density will be maximum at the ground receiver.

The ground-based receiver will consist of a receiving aperture, secondary optics, and a duplex heterodyne detector. The energy received will be circularly polarized light. The duplex receiver will provide a capability for detecting both vertically and horizontally polarized light. The local oscillator laser beam will be mixed with the incoming signal and be detected, in accordance with the transmitter frequency, by either photomultipliers or cooled semiconductor detectors. The detector output will be a function of the difference frequency.

The performance of this space-to-ground system is affected not only by the efficiency of the transmitting lasers, but also by the efficiency of the detectors on the ground. In the visible wavelengths, photomultipliers will provide reasonable efficiency plus gain through the multiplier sections, raising the output level above the thermal noise level of the electronic system. In the infrared region, photomultipliers are not available, and diode detection or photoconductive detectors will be required. The output of these detectors will not have the benefit of photomultiplication, and their output level may be considerably lower than the thermal noise level at the input of the electronics. One advantage of the heterodyne technique is its ability to raise the received signal to a level above thermal noise.

Input power on the spacecraft is limited, and this will limit the maximum output power for some types of lasers. It is planned to use two wavelengths in the spacecraft transmitter. These will be helium neon at 0.6328 micron and N_2-CO_2 at 10.6 microns. The expected laser output power that can be obtained in the spacecraft will be in the order of 10 milliwatts at 0.6328 micron and one watt at 10.6 microns. All power not transmitted will be dissipated as heat. Provision will be made for the conduction or radiation of this heat from the exterior surface of the laser assembly to the exterior of the spacecraft for radiation to space.

The principal environmental hazards to the proper operation of the heterodyne link are atmosphere and vibration. Although the heterodyne system is not affected by background illumination, the transmitter and receiver apertures must not be pointed to within 10° of the sun since the solar energy collected will create a temperature in excess of 500°C at the focal point, even for a 15-cm stopped aperture.

For a heterodyne system, transmission of the optical beam through the atmosphere is of special concern. Lateral spatial coherence of the beam is restricted to approximately 15 to 25 cm in the visible spectrum under normal conditions, due to turbulence in the atmosphere. Use of the receiving aperture larger than this coherence diameter will cause a reduction in the total received signal because of destructive interference between out-of-phase components. Furthermore, atmospheric constituents and impurities will attenuate the signal. Measurement of the system performance will be correlated with the atmospheric conditions to determine the proportion of signal degradation due to each separable characteristic.

The requirement for a temporal and spatial coherence of the beam places serious constraints on the allowable magnitude of vibration in the spacecraft. The structural assembly and alignment of components must be adequate to assure diffraction-limited performance of the beam while the necessary attitude control devices are operating. It must be emphasized that the diffraction-limited performance requirement is imposed to obtain a maximum energy density in the transmitted or received beam. Any disturbances such as vibration or shock that will cause optical misalignment will reduce the energy density of the beam.

The operation of the spaceborne equipment will be remote-controlled, and will consist of turning on and turning off appropriate lasers and the associated frequency stabilization circuitry, turning on and off the modulator, and selecting the several signal sources to be used with the modulator. Control of the transmitting optics will be handled through the telescope control. Although the laser will be designed to to be automatically tuned and adjusted, remote adjustment of the laser cavity may be required.

9.6.1.3 Measurement Objective

A space-to-ground link will be established. The ground-based receiver will use both optical heterodyne and direct detection of the signal transmitted from the spacecraft. The spacecraft may transmit two laser wavelengths simultaneously, and they will both be processed through the same ground receiving telescope aperture

Several parameters will be measured at each receiver. They are:

a. amplitude fluctuation of the heterodyne signals;

b. intensity fluctuation of the direct signals (total received energy fluctuation);

c. frequency (or phase) fluctuations in the heterodyne signals;

d. receiving aperture size and field of view;

e. atmospheric conditions such as temperature profile, winds aloft, haze conditions.

These parameters can be combined to give further results:

a. heterodyne mixing efficiency: the degradation of heterodyne efficiency can be found by normalizing the instantaneous heterodvne signal to the total received power level;

b. polarization fluctuation: since each direct and each heterodyne receiver is sensitive to orthogonal polarizations, any differential treatment by the atmosphere can be detected.

Several important kinds of experiments can be carried out with the optical heterodyne receivers in the satellite and on the ground. They are:

a. Atmospheric effects measurements. This group of experiments is designed to determine the atmosphere properties that significantly affect space-to-ground laser communication links. These are experiments that can only be made from a satellite vehicle that is well above the Earth's atmosphere and moving at angular rates slow enough to simulate those that will be encountered on interplenetary probe missions. The objective is to determine experimentally the types and rates of modulation that the atmosphere will support. Heterodyne receivers at the spacecraft will measure

(1) Scintillation in received signal amplitude. Predictions have been made [23] that the power spectra of amplitude scintillation observed from a satellite will be larger and peaked at higher frequencies than that observed at the ground. Verification of theoretical predictions will establish the useful bounds on fade rates for an optical up-link.

(2) Fluctuations in optical phase on a coherent signal passing through the entire atmosphere. The magnitude and rate of such phase fluctuations will establish the usefulness of optical FM modulation for communication. The frequency, or phase stability of the spacecraft local oscillator, may not be good enough to permit definitive measurements to be made except when acoustic disturbances aboard the vehicle are absent.

(3) Polarization fluctuation. The spacecraft heterodyne receivers can detect any differential in amplitude or phase fluctuations between orthogonally polarized input beams. Correlation between any of the fluctuations in the two channels will allow estimates of atmospheric depolarizing effects to be made after normalizing to correct for scintillation effects.

Each of these measurements can be carried out in the visible and in the infrared regions to obtain the wavelength dependence of these effects.

Heterodyne receivers on the ground will measure:

(4) Angle-of-arrival fluctuations. The extremely narrow beamwidth of a heterodyne receiver makes it useful for detecting small chang in angle of arrival of a signal from the spacecraft. The fluctuations in receiver output due to angle of arrival cannot be separated from those due to amplitude scintillation. A second detector with a wider field of view is necessary to separate the effects. When this is done, the fade rates for ground-based heterodyne systems of varying beamwidths can be measured.

(5) Phase fluctuations on the received signal. The phase noise generated by the atmosphere on the downlink can be measured when both ecraft transmitter and the local oscillator on the ground sturbed by external vibrations.

(23) R. J. Munick, "Turbulence-Produced Irradiance Fluctuations in Ground-to-Satellite Light Beams," NAA--Space & Information Systems Division, Repc No. SID 64-2222, December 28, 1964.

(6) Polarization fluctuations. These ground-based measurements will be made in the same way as done aboard the spacecraft.

(7) Wavelength dependence of receiver diameter. The effective collecting area of an optical heterodyne receiver can be measured as a function of wavelength over the range from visible (0.6328 micron) to the far infrared (10.6 microns). These experiments will determine whether the gain in system performance that is predicted for the infrared system can be achieved.

b. Optical communications experiments. This group of experiments will test alternative modulation techniques, with the objective of testing their capability for communication with 10-MHz bandwidths over a space-to-ground link.

9.6.1.4 Equipment Design

The block diagram of the equipment required for the Optical Heterodyne Detection on Earth experiment is shown in figure 9.6.1.4-1. It consists of (a) a dual 0.6328-micron multimode laser, with its power supply, mode stabilization controls, and automatic frequency control; (b) electro-optic modulator with the modulator driver, power supply, and signal source; and (c) telescope, including secondary optics, beam deflection subsystem, and pointing and tracking controls. The ground receiver will be made up of the following subsystems: a) ground telescope, including its secondary optics, beam deflection subsystem, and pointing and tracking controls; b) dichroic mirror; c) optical filter; and d) duplex heterodyne receiver.

More detailed block diagrams of the spaceborne equipment, and the optical layout, are shown in figures 9.6.1.4-2, 9.6.1.4-3, 9.6.1.4-4, 9.6.1.4-5, and 9.6.1.4-6 for the three laser telescopes.

9.6.1.4.1 Spaceborne Transmitting System

The requirements for spaceborne transmitters in the heterodyne detection case are more severe than for the direct detection case. A heterodyne receiver with its narrow inherent bandwidth must have a single-frequency transmitter, or, as is proposed here, it must use only one of the several frequencies that a transmitter laser may be generating as its signal source. In addition, the frequency stability of the transmitter laser is most important, whether it be a multimode or a single-frequency laser.

The spaceborne transmitter system, which will consist of multifrequency laser transmitters at 0.6328 microns and a single frequency laser at 10.6 microns will be capable of broadcasting at these two optical frequencies simultaneously, so that comparison of the effects of the atmosphere on these two wavelengths could be made

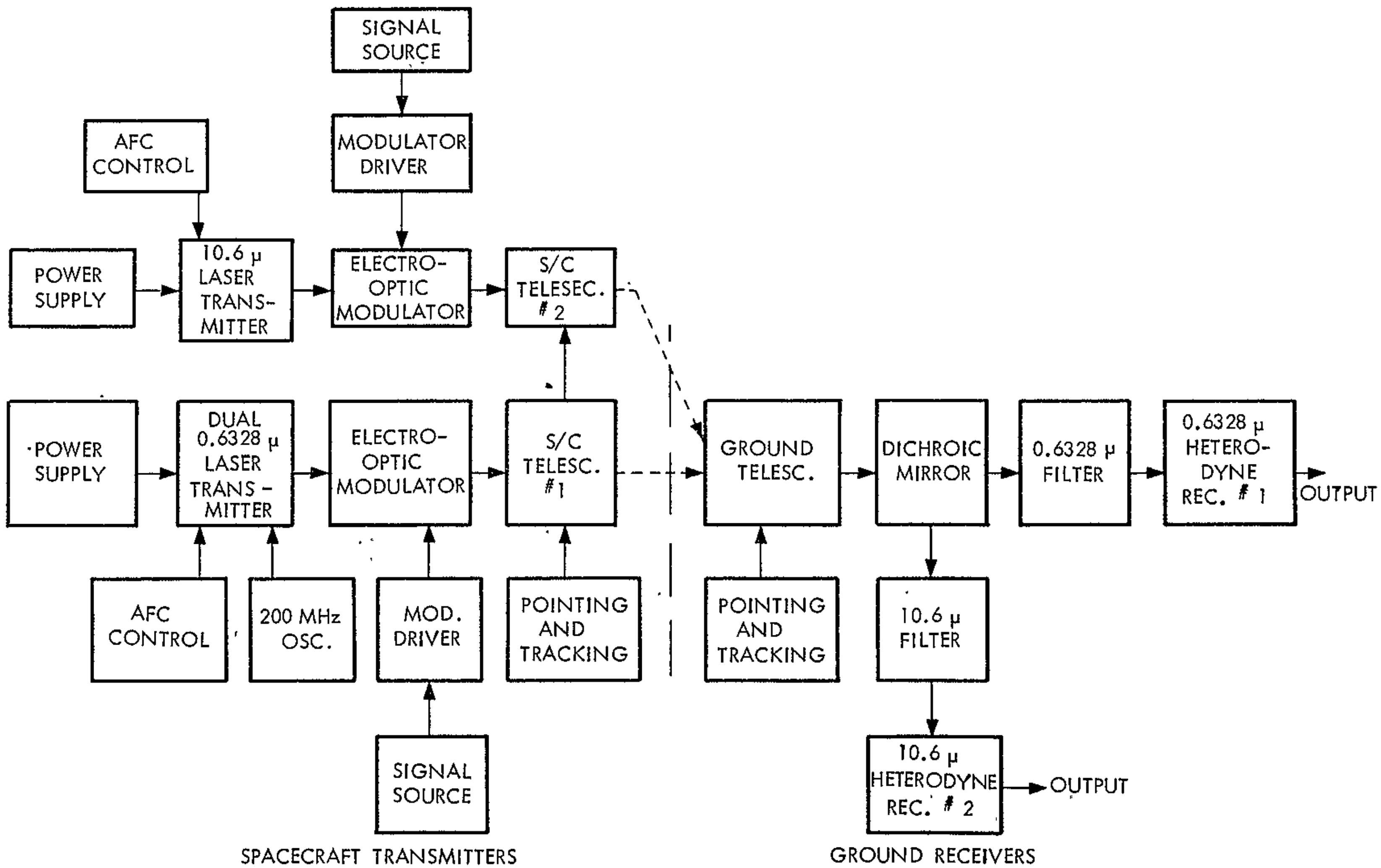

Figure 9.6.1.4-1. Block Diagram of Heterodyne Detection on Earth Experiment - 0.6328 Micron and 10.6 Microns

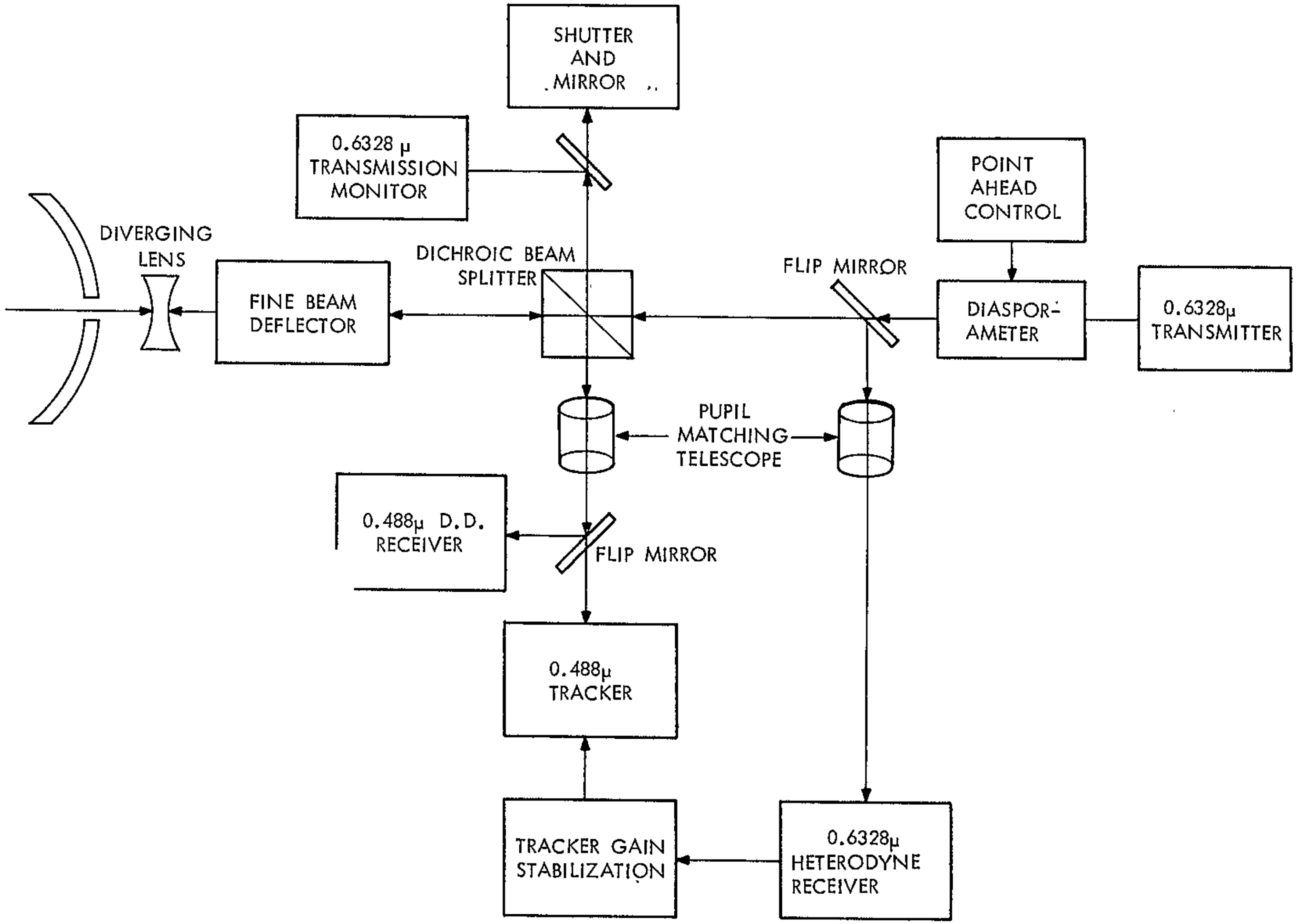

Figure 9.6.1.4-2. Block Diagram of Telescope No. 1: 1.0-Meter - Gimbaled

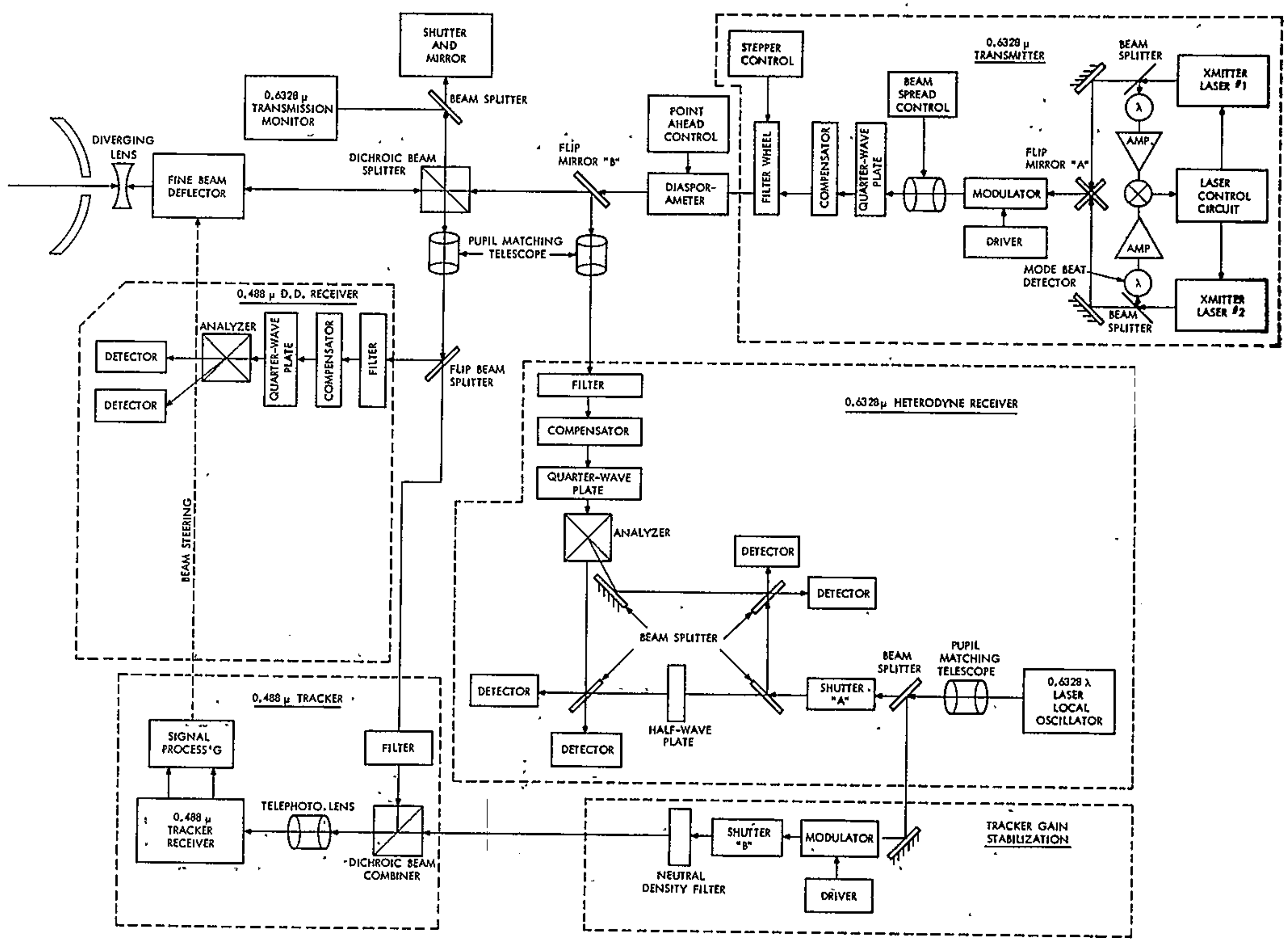

Figure 9.6.1.4-3. Block Diagram of Telescope No. 1: 1.0-Meter - Gimbaled

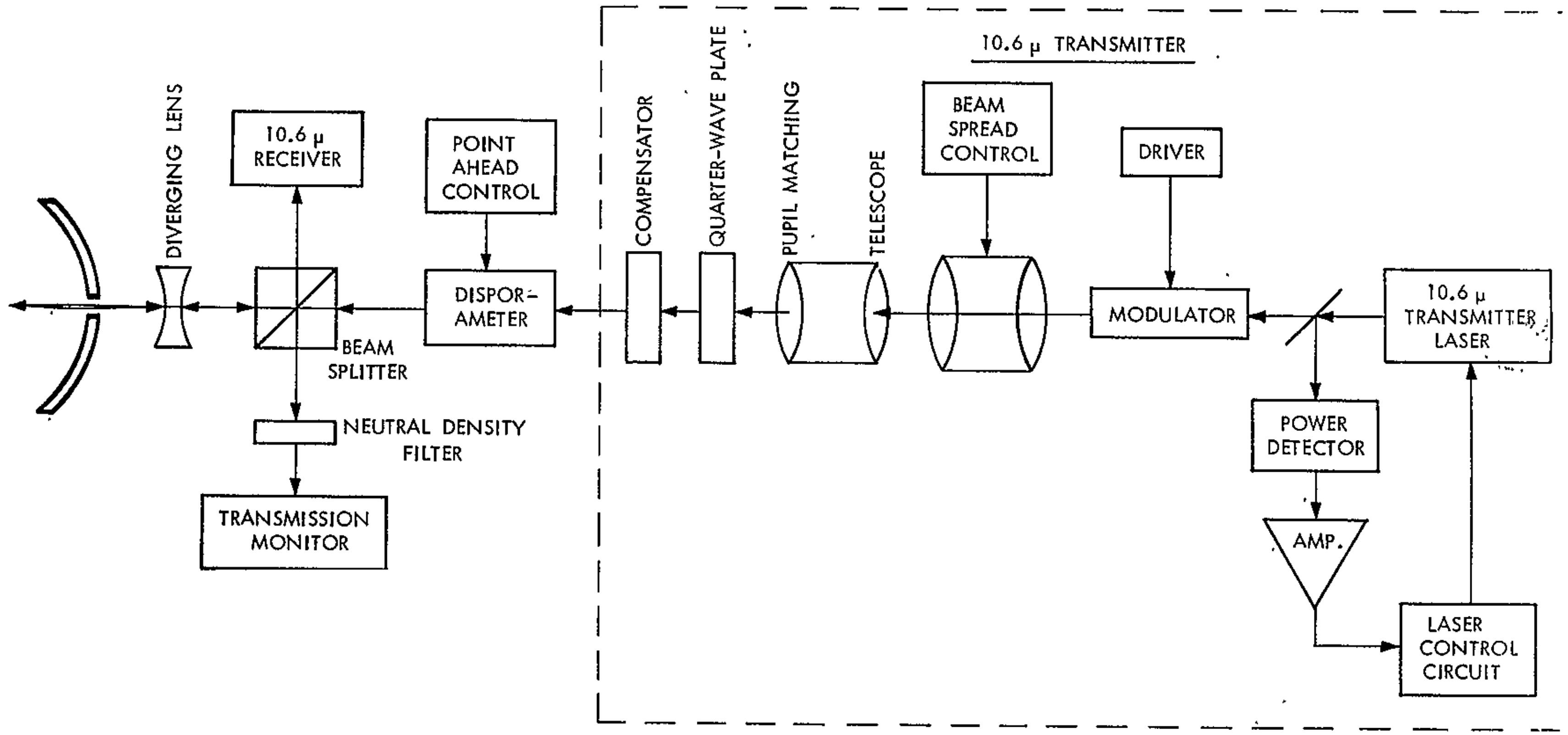

Figure 9.6.1.4-4. Block Diagram of Telescope No. 2: 0.3-Meter Strap-On

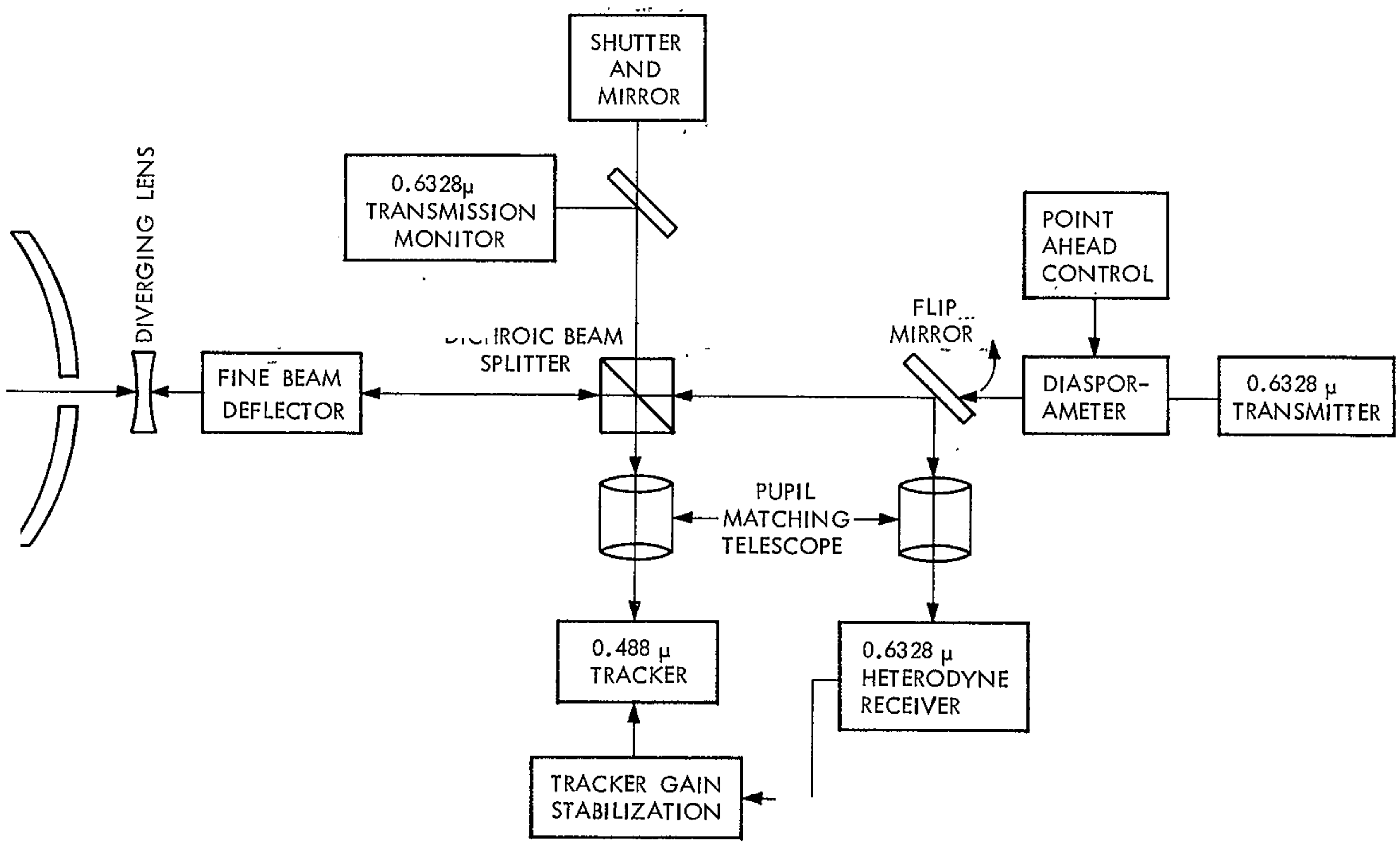

Figure 9.6.1.4-5. Block Diagram of Telescope No. 3: 0.3-Meter - Separately Gimbaled

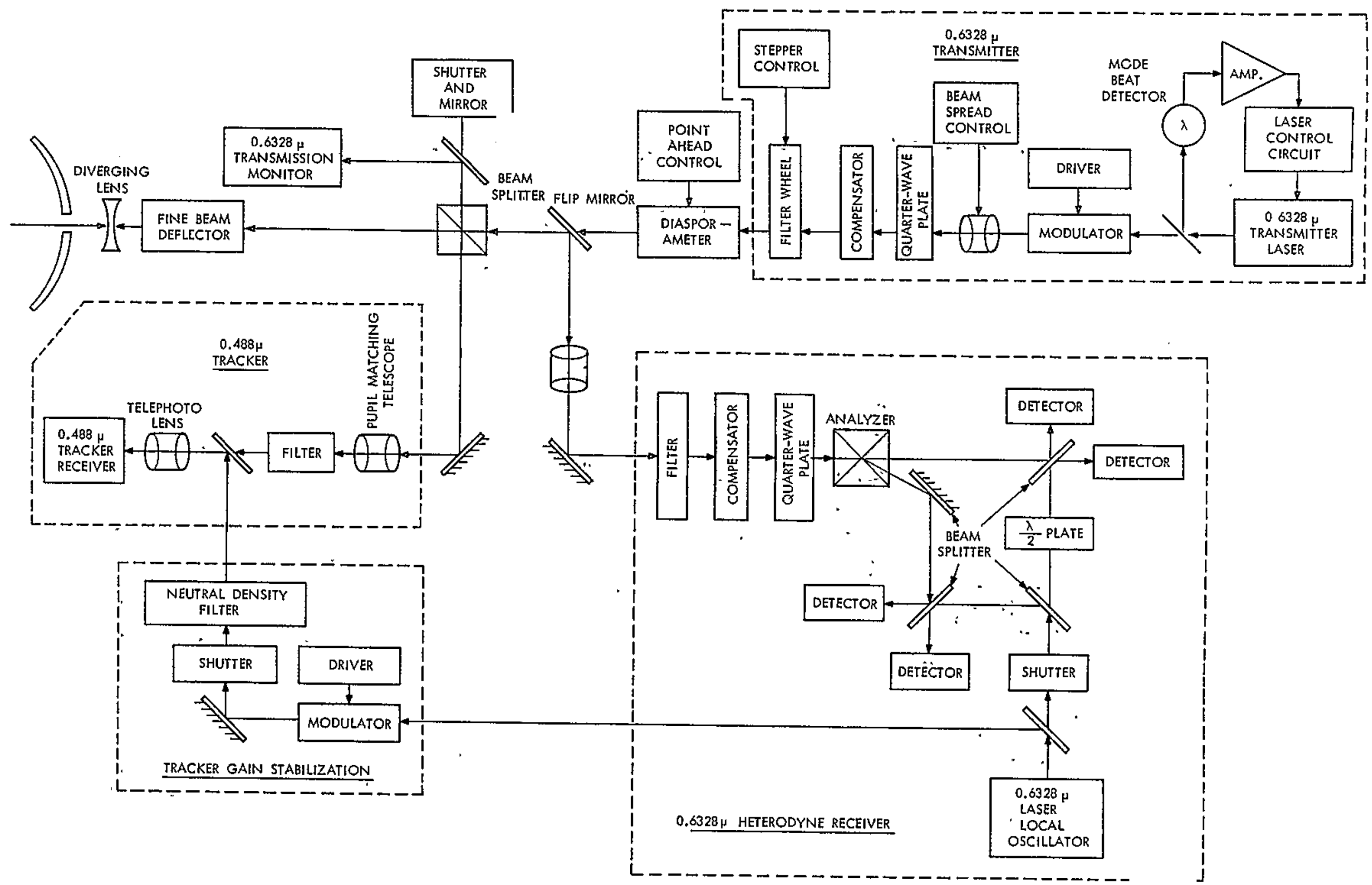

Figure 9.6.1.4-6. Block Diagram of Telescope No. 3: 0.3 Meter--Separately Gimbaled.

simultaneously at the ground receiver station. The selection of radiating wavelengths and their frequency offset from line center in the case of the mode-coupled multi-frequency laser will be controlled by a radio command from the ground station.

Circularly polarized radiation will be transmitted to allow any atmospheric depolarizing effects to be detected.

Each of the spacecraft transmitter lasers can be expected to drift in frequency at rates of a few megahertz per minute because of thermal changes alone. These slow drifts are caused by expansion or contraction in the supports that separate the cavity mirrors. Good mechanical and thermal design can minimize, but can never eliminate, these motions in the presence of diurnal heat input fluctuations and the turning on and off of other equipment.

In addition, there are more rapid disturbances to be contended with because of acoustic vibrations carried to the laser structure from other parts of the spacecraft. Mechanical actuators, gyros, reaction jet valves, transformers, etc., all can generate disturbances at audio and ultrasonic frequencies, causing frequency jitter in the transmitter lasers if they are not compensated.

For these reasons, various laser stabilization techniques must be used. In the case of the helium-neon laser at 0.6328 micron, the FM laser technique can be used to stabilize the output frequency to a point near the laser line center.[24,25] In the case of the carbon dioxide laser at 10.6 microns the inherent linewidth of the carbon dioxide fluorescence is only about 50 MHz, and the laser will operate at a single frequency without the necessity for mode-coupling schemes. It will, however, need to be stabilized near line center to keep the output at full power, and to keep acoustically induced frequency jitter in the transmitter from showing up as a spurious signal in a heterodyne ground receiver.

Recent experimental results at Sylvania[26] using super-mode and FM laser techniques have indicated the use of a multimode FM laser for the 0.6328-micron He-N optical heterodyne experiments. Two alternatives which, at first, appear more efficient (converting most of the available power of a multimode laser to single frequency) have been rejected: (a) a frequency selective etalon output coupler with...

(24) S. E. Harris, M. K. Oshman, B. J. McMurtry, E. O. Ammann, "Proposed Frequency Stabilization of the FM Laser," Appl. Phys. Lett., vol. 7, no. 7, October 1, 1965, p. 185.

(25) S. E. Harris and B. J. McMurtry, "Frequency Selective Coupling to the FM Laser," Appl. Phys. Lett., vol. 7, no. 10, November 15, 1964.

(26) R. Targ et al., "Techniques for Super-Mode Oscillation," Interim Engineering Report Nos. 4, 5, and 6, 1 March 1966 - 31 December 1966. Contract No. AF 33(615)-2884.

an internal FM modulator or (b) an external super-mode modulator with the internal mode coupling modulator. The first technique (etalon output coupling), although experimentally demonstrated to give about 50 per cent of the available energy at a single frequency has been discovered to be subject to some very unattractive instabilities. The technique is sensitive to the level of laser power coupled out as well as the level of internal phase modulation. Also, acoustic vibrations of the output etalon were shown to induce AM fluctuations which could only be compensated for by a high frequency response servo system. The super-mode approach has been experimentally demonstrated as a superior technique to obtain single-frequency operation. However, this technique requires an additional external phase modulator which must be driven at a modulation index equal and opposite in phase to the internal FM modulator. The additional spacecraft hardware involved with single-frequency operation is to be avoided where possible.

Therefore, the following approach has been taken in selecting 0.6328-micron He-N transmitters for the optical heterodyne experiments. First, the spacecraft lasers, normally multimode lasers, will be operated as FM lasers when used as heterodyn transmitters. FM operation or mode-coupling by an internal optical phase modulat greatly reduces the low-frequency amplitude modulation noise as well as the high-frequency beat signals associated with the free-running modes. In fact, Targ [26] has measured a 20 dB AM noise reduction and a 30-40 dB suppression for the high-frequency beat signals in an FM laser. Since the video signal used in the heterodyr downlink has an information bandwidth considerably less than the laser intermode frequency spacing, the FM laser should be a sufficiently quiet transmitter. Single side-band FM laser output power, although less than the multimode laser by approximatel 1/n where n is the number of free-running modes, is still adequate for high signal-to noise link performance. The ground heterodyne transmitter has considerably more design flexibility and the super-mode technique is used to both convert the multimo output to a single frequency and simultaneously stabilize the output frequency to a point near the center of the fluorescence line.

The optical configuration of a frequency-stabilized, multimode, FM laser is shown in figure 9.6.1.4.1-1. The resonant cavity of the laser system is formed by an opaque mirror at one end and a highly reflective mirror at the other end. Inside the cavity formed by the mirrors is a laser tube that provides gain, and a phase modulator that is made of a material such as KDP, which has a high electro-optic coefficient. When the phase modulator is driven with a frequency that is very near to the frequency spacing between the axial modes of the laser itself, the modes become coupled together and are converted from independent free-running oscillations into mutually dependent, coupled oscillations at nearly the same optical frequencies

The amplitude and phase of each of the previously independent oscillations is altered by the presence of significant coupling between the modes, so that the laser modes become sidebands of a single, coherent signal. Both AM and FM coupling have been observed.[27,28]

The FM mode coupled, or "FM laser," has an additional advantage, however: the light inside the cavity is effectively frequency-modulated at a rate controlled by the intracavity phase modulator, and the amount of AM distortion on this signal strongly depends on the optical frequency difference between the center of the FM mode pattern and the center of the fluorescence line. This dependence can be used to measure the absolute frequency drift of the mode pattern, and thus the drift in the cavity mirror separation, and to provide an error signal to correct drift or jitter as it occurs. An FM laser can thus be stabilized to line center without the need for "dithering" the output to get an error signal.

Feedback control systems are needed in order to operate the laser in this way. The Laser AFC Subsystem monitors the AM distortion on the FM light within the laser cavity and adjusts the cavity length to the correct value. This is accomplished by moving one end mirror (the single end mirror) with a piezoelectric transducer. In this fashion the spectrum of oscillating modes can be placed on the center of the resonance fluorescence line of the laser.

9.6.1.4.2 Ground Receiver

The heterodyne ground receiver system will have its useful collecting aperture diameter limited by atmospheric turbulence effects, as discussed in paragraph 9.1.3.4.[29,30] The atmosphere produces random phase variations on the order of $\pi/2$ or more between optical paths separated from each other by no more than a few inches, during usual clear weather conditions. For this reason, a 0.6328-micron heterodyne receiver immersed in the atmosphere will have a useful collector only 15 to 25 cm in diameter. It is anticipated that a larger diameter could be used in the far infrared at the 10-micron band, but this remains to be experimentally verified.

---

(27) S. E. Harris and O. P. McDuff, "FM Laser Oscillation--Theory," Appl. Phys. Lett., vol. 5, no. 10, November 15, 1964.

(28) E. O. Ammann, B. J. McMurtry, and M. K. Oshman, "Detailed Experiments on He-Ne FM Lasers," IEEE Journal of Quantum Electronics, vol. QE-1, no. 6, September 1965.

(29) Goldstein, Chabot, and Miles, "Heterodyne Measurements of Light Propagation through Atmospheric Turbulence," Proc. IEEE, vol. 53, no. 9, September 1965, pp. 1172-1180.

(30) D. L. Fried, "Optical Heterodyne Detection of an Atmospherically Distorted Signal Wave Front," Proceedings of the Conference on Atmospheric Limitations to Optical Propagation, National Bureau of Standards, Boulder, Colo., 1965.

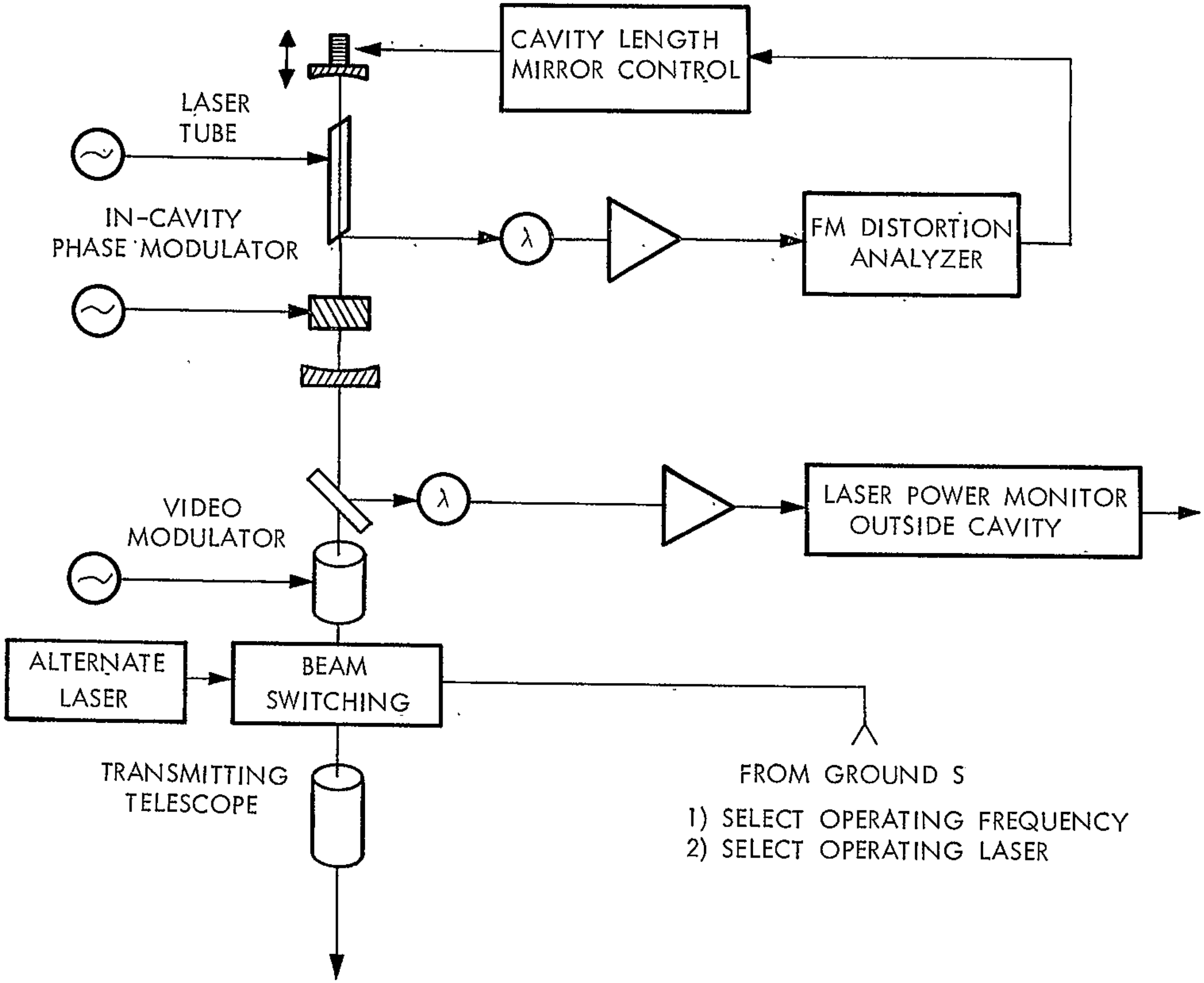

Figure 9.6.1.4.1-1. FM Laser Spacecraft Transmitter (0.6328 Micron)

The ground heterodyne receiver system will use a collecting aperture, which, for purposes of finding the dependence of receiver diameter on atmospheric conditions, will be 1.0-meter in diameter. The full aperture of this system would not be effectively used at short wavelengths or perhaps under poor conditions, but it will provide an aperture large enough to make tests of the atmospheric turbulence wavelength dependence. A set of two laser heterodyne receivers will be mounted near the focus of the optical system, and a set of dichroic mirrors or prisms will be used to separate the incoming wavelengths and direct them to their respective heterodyne receivers. The operating wavelengths will be at 0.6328 micron and 10.6 microns. The instantaneous field of view of each receiver system could be as small as the diffraction limit of the receiver aperture, which, for the case of visible radiation, is on the order of 0.2 second of arc, but this narrow a field of view would not be usable in general because of the atmospherically induced variations in angle of arrival of the signal as seen by the receiver.

The receiver must either: (a) track the incoming signal in angle; or (b) operate with a larger instantaneous field of view and operate with some sacrifice in sensitivity. The latter method will be used. The field of view can be increased over the diffraction limit by deliberately spreading the local oscillator beam so that mixing takes place over a larger angle. This is fully equivalent to masking the aperture size down to that having an equal diffraction-limited angular resolution.

The heterodyne receiver configuration is shown in figure 9.6.1.4.2-1. The received circularly polarized energy is divided by dichroic beam splitters and sent to the appropriate receiver units. Within each unit, the received energy is prefiltered and then analyzed by a quarter-wave plate, which converts right or left circularly-polarized input radiation into orthogonal plane polarized beams. These are then separated by a polarization-sensitive prism and sent to one of two basic heterodyne receivers. Both basic receivers are fed by the same laser local oscillator, but are sensitive to opposite polarizations. This configuration is called a polarization diversity optical heterodyne receiver. It is capable of processing the two polarization channels simultaneously. The local oscillator's power is divided equally by a beam splitter between the two channels. The beams are superimposed at the two mixer beam splitters. Their directions and phase fronts are matched so that they will beat coherently to produce a signal at their difference frequency at the output of the detector. This is then amplified by the IF amplifiers.

Each of the polarization channels uses two detectors in a balanced mixer configuration. The signals from the two detectors are out of phase because of the phase reversal produced on the light by reflection at the beam splitter. One of the legs of the circuit has an inverter that restores the signal to its correct polarity. Then it is added to the signal from the other leg, and a heterodyne signal of full amplitude is obtained without wasting any of the incoming signal light or any of the local oscillator power. This basic configuration is used for heterodyne reception at each wavelength. The details of the implementation will differ, particularly in the case of the detectors that at longer wavelengths require cooling and the attendant cooling equipment.

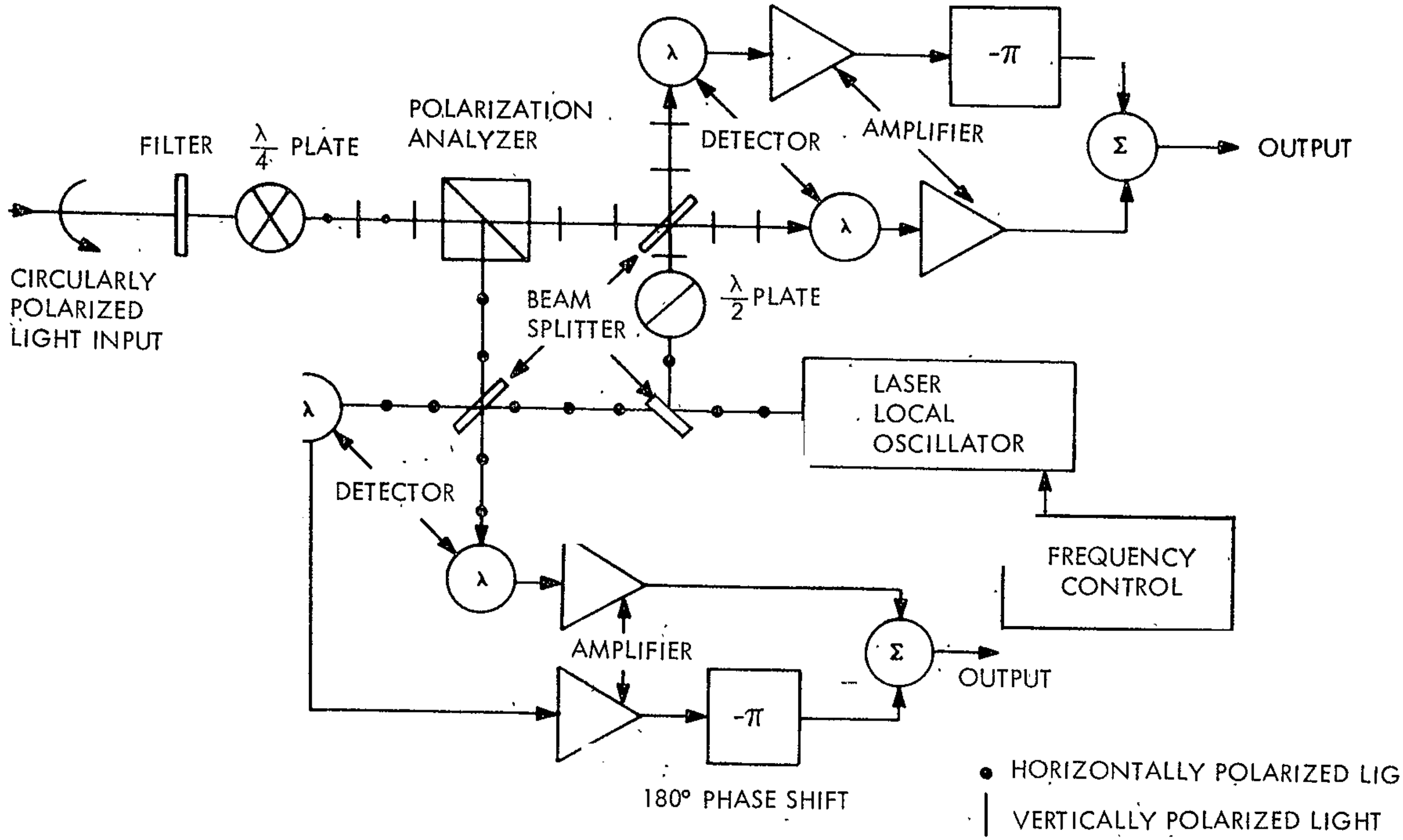

Figure 9.6.1.4.2-1. OTAES Polarization Diversity Heterodyne Receiver--Ground Based.

The frequency of the laser local oscillator must be stabilized to a fixed frequency offset from the frequency of the optical signal being received. The difference frequency to be detected must lie within the bandpass of the photodetector. In the visible and near infrared spectrum, there are available broadband detectors [31, 32] that permit the laser local oscillator to operate as far as 3 GHz away from the frequency of the incoming signal. A second electronic conversion with a tracking local oscillator can always move the signal to a convenient intermediate frequency. At 10.6 microns, the available detectors have bandwidths in excess of 400 MHz.

9.6.1.4.3 Equipment Required

The Optical Heterodyne Detection on Earth Experiment equipment list follows. The spaceborne equipment can be operated from either the astronaut console (left panels, figure 9.6.1.4.3-1) or the ground station (console no. 3, figure 9.6.1.4.3-2).

SPACEBORNE EQUIPMENT

a. DUAL 0.6328-MICRON LASER TRANSMITTER ASSEMBLY (Only one laser activated for experiment)

   Wt. - 80 lbs. L - 36 in. W - 12 in. H - 10 in.

   No. 1 -- 0.6328-MICRON LASER TRANSMITTER (FM OPERATION)

   He-Ne Laser
   Internal Cavity Modulator
   Internal Cavity Modulator Driver Amplifier
   Pupil Matching Optics
   Beamsplitter
   Stabilization Circuit Photodetector/Preamplifier

   No. 2 -- 0.6328-MICRON LASER TRANSMITTER (FM OPERATION)

   He-Ne Laser
   Internal Cavity Modulator
   Internal Cavity Modulator Driver Amplifier
   Pupil Matching Optics
   Beamsplitter
   Stabilization Circuit Photodetector/Preamplifier

---

(31) M. B. Fisher, "A Multiplier Travelling Wave Phototube," presented at the Conference on Electron Device Research, University of Illinois, Urbana, Ill., June 23, 1965 (to be published).

(32) L. K. Anderson, L. A. D'Asaro, and A. Goetzberger, "Microwave Photodiodes Exhibiting Microplasma--Free Carrier Multiplication," Appl. Phys. Lett., vol. 6, no. 4, February 15, 1965.

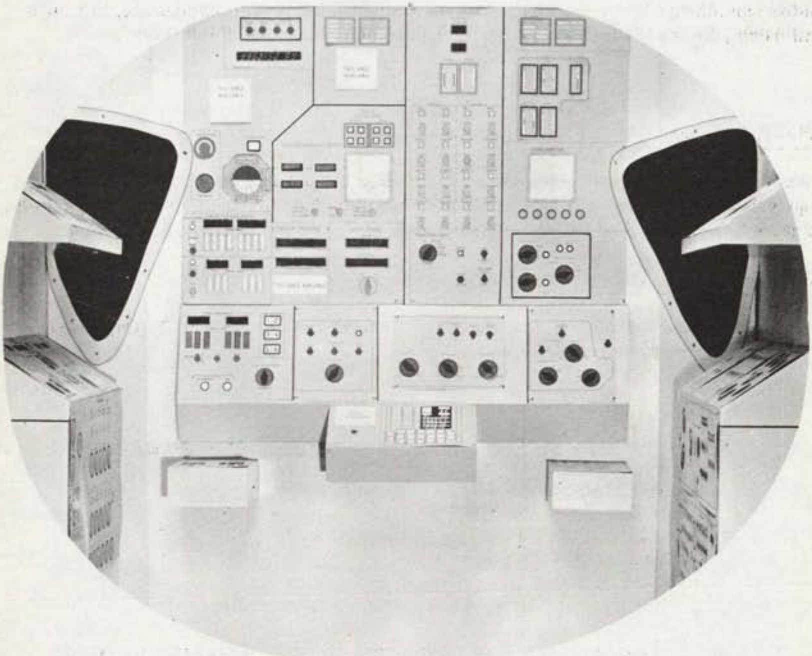

Figure 9.6.1.4.3-1. Mockup of Interior of LM/OTAES Spacecraft.

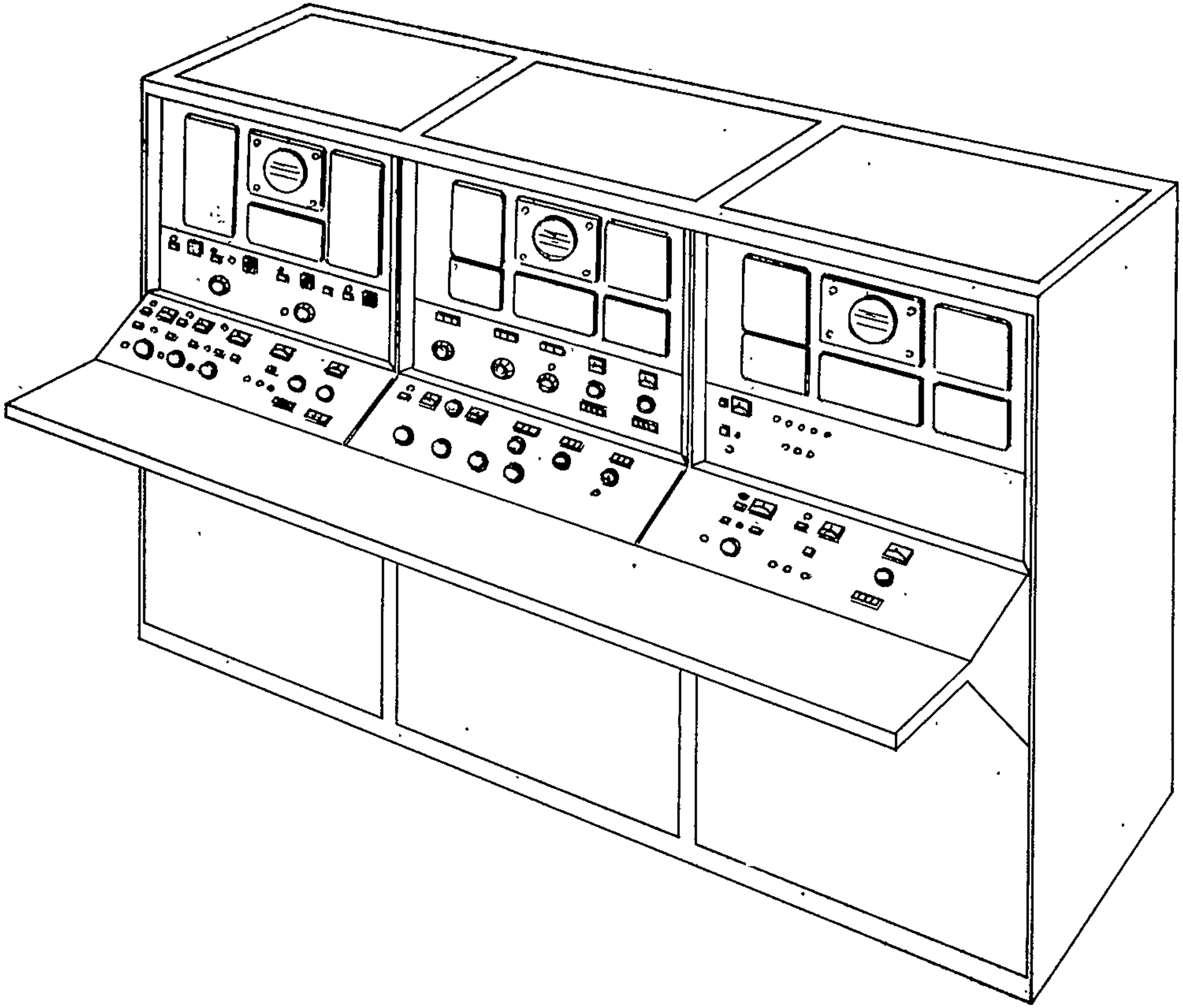

Figure 9.6.1.4.3-2. Console--Experiments 1,2,8, and 9.

EQUIPMENT SHARED BY 0.6328-MICRON LASERS NO. 1 & 2

Flip Mirror (2 Position)
Output Power Monitor
Main Control and Power Circuits
Cavity Tuning Control and Frequency Stabilization Circuits
Internal Modulator Control and Power Circuits

VIDEO MODULATOR SUBASSEMBLY

Modulator
Modulator Control and Power Circuits
Modulator Driver Amplifier
Signal Generator or Encoder
Photodetector and Preamplifier
Signal Comparator
Flip Mirror

b. 10.6-MICRON LASER TRANSMITTER ASSEMBLY

Wt. - 60 lbs. L - 32 in. Dia. - 18 in.

CO_2 Laser (Single-Frequency)
Laser Control and Power Circuits
Cavity Tuning Control and Frequency Stabilization Circuits
Stabilization Circuit Photodetector and Preamplifier
Thermo-Electric Cooler (Optional)
Beam Splitter
Pupil Matching Telescope
Output Power Monitor

VIDEO MODULATOR SUBASSEMBLY

Modulator
Modulator Control and Power Circuits
Modulator Driver Amplifier
Signal Generator or Encoder (maybe shared with telescope #1)
Photodetector and Preamplifier
Signal Comparator
Flip Mirror

c. BACK-UP 0.6328 MICRON LASER TRANSMITTER ASSEMBLY

Wt. - 50 lbs. L - 36 in. Dia. - 6 in.

He-Ne Laser (FM Operation)
Main Control and Power Circuits
Cavity Tuning Control and Frequency Stabilization Circuits
Stabilization Circuit Photodetector and Preamplifier
Internal Cavity Modulator
Internal Cavity Modulator Driver Amplifier
Internal Modulator Control and Power Circuits
Output Power Monitor
Beamsplitter
Pupil Matching Telescope

VIDEO MODULATOR SUBASSEMBLY

Modulator
Modulator Control and Power Circuits
Modulator Driver Amplifier
Signal Generator or Encoder (maybe shared with telescope #1)
Photodetector and Preamplifier
Signal Comparator
Flip Mirror

d. SIGNAL WAVEFORM ANALYZER/DISPLAY UNIT

e. TELEMETRY SIGNAL CONDITIONER CIRCUITS

f. 1.0-METER TRANSMITTING TELESCOPE WITH BEAM COMBINING OPTICS

g. 0.3-METER STRAP ON TRANSMITTING TELESCOPE FOR 10.(MICRON LASER WITH BEAM COMBINING OPTI(

h. 0.3-METER SEPARATELY GIMBALLED TRANSMITTING TELESCOPE WITH SUITABLE BEAM COMBINING OPTICS

GROUND BASED EQUIPMENT

a. 0.6328 MICRON AND 10.6 MICRON DUPLEX HETERODYNE RECEIVERS

He-Ne (Single-Frequency) and CO_2 (Single-Frequency) Laser
(2) Narrow-band Interference Filters
(2) Quarter-Wave Plate and Polarization Compensator
(2) Polarization Analyzer/Optical Mixer Subassembly
(2) Shutters
(2) 4 Wideband Photodetectors
(2) Photodetector Control and Power Circuits
(2) Signal Processing and Demodulation Circuits
(2) Laser Control and Power Circuits
(2) Cavity Tuning Control and Frequency Stabilization Circuits
(2) Automatic Frequency Control Circuits
(2) Power Monitor
(1) Dichroic Beam Splitter

b. 1.0-METER RECEIVING TELESCOPE WITH SUITABLE BEAM COMBINING OPTICS

c. EXPERIMENT CONTROL, SEQUENCING, AND MEASUREMENTS SYSTEM

Signal Processing Circuits
Telemetry Storage/Computation Facilities
Heterodyne Downlink Control/Display Console

Recent developments in 10.6-micron detector and modulator technology have considerably enhanced the bandwidth capability of CO_2 laser optical communication systems. Detectors sensitive at 10.6 microns with bandwidths in excess of 100 MHz have been demonstrated. Yardley and Moore [33] using a special high-frequency dewar construction, measured a Ge:Cu detector frequency response of 100 MHz at 3.39 microns by detecting the mode beats of a He-Ne laser. Additional measurements by Picus [34] have shown a compensated Ge:Hg detector with flat frequency response to 450 MHz at 3.39 microns and a Ge:Cu flat to 286 MHz. Although these detectors have spectral responsivity at 10.6 microns which is actually higher than at 3.39 microns, the measurements were performed at 3.39 microns because high-frequency modulation sources were not available at the longer wavelength. More recently,

(33) J. T. Yardley and C. B. Moore, "Response Times of Ge:Cu Infrared Detectors," Appl. Phys. Lett. vol. 7, December 1, 1965, pp. 311-312.
(34) G. S. Picus, Hughes Research Laboratory, Interim Technical Report No. 2, Contract No. AF 33(615)-3847.

Verie and Ayas [35] have developed p-n junction $Cd_x Hg_{1-x} Te$ photovoltaic detectors and measured their performance at 10.6 microns by observing the mode beats on the continuous output of a low-power CO_2 laser. A frequency response, possibly limited by the oscilloscope used, of 25 MHz was observed. The junction devices were operated at 77°K with D* from 1 to 5 x 10^9 cm - W^{-1} - $Hz^{1/2}$ in the range 3-14 microns.

Modulator development for the 10.6 micron CO_2 laser has also progressed at a rapid rate. Walsh [36] has constructed GaAs electro-optic modulators and obtained a modulation depth of 70 per cent at 10.6 microns using a peak applied voltage of 600 volts. A modulation bandwidth of about 100 MHz is quoted for a commercial unit. [37] An experimental program currently in progress at Sylvania [38] using a GaAs modulator at 10.6 microns will also measure GaAs modulator properties.

The 10.6-micron link represents the highest degree of technical risk in this experiment. No element of such a link has been space tested. Very few transmission materials are available and those refractive elements which have been tested have proven difficult to fabricate. Although the 10.6-micron link has the greatest potential for deep space application, from the standpoint of reliability, the Heterodyne Detection on Earth experiment has been designed to rely most heavily on the 0.6328-micron link.

Thus, from an experiment viewpoint the critical element is the He-Ne link. At 0.6328 microns all necessary components and their coatings are adequately developed and, in the case of optical elements and beam splitters, have already been proven in space. Optical heterodyne links have been demonstrated under field conditions on earth. [34] Only the laser, the modulator, and the heterodyne technique itself now require space qualification testing.

A technology plan is advocated herein which would test these components, and a rudimentary heterodyne space-to-ground link, in an early, piggyback experiment. Such a procedure, and the preceding development efforts which it implies, would serve to eliminate much of the risk associated with the 0.6328 micron portion of this experiment. It appears that the highest element of risk for both laser wavelengths may be the frequency stability of the lasers in both transmitters and receivers, a

---

(35) C. Verie and J. Ayas, "$Cd_x Hg_{1-x}$ Te Infrared Photovoltaic Detectors," Appl. Phys. Lett. vol. 10, May 1, 1967, pp. 241-243.

(36) T. E. Walsh, "Gallium-Arsenide Electro-Optic Modulators," RCA Review, September 1966, pp. 323-335.

(37) RCA data sheet describing Type J2036V1 Infrared Electro-Optic Modulator.

(38) R. Targ, D. E. Caddes, and P. J. Titterton, "Techniques for Super-Mode Oscillation," Interim Engineering Report No. 7, January 1, 1967 to March 31, 1967. Contract No. AF 33(615)-2884.

deficiency which could be partially solved through acoustic decoupling from their surroundings.

9.6.1.5 Data Management

A block diagram of the signal processing system following the photodetectors is shown in figure 9.6.1.5-1. The IF signal from each balanced photomixer pair is amplified at the IF frequency. The AGC circuit compensates for large changes i received signal strength. The IF signals from the two channels are processed ir several ways, depending on the type of experiment being performed.

a. [illegible]imiter-discriminator combination is sensitive to optical frequency modulation, and is also used to control the frequency of the laser local oscillator to the desired fixed offset. The frequency offsets due to Doppler effects aboard the OTAES will not be large compared to those obtained on an inter-planetary mission. It is therefore very difficult to simulate them on a stationary satellite-to-ground-station experiment. The ground receiver, however, should be capable of tracking Doppler shifts over a bandwidth well above that required so that experiments with different orbit configurations could be carried out.

b. A set of gated second detectors followed by a PCM demultiplexing syster is used for digital transmission tests. It should be noted that if alternate pulses of right and left circularly-polarized light are used, the received pulse will always be present in one channel or the other.

c. A set of video bandwidth AM detectors are used for analog AM transmission tests and beat amplitude scintillation measurements. The heterodyne receiver can also be used for angle of arrival fluctuation measurements.

d. The polarization measurement technique shown involves taking the difference in the photodetector output of the orthogonal components ("e" and "o" rays) obtained from a polarization-sensitive prism. Such a technique is valid only if the light beam input to the prism has a constant value unless the difference is zero. Consequently, the changes in polarization are to be measured and normalized by considering the sum of the detector output as well as their differenc to avoid this error.

No spacecraft crew display of signals received by a ground-based heterodyne re ceiver is needed. However, the status of the stable laser transmitters will be displayed via: (a) out-of-tolerance warning lights for laser AFC circuits, (b) laser output power monitor via panel meters, and (c) a CRT display of selectec circuit test points.

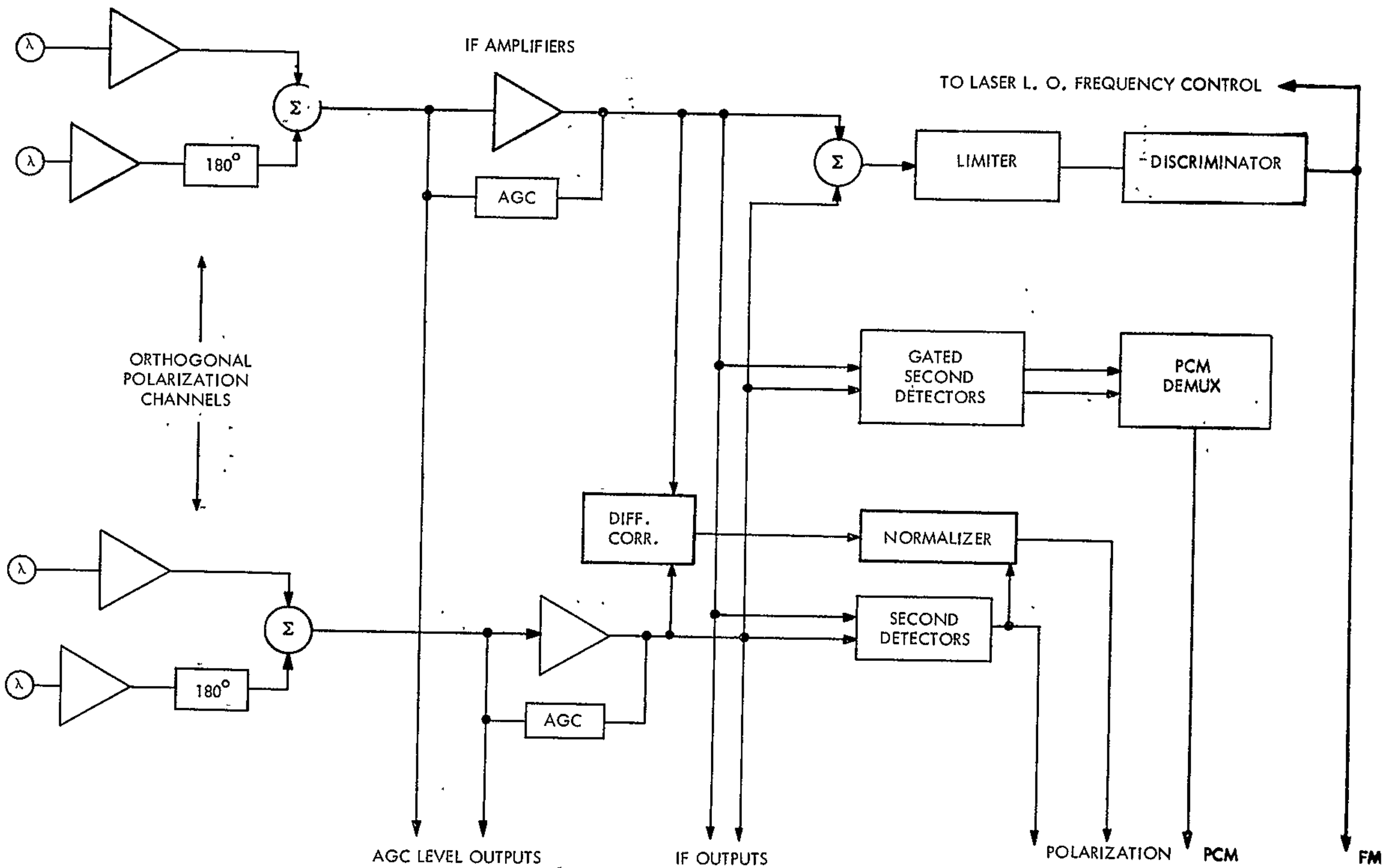

Figure 9.6.1.5-1. Heterodyne Receiver Electronic System.

The equipments aboard the spacecraft that must be operated include:

a. a 0.6328-micron stabilized laser transmitter

b. a 10.6-micron stabilized laser transmitter

c. either the 1.0-meter or the 0.3-meter telescope, in a transmit mode

d. the 0.3-meter strap-on telescope (no. 2) in transmit mode

e. a 0.4880-micron tracker for telescope no. 1 and/or no. 3

f. transmission monitors for telescope nos. 1, 2, 3

g. transmitter beam spread controls for telescope nos. 1, 2, 3

h. transmitter beam point-ahead controls for telescope no. 1 and/or no. 3

i. transmitter optical attenuators for telescope no. 1 and/or no. 3

j. electro-optic video modulators for all telescopes

k. RF telemetry and beacon system

The astronaut can operate these equipments using the laser control panels (figures 9.6.1.5-2, 9.6.1.5-3, and 9.6.1.5-4). Alternatively, this experiment can be operated from the ground OTTOS-OTAES Control Room (figure 9.6.1.5-5) using consoles 1 and 3 (figures 9.6.1.5-6 and 9.6.1.5-7). The OTTOS panels used to operate experiment 1 are shown in figures 9.6.1.5-8 through 9.6.1.5-13.

9.6.1.5.1 Spacecraft Equipment Test and Checkout

To assure satisfactory performance, the equipment alignment and tuning must be optimized and periodically repeated. Alignment of the laser, modulator, and telescope can be determined by operating the boresight error measurement equipment on the control panel and determining the magnitude of this error. Adjustment of alignment controls will be made to minimize the boresight error. Tuning of the laser to obtain optimum efficiency will be done by adjusting the laser mirror controls to maximize output power for fixed input power. Laser AFC circuits are automatic in operation and require only recheck of status indicator lamp. Telescope fine tracking functions are also automatic once they are initiated.

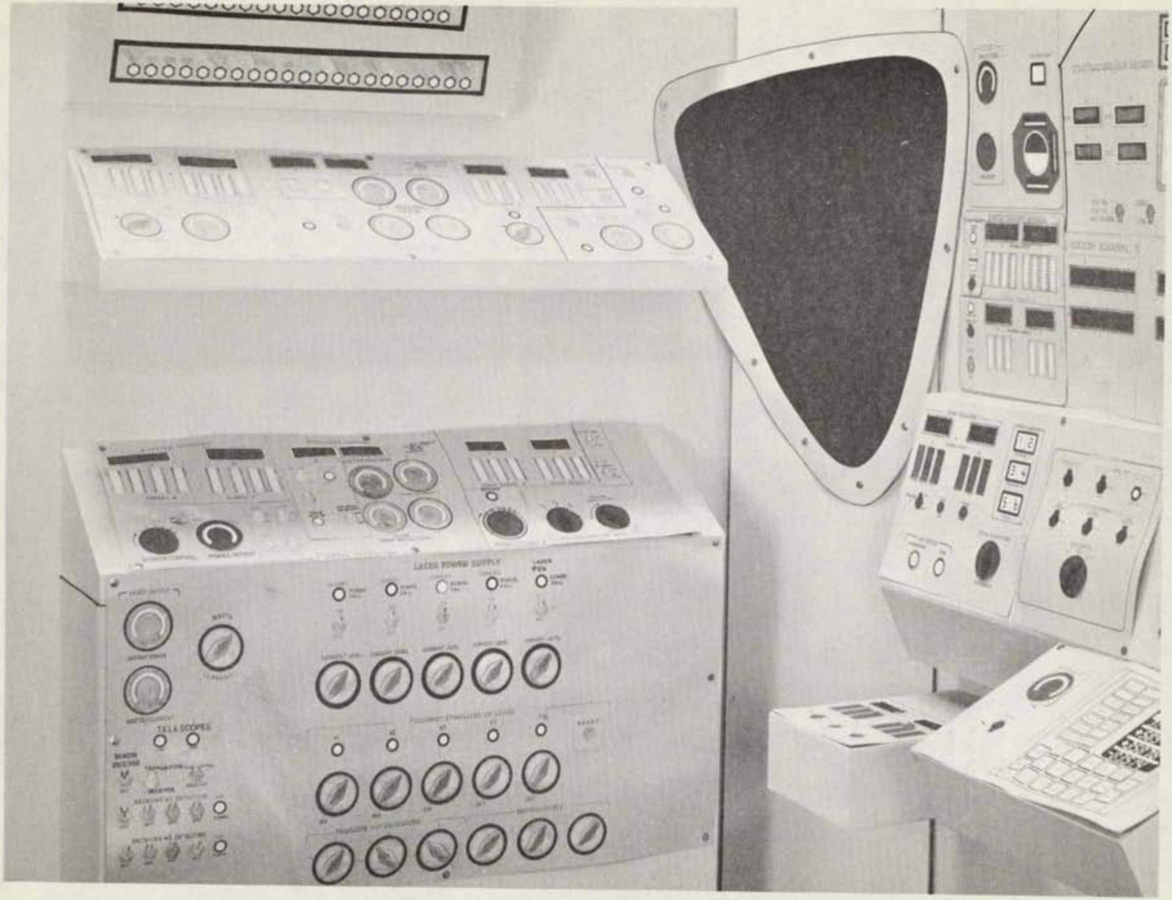

Figure 9.6.1.5-2, -3, and -4. 1-Meter and 0.3-Meter Telescope Panels and Laser Power Supply Panel.

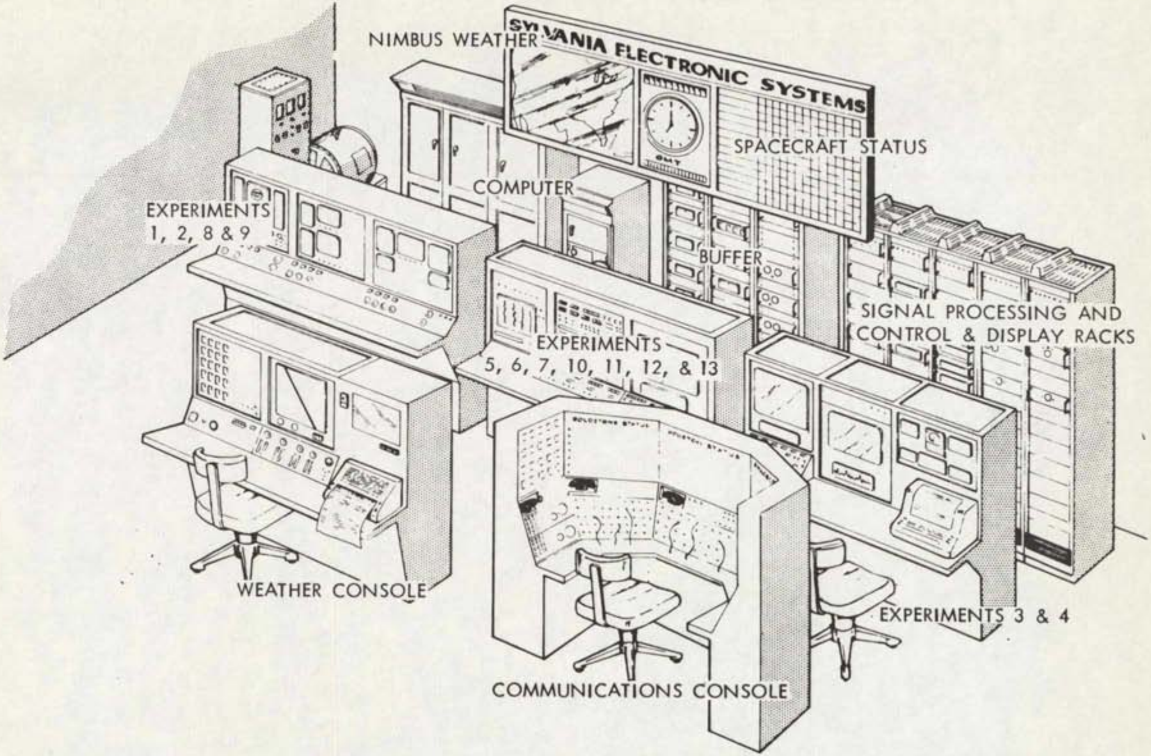

Figure 9.6.1.5-5. OTTOS/OTAES Control Room

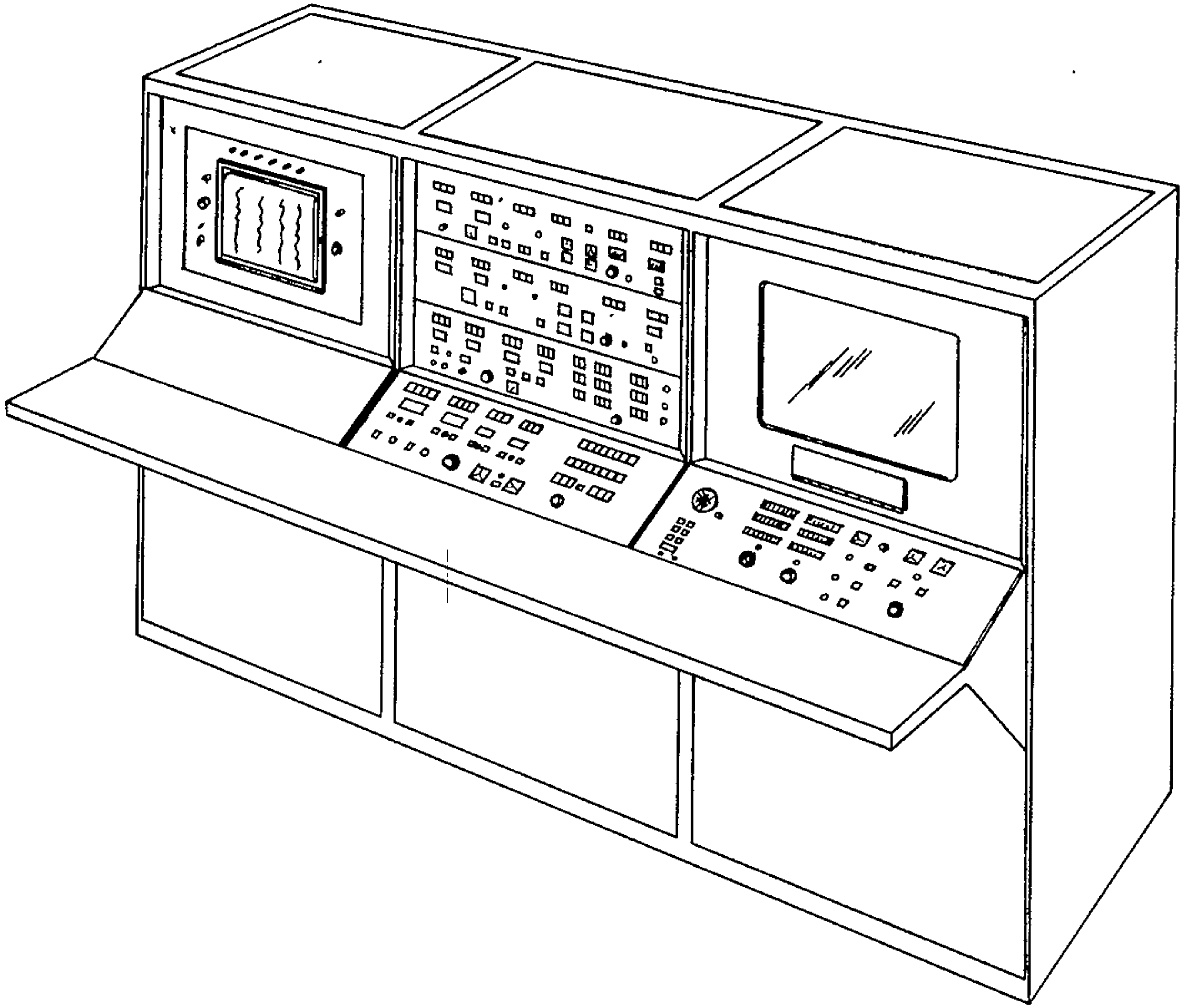

Figure 9.6.1.5-6. Console - Experiments 5, 6, 7, 10-13

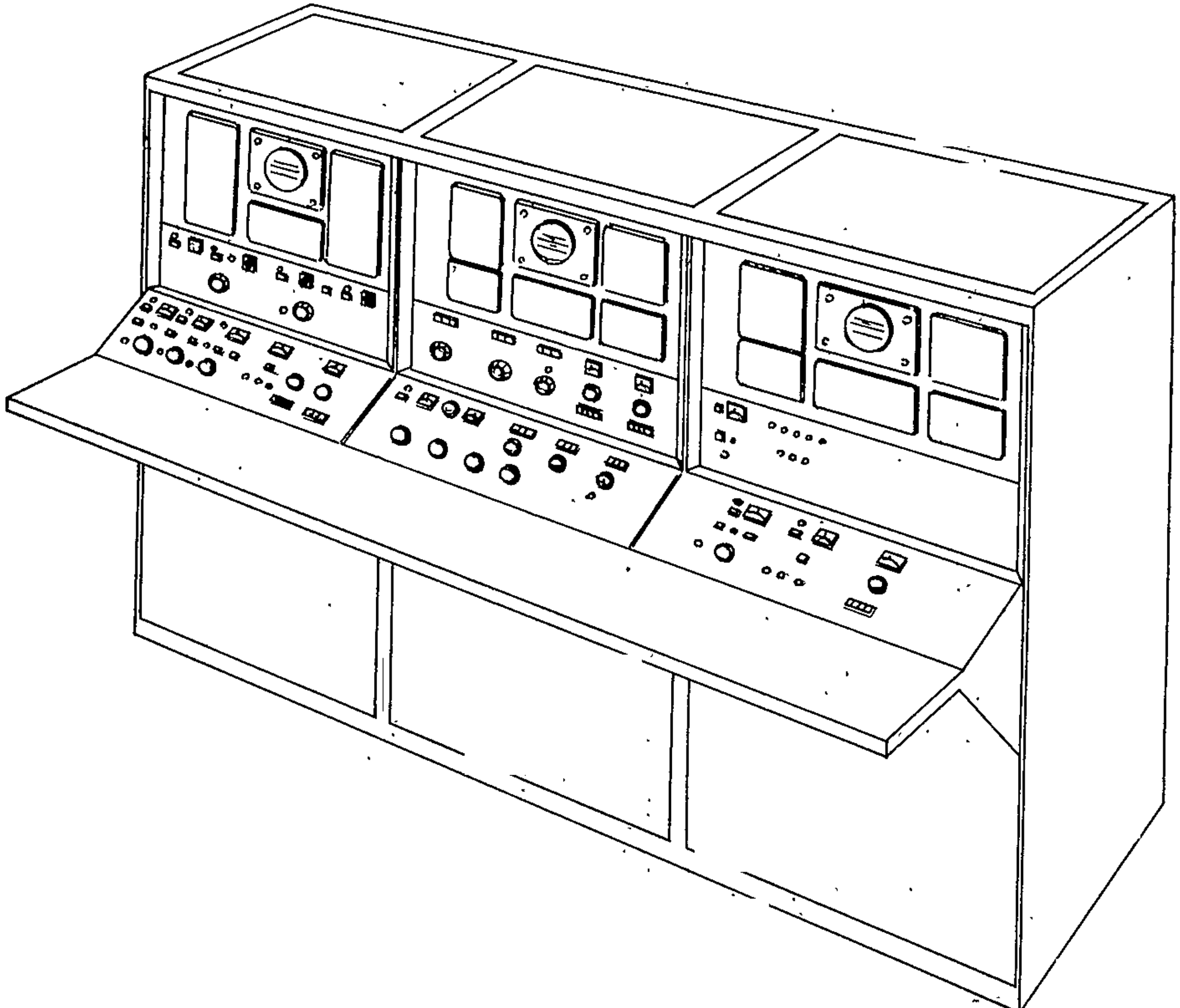

Figure 9.6.1.5-7. Console - Experiments 1, 2, 8 and 9

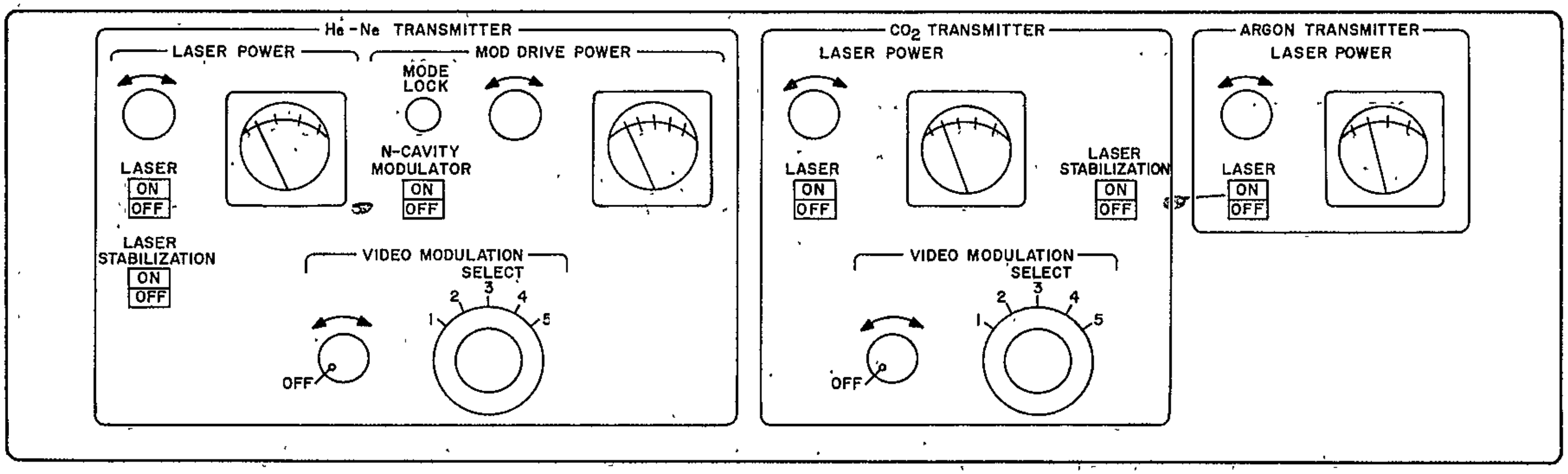

Figure 9.6.1.5-8. Panel, Transmitters; Experiments 1,2,8, and 9.

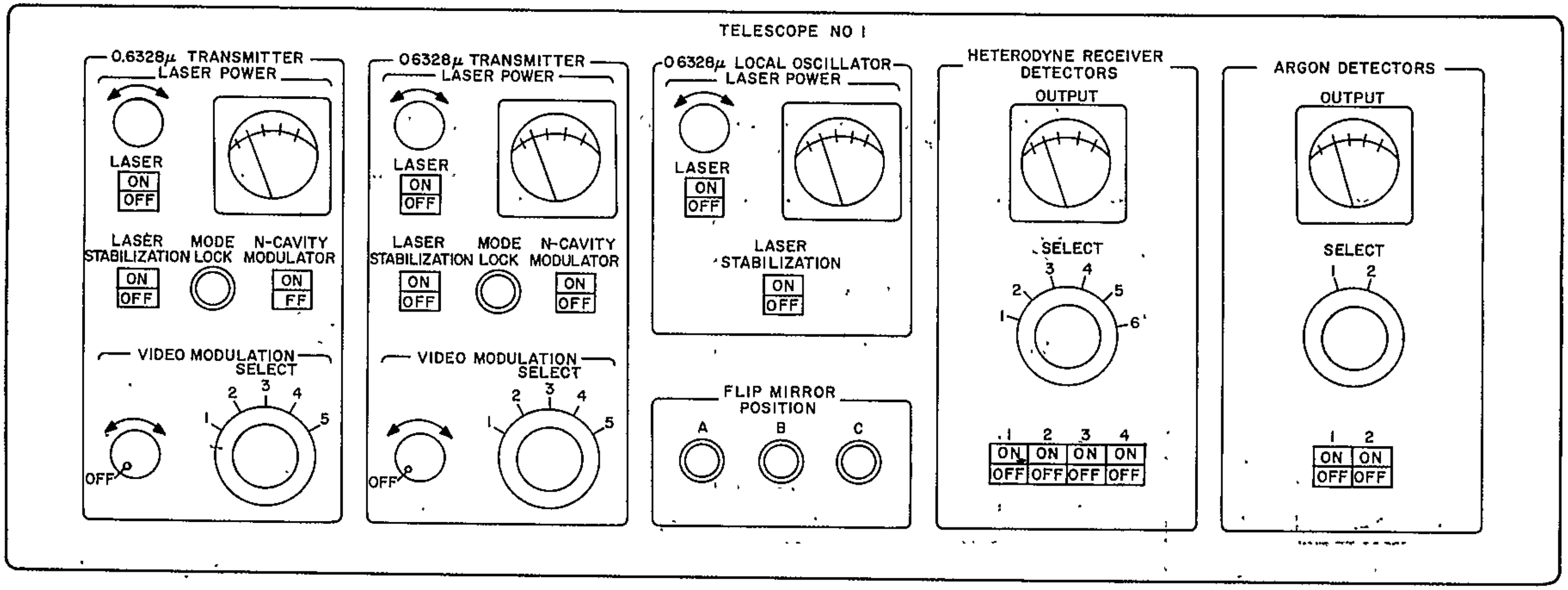

Figure . 9.6.1.5-9. Panel, Telescope No. 1; Experiments 1,2,8, and 9.

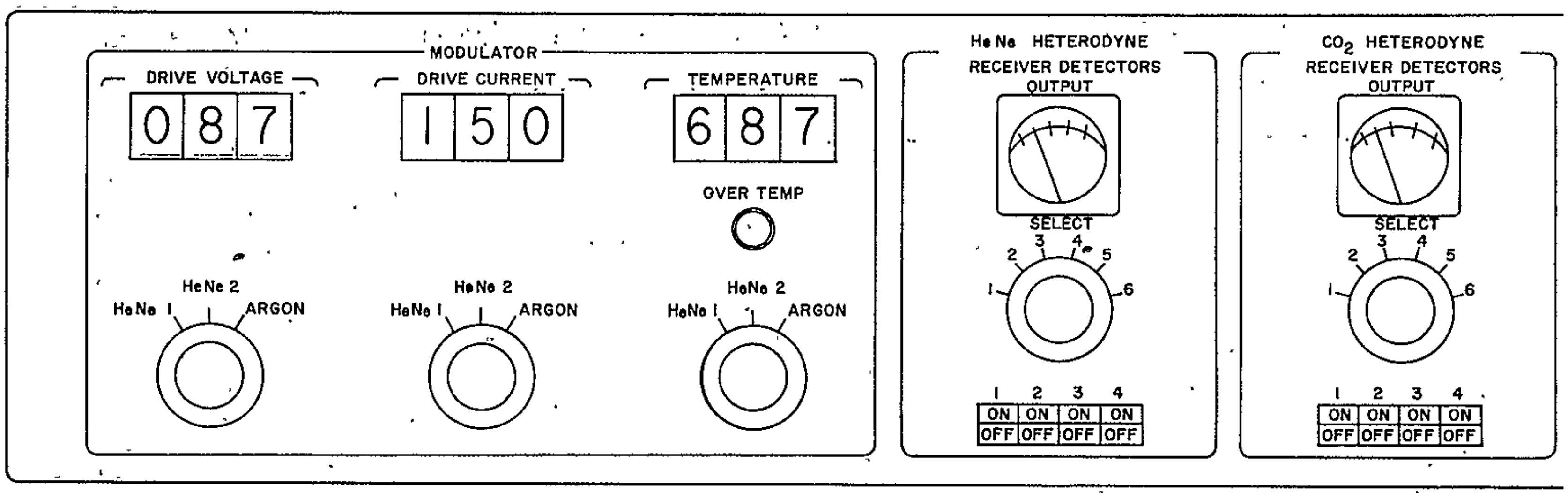

Figure 9.6.1.5-10. Panel, Modulator, and RCVR Detectors; Experiments 1,2,8, and 9.

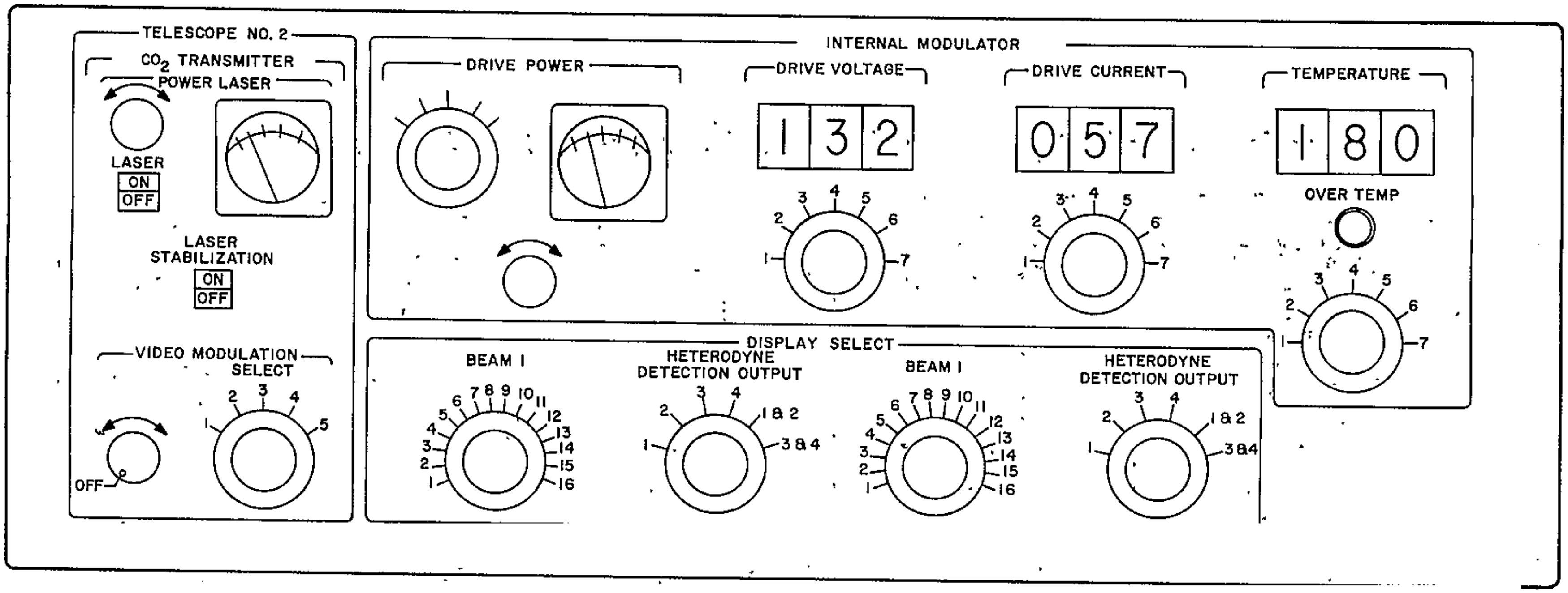

Figure 9.6.1.5-11. Panel, Telescope No. 2, Modulator, and Detection Output; Experiments 1,2,8, and 9.

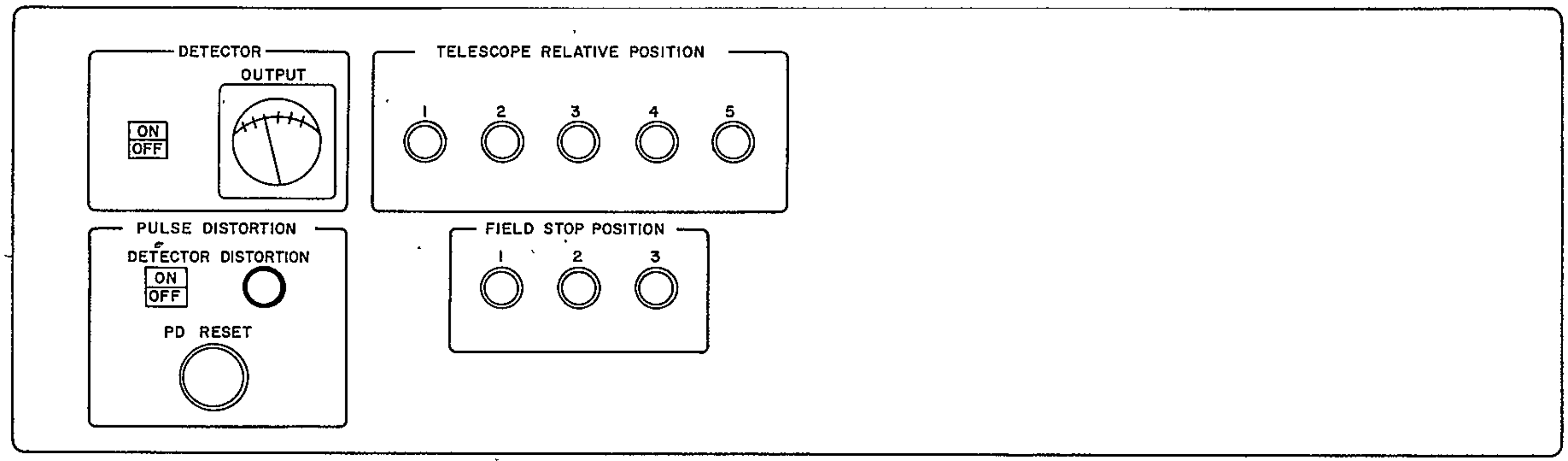

Figure 9.6.1.5-12 Panel, Telescope, and Field Position; Experiments 1,2,8, and 9

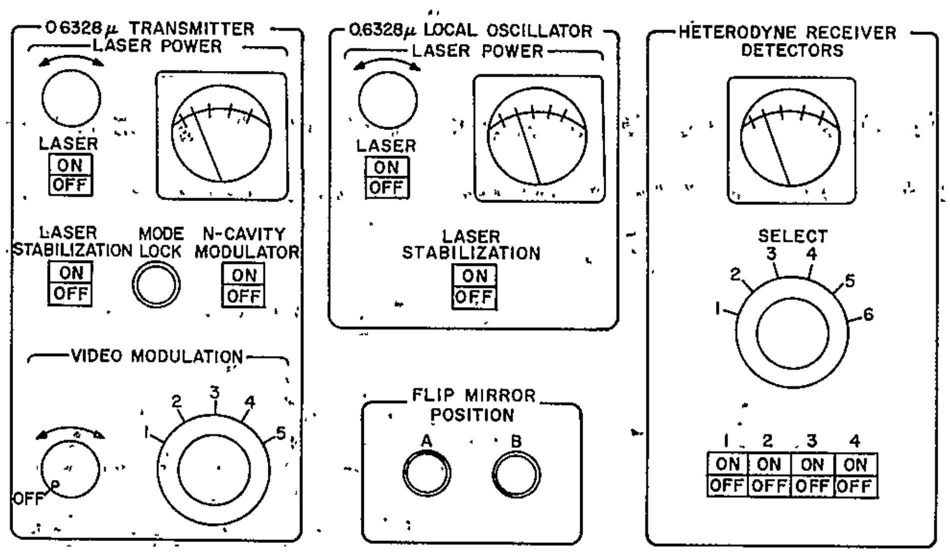

Figure 9.6.1.5-13. Panel, Telescope No. 3; Experiments 1,2,8, and 9.

Several portions of the spacecraft equipment shown, in the laser telescope block diagrams (figures 9.6.1.4-2, 9.6.1.4-3, 9.6.1.4-4, 9.6.1.4-5, and 9.6.1.4-6), are used for checking out the spacecraft laser transmitters, as described in the previous section. The equipments used for checkout include, for each laser telescope:

a. Transmission monitor, of both the average power level and the video signals modulated on the outgoing beams.

b. Laser input current and voltage meters.

c. Laser AFC circuits, with automatic out-of-limit status display indicators.

d. Laser Mode-Lock verification circuits, with panel indicators.

e. Boresighting mirror, with shutter.

f. Modulator and shutter for 0.4880-micron tracker calibration and balance.

g. Temperature sensors, in the laser package and the electronic units.

h. Oscilloscope display of all critical electronic test points.

i. Control and display panels for the laser transmitters in the crew cabin area.

The checkout and operation of the laser transmitters is relatively straightforward. They can be effectively monitored and operated by ground control. The required adjustments do not need special optical test fixtures, which might require a human being to be present to set up and to interpret the results.

9.6.1.5.2 Ground Equipment Test and Checkout

The ground-based equipment required for this experiment will include:

a. the 1.0-meter aperture heterodyne receiving telescope

b. pointing and positioning equipment

c. 0.6328-micron and 10.6-micron heterodyne receivers

d. receiving electronics and data handling equipment

e. control and display consoles for receiving telescope, receivers, data processing, and recording

f. 0.4880-laser beacon transmitter

g. microwave tracker to provide pointing information

h. spacecraft telemetry command and display

The ground-based equipment will be checked for operability before the experiment is begun. All of the lasers (0.4880-micron beacon, 0.6328-micron, and 10.6-micron local oscillators) will be turned on and thermally stabilized, and AFC circuits turned on. Cryogenic cooling will be supplied to the 10.6-micron heterodyne receiver. Internal checking of the receiving electronics will be done by injecting an optical signal directly into the photodetectors and checking the output against the input for gain and distortion. These functions will all be controlled from the ground station control consoles. Signal processing electronics will be self-checked in a similar manner.

The beacon modulator will be operated with selected test signals, and the beacon output will be measured. Pointing of the beacon will be done by using the inputs from the RF tracking stations such as Goldstone, and the RF tracking equipment at the optical ground site.

The 1.0-meter heterodyne receiving telescope is pointed at the spacecraft, using the same pointing signal inputs. More accurate pointing will be done after the spacecraft signal is acquired by the receiving telescope.

The RF telemetry system will be checked for operational status at the spacecraft status display and control console.

9.6.1.5.3 Experiment Performance

Radiosonde balloons will be released over a period of several hours prior to, and during, optical measurements, in order to record upper air conditions. Local meteorological conditions will be measured near the receiving telescope. When there is no interference from clouds, the spacecraft will be commanded to acquire the 0.4880-micron ground beacon, to begin fine tracking, and to transmit test signals on the optical down links. The pointing of the ground receiver and the beacon transmitter is updated, so that spacecraft and ground station are accurately illuminating each other. The modulation of the transmitter beams will be a selected narrow-band signal so that the receiver bandwidth may be narrowed accordingly, giving a good signal-to-noise ratio for the reduced signal intensities obtained with wide transmitter beamwidths.

As the pointing accuracy of the spacecraft is improved, the transmitter beam may be narrowed in increments and link performance determined as a function of beamwidth and pointing performance requirements of the spaceborne transmitter. Fading rate, signal dropouts, and signal-to-noise ratios may be determined for various bandwidths over extended periods of time. Various forms of modulation such as amplitude, polarization, and frequency modulation may be accomplished on the downlink by changing the operational mode of the modulators, at both the 0.6328-micron and 10.6-micron wavelengths.

The effective received coherence diameter will be measured over extended periods of time by varying the telescope entrance aperture diameter and measuring heterodyne mixing efficiency. These data will be displayed at the heterodyne receiver control console, and automatically recorded. Fluctuations in beam polarization will be continually measured, and unexpected anomalies displayed and recorded.

Phase noise introduced by the atmosphere will be measured, and selected portions of data will be recorded.

Many of these measured quantities may be varying at up to 1 kHz. Extensive pre- processing will be used before data are recorded. The magnitude of, and the statistical distributions of, the data are the most important information. Raw dat from the heterodyne receivers will be stored only while processing takes place, a then erased. Anomalous, or out-of-limit, data will automatically be retained for later analysis.

The duration of the heterodyne detection on Earth experiment will be determined primarily by weather conditions, and secondarily by the conflicting needs of other experiments, such as the transfer of tracking from one ground station to another. Data should be taken over periods of several hours at a time, especially when wea conditions are changing.

After the basic information on vertical-path propagation is built up, some further tests will be made. These include attenuating the transmitted beam at the spacecraft to simulate signals from planetary ranges, detection of signals under very high background conditions, and comparison of various types of modulation and coding formats.

9.6.2 Optical Heterodyne Detection in Space

Earth satellites have opened new areas of investigation in the atmospheric sciences. One important aspect of optical propagation in a turbulent atmosphere (Section 9.1) is the behavior of a coherent laser beam transmitted from the Earth's surface into space. Such a beacon signal could be extremely useful as: (a) a reference for spaceborne precision tracking and pointing devices (paragraphs 9.6.5, 9.6.6, and 9.6.7), (b) an optical communication uplink, and (c) a possible technique for planetary atmosphere analysis. Yet, the character of such a beam is neither theoretically described nor has it been measured. A spaceborne heterodyne receiver monitoring a ground-based laser transmitter can measure both the amplitude and phase perturbations on the signal due to the atmospheric disturbance.

A coherent propagation link will be established from Earth to the OTAES spacecraft (figure 9.6.2-1). Propagation theory indicates that a disturbance introduced in the near field will cause perturbations which should differ significantly from those produced when an identical disturbance is introduced in the far field. At visible frequencies, the atmosphere constitutes a disturbance in the near field on the uplink and in the far field on the downlink. This experiment (paragraph 9.6.2), when performed in conjunction with the space-to-Earth experiment (paragraph 9.6.1), can provide simultaneous up- and downlinks. Both direct and heterodyne optical receivers will be used aboard the spacecraft for comparison under a variety of atmospheric conditions. Such measurements would support the body of theoretical work which attempts to define, both qualitatively and quantitatively, the effects of a turbulent atmosphere on the propagation of optical waves, and would develop the fundamental basis for extrapolating the tracking and pointing experiments (paragraphs 9.6.5, 9.6.6, and 9.6.7).

This experiment can only be usefully performed in space. Data must be gathered for a long enough time to permit meaningful statistical analysis and correlation with gross measurables such as winds, temperature profiles, humidity, and seeing. Measurements will be most valuable at small zenith angles where ground-based measurements provide very limited data. Measurements from high altitude balloons can give limited but useful preliminary results incorporating much, but not all, of the sensible atmosphere in weather conditions suitable for balloon launching. Aircraft tests are not feasible because of the high vibration and turbulence environment. A comparison of heterodyne measurements made over the ground-to-space path with those made in the opposite direction along the same path will aid in understanding the detailed properties of the atmosphere and extend existing solutions of the turbulence theory.

9.6.2.1 Justification

Atmospheric theory suggests that a narrow beam transmitted through the whole atmosphere to an orbiting satellite may suffer severe breakup, or "tearing."

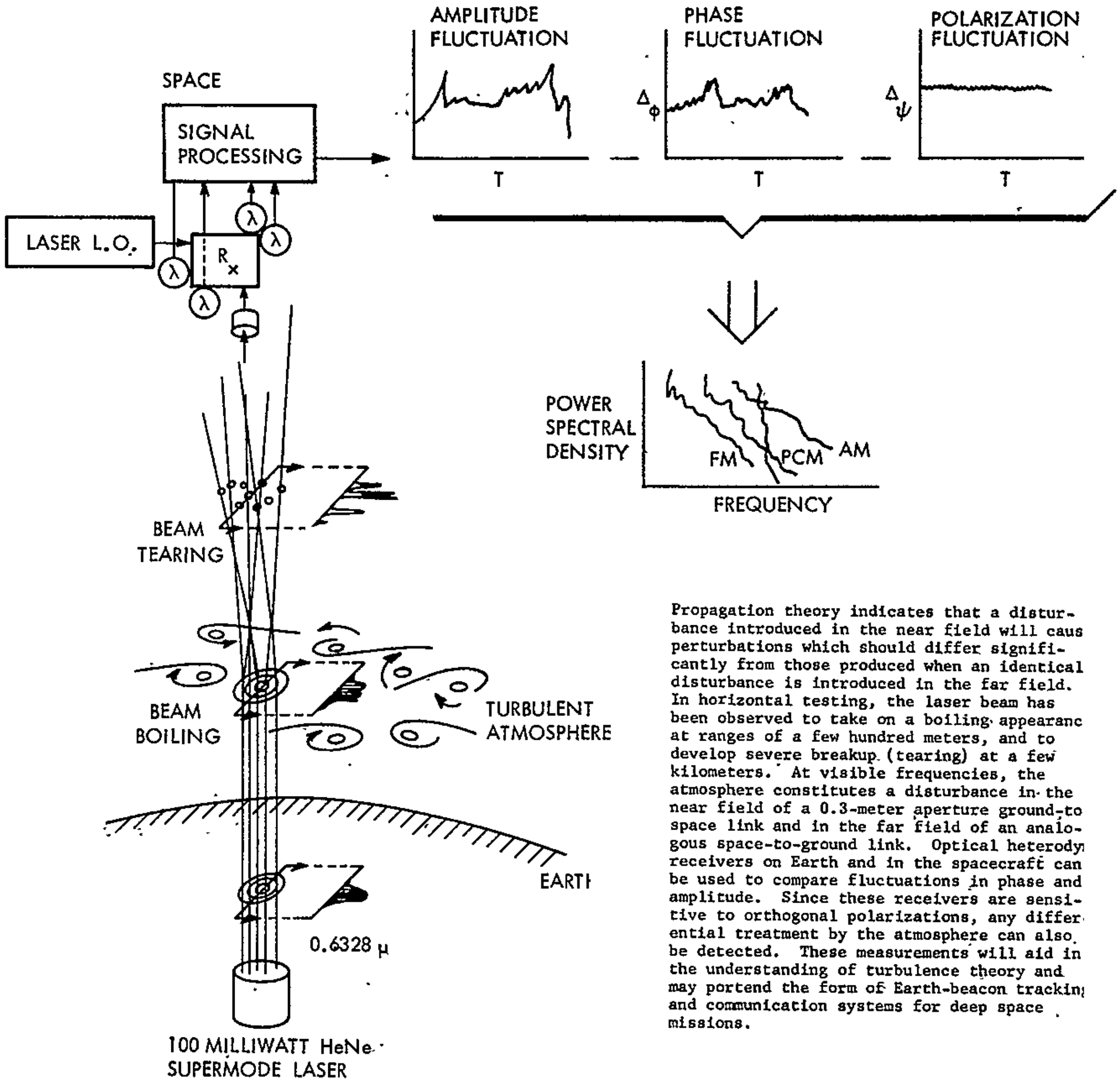

Propagation theory indicates that a disturbance introduced in the near field will caus perturbations which should differ significantly from those produced when an identical disturbance is introduced in the far field. In horizontal testing, the laser beam has been observed to take on a boiling appearanc at ranges of a few hundred meters, and to develop severe breakup (tearing) at a few kilometers. At visible frequencies, the atmosphere constitutes a disturbance in the near field of a 0.3-meter aperture ground-to space link and in the far field of an analogous space-to-ground link. Optical heterody receivers on Earth and in the spacecraft can be used to compare fluctuations in phase and amplitude. Since these receivers are sensitive to orthogonal polarizations, any differential treatment by the atmosphere can also be detected. These measurements will aid in the understanding of turbulence theory and may portend the form of Earth-beacon trackin and communication systems for deep space missions.

Figure 9.6.2-1. Optical Heterodyne Detection in Space.

Evaluation of such a theoretical finding could impact the development of precision Earth beacon tracking techniques as well as the obvious support to physical theory. In horizontal propagation, the transition from a beam-boiling appearance to gross beam-tearing (characterized by spots whose size seems independent of further increases in range) occurs at ranges in excess of 5 km.(1, 2) Along slant and near-vertical paths, this critical range should extend to tens of kilometers. Hence, measurements should be taken well above the turbulence layers (20 km). The measurement altitude should thus be greater than 40 km, the present bound on test aircraft and balloon operation.

A heterodyne receiver in space can provide the data needed to determine the types and rates of modulation that can be supported by the atmosphere. The results of this experiment can also help to establish the design choices for future laser communication systems since wavelength, modulation, and detector techniques can only be decided on the basis of a thorough knowledge of atmospheric effects. For this reason, various modulations will be placed on the link. The quantities to be measured in space are received signal power, heterodyne signal power, and fluctuations in both polarization and phase.

9.6.2.2 Experiment Design

By implementing a ground-to-space heterodyne link, it will be possible to determine scintillation spectra, optical phase fluctuations, and polarization fluctuations (paragraphs 9.1.3.1 and 9.1.3.5) in the absence of significant angle-of-arrival effects, which are always present in space-to-ground measurements. By imposing various modulations, it will also be possible to find the types and rates of modulation which can be supported by the atmosphere, and these can be compared with downlink measurements. Should future system designers consider adaptive optical communication from space to Earth, an optical uplink could sense the capacity of the transmission path for adaptive feedback purposes. Polarization measurements will be useful in evaluating polarized light communication techniques. Phase measurements can be used to assess optical phase or frequency modulation methods.

The functional description of the heterodyne uplink is identical to that for the heterodyne downlink given in paragraph 9.6.1.2. Indeed, simultaneous operation of two identical functioning links is important. However, location of the transmitter on the ground will permit detailed instrumentation differences, chief of which will be the use of a single-frequency (super-mode) laser. The 0.6328-micron receiver in

---

(1) W. R. Hinchman and A. L. Buck, "Fluctuations in a Laser Beam over 9 and 90 Mile Paths," Proc. IEEE (Correspondence), vol. 52, March 1964, pp. 305-306.

(2) J. R. Whitten, G. F. Prehmus, and K. Tomiyasu, "Q-Switched Laser Beam Propagation over a 10-Mile Path," Proc. IEEE (Correspondence), vol. 53, July 1965, p. 736.

the 1.0-meter spaceborne telescope will be essentially identical to the ground receiver described in paragraph 9.6.1.4.2. A similar 0.3-meter spaceborne 0.6328-micron receiver will provide additional field of view and backup reliability.

An argon beacon will be available (paragraph 9.6.5) for uplink direct (energy) detection experiments at 0.488 micron. Although this beacon could be instrumented as a ground-based heterodyne transmitter, severe problems are associated with the implementation of a spaceborne 0.488-micron heterodyne receiver which primarily have to do with the feasibility of developing the laser local oscillator having high enough stability and reliability. They are:

a. A development program about 24 months long will be required to evolve a laser design with the lifetime and reliability needed for the OTS missio There is at this time no reasonable assurance that the desired result will in fact be obtained. The present problems are in designing laser tubes to withstand the high current densities needed without erosion of the tube walls and electrodes.

b. The primary electrical power needed by the Argon laser local oscillator cannot be reduced below the 250-watt level, even for output powers of a few milliwatts. This high power drain not only imposes restrictions on the performance of other experiments but creates a serious heat dissipation problem inside a telescope well.

c. The Argon laser tube will need cooling with a circulating fluid. Simple radiative cooling of the laser tube will not be adequate. The vibrations set up by the fluid flow and pump will make the stabilization of the cavity length difficult, as well as couple into the pointing and tracking experiments. In addition, the 0.4880- and 0.6328-micron wavelengths are close together, so that atmospheric perturbations on the two wavelength will be nearly identical.

The 10.6-micron wavelength attainable with the highly efficient CO_2-N_2 laser is also an interesting subject for experimentation. Here, the arguments against a 10.6-micron heterodyne uplink revolve about detector technology. In the infrare region, photomultipliers are not available; hence, diode detection or photoconductive detectors will be required. Present bulk detectors are noisy. Their per formance could be improved by incorporating cooled spectral filters such that the detector does not see the total blackbody radiation from the optical antenna surfa Ideally, photon noise-limited operation would then prevail. However, tests with narrow detector fields of view indicate that with background noise removed sensitivity may still be limited by other noise mechanisms in the detector. This uncertainty in present development and the need for cryogenic cooling in the spacecraft to achieve kilohertz bandwidths dictates omission of a 10.6-micron heterodyne uplink.

A narrow-band 10.6-micron (energy) detection measurement on the spacecraft will be included in the direct detection experiment (paragraph 9.6.3).

9.6.2.3 Measurement Objective

A ground-to-space link will be established to make measurements of the phase and amplitude scintillation on the upgoing beam without the additional perturbing effects of angle-of-arrival and coherence diameter fluctuation. The spacecraft will receive 0.6328-micron radiation through either the 1.0-meter aperture or the 0.3-meter aperture (figure 9.6.2.3-1).

Several parameters will be measured at the spacecraft heterodyne receivers. They are:

a. Amplitude fluctuation of heterodyne signals.

b. Frequency (or phase) fluctuations in the heterodyne signals.

c. Polarization fluctuation: Since each heterodyne receiver is sensitive to orthogonal polarizations, any differential treatment by the atmosphere can be detected.

Circularly polarized light will be transmitted from the ground for most experiments, so that any atmospherically induced depolarizing effects can be analyzed at the spacecraft.

Various modulators will be used, as in the spacecraft transmitter, in order to evaluate their effectiveness on an optical uplink, whose scintillation properties are not the same as a downlink. Optical AM, FM, and Polarization PCM modulation will be used in turn, under various weather conditions.

9.6.2.4 Equipment Design

The block diagram of the equipment required for the Optical Heterodyne Detection on the Spacecraft experiment is shown in figure 9.6.2.3-1. The 0.6328-micron ground transmitter will be made up of the following subsystems: (a) super-mode laser with its power supply, mode stabilization controls, and automatic frequency control; (b) electro-optic modulator with the modulation driver, power supply, and signal source. The telescope, including secondary optics, beam deflection subsystem, and pointing and tracking controls, will be shared with the beacon. Each spacecraft receiver will be made up of the following subsystems: (a) spacecraft telescope, including its secondary optics, beam deflection subsystem, and pointing and tracking controls; (b) dichroic mirror; (c) optical filter; and (d) duplex heterodyne receiver.

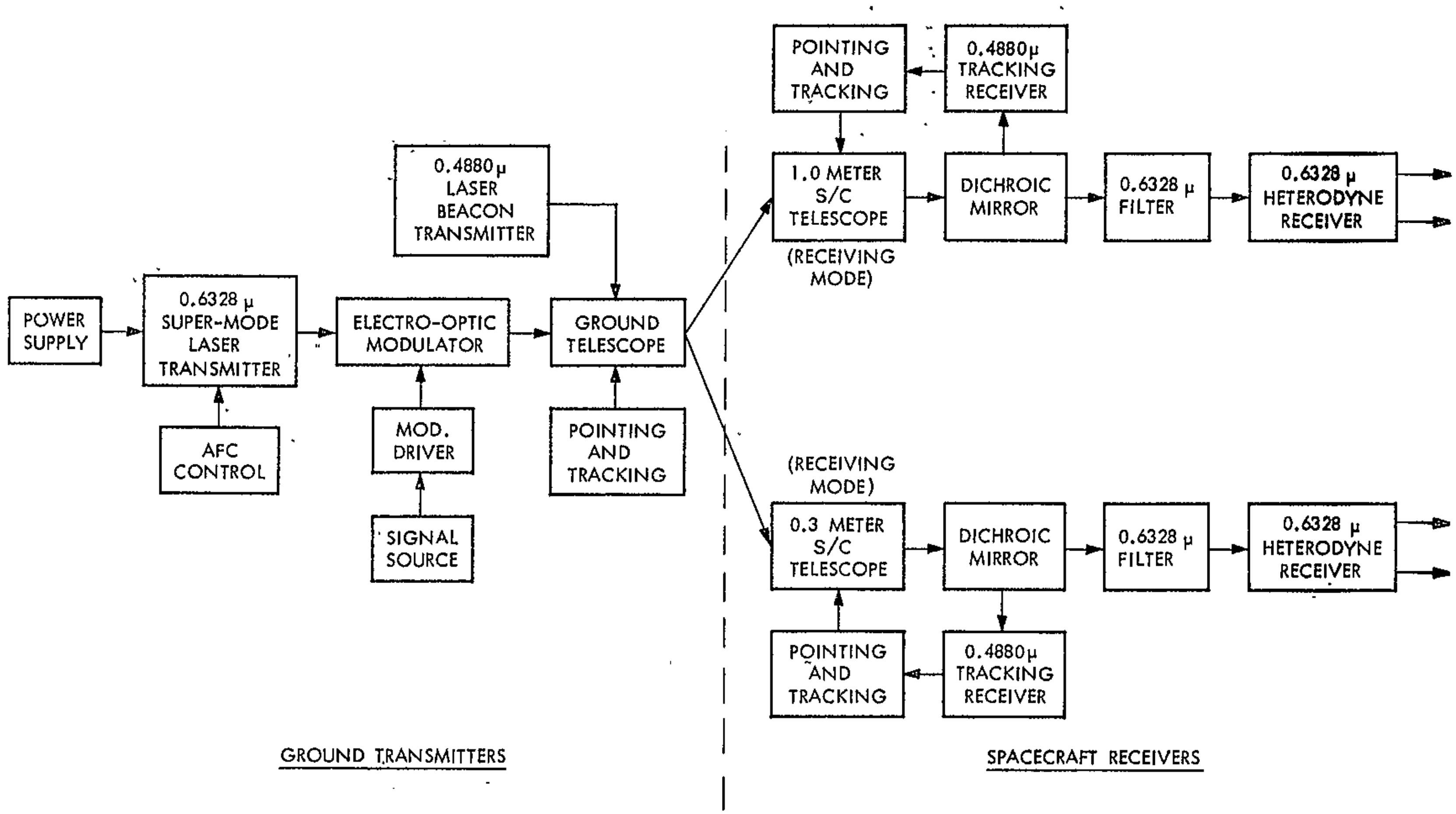

Figure 9.6.2.3-1. Block Diagram of Heterodyne Detection on the Spacecraft Experimen

The locations of the heterodyne receivers are in telescope no. 1 and no. 3 (see figures 9.6.1.4-3 and 9.6.1.4-5 for equipment block diagrams within each of these telescopes). A flip mirror is used within each telescope to convert between transmitting and receiving modes. One of the telescopes can be receiving while the other is simultaneously transmitting.

9.6.2.4.1 Spaceborne Receivers

The spaceborne receivers for the heterodyne detection experiments will be, like the ground receivers, polarization diversity receivers that can process orthogonal polarization states simultaneously. The spaceborne heterodyne receiver may enjoy the immense advantage of being able to use the entire area of the collector efficiently outside of the atmosphere. All optical components can be used at their diffraction limit.

The heterodyne receiver configuration is shown in figure 9.6.2.4.1-1. The received, circularly polarized energy is picked off by a flip mirror and sent to the receiver unit. Within each unit, the received energy is prefiltered and then retarded by a quarter-wave plate, which converts right or left circularly-polarized input radiation into orthogonal plane polarized beams. These are then separated by a polarization-sensitive prism and sent to one of two basic heterodyne receivers. Both basic receivers are fed by the same laser local oscillator, but are sensitive to opposite polarizations. This configuration is called a polarization diversity optical heterodyne receiver. It is capable of processing the two polarization channels simultaneously. The local oscillator's power is divided equally by a beam splitter between the two channels. The beams are superimposed at the two mixer beam splitters. Their directions and phase fronts are matched so that they will beat coherently to produce a signal at their difference frequency at the output of the detector. This is then amplified by the IF amplifiers.

Each of the polarization channels uses two detectors in a balanced mixer configuration. The signals from the two detectors are out of phase because of the phase reversal produced on the light by reflection at the beam splitter. One of the legs of the circuit has an inverter that restores the signal to its correct polarity. Then it is added to the signal from the other leg, and a heterodyne signal of full amplitude is obtained without wasting any of the incoming signal light or any of the local oscillator power. This configuration is used for heterodyne reception in both telescopes.

The frequency of the laser local oscillator must be stabilized to a fixed frequency offset from the frequency of the optical signal being received. The difference frequency to be detected must lie within the bandpass of the photodetector. In the visible

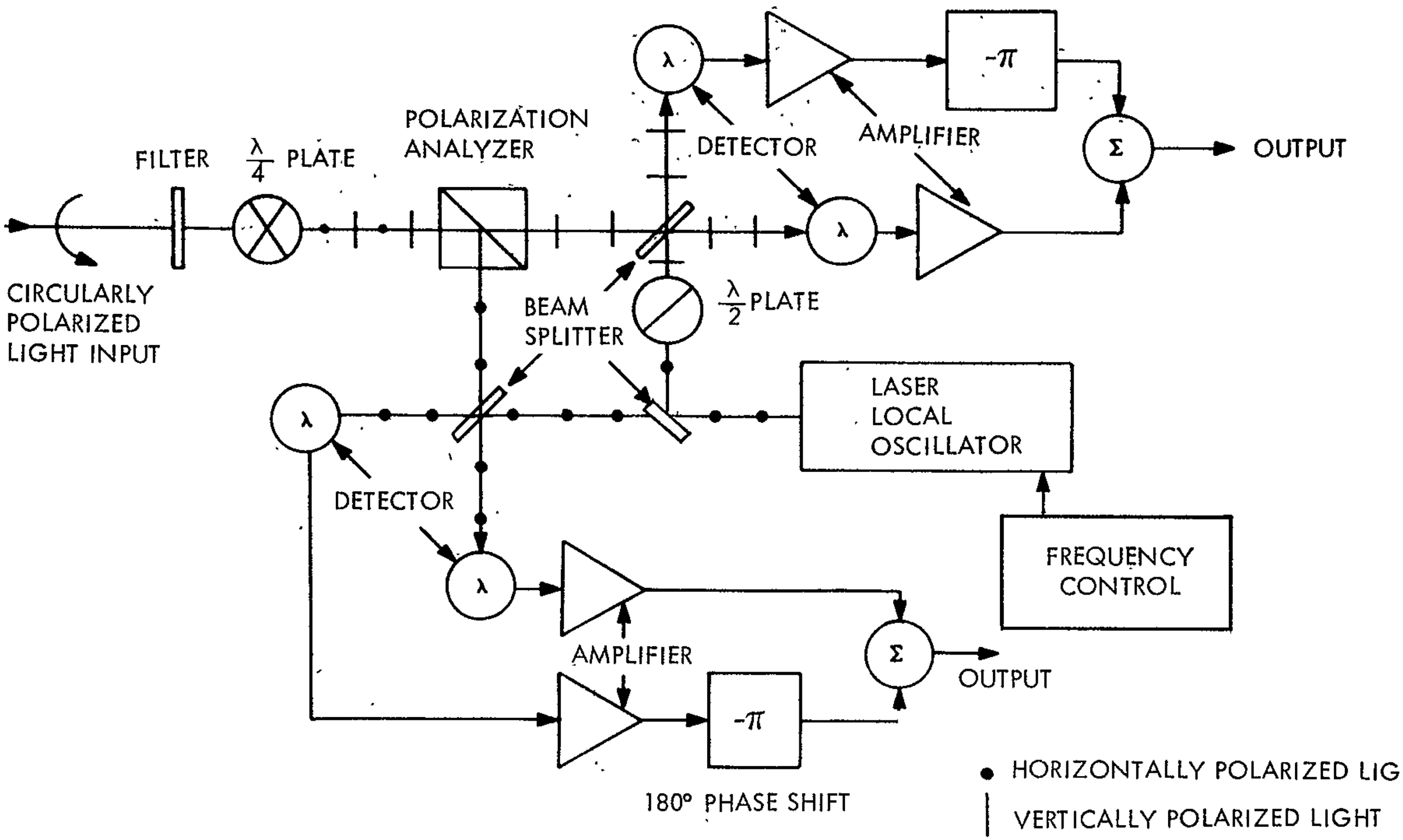

Figure 9.6.2.4.1-1. OTAES Polarization Diversity Heterodyne Receiver.

and near infrared spectrum, there are available broadband detectors [3,4] that permit the laser local oscillator to operate as far as 3 GHz away from the frequency of the incoming signal. A second electronic conversion with a tracking local oscillator can always move the signal to a convenient intermediate frequency.

In the past few years several frequency stabilized lasers have been constructed. A variety of methods are now suitable for the development of a frequency stabilized local oscillator laser to be used in the spacecraft. [5,6,7,8,9] The most common laser is the short single frequency laser with about 0.25 mW output at 0.6328 micron. Multimode lasers may also be stabilized. [10] Typically line widths of about 2 parts in 10^{10} or 0.1 MHz is ordinarily obtained. [6,8] The methods which employ a frequency dither will have a residual FM modulation that can be about 5 MHz. [5,6]

For the OTAES experiment a simple mirror tuning system that maximizes the L. O. laser output power is sufficient; once a signal from the ground station is acquired the AFC system will use it as a first-order reference and track at a fixed frequency offset.

---

(3) M. B. Fisher, "A Multiplier Travelling Wave Phototube," presented at the Conference on Electron Device Research, University of Illinois, Urbana, Ill., June 23, 1965 (to be published).

(4) L. K. Anderson, L. A. D'Asaro, and A. Goetzberger, "Microwave Photodiodes Exhibiting Microplasma--Free Carrier Multiplication," Appl. Phys. Lett., vol. 6, no. 4, February 15, 1965.

(5) W. R. C. Rowley and D. C. Wilson, "Wavelength Stabilization of an Optical Laser," Nature, vol. 200, 1963, p. 745.

(6) Koichi Shimoda, "Frequency Stabilization of the He-Ne Laser," IEEE Trans on Instrumentation and Measurement.

(7) A. D. White, E. I. Gordon, and E. F. Labuda, "Frequency Stabilization of Single Mode Gas Laser," Appl. Phys. Lett., vol. 5, 1964, p. 97.

(8) M. S. Lipsett and P. H. Lee, "Laser Wavelength Stabilization with a Passive Interferometer," Appl. Optics, vol. 5, 1965, p. 823.

(9) A. D. White, "A Two-Channel Laser Frequency Control System," IEEE Journal of Quantum Electronics (Correspondence), vol. QE-1, 1965, p. 322.

(10) S. E. Harris, M. K. Oshman, B. J. McMurtry, and E. O. Ommann, "Proposed Frequency Stabilization of the FM Laser," Appl. Phys. Lett., vol. 7, 1965, p. 185.

(11) A. Heller, "A High-Gain Room-Temperature Liquid Laser: Trivalent Neodymium in Selenium Oxychloride," Appl. Phys. Lett., August 1, 1966.

A. Lempicki and A. Heller, "Characteristics of the $Nd^{+3}SeOCl_2$ Liquid Laser," ibid.

9.6.2.4.2 Ground Transmitters

The requirements for a ground-based laser transmitter are the same, in essence, as those for the spaceborne transmitters. Stable single-frequency operation is needed, and this will be obtained in the same way as in the spacecraft transmitter system, i.e., with a combination of mode-coupling techniques and acoustic isolation. However, the ground transmitter is not subject to the constraints which led to elimination of the super-mode technique on the spacecraft. Thus, using the super-mode technique, the ground transmitter can transmit nearly all of its power in a single frequency.

For the He-Ne laser at 0.6328 micron, the FM laser-supermode laser technique can be used to convert the output of a multimode laser to a single frequency, and simultaneously to stabilize the output frequency to a point near the laser line center.[12,13] The optical configuration of a frequency-stabilized, multimode, single-frequency output laser is shown in figure 9.6.2.4.2-1. The resonant cavity of the laser system is formed by an opaque mirror at one end and a highly reflective mirror at the other end. Inside the cavity formed by the mirrors is a laser tube that provides gain, and a phase modulator that is made of a material such as KDP, which has a high electro-optic coefficient. When the phase modulator is driven with a frequency that is very near to the frequency spacing between the axial modes of the laser itself, the modes become coupled together and are converted from independent free-running oscillations into mutually dependent, coupled oscillations at nearly the same optical frequencies. The amplitude and phase of each of the previously independent oscillations is altered by the presence of significant coupling between the modes, so that the laser modes become sidebands of a single, coherent signal. Both AM and FM coupling have been observed.[14,15]

The FM mode coupled, or "FM laser," has an additional advantage, however: the light inside the cavity is effectively frequency-modulated at a rate controlled by the intra-cavity phase modulator, and the amount of AM distortion on this signal strongly depends on the optical frequency difference between the center of the FM mode pattern and the center of the fluorescence line. This dependence can be used to measure the absolute frequency drift of the mode pattern, and thus the drift in the cavity mirror separation, and to provide an error signal to correct drift or jitter as it occurs.

---

(12) S. E. Harris, M. K. Oshman, B. J. McMurtry, E. O. Ammann, "Proposed Frequency Stabilization of the FM Laser," Appl. Phys. Lett., vol. 7, no. 7, October 1, 1965, p. 185.

(13) S. E. Harris and B. J. McMurtry, "Frequency Selective Coupling to the FM Laser," Appl. Phys. Lett., vol. 7, no. 10, November 15, 1964.

(14) S. E. Harris and O. P. McDuff, "FM Laser Oscillation--Theory," Appl. Phys. Lett., vol. 5, no. 10, November 15, 1964.

(15) E. O. Ammann, B. J. McMurtry, and M. K. Oshman, "Detailed Experiments on He-Ne FM Lasers," IEEE Journal of Quantum Electronics, vol. QE-1, no. 6, September 1965.

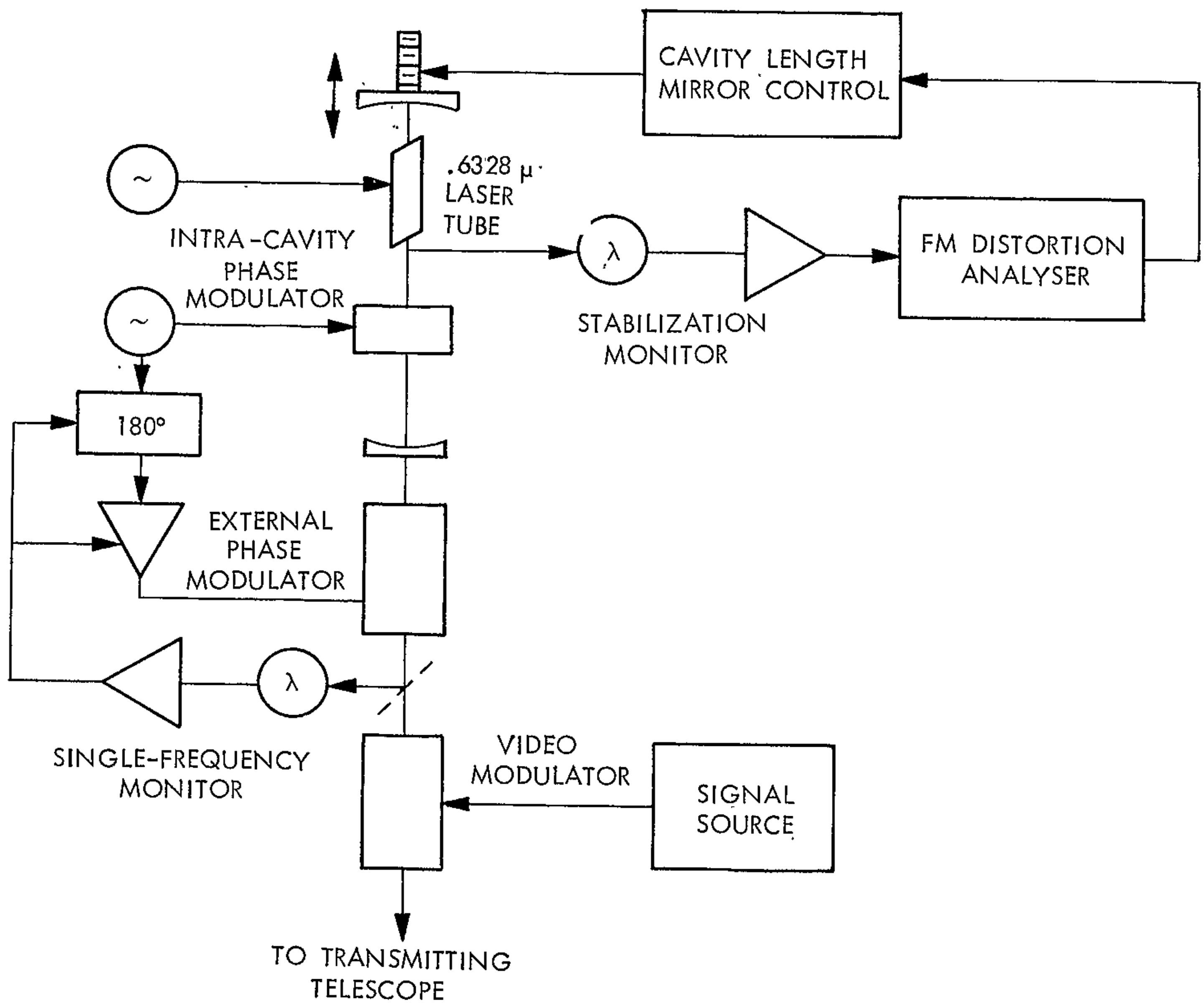

Figure 9.6.2.4.2-1. Single Frequency Super-Mode Laser Transmitter.

The multiple frequencies in the laser output can also be combined coherently into a single frequency, because of the fact that they all have the amplitudes and phases equivalent to a single FM-modulated optical carrier. An external optical phase modulator, driven 180 degrees out of phase with the FM-locking intracavity modulator, acts on the light beam to "un-modulate" it, and restore all sideband power into a single carrier frequency. An FM laser can thus be stabilized and deliver its full power into a single frequency simultaneously.

Two feedback control systems are needed in order to operate the laser in this way. They are:

a. The Laser AFC Subsystem. This subsystem monitors the AM distortion on the FM light within the laser cavity and adjusts the cavity length to the correct value. This is accomplished by moving one end mirror with a piezoelectric transducer. In this fashion the spectrum of oscillating modes can be placed on the center of the resonance fluorescence line of the laser.

b. The Super-Mode Modulator Subsystem. The drive power to the external modulator must always be adjusted to produce inverse modulation; i.e., equal and opposite to the FM modulation coming from the laser. This is accomplished by sensing any residual FM (or AM) sidebands on the output beam and driving them to zero, by adjustment of the gain and phase shift circuits driving the external modulator.

The major equipment necessary to conduct optical heterodyne detection in space is listed below. The spaceborne equipment can be operated by the astronaut using the left-hand panels shown in figure 9.6.2.4.2-2 or, alternatively, from the optical ground station using console 3 (figure 9.6.2.4.2-3).

SPACEBORNE EQUIPMENT

a. 0.6328-MICRON DUPLEX HETERODYNE RECEIVER - (Two Identical Units; One Located in 1-Meter Telescope and Other in 0.3-Meter Telescope)

Local Oscillator Laser Assembly Specifications:

Wt. - 15 lbs. L - 8 in. Dia. - 6 in.

He-Ne Laser (Single Frequency)
Narrow-band Interference Filter - 0.6328 micron
Quarter Wave Plate and Polarization Compensator
Polarization Analyzer/Optical Mixer Subassembly
Shutter
4 Wideband Photomultiplier Photodetectors

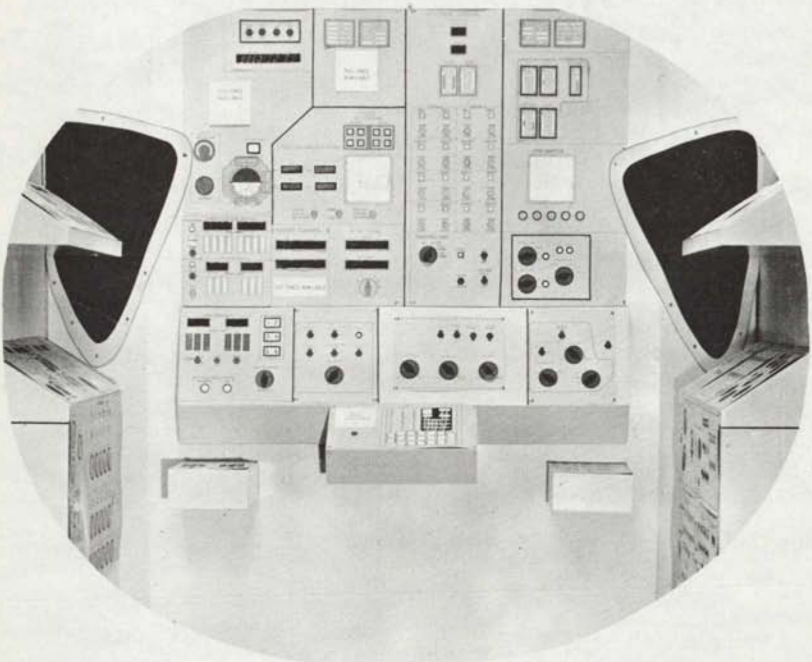

Figure 9.6.2.4.2-2. Mockup of Interior of LM/OTAES Spacecraft.

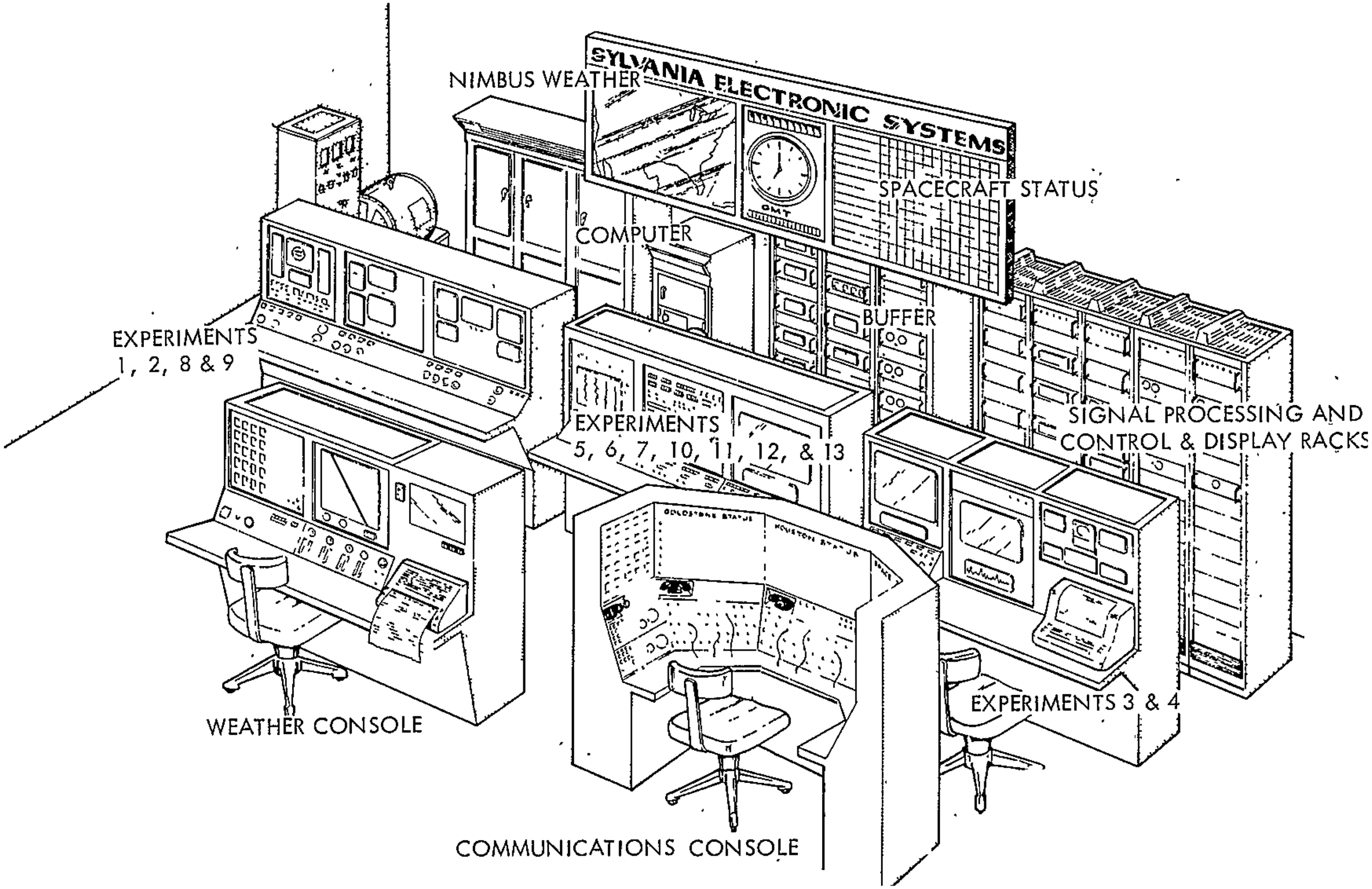

Figure 9.6.2.4.2-3. OTTOS/OTAES Control Room.

Photomultiplier Control and Power Circuits
Signal Processing and Demodulation Circuits
Laser Control and Power Circuits
Cavity Tuning Control and Frequency Stabilization Circuits
Power Monitor

b. 1.0-METER RECEIVING TELESCOPE WITH SUITABLE BEAM COMBINING OPTICS

c. 0.3-METER RECEIVING TELESCOPE WITH SUITABLE BEAM COMBINING OPTICS

d. SIGNAL WAVEFORM ANALYZER/DISPLAY UNIT

e. TELEMETRY SIGNAL CONDITIONER CIRCUITS

GROUND BASED EQUIPMENT

a. 0.6328-MICRON LASER TRANSMITTER ASSEMBLY

He-Ne Laser (100-milliwatt single frequency "supermode")
Main Control and Power Circuits
Cavity Tuning Control and Frequency Stabilization Circuits
Stabilization Circuit Photodetector and Preamplifier
Internal Cavity and External Supermode Modulator
Internal Cavity and External Supermode Modulator Driver Amplifier
Internal Modulator and External Supermode Control and Power Circuits
Output Power Monitor
Pupil Matching Telescope

VIDEO MODULATOR SUBASSEMBLY

Modulator
Modulator Control and Power Circuits
Modulator Driver Amplifier
Signal Generator or Encoder
Photodetector and Preamplifier
Signal Comparator

b. 0.5-METER TRANSMITTING TELESCOPE WITH SUITABLE BEAM COMBINING OPTICS

c. EXPERIMENT CONTROL, SEQUENCING, AND MEASUREMENTS SYSTEM

Signal Processing Circuits
Telemetry Signal Storage/Computation Facilities
Heterodyne Up-Link Control/Display Console (Transmitter and Receive: Waveform Display)

9.6.2.4.3 Feasibility

The development of ground-based optical heterodyne receivers has advanced to a point where the design considerations can now be extrapolated for use in a satellite-borne heterodyne receiver. The local oscillator laser has not yet been developed and qualified for space applications, but a reasonable design can be developed based on the present state-of-the-art of lasers and present knowledge of the space environment. Alignment of the various elements making up the heterodyne receiver can be maintained under the rigors of launch, using standard optical assembly techniques such as drilling and pinning each element in position after final alignment has been accomplished. Detectors for spacecraft application are available for all frequencies of interest, but require cooling to 30°K or lower for the far infrared wavelengths. The ground equipment and facilities needed for this experiment are within the present state-of-the-art.

For the visible wavelength of 0.6328 microns, critical components such as modulators, beam splitters, detectors, optical elements and their coating have been demonstrated in environments similar to those expected for this OTAES experiment. Design and space qualification testing of lasers must be started soon since laser reliability and lifetime estimates are still low. Only the laser and the heterodyne receiver assembly remain to be space tested. However, earth-based optical heterodyne links have been demonstrated over kilometer distances. The most critical parameter is the frequency stability of the spaceborne laser local oscillators, which brings about the requirement that they be acoustically decoupled from their surroundings.

9.6.2.5 Data Management

The signal processing electronic subsystems will operate in the same fashion as their ground-based counterparts; AM, FM, and Polarization PCM signals can be received, and the laser local oscillator will track the received signal at a fixed frequency offset as described in paragraph 9.6.1.4.1. The pseudo-random signal comparison technique (section 28.0) will be used for display and recording in the normal data management mode. However, the true signal from the spacecraft heterodyne receivers can be displayed to the crew, using either an oscilloscope or TV monitor-type display. The status of the frequency tracking (AFC) circuits will be displayed with out-of-status warning lights, indicating loss of lock-on or excessive frequency jitter due to spacecraft vibrations. Laser input electrical power and optical output power will be displayed with panel meters.

The equipments aboard the spacecraft can be operated from either the astronaut console panels (figures 9.6.1.5-2, 9.6.1.5-3, and 9.6.1.5-4) or from console 3 in the ground station OTTOS-OTAES Control Room (figures 9.6.1.5-7, 9.6.1.5-9, 9.6.1.5-10, 9.6.1.5-11, 9.6.1.5-12, and 9.6.1.5-13). These spaceborne equipments include:

a. either the 1.0-meter (no. 1) or the 0.3-meter (no. 3) gimbaled telescope, in a receive mode

b. an 0.4880-micron tracker for telescope no. 1 and/or no. 3

c. a 0.6328-micron laser local oscillator

d. heterodyne receiver detectors, electronics, and data handling equipment

e. RF telemetry and beacon system

9.6.2.5.1 Spacecraft Equipment Test and Checkout

To assure satisfactory performance, the equipment alignment and tuning must be optimized and periodically repeated. Tuning of the laser to obtain optimum efficiency will be done by adjusting the laser mirror controls to maximize output power for fixed input power. Laser AFC circuits are automatic in operation and require only recheck of status indicator lamp. Telescope fine tracking functions are also automatic once they are initiated.

Several portions of the spacecraft equipment in laser telescope nos. 1 and 3, whose block diagrams are shown in figures 9.6.1.4-3 and 9.6.1.4-5, are used for checking out the laser local oscillators and heterodyne receivers, as described in the previous section. The equipments used for checkout in these two telescopes include

a. Local oscillator laser power output meter

b. Laser input current and voltage meters

c. Laser tuning and AFC circuits, with lock-on display indicator

d. Shutter for blocking local oscillator radiation out of the photodetectors during initial adjustments

e. Temperature sensors in the laser package and the electronic units

f. Oscilloscope display of all critical electronic test points

g. Control and display panels for the laser local oscillators in the crew cabin area

The checkout and operation of the heterodyne receivers consists mostly of electronic adjustments. They can be effectively monitored and operated by ground control. The required adjustments do not need special optical test fixtures, which might require a human being to be present to set up and to interpret the results.

9.6.2.5.2 Ground Equipment Test and Checkout

The ground-based equipment required for this experiment will include:

a. The 0.5-meter aperture transmitting telescope

b. Pointing and positioning equipment

c. 0.6328-micron and 10.6-micron laser transmitters, including modulators

d. Power supplies and electronic data handling equipment

e. Control and display consoles for transmitting telescope, transmitter lasers, data processing, and recording equipment

f. 0.4880-laser beacon transmitter

g. Microwave tracker to provide pointing information

h. Spacecraft telemetry command and display

The ground-based equipment will be checked for operability before the experiment is begun. All of the lasers (0.4880-micron beacon, 0.6328-micron and 10.6-micron transmitters) will be turned on and thermally stabilized, and AFC circuits turned on. Internal checking of the modulator electronics will be done by injecting a signal directly into the modulator and checking the modulated output against the input for gain and distortion. These functions will all be controlled from the ground station control consoles. Signal processing electronics will be self-checked in a similar manner.

The beacon modulator will be operated with selected test signals, and the beacon output will be measured. Pointing of the beacon will be done by using the inputs from the RF tracking stations such as Goldstone, and the RF tracking equipment at the optical ground site.

The 0.5-meter transmitting telescope is pointed at the spacecraft, using the same pointing signal inputs. More accurate pointing will be done after the signal is acquired by the receiving telescope on the spacecraft.

The RF telemetry system will be checked for operational status at the spacecraft status display and control console.

9.6.2.5.3 Experiment Performance

Radiosonde balloons will be released over a period of several hours prior to, and during, optical measurements, in order to record upper air conditions. Local meteorological conditions will be measured near the transmitting telescope. Whei there is no interference from clouds, the spacecraft will be commanded to acquire the 0.4880-micron ground beacon, to begin fine tracking, and to receive test signa on the optical uplinks. The pointing of the ground transmitter and the beacon trans mitter is updated, so that the spacecraft is accurately illuminated by the ground station. The modulation of the transmitter beams will be a selected narrow-band signal so that the receiver bandwidth may be narrowed accordingly, giving a good signal-to-noise ratio for the reduced signal intensities obtained with wide transmit beamwidths, of a few milliradians.

As the pointing accuracy of the beacon is improved, the ground transmitter beam may be narrowed in increments and link performance determined as a function of beamwidth and pointing performance requirements of the spaceborne receiver. Fading rate, signal dropouts, and signal-to-noise ratios may be determined for various bandwidths over extended periods of time. Various forms of modulation such as amplitude, polarization, and frequency modulation may be accomplished on the uplink by changing the operational mode of the modulators, at both the 0.6328-micron and 10.6-micron wavelengths.

Fluctuations in beam polarization will be continually measured, and unexpected anomalies telemetered to the ground and displayed. These data will be displayed at the heterodyne receiver control console, and automatically recorded.

Phase noise introduced by the atmosphere will be measured, and selected portions of data will be telemetered and recorded.

Many of these measured quantities may be varying at up to 1 kHz. Extensive pre-processing on the ground will be used before data are recorded. The magnitudes of, and the statistical distributions of, the data are the most important information. Telemetered raw data from the heterodyne receivers will be stored only while processing takes place, and then erased. Anomalous, or out-of-limit, data will automatically be retained for later analysis.

The duration of the heterodyne detection in space experiment will be determined primarily by weather conditions, and secondarily by the conflicting needs of other experiments, such as the transfer of tracking from one ground station to another. Data should be taken over periods of several hours at a time, especially when weather conditions are changing.

After the basic information on vertical-path propagation is built up, some further tests will be made. These include attenuating the transmitted beam, detection of signals under very high background conditions, and comparison of various types of modulation and coding formats.

9.6.3 Direct Detection on Earth

One potential application for lasers is communication at very long ranges. But, before an optical communication link can be proposed as an operational tool, its efficacy must be established. A foundation of spaceborne optical communication engineering data must be obtained to allow comparison with conventional techniques. The preceding experiments have treated the optical heterodyne technique. Direct detection also applies as an alternative communication form that has planetary distance potential.

There are three salient advantages to the direct detection concept: system simplicity, lenient pointing tolerances, and an advanced state of ground-based development. In fact, direct detection system tests can be implemented on OTAES by defocusing the telescope, in the same fashion that is prerequisite to the precision tracking experiment (paragraph 9.6.5), and by using the optical heterodyne transmitter. Thus, at the expense of a few logic elements in its test program sequencer, the OTAES spacecraft can be adapted for the direct detection experiment.

There is a second advantage to the inclusion of a direct detection link in OTAES: probability of experiment success. In the direct system, beam pointing and collimation requirements are traded off at the expense of enlarging the ground-based optical collector, thereby enhancing the reliability of the space-to-earth communication link. Since those atmospheric measurements predicated upon amplitude and polarization sensing can be accomplished with the spaceborne optical transmitter in the direct detection communication mode, inclusion of the direct detection link enhances the success of that portion of the atmospheric experiments.

The one element of an optical direct detection system that remains to be developed is the large, earth-based optical collector (depicted in figure 9.6.3-1). For a meaningful comparison (i.e., in a planetary communication context) with alternative techniques, this aperture should be 8 meters in diameter. In this size, solar furnace technology and conventional RF antenna tracking techniques apply.

Given such an earth-based receiving system and a relaxed tolerance spaceborne laser transmitter, portions of the 10-MHz communication, pulse distortion, and fading experiments can be accomplished. To be of full value to atmospheric physicists and to develop meaningful space-to-earth communication engineering data, such measurements must be made through the whole atmosphere. This atmospheric measurement requirement, and the opportunity to make exact and simultaneous comparison with an alternative communication form, constitute the justification for performing the direct detection optical communication experiment in space.

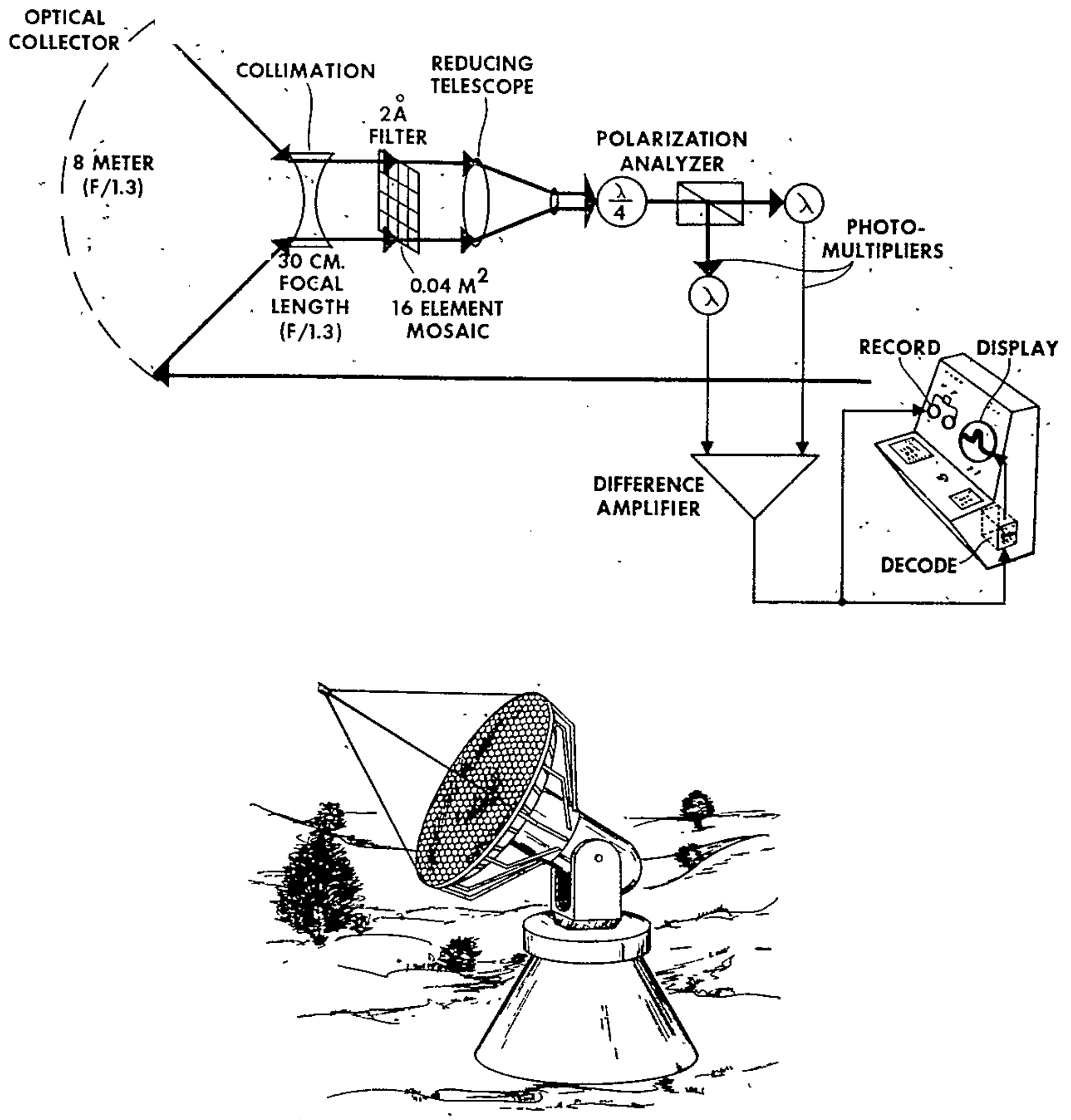

Figure 9.6.3-1. Direct Detection Telescop

9.6.3.1 Justification

The frequently expressed need [1] for television bandwidth deep space-to-earth data links suggests the use of a wide bandwidth laser communication system in which all the short wavelength optical energy can be concentrated into a very narrow diffractioı limited beam by using relatively small apertures. Assuming all other factors to be equal, the narrower the beamwidth the greater the capability of the communication system. However, the ability to transmit submicroradian beams with apertures less than a meter in diameter presents the designer with problems of precision pointing, alignment, and atmospheric refraction effects comparable in difficulty to those of the microwave communication system designer, who must construct and point massive space antennas in order to increase the present microwave systems capability.

The Direct Detection Optical Communication System concept, shown in figure 9.6.3.1-1, represents a compromise of the theoretical ultimate. In direct or energy detection, the light beam is detected directly by a photocell that is sensitive to changes in input beam power. This is analogous, in the RF spectrum, to the early crystal sets. However, since the direct detection optical communication system is independent of the atmosphere coherence diameter limitation, a large aperture collector can be used. A large receiving aperture will provide an excess of aperture gain that may be traded off to relax the pointing requirements both on the earth and in the spacecraft, preserving the capability for megahertz bandwidth communications. The direct detection system technique accepts a detector efficiency of 10^{-1}, laser efficiencies of 10^{-4}, pointing accuracies of tens of microradians, and non-diffraction-limited optics. The signal-to-noise ratio for an optical communication link using direct detection, neglecting dark current in the photodetector, is (paragraph 9.9.2.3):

---

(1) M. C. Adams, Hearings before the Committee on Science and Astronautics, United States House of Representatives, Eighty-ninth Congress, February 23, 24, 25, and 28 thru March 1, 2, 3, 7, and 8, 1966, Part 4, p. 97.

A. J. Kelley, "NASA's New Electronic Research Center," Astronautics and Aeronautics, vol. 3, no. 5, May 1965, pp. 58-63.

H. E. Newell, Hearings before the Committee on Aeronautical and Space Sciences, United States Eighty-ninth Congress, March 22, 23, 24, 25, and 30, 1965.

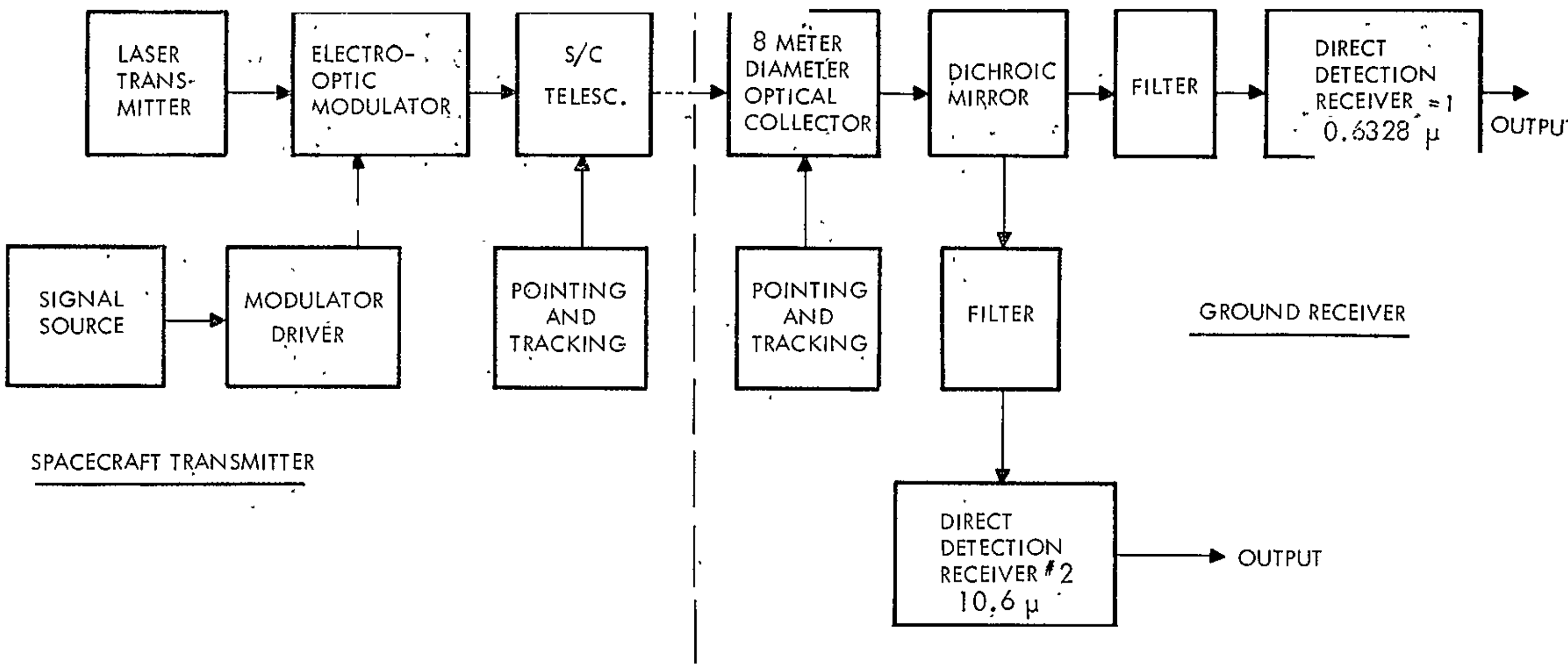

Figure 9.6.3.1-1. Direct Detection on the Ground.

$$\frac{S}{N}_{\text{Space to Ground}} = \left(\frac{P_t \rho A_r T_o T_A}{2e\Delta f \Omega_t R^2}\right)\left\{\frac{1}{1 + \dfrac{\Omega_r N_\lambda \Delta\lambda}{\dfrac{P_t T_A}{\Omega_t R^2}}}\right\}$$

where

ρ = The responsivity of the photo-surface $= \frac{e\eta}{h\nu}$
P_s = The signal power received at the photomultiplier (watts)
P_B = The background power received at the photomultiplier (watts)
e = The electronic charge
Δ_f = The electrical noise bandwidth of the system (hertz)
η = Quantum efficiency (number of charge carriers per photon)
h = Planck's constant
ν = Optical frequency (hertz)
Ω_r = The field of view of the receiver
N_λ = Average spectral radiance of the sky in the optical filter bandwidth, Δ_λ, as measured at the telescope receiver aperture, A_r
P_t = Transmitted power (watts)
Ω_t = Transmitter half-power solid angle beamwidth (steradians)
A_r = Effective area of the receiver collecting optics (Square meters)
T_o = Optical transmission
T_A = Atmospheric transmission
R = Range (meter).

The term in the first parentheses is the expression for signal photon noise-limited operation. The term in the second parentheses represents the effect of background in reducing the signal-to-noise ratio for signal photon noise-limited operation. The 8-meter collector can thus be used to compare direct detection to heterodyne optical communication techniques in 24-hour earth orbit at visible frequencies.

The background problem at 10.6 microns is less severe than at 0.63 micron. The background power incident upon the detector is small compared to the total black-body radiation from the optical antenna that is viewed by the detector.

Solving for the transmitter radiance (paragraph 9.9.2.3) gives:

$$\frac{P_t}{\Omega_t} = \frac{R^2 \left(\frac{S}{N}\right)_v (\Delta f A_c)^{1/2}}{D^* T_o T_A A_r}$$

where

$\left(\frac{S}{N}\right)_v$ = The voltage signal-to-noise ratio

P_s = The signal power in watts

Δ_f = The noise bandwidth in hert

A_c = The detector area in cm^2.

Typical D* values of Ge-Hg[5] are 3×10^{10} $\frac{cm(Hz)^{1/2}}{watt}$ for an f/1.3 detector aperture ratio and a $4^{o}K$ operating temperature. The minimum area of the detector, determined by the optics circle of confusion, would be $0.25\ cm^2$

Using the parameters from table 9.6.3.1-1 in addition to those properties of the detector, and requiring a 30-dB signal-to-noise ratio, the required transmitter radiant intensity is

$$\frac{P_t}{\Omega_t} = 7 \times 10^7 \text{ watts/steradian}$$

Hence, t S CO_2-N_2 laser is adequate to demonstrate 10-MHz Direct Detection communication using the OTAES 0.3-meter transmitting aperture ($\Omega_t = 1.4 \times 10^{-8}$).

9.6.3.2 Experiment Design

This experiment will provide a high-confidence link for atmospheric propagation measurements and will compare alternative optical communication forms. The specific objective is to evaluate the performance of a wideband space-ground laser communications technique that uses state-of-the-art components, but does not require diffraction-limited optics, extreme pointing accuracy, or excessive power consumption.

The implementation of a direct detection experiment in earth orbit would thus test and evaluate a simple laser communications system concept, and provide means for performing atmospheric propagation measurements. As lasers and detectors are made more efficient and as space optical and pointing problems are solved, the direct system will then become a means for high data-rate optical communications at interplanetary distances

TABLE 9.6.3.1-1
TYPICAL VALUES REQUIRED FOR DIRECT DETECTION EXPERIMENT

System Parameters	Space-to-Ground Noncoherent
Range	3.22×10^7 meters (20,000 miles)
Laser Power (a)	10^{-3} watts
Beamwidth (a)	1.4×10^{-5} radians
Wavelength	6.328×10^{-7} meters (6328 A)
Filter Bandwidth (b)	2 A
Modulation Type	Polarization
Filter Transmission (b)	0.4
Nominal Optics Efficiency	0.75
Nominal Atmospheric Transmission (c)	0.5
Typical Background Radiance Observed by Receiver (d)	Blue Sky at Zenith (*) 2×10^1 watts/m^2-stermicron
Optical Collector Area	50 meters^2
Minimum Receiver Field of View	5×10^{-4} radians
Phototube Type	S-20 (C70038D)
Peak Signal to RMS Noise (a)	30 dB
System Bandwidth	10 MHz

(a) Possible system parameters as indicated on curve.
(b) Spectralab mica interference filter.
(c) Less than standard clear atmosphere at 60° from zenith.
(d) Angle of sun and observer neglected for simplicity.

(*) F. Moller, "Optics of the Lower Atmosphere," Applied Optics, vol. 3, no. 2, February 1964, p. 161.

The development of a space-to-ground direct laser communications technology with interplanetary capabilities requires the development of a spacecraft transmitter and ground-based receiver techniques. In addition to critical component development, numerous experiments are required to develop design parameters affected by transmission of laser beams down through a turbulent atmosphere. Furthermore, once a system has been designed it should be constructed and then tested to determine its performance. This could be accomplished partially by using balloon-borne laser sources and receivers.

In evaluating the alternative to spaceborne equipment, it is necessary to determine the minimum requirements for developing direct detection technology. The direct detection system is a communications system. Its design objective is to minimize the fading effects introduced by the atmosphere. It is insensitive to wavefront phase distortion and can operate either in the near or far field of a transmitter.

Turbulent air containing eddies of different index of refraction produces the seeing and scintillation effects commonly observed by astronomers. (2) Generally speaking, there are two regions of turbulent air. The common seeing effects such as angle of arrival, defocusing, shimmer, etc., all occur in the turbulent layer within a few hundred feet of the ground. A second region of turbulence is within 10,000 feet of the tropopause. Scintillation or intensity fluctuations for the most part originate in this region which is at altitudes between 20,000 and 60,000 feet, depending upon location to the earth. The subject of atmospheric characteristics is discussed more thoroughly in section 9.1.

Scintillation is introduced at the tropopause. A simple model of this effect is that a corrugated shaped interface produces a corrugation in a wavefront passing through the region. For starlight, mottled light and dark areas are produced at the earth's surface. Protheroe (3) has measured the correlation distance of starlight at the earth's surface to be 11 inches. In his measurements the predominant structure size of the light and dark patterns range between 5 and 10 inches. Laser light, because of its single frequency would have a finer structure. The direct detection system antenna is composed of approximately 900 12-inch diameter elements. If the structure scintillation is random, the root mean square fluctuation is approximately $\sqrt{900}$ and the signal fluctuation would be 3 per cent.

In fact, the observed structure is often only the order of 0.03 to 0.04 meter. (4) The 8-meter diameter aperture area is 50 m^2. Thus, if the structural area is 10^{-3} meter^2, then the root mean square fluctuation would be 0.5 per cent.

---

(2). G. Kuiper and B. Middlehurst, Telescopes, University of Chicago Press, 1960, pp. 138-139.

(3) W. Protheroe, "Determination of Shadow Band Structure from Stellar Scintillation Measurements," J. Opt. Soc. Am., 1956, p. 851.

(4) J. Meyer-Arendt and C. Emmanual, "Optical Scintillation," NBS Technical Note 225, April 1966, p. 31.

9.6.3.3 Measurement Objective

The probability of success of the direct detection experiment is high. The experiment does not add complexity to the spacecraft and yet allows a relaxation of laser pointing and beam forming. Thus, the experiment provides a highly reliable mean to measure fading depth and fading rate statistics for noncoherent communications between space and ground.

It also provides a high gain antenna to facilitate the measurement of channel bandwidth and provides an intense point source in space to facilitate testing of the large aperture optical antenna and the comparison of laser light with starlight and sunlight. Following the communications experiments and the development of new key components, the direct detection technique would be available to deep space communications problems.

9.6.3.4 Equipment Design

The implementation of the optical communication system for direct detection optica communication from space-to-ground is shown in the block diagram in figure 9.6.3.1-1. The laser transmitter will produce an output of the selected wavelength.

The ground-based receiver, shown in figure 9.6.3-1, will be an 8-meter diameter optical collector made of long focal length hexagonal mirrors approximately one foot across. Each mirror would be an f/30 parabolic or spherical surface.. The overall optical collector would be a nominal, moderate quality f/1.3 system. Th ultimate resolution could be less than 0.1 milliradians. It would be mounted on a large tracking mount to point and track the incoming signal. Pointing and tracking will be done open loop; that is, it will receive pointing and tracking data from another source and will position itself in accordance with the data, but will not generate any error information to correct the incoming data. The data must be accurate to within 0.05 milliradians. Secondary optics will provide a collimated beam for the direct detection receiver.

Figure 9.6.3.4-1 is a block diagram of the direct detection receiver. The dichroic mirror will be used to separate different operating wavelengths. In the 0.6328-micron receiver, the filter is used to reject much of the background radiation that would otherwise reduce the signal-to-noise ratio of the detected signal, and, under, conditions of high levels of background radiation, would overload the detector.

The filter pass-band will be 0.0002-microns wide, centered at the transmitted wavelength. For PCM/PL the quarter-wave plate will convert circularly polarized light to plane-polarized light.

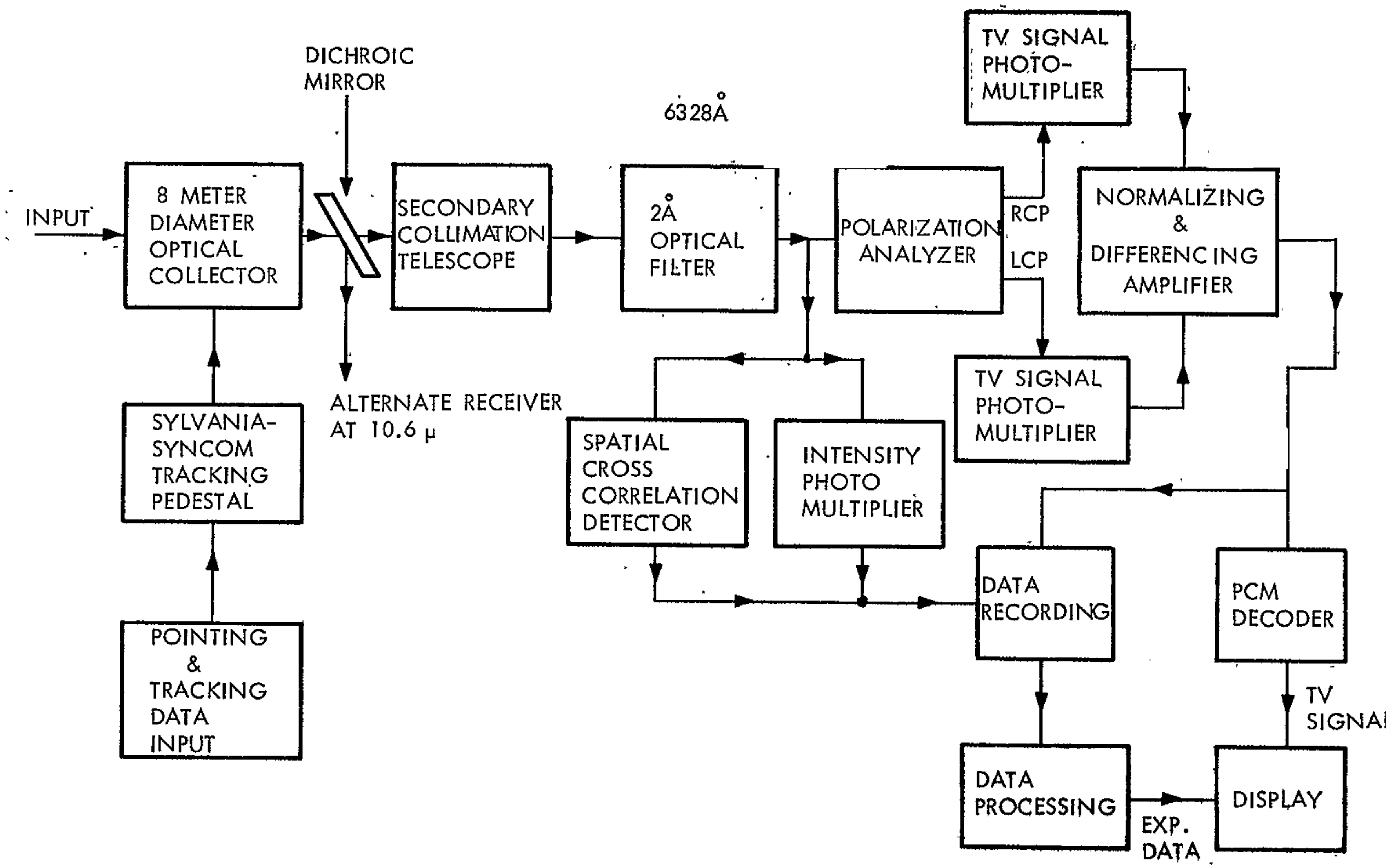

Figure 9.6.3.4-1. Ground Receiver for Direct System

Light entering the polarization analyzer will contain left and right circularly-polarized light. The analyzer will separate the two types of polarization. The detectors will convert the light energy to electrical signals, and the output will then be processed by the data-handling electronics to provide a display of the incoming data. The signal fluctuations observed in the intensity photomultiplier will be a measure of the fading depth and fading rate. The spatial correlation detector will provide a means of measuring signal correlation across the aperture.

9.6.3.4.1 Feasibility

The direct system has been designed to discriminate against sunlight scattering due to normal air and aerosol concentrations by using optical filters and restricting the optical field of view. The design of the direct system provides a means of discrimination against seeing and scintillation effects. A primary characteristic of the direct system concept is simplicity, reliability, and low cost. At 0.6328 microns, it can be implemented with state-of-the-art components. For example, in the direct space transmitter, the laser, beam-forming optics, laser pointing, the electro-optic modulator, and modulation driver have commercial counterparts in existence. A nominal 1-milliwatt laser approximately 30-cm long and 10-cm in cross-section, weighing 6 kg and requiring 10 watts of prime laser tube power, such as the Spectra Physics Model 130 laser, can serve as the starting point for the design of a space-qualified laser. In addition, the Sylvania V2 electro-optic modulator and solid-state modulation driver requiring 5 watts of power for 10-MHz modulation are the basis for the space optical modulator. Furthermore, the beam-forming optics for the direct system do not have to be diffraction limited. Small collimating telescopes for lasers, similar to the Spectra Physics Model 331 beam-expanding telescope, can easily form the beam required by the direct detection system.

Recent ground-to-air tracking experiments (5) have been performed using a narrow laser beam pointed at a retroreflector mounted on an aircraft. The return signal has been tracked at 14-km slant ranges with an accuracy of 25 microradians, rms. These experiments demonstrate accurate tracking and laser pointing in a turbulent atmosphere with the precision required for a direct detection optical communication link.

The 8-meter ground-based optical collector contemplated for this experiment is very similar to the 6.5-meter Narrabri Observatory multi-element optical collector. (6)

---

(5) R. F. Lucy, C. J. Peters, E. J. McGann, and K. T. Lang, "Precision Laser Automatic Tracking System," Applied Optics, vol. 5, April 1966, pp. 517-524.

(6) R. H. Brown, "The Stellar Interferometer at Narrabri Observatory," Sky and Telescope, vol. 28, no. 2, pp. 64-69.

H. Messel, and S. Butler, Space Physics and Radio Astronomy, MacMillan and Co., Ltd., London, 1964.

This array of 252 hexagonal segments can form a 3-milliradian star image. An existing Syncom [7] microwave antenna tracking mount design could be adapted for the 8-meter optical collector. This mount has demonstrated accuracies of 50 microradians when tracking celestial objects from programmed data sources.

9.6.3.5 Data Management

Direct system experiments must be performed and statistical data recorded under a variety of night and day conditions and zenith angles in order to adequately evaluate this mode of communication. Typical experiment variables, most of which are interrelated and uncontrollable, will be:

a. Meteorological conditions

b. Atmospheric path conditions

c. Background radiance

d. Angular location of sun and/or moon

e. Angular location of satellite.

In addition, it is desirable to perform these experiments at more than one laser frequency.

Most of the optical power measurements are straightforward. Total signal power and depolarization effects are measurable with the system detectors. Detailed examinations of portions of the input apertures for correlation measurements can be made by scanning the post focal region with a mechanical scanner or image tube. If simultaneous measurements are made across the aperture, the aperture scan rate must be much greater than the signal fluctuation rate. Angle of arrival fluctuations can be measured by observing signal motion in the optics focal plane. Available signal power, background, and bandwidth will limit the measurements and their accuracies. The relative accuracy of measurement will be equal to $\sqrt{S/N}$.

The ground station will determine the length of each run, based upon meteorological conditions, from real-time data processing and analysis. It will be necessary to collect both short- and long-term data.

In order to evaluate the space-to-ground direct system, the following measurements should be made. In each case, we are measuring and recording the output of photodetectors.

(7) Advent Ground Antenna Systems, Contract No. DA 36-039-SC-87365, U. S. Signal Supply Agency, Ft. Monmouth, N. J.

1a) Measure the magnitude of the received power to check losses and fading phenomena. In this experiment, the output of the photodetectors is continuously recorded (section 28.0) to provide a chronological record of the instantaneous received power. These data can be correlated with meteorological and spacecraft data to determine the intensity fading characteristics of the propagation path for the large aperture collector. This meas urement should show the ability of the large aperture collector to smooth scintillation introduced by the atmosphere.

1b) Measure the signal power in the post focal image plane of the large parabola to determine the point-by-point instantaneous intensity structure of the optical signal across the input aperture. In this experiment, a scanning photomultiplier or a matrix of detectors could be used to measure the intensity fading characteristic of each section of the large collector. A comparison of small sections with large sections can be made to determine intensity fading as a function of aperture size. This is an intensity cross-correlation experiment.

2) Determine the error rate and/or overall communication channel quality. In this experiment, modulation methods are being evaluated. Thus, if PCM or other pulse modulation is used, the receiver will measure the error rate. If analog modulation is used, the instantaneous received signal-to-noise is measured. The television signal will be monitored at the ground station to determine channel quality. In addition, signal depolarization effects produced by the atmosphere will be determined.

3) Measure the effects of varying the transmitter beamwidth on system parameters. In this experiment, two effects are being observed. One is attributable to lateral motion of the beam on the received signal. This would introduce a modulation on the signal received by the phototubes. The modulation would be a function of the beam intensity distribution and the beam motion as it sweeps across the aperture. The second effect would involve the communication channel bandwidth. As the beam is spread, multipath scattering effects introduced primarily at the tropopause will degrade the communication channel. This effect will become pronounced as the differences in multipath transit times approach the periodicity of the laser modulation signal. Thus, large beams may have a lower bandwidth than narrow beams because they illuminate scatterers traveled from the scattering effects in the tropopause, which are farther from the beam center. This measurement could be performed by the pulse distortion technique at several beamwidths.

On board the spacecraft, several equipments must be operated to perform this experiment. The equipment includes: (a) a 0.6328-micron laser transmitter, (b) a 1.0-meter telescope, (c) a 0.6328-micron direct detection receiver,

(d) a 10.6-micron laser transmitter, and (e) a 0.3-meter telescope strapped onto (b). The operation of this equipment to perform the Direct Detection experiment can be accomplished by the astronaut, using the left panels in figure 9.6.3.5-1, or from the OTTOS-OTAES Control Room on the ground (figure 9.6.1.5-5), using console 3 (figure 9.6.3.5-2).

9.6.3.5.1 Spacecraft Equipment Test and Checkout

Initiation and gross operation of the equipment have been described above. To assure satisfactory performance, the equipment alignment and tuning must be optimized. Alignment of the laser, modulator, and telescope can be determined by operating the boresight error measurement equipment on the control panel (figure 9.6.3.5.1-1) and determining the magnitude of this error. Adjustment of alignment controls will be made to minimize the boresight error. Tuning of the laser to obtain optimum efficiency will be done by adjusting the laser mirror controls to maximize output power for fixed input power.

9.6.3.5.2 Ground Equipment Test and Checkout

The ground-based equipment required for these experiments will include: (a) the large aperture (8-meter) receiver dish, (b) pointing and positioning equipment, (c) receiving electronics and data-handling equipment, and (d) ground station control console. Auxiliary to this equipment will be: (a) the ground beacon, (b) beacon modulator and drive equipment, and (c) the microwave tracker to provide pointing information.

The ground-based equipment will be tested by operating the beacon and measuring its output. The beacon modulator will be operated with selected test signals, and the beacon output will be measured. Pointing of the beacon will be done by using the inputs from the RF tracking stations such as Goldstone and, when possible, switching over to the optical fine tracking system when lock-on has been obtained.

When the spacecraft tracker is locked onto the ground beacon and is transmitting, the 8-meter dish will be pointed at the spacecraft and the receiving electronics will be activated. Internal checking of the receiving electronics will be done by injecting an optical signal directly into the photodetectors and checking the output against the input for gain and distortion. These functions will all be controlled from the ground station control consoles.

9.6.3.5.3 Experiment Performance

With the establishment of the down-communication link (spacecraft transmitter being received by the 8-meter diameter dish), the Direct Detection Experiment is ready to be performed. This experiment was developed on the basis that precise pointing

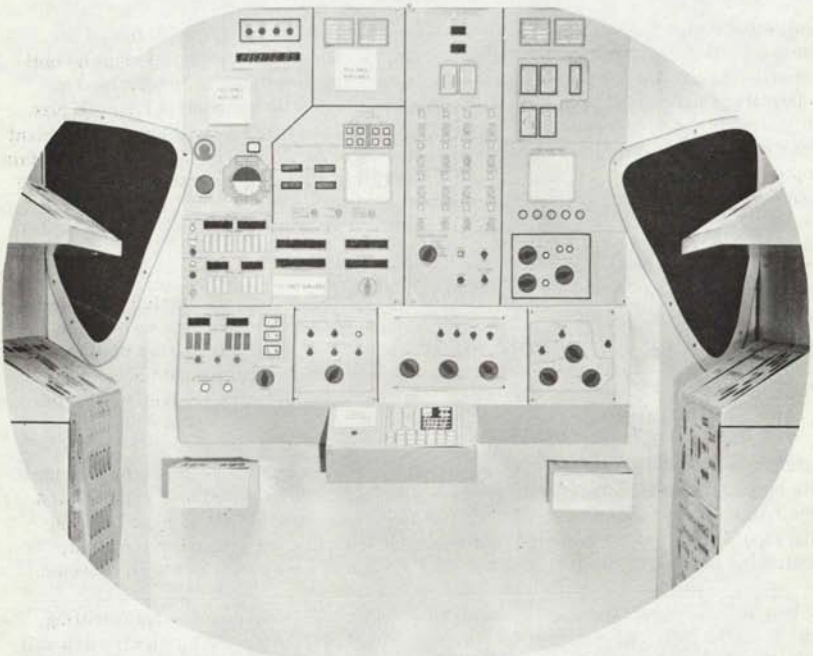

Figure 9.6.3.5-1. Mockup of Interior of LM/OTAES Spacecraft.

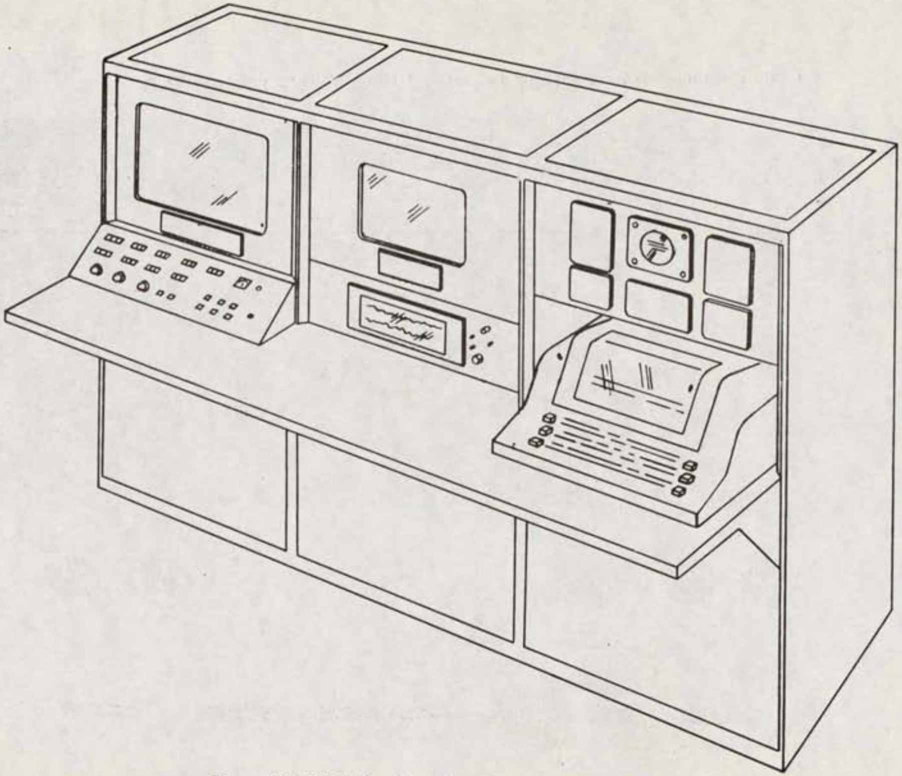

Figure 9.6.3.5-2. Console - Experiments 3 and 4

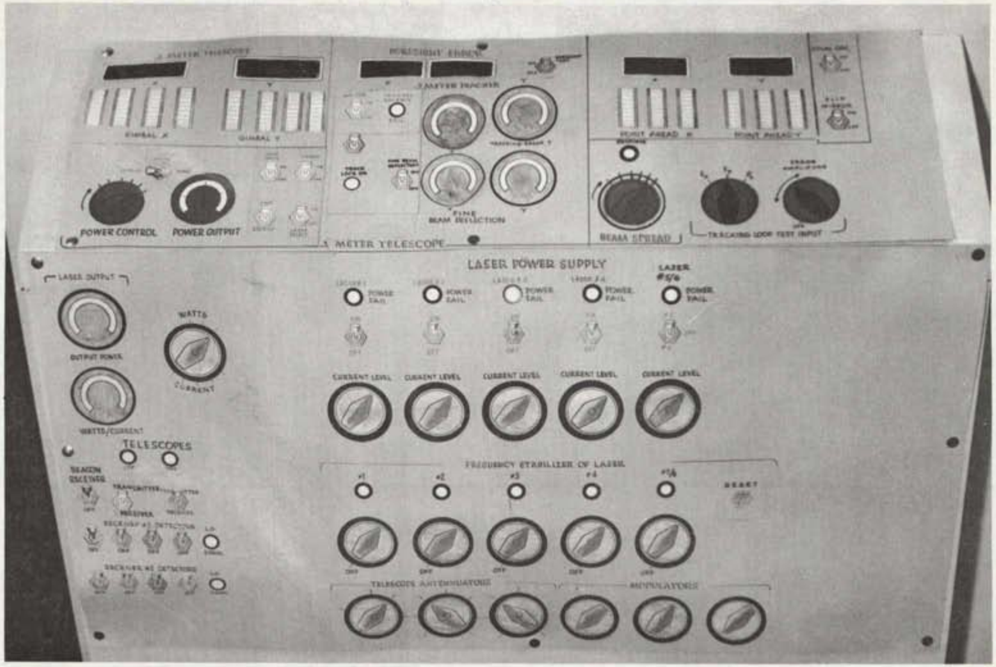

Figure 9.6.3.5.1-1. Panel, Laser and Starlight: Experiments 3 and 4

would not be needed for performance of the experiment; therefore, the spaceborne transmitter may be defocused to obtain a beam of 3 arc seconds. The modulation of the transmitter beam will be a selected narrow-band signal so that the receiver electrical bandwidth may be narrowed accordingly, giving a good signal-to-noise ratio for the reduced signal intensity.

The transmitter beam may be narrowed in increments and link performance determined as a function of beamwidth and pointing performance requirements of the spaceborne transmitter. Fading rate, signal dropouts, and signal-to-noise ratios may be determined for various bandwidths over extended periods of time. Various forms of modulation such as amplitude, polarization, and FM/AM may be accomplished on the downlink by changing the operational mode of the modulator.

It will be possible to use the direct detection link to measure beam shape of the transmitting laser in the spacecraft. A sinusoidal signal of predetermined amplitude and frequency can be used to drive the beam deflector, causing the beam to be swept in a sinusoidal manner across the receiving aperture. By inserting a very low-pass electrical filter in the tracker output signal line, the tracker will not correct for the sinusoidal variations but only for slow drift in the position of the spacecraft. Providing that the sweep frequency is within the range of operation of the receiver's bandwidth and capability of the beam deflector, the intensity of the beam may be plotted as a function of deflection voltage, which will have been previously calibrated as a function of beam angle. Beam axis and tracker offset may be determined with this procedure.

Modulation of the beacon signal will provide a communication uplink. Comparison of performance between the downlink and the uplink will determine the reciprocal and nonreciprocal characteristics of the propagation medium. The output of the spaceborne receiver will be telemetered back. The spaceborne receiver will not only measure the intensity of the signal but also polarization distortion, therefore requiring two receiver outputs -- one for intensity and one for polarization error.

9.6.4 Megahertz Optical Communication

The rapidly increasing data gathering capabilities of deep space probes have made necessary the development of techniques for transmitting data at maximum rates using a minimum of spacecraft power. The rate at which data can be transmitted varies directly as the bandwidth of the communication channel. Optical communication, using wide bandwidth modulation and detection techniques, offers a potential solution for this need. Very narrow beamwidths are obtainable at optical wavelengths using nominal apertures, providing high energy density in the beam for reasonable amounts of transmitted power. The high energy density will support wide bandwidth communication with high signal-to-noise ratio.

Performance of wide bandwidth optical communication systems can be analytically determined by making assumptions about the propagation path and assuming mathematically ideal system components. However, it can be expected that a communication system placed in orbit will depart from this mathematical ideal. Determination of the effect of these departures on system performance can best be measured by placing them in the orbital environment. Because the atmosphere is neither homogeneous nor isotropic, and because the applicable theory is not developed for the general case, it is necessary that the measurements be made along actual transmission paths through the entire atmosphere. The few measurements made to date have been over relatively short, nearly horizontal paths which cannot be considered representative of an actual space-to-ground transmission path. Present knowledge of the atmosphere does not permit accurate estimates to be extrapolated from measurements made along these horizontal paths. This can only be accomplished from an orbiting satellite (figure 9.6.4-1). Variations of the atmosphere and its effect on the system performance must be measured over a long time period to obtain statistical data. These measurements will be made simultaneously at different wavelengths. The atmospheric characteristics at several altitudes will be recorded during the measuring period for correlation with the communication data.

9.6.4.1 Justification

The experiment will gather and analyze engineering data that may be applied in evaluating alternative communication systems. The results will provide the information required to make a realistic assessment of the relative merits of optical and radio frequency communications. The optical measurements will compare different optical wavelengths and both coherent and noncoherent detection methods. Statistical data of fading depth and fading rates would be collected while propagating both ways along complete atmospheric paths at different zenith angles, weather conditions, and time of year. From the fading data the experiment would determine the relative merits of different forms of optical communication techniques.

The performance of a transmission medium in supporting wide bandwidth propagation is most positively determined by direct measurement. Although inference of performance may be made by measuring certain parameters which are considered to be most influential, this technique is not positive. Because of the variability of the atmosphere, continuous long-term measurements need to be made to gather statistically significant performance data. Transmission of signal energy through the whole atmosphere will be required to provide the necessary data. For ease of data reduction, a variable clock rate pseudo-random pulse code generator will provide the modulation of the signal. A synchronized generator on the ground will be used for detecting errors. Evaluation of error rate for different atmospheric conditions and several power levels will determine optimum power levels for the desired bandwidth, under given weather conditions.

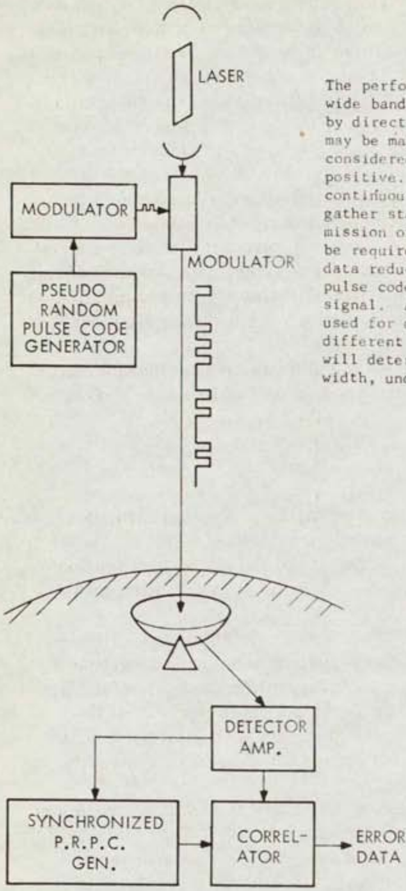

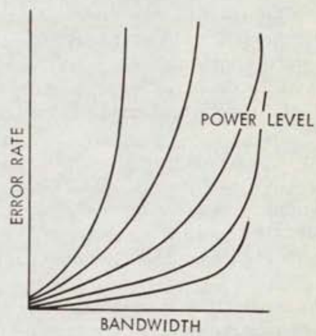

Figure 9.6.4-1. Communication with 10 MHz Bandwidth

In his congressional testimony, Newell (1) pointed out that approval of the Voyager program had to be delayed until a minimum communication capability of 8,000 bits per second could be assured. The data error rates associated with these bit rates are of the order of 5×10^{-3}. Reduced error rates can be obtained at the expense of bandwidth. Conversely, increased bandwidth can be obtained at the cost of greater error rates. It has been estimated by Kelley (2) that in the 1970-71 period, data needs for exploration of the near planets will require 10^7 bits per second system capacity.

Various combinational modulation forms have been used at radio frequencies to optimize satellite system performance for its analog and digital communication needs. Future space missions using optical communications will also have special characteristics, requiring a particular modulation form to optimize the performance for each mission. Development of performance data will provide communication system engineers a basis for optimizing the modulation form for each mission.

If it can be proven that an optical communication system can provide megahertz bandwidths at planetary ranges, the system performance of future space probes can be greatly enhanced.

9.6.4.2 Experiment Design

From the point of view of deep space optical communication, the signal transfer characteristics of the atmospheric transmission link are desired. For all except the most simple cases, results based on measurements of the actual propagation link will provide the most realistic solution to the problems of information transmitted through the whole atmosphere.

That is, the designer of an optical communications system of a space-to-ground link must know the statistical behavior of the noisy propagation medium before an efficient system can be designed. Knowledge of the fading characteristic of the medium will direct the engineer to choose between an analog or digital system, a threshold or nonthreshold detection technique, a redundant or nonredundant code.

If the modulation system chosen is analog, such as amplitude modulation, sufficient power reserve is necessary to provide full dynamic range in the midst of a deep fade. If a threshold system such as FM or PCM is chosen, the signal-to-noise ratio should not drop below a minimum level or severe degradation results. In

(1) H. E. Newell, Hearings before the Committee on Aeronautical and Space Sciences, United States Senate, Eighty-ninth Congress, March 22-25 and 30, 1965.

(2) A. J. Kelley, "NASA's New Electronics Research Center," Astronautics & Aeronautics, vol. 3, no. 5, May 1965, pp. 58-63.

addition, in order to provide a reliable message transmission by means of message redundancy, the duration and depth of fades must be known. Furthermore, the design of adequate automatic gain control systems requires fading depth (dynamic range) and fading rate (response time) data. Also, if diversity (multiple) transmission or reception techniques are to be employed, it is necessary to know the spatial dependence of the fading characteristics.

Another extremely important input to the engineer is the frequency and time spread introduced by the medium. Doppler effects produce frequency or phase distortion. Multipath transmission caused by scatter introduces transit time spread that distorts the message (figure 9.6.4.2-1). Time spread can also be introduced by index of refraction variations with frequency. All these effects tend to limit the channel bandwidth or information rate. Simple calculations (e.g., figure 9.6.4.2-1) show these effects are not important at optical wavelengths in the megahertz range but are important in the 100 MHz and above frequency range, and thus will tend to limit an outstanding potential of optical communication, namely ultrawide bandwidth. Consequently, to evaluate the ultimate potential of laser communication from space to ground, the channel bandwidth must be measured. This is especially important in modulation techniques such as FM or PCM where wider bandwidths are necessary to transmit narrower band information more efficiently than with straight analog amplitude modulation.

In addition, if polarization distortion occurs, the designer must know this to adequately design a system using polarization modulation. In noncoherent systems only intensity fluctuations and possibly polarization distortion are important. In coherent systems amplitude, phase, and polarization distortion data is necessary.

9.6.4.3 Measurement Objective

This experiment will provide the statistical data required to evaluate optical communication techniques at different wavelengths from space to ground and ground to space. Fading depth, rate, and duration data will be collected over different propagation paths under different weather and seasonal conditions in both directions. A minimum downlink channel bandwidth of 100 MHz will be verified, and a 10-MHz space-to-ground laser communications link will be established. Coherent and noncoherent detection techniques will also be compared.

The transmitter parameters to be measured on the spacecraft include laser power, laser noise, modulation, beam divergence, and pointing accuracy for each laser transmitter. In addition, all the optical receiver outputs, both coherent and noncoherent, would be monitored. On the ground the corresponding receiver and transmitter measurements would also be made.

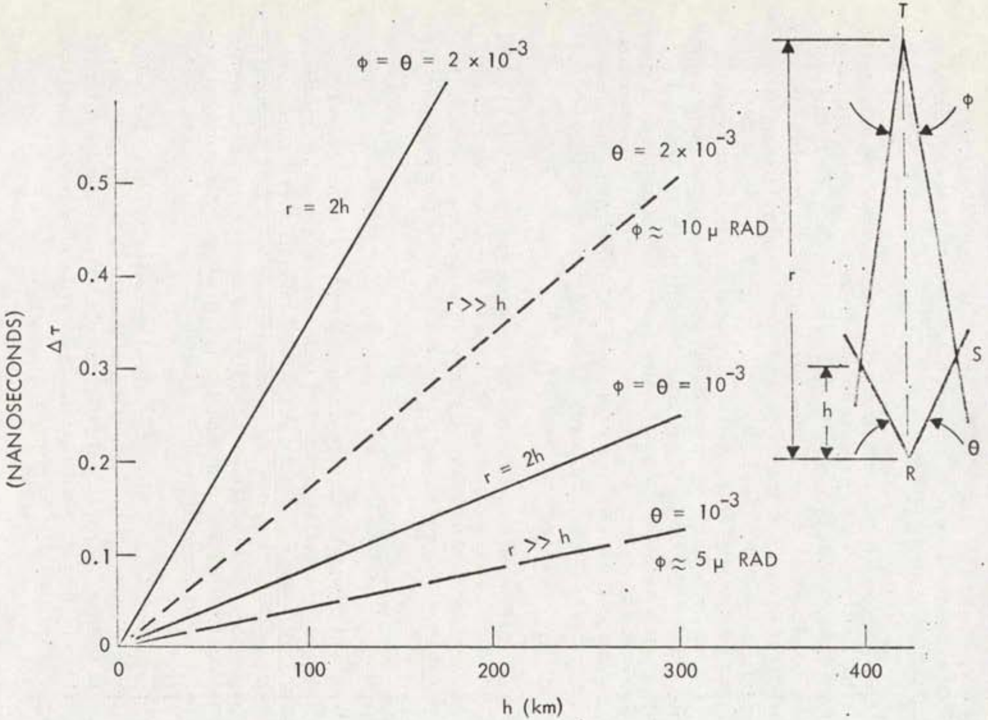

Figure 9.6.4.2-1. Multipath Delay.

9.6.4.4 Equipment Design

The equipment used for this experiment will be the same equipment used for heterodyne detection on the ground, heterodyne detection in space, and direct detection on the ground. The spaceborne equipment will use three telescopes, one having an aperture of 1.0 meter and the other two having apertures of 0.3 meter. Telescope no. 1 will be used for transmission of the 0.6328-micron wavelength and a backup of the 0.6328-micron heterodyne receiver as shown in figure 9.6.4.4-1. Telescope no. 2 has a 0.3-meter aperture and will be used only for the 10.6-micron wavelength as shown in figure 9.6.4.4-2. Telescope no. 3 has a 0.3-meter aperture and will be used for reception of the 0.6328-micron wavelength as shown in figure 9.6.4.4-3. The 0.6328-micron transmitter in telescope no. 3 is a backup for the transmitter in telescope no. 1.

The heterodyne receiver output in telescope no. 3 will be monitored over at least a 1 kHz bandwidth to give a measure of scintillation in the coherent uplink. Also in telescope no. 3 the local oscillator will have to be disabled to measure the corresponding scintillation in a noncoherent uplink. A 10.6-micron noncoherent receiver is included in telescope no. 2 to measure scintillation in the 10.6-micron uplink. This receiver, consisting of a thermistor bolometer and amplifier, does not have to be cooled. Even though the receiver is relatively insensitive, it will provide a 30-dB signal-to-noise ratio to measure scintillation from 0-1 kHz, providing the ground transmitter radiates 100 watts in a 0.1-milliradian beamwidth.

The transmission monitors which are photodetectors are used to measure laser power, laser noise, and modulation.

At 6328 Å the Sylvania V-2 modulator, which operates at frequencies up to 100 MHz with 30 watts of prime power, is used to modulate the laser beam. Figure 9.6.4.4-4 shows the V-2 modulator and a transistorized driver. This driver with less than 2.5 watts of input power can provide 100 per cent modulation at 5 MHz. The V-2, which is basically a polarization modulator, can be operated using any pulse, analog, or FM/AM method.

On the ground the received signals would be recorded at the heterodyne and direct detection systems outputs. Transmitted power and beam divergence would also be measured with monitors for the 6328 Å and 10.6-micron transmitters. Pointing accuracy and stability measurements are also required for both transmitters and receivers. This data would originate from the tracking error signals and calibrations of the optical tracking mounts associated with beacons and receivers.

9.6.4.4.1 Feasibility

This experiment is to be performed at two optical wavelengths. The degree of perfection of the several critical elements required for communication at these

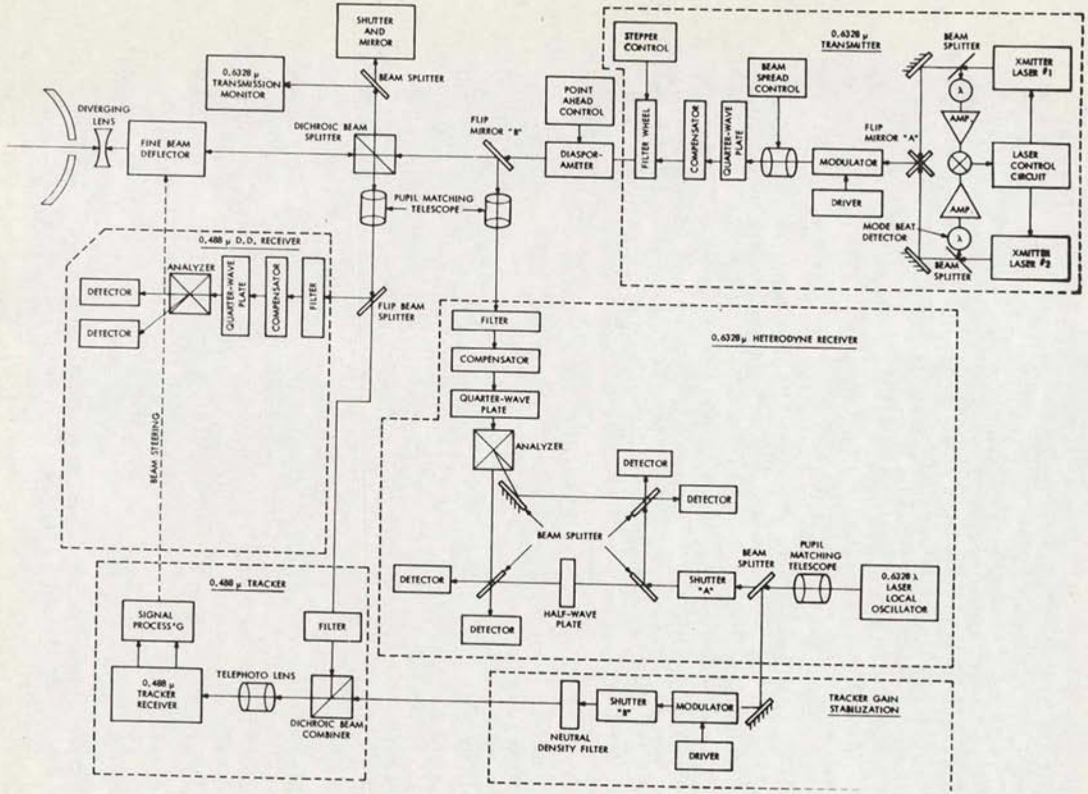

Figure 9.6.4.4-1. Block Diagram of Telescope No. 1: 1.0 Meter--Gimbaled.

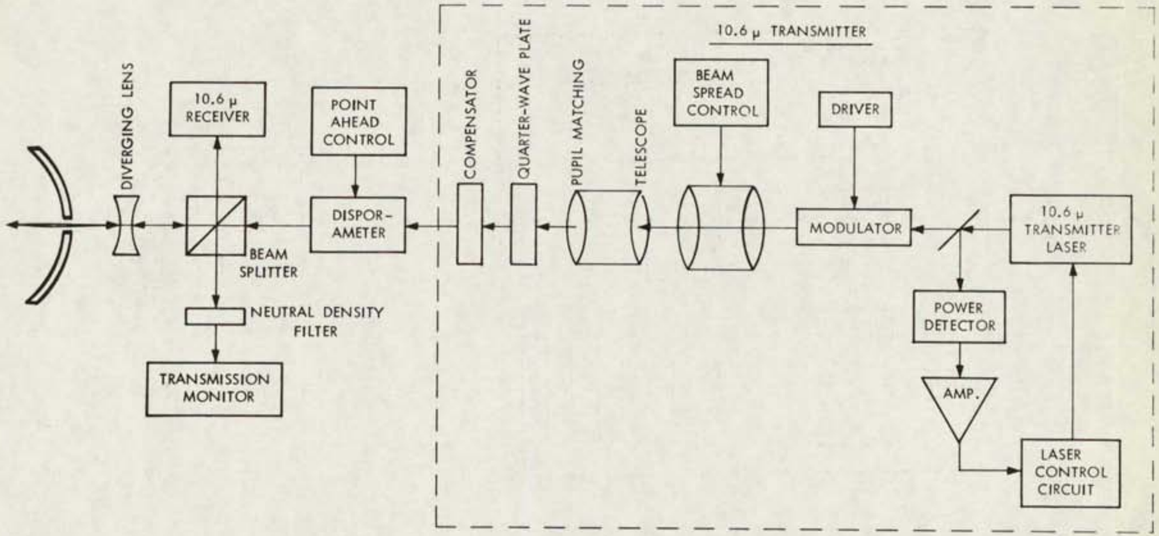

Figure 9.6.4.4-2. Block Diagram of Telescope No. 2: 0.3 Meter-Strap-On.

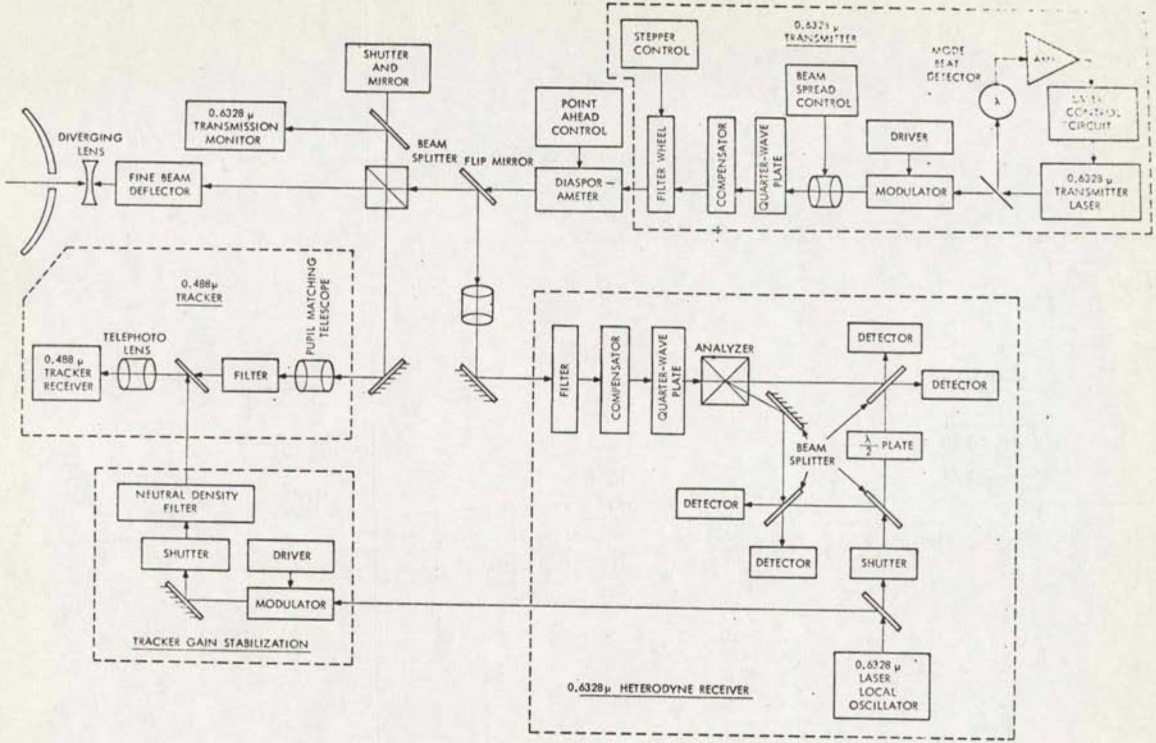

Figure 9.6.4.4-3. Block Diagram of Telescope No. 3: 0.3 Meter--Separately Gimbaled.

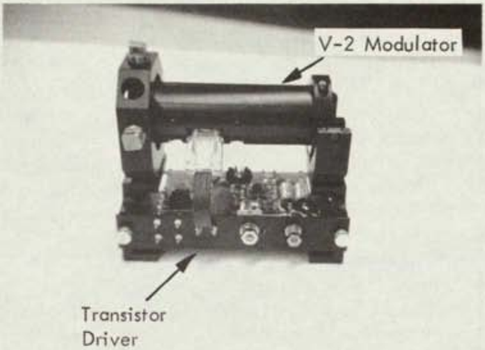

Scale 1:4

Figure 9.6.4.4-4. Sylvania V-2 Modulator and 5-MHz Driver

wavelengths varies markedly with the wavelength under consideration. For visible wavelengths, such as 0.6328 micron, all critical components such as lasers, modulators, beam splitters, and optical elements and their coatings have reached a state of development where some items such as optical elements, beam splitters, and detectors have demonstrated reliable performance on rockets and satellites; other items such as lasers and modulators have been operated in experimental communication links carrying television signals over distances of 2 km. [(3)] Reliability and lifetime estimates are still low for OTAES applications and will need to be improved.

At the 10.6-micron wavelength of the CO_2-N_2 laser, operation of most component parts in the space environment is relatively unknown. The number of transmission materials available for selection is limited, and suitable reflection and antireflection coatings are also limited. Until the recent availability of the CO_2-N_2 laser, work in the infrared region was spread over the band; but it can be expected that considerable effort will be concentrated at the 10.6-micron wavelength because of the availability of a coherent source of high energy and the great need of materials to be used with this source. Development of devices for operation at this wavelength can also be expected to keep pace with material development. Sensitive detectors for operation at 10.6-microns are limited to the photodetectors such as gold- or mercury-doped germanium, and they require cooling to liquid helium temperatures for proper operation. Present devices can be operated at MHz bandwidths. Further development will be required to obtain 10-MHz bandwidths with long life and high reliability. Modulator development has progressed at a rapid rate. Walsh [(4)] has obtained a modulation depth of 70 per cent at 10.6-microns by applying 600 volts to a GaAs modulator. 100 MHz has been quoted for a commercial unit at unspecified voltage and modulation depth. Other suitable materials are also available that can be operated in modulators at wide modulation bandwidths. An efficient modulator at 10.6 microns is the primary high risk component for this experiment because of the large drive powers presently required.

9.6.4.5 Data Management

Optical transmitter power in the spacecraft is measured using photodetectors, which produce either a voltage or current output. The average power will be represented by a dc signal. Noise is a fluctuation on the dc signal. When the modulation is turned on, the ac component will be a measure of the modulation superimposed. In the spacecraft these electrical signals will be sent by telemetry to the ground for storage, processing, and display. Similarly, the ground measured parameters will be recorded, processed, and displayed as necessary at the ground station.

(3) C. J. Peters, et al., "Laser-Television System Developed with Off-the-Shelf Equipment," Electronics, February 8, 1965, pp. 75-78.

(4) T. E. Walsh, "Gallium-Arsenide Electro-optic Modulators," RCA Rev., September 1966, pp. 323-335.

The recorded analog data will be analyzed to provide:

a. probability density distributions of signal fading

b. power spectrum of signal fluctuations

c. transmission losses

d. beam pointing and spreading effects

e. signal-to-noise ratios/error rates

f. polarization distortion

g. television picture quality

h. channel bandwidth

9.6.4.5.1 Spacecraft Equipment Test and Checkout

Verification of laser performance will be done by checking that the alignment servo for the laser mirrors is operating satisfactorily and checking the transmission monitor output power. For satisfactory performance, the equipment alignment and tuning must be optimized. Alignment of the laser, modulator, and telescope can be determined by operating the boresight error measurement equipment on the control panel and determining the magnitude of this error. Adjustment of alignment controls will be made to minimize the boresight error.

Modulator performance will be tested by measuring the amount of drive voltage required to shift the signal polarization by 90° (i.e., full on to full off) and by adjusting the modulator driver gain to obtain the required output. A polarization analyzer will be included in the transmission monitor for this purpose, and the monitor output will be used for measuring the modulator performance.

9.6.4.5.2 Ground Equipment Test and Checkout

The ground-based equipment required for this experiment will include: (a) the heterodyne ground receiver, (b) the large aperture (8-meter) receiver dish, (c) pointing and positioning equipment, (d) receiving electronics and data-handling equipment, and (e) ground station control consoles. Auxiliary to this equipment will be: (a) the ground beacon, (b) beacon modulator and drive equipment, and (c) the microwave tracker to provide pointing information.

The ground-based equipment will be tested by operating the beacon and measuring its output. The beacon modulator will be operated with selected test signals, and the beacon output will be measured. Pointing of the beacon will be done by using the inputs from the RF tracking stations such as Goldstone and, when possible, switching over to the optical fine tracking system when lock-on has been obtained.

On board the spacecraft, the equipments required for performing the Heterodyne Detection on Earth, the Heterodyne Detection on board the Spacecraft, and the Direct Detection on Earth experiments will be needed for this experiment. Also required for this experiment will be the direct detection receivers for 0.6328 micron and 10.6 microns. Experiment control can be exercised by either the astronaut (figure 9.6.4.5.2-1, left-side panels; and figures 9.6.1.5-2, 9.6.1.5-3, and 9.6.1.5-4) or the experimenter at the OTTOS ground site (figures 9.6.4.5.2-2, 9.6.4.5.2-3, and 9.6.4.5.2-4 and figures 9.6.1.5-5, 9.6.1.5-6, 9.6.1.5-7 through 9.6.1.5-13, and 9.6.3.5-1).

9.6.4.5.3 Experiment Performance

Prior to the commencement of the experiment, the ground station must be continuously illuminated by the selected spacecraft laser. Data is required defining:

a. Laser beam radiant intensity distribution as a function of beam divergence

b. Laser noise characteristics

c. Spacecraft beam-pointing accuracy and fluctuations.

When the spacecraft tracker is locked onto the ground beacon and is transmitting, the heterodyne receiver telescope and the 8-meter dish will be pointed at the spacecraft and the receiving electronics will be activated. Internal checking of the receiving electronics will be done by injecting an optical signal directly into the photodetectors and checking the output against the input for gain and distortion. These functions will all be controlled from the ground station control consoles.

To obtain the statistical fading characteristics of the propagation medium, this experiment will require data from the other propagation experiments while they are in progress. In addition, meteorological and path data will also be required. Explicitly, the following outputs are recorded and monitored by the experimenter on the ground.

Ground Equipment

a. Direct detection at 6328 Å and 10.6 microns

b. Heterodyne detection at 6328 Å and 10.6 microns

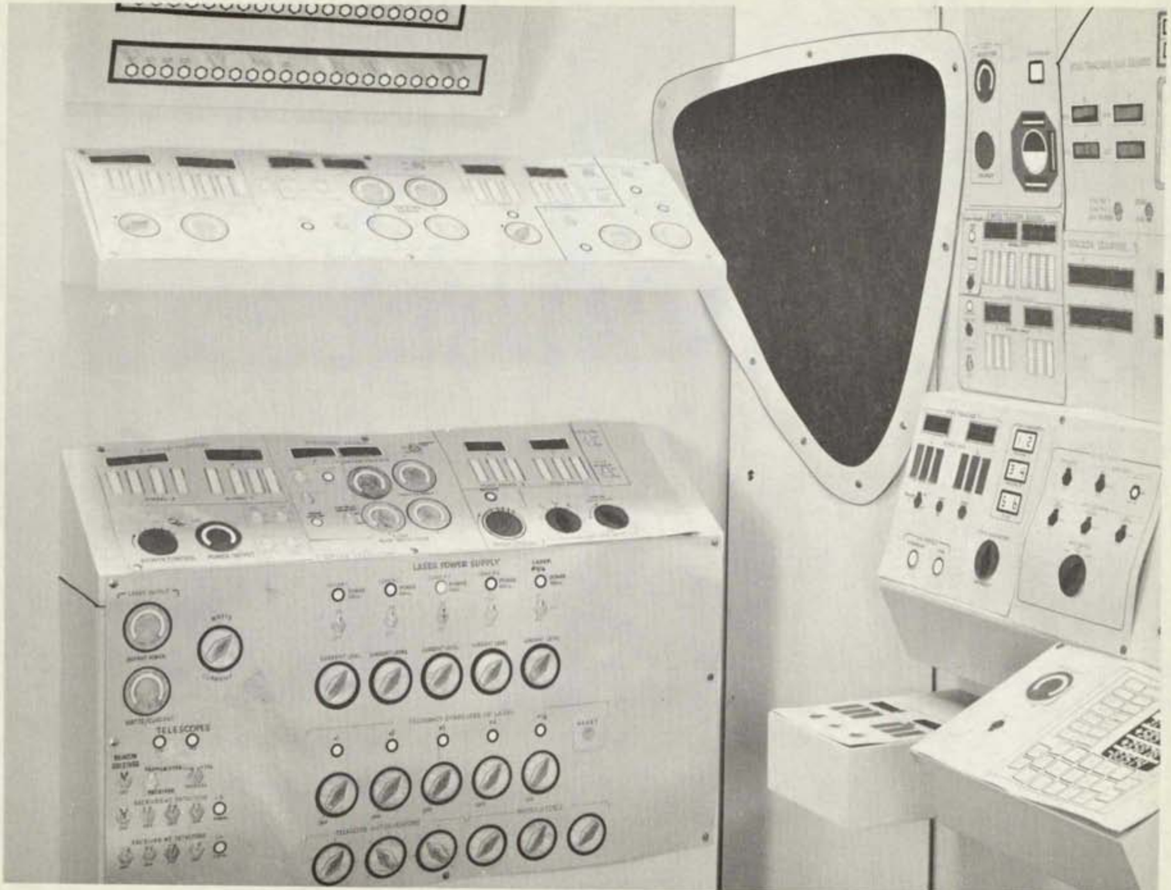

Figure 9.6.4.5.2-1. Spacecraft Laser Telescope Control Panels

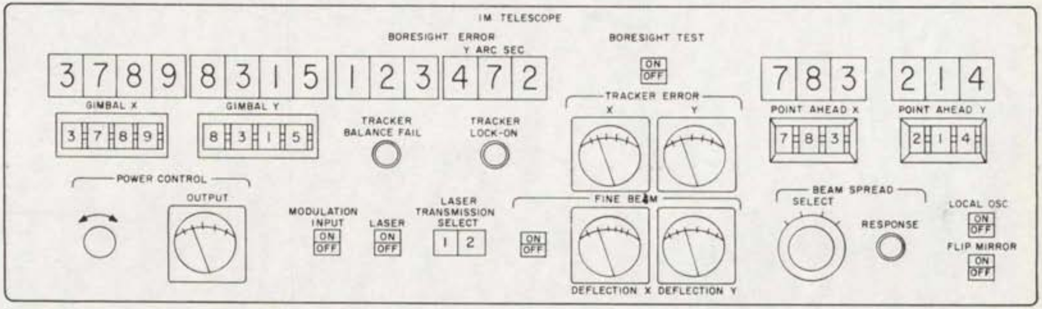

Figure 9.6.4.5.2-2. Panel, 1.0 -Meter Telescope; Experiments 5,6, and 7.

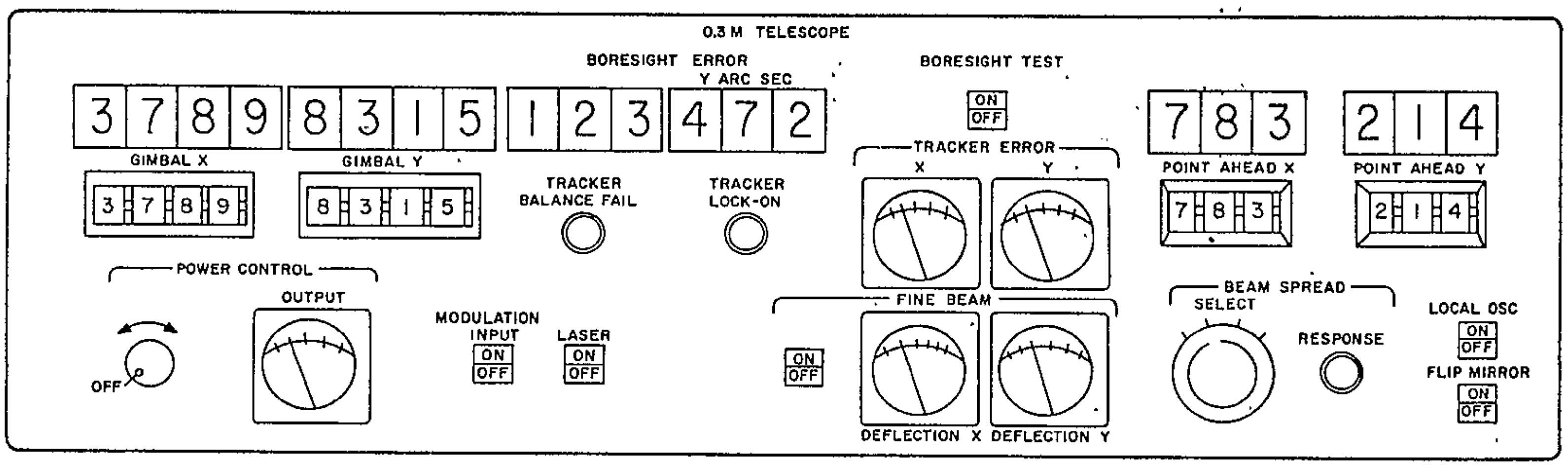

Figure 9.6.4.5.2-3. Panel, 0.3 -Meter Telescope; Experiments 5,6, and 7.

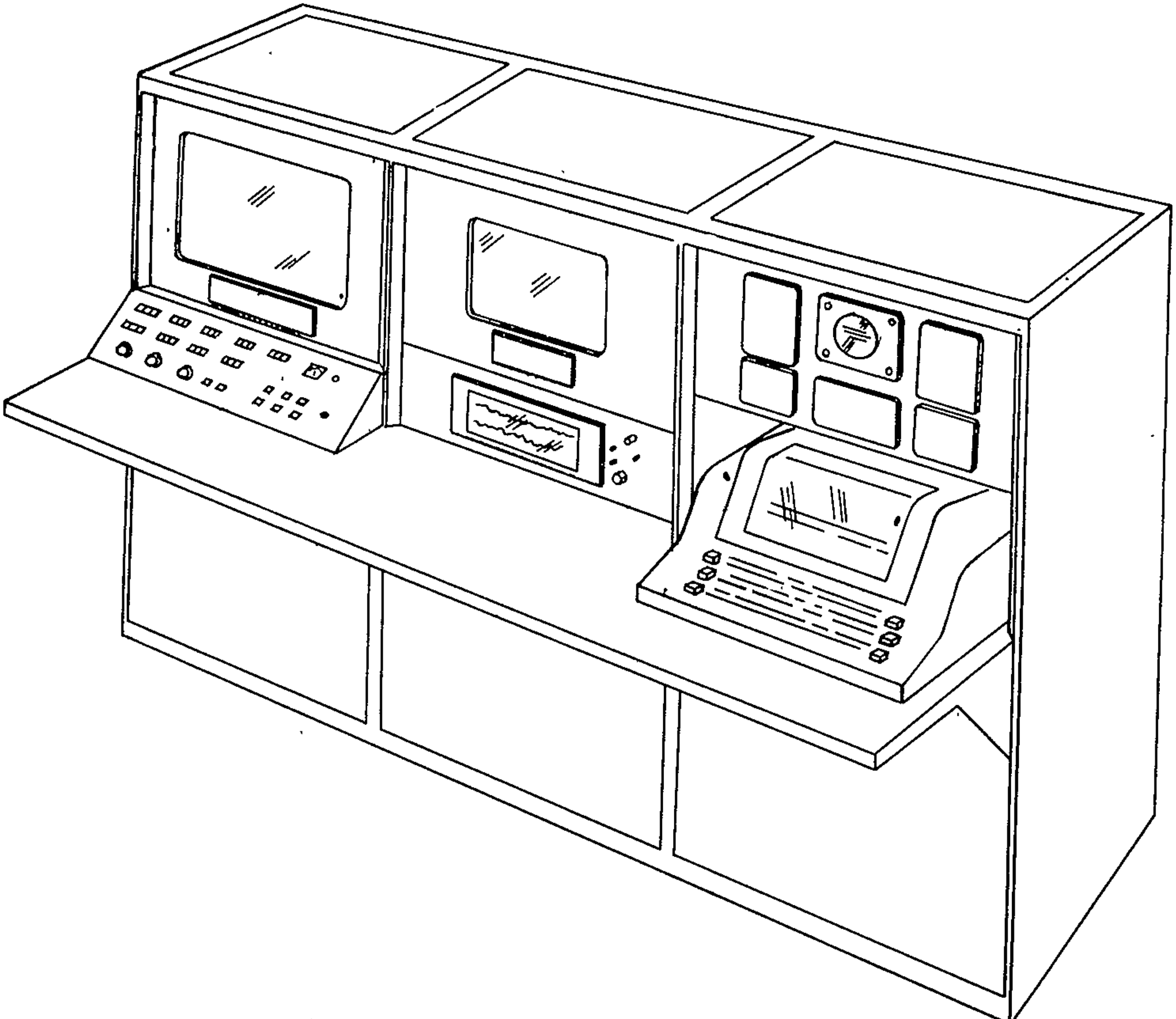

Figure 9.6.4.5.2-4. Console -- Experiments 3 and 4.

c. Ground transmitter outputs and pointing data at 6328 Å and 10.6 microns.

Spacecraft Equipment:

a. Direct and heterodyne detection at 6328 Å and direct detection at 10.6 microns

b. Spacecraft transmitters and pointing data at 6328 Å and 10.6 microns.

This experiment will also require direct detection receiver outputs on the spacecraft. At 6328 Å, the direct output is obtained from a heterodyne receiver detector. In order to eliminate the shot noise produced by the local oscillator, it will be necessary to block out with a shutter, or turn off the local oscillator for this measurement.

A direct receiver at 10.6 microns has been incorporated in telescope no. 2 as shown in figure 9.6.4.4-2. This receiver will be prealigned in the telescope. It will be designed to operate while the 10.6 micron laser is in operation. (This is possible because the 10.6-micron laser is polarization modulated and will only appear as a bias offset in the receiver. The receiver will not be degraded by the photon noise of the 10.6-micron transmitter.) This receiver will be activated by a switch on the control panel for telescope no. 2.

The communication experiments using modulation are planned to be operated as an extension of the Heterodyne Detection on Earth Experiment and the Direct Detection Experiment. For example, the first experiment that is expected to be performed will be the Direct Detection Experiment. When it has been determined that the Direct Detection Experiment on Earth is operating satisfactorily, the modulator can be supplied a signal such as: (a) tones, (b) voice, (c) TV test pattern, (d) TV picture, and (e) pulses.

The tones and TV test pattern will be used to make quantitative measurements of the system performance, and the voice and TV picture will be used for subjective evaluation of the system. The tones spaced at decade intervals up to 100 MHz will provide a means of measuring the frequency response of the space-to-ground channel.

The TV test pattern will provide another means of determining system performance by correlation of many successive received signals. The pulse signal will provide a means of measuring error rate of the received signal with a minimum of data processing. Both analog and digital modulation methods can be used with the same modulator and modulator driver.

These measurements will be made using both 6328 Å and 10.6-micron receivers in the spacecraft. Although uplink optical communications are not a part of this experiment, they will provide data on the upward path and will aid in the interpretation of the downward transmission. In addition, depending upon the upward laser beamwidths and the atmospheric turbulence scale in the tropopause, it is conceivable that deep fading could occur. This fading would be due to beam breakup and the fact that the long range between the tropopause and spacecraft will accent the breakup. For example, a 1-micron radian refraction will displace that portion of the beam by about 37 meters at the synchronous orbit distance.

9.6.5 Precision Tracking of a Ground Beacon

Due to space power limitations, wide bandwidth laser communication links for space application will require that the laser power be concentrated in very narrow beam widths. In order to utilize narrow beams (divergence of 0.15 arc second at the 3 db power points) a pointing capability commensurate with the beam angular divergence is required. Pointing a laser to this accuracy from the spacecraft to a ground site would be virtually impossible without a reference line of attitude. This reference line of sight will be provided by an earth laser beacon whose angular beam spread can be considerably larger than the spacecraft's due to the greater power available at the ground site. The Deep Space Information Facility (DSIF) microwave link can establish the spacecraft's position to an accuracy of ± 22.5 sec. Thus, a 50 sec beam from the earth will insure illumination at the space vehicle initially. It can be narrowed down after the spacecraft has acquired the beacon, and in turn transmitted a wide down beam (3 sec.) to the ground. Narrowing the up beam to 6 sec. increases the signal-to-noise ratio in the spacecraft tracker to make theoretically possible (see supporting analysis 9.9.1.3) the desired tracking precision in the face of variable earth-shine.

Line of sight aberrations of high frequency due to spacecraft disturbances and atmospheric perturbations are compensated by optical gimballing within the telescope (fine beam deflector system). Errors due to differential detector drift and telescope optics misalignment are corrected by features of telescope design such as detector balancing and boresight compensation loops. Point ahead of the down going beam, required by the finite velocity of light, is accomplished on an open loop basis in this experiment using a pre-calculated value.

The purpose of this experiment is to investigate the practicability of tracking a ground based laser to an accuracy of 0.1 arc-second from the space vehicle. Overall tracking conditions will be simulated from synchronous orbit. Tests will be performed in a manner such that results can be extrapolated to obtain expected tracking performance for a deep-space mission.

9.6.5.1 Experiment Design

9.6.5.1.1 Experiment Concept

A ground station laser transmitter (beacon) beam is pointed at the spacecraft. The Deep Space Information Facility, DSIF, which tracks the spacecraft, furnishes the pointing information. In the spacecraft, telescopes with laser transmitting and receiving equipment must also track the earth laser beacon. Initial telescope pointing will require assistance from an on-board microwave tracking system, and from star trackers or planet trackers needed for complete determination of spatial orientation of the telescope. Of course, the spacecraft's attitude control system must initially orient the spacecraft so that the gimballed telescopes will be able to acquire the earth's beacon. Because of the importance of successful beacon tracking to other experiments, two gimballed telescopes, of differing fields of view and performance characteristics, are being proposed for this experiment. (See subsection 9.4 for further discussion on the selection of the number of laser telescopes.)

The laser communication link is not complete until spacecraft transmission is received at an earth station. Because of the relative velocity between the spacecraft and the ground station, the spacecraft transmission must not be beamed coaxially with the upcoming transmission; rather the down-going beacon must be "pointed ahead". The manner in which this is done in a closed-loop feedback manner is the subject of another experiment, POINT AHEAD AND SPACE-TO-GROUND-TO-SPACE LOOP CLOSURE, subsection 9.6.6. The initial point-ahead angle is supplied from the earth station computer facility. The processed signal at the ground can be used in evaluating the tracking performance of the experiment being discussed. For this reason and to make possible illumination of the ground receiver, the open loop insertion of point-ahead angles is considered a part of this experiment. Details of current practice in spacecraft attitude control and microwave-link operation are important to the success of the experiment. However, in the discussion much of this will be assumed, and emphasis will be placed on the new frontier of laser space telescope tracking technology.

The experiment is to be conducted from synchronous orbit, thereby eliminating the effects of image dancing and requiring only one ground station. Consequently, there will not be any systematic slewing or reacquisition requirements, as would be the case for lower orbits. This does not, however, eliminate the atmospherically produced fluctuations of the wave-front angle which produce scintillation or "twinkling", a fluctuation of the received intensity. The relatively large receiving apertures will, however, reduce the average amplitude of these fluctuations, especially at higher frequencies, where they are virtually eliminated. The effect of these intensity variations is to vary the signal level (fading), and hence, to degrade the signal to noise level which can be relied upon. Available data for a quantitative evaluation of this effect is scarce; one of the primary aims of these experiments is to provide useful measurements for its evaluation. Reacquisition will be investigated, and slew is a part of the TRANSFER TRACKING FROM ONE GROUND STATION TO ANOTHER experiment, subsection 9.6.7.

9.6.5.1.2 Acquisition and Tracking of Ground Beacon

9.6.5.1.2.1 Spacecraft Orientation

The spacecraft and its telescopes must be properly oriented for the latter to receive the illuminating beacon signal. The spacecraft attitude will be referenced to both a line of sight to the sun and to the star Canopus. Two alternative means of acquiring Canopus are being considered: One is to orient the spacecraft in roll by having an on-board microwave tracker track a ground beacon and then issue gimbal commands to a star tracker to search for and acquire Canopus. The second method is to issue gimbal commands to the star tracker such that it will acquire Canopus if the correct roll attitude around a sun line exists and then program a spacecraft roll about the sun LOS as in the recent Mars-Mariner flight or as had been planned for the Advanced Orbiting Solar Observatory.

9.6.5.1.2.2 Acquisition and Tracking

Spacecraft position is known to the earth station within a 3 sigma cone of uncertainty of a half-angle of 22.5 sec. from the D.S.I.F. network. Allowing for degradation due to data transfer, encoding and other earth station mount errors, a value of 25 sec. is reasonable for the overall uncertainly (cone half angle.)

On this basis, a beacon with a beam spread of 50 sec. is pointed toward the spacecraft. The beacon is operated in a pulsed mode to facilitate acquisition and tracking.

The position of the earth station is known at the spacecraft to a cone of uncertainty of half-angle of 30 min., from the on-board microwave tracker. This information is used to point a planet tracker with a field of view of about ± 1 deg. toward the earth (or simulated earth, white light beacon.)

The planet tracker tracks the earth (or beacon) to ± 10 sec. (± 30 sec., 3 sigma). The planet tracker is boresighted to the 0.3 meter gimballed telescope, and tracks the earth by using its error signals to drive the gimbals of the 0.3 meter telescope. As a result, the 0.3 meter telescope will now be pointed to within ± 30 sec. (3 sigma) of the earth (or simulated earth).

Since the field of view of the 0.3 meter telescope is ± 45 sec., it will now acquire and track the ground beacon to an accuracy of about ± 1.5 sec

The calculated point-ahead angle required is inserted between the 0.3 meter receiver and transmitter, and a beam of 3 sec. divergence is transmitted to the earth station. Internal boresight alignment is accomplished prior to this step.

The earth station tracks this beam, sharpening its knowledge of the spacecraft position. The uncertainty of this tracking is as follows:

a. Atmospheric error, typically 2 sec. for one aperture, or, averaged over 16 apertures, about 0.5 sec.

b. Tracking resolution, boresight and other errors, estimated to be on the order of 0.3 to 0.5 sec. with a 3 sec. beam.

The probable total uncertainty in the earth station's knowledge of spacecraft position will then be on the order of 0.6 to 0.8 arc seconds.

Based on improved knowledge of spacecraft position, and hence, improved earth beacon pointing, the earth laser divergence is gradually reduced to a value of 6 arc seconds. With this divergence, the spacecraft will track the earth beacon to approximately 0.15 arc second.

The spacecraft transmitter can now be narrowed to a beam width of 0.5 arc second (0.3 meter telescope).

The gimbal angles and fine beam deflector voltages from the 0.3 meter telescope are transferred to the 1.0 meter telescope.

The 1.0 meter telescope tracks the earth beacon (which has a 6 arc second spread) to within approximately 0.1 arc second.

The 1.0 meter telescope transmits a laser beam to the earth station with an initial beam width of 1.0 arc second, gradually reducing it to a value on the order of 0.15 second.

The parameters of acquisition are given graphically in Figure 9.6.5-1.

9.6.5.1.2.3 Testing of Tracking Loop

Dynamic testing of the tracking loop operation will be performed on both the 0.3 meter and the 1.0 meter telescopes. In the case of the 0.3 meter telescope, the testing will be performed after the ground beacon has been narrowed down to 6 arc seconds, before transfer of tracking to the 1.0 meter telescope. Loop testing will be performed on both axes of both telescopes. Although the overall beam-pointing correction (space-ground-space) loop is not closed during this experiment, the earth stations's beam pointing error outputs may be utilized as a measure of the behavior of the line-of-sight during this testing. To facilitate this, a known increment (e.g. - perhaps 0.2 of the transmitted beam width) may be added to the commanded point-ahead angle, and its effect measured at the ground, thus calibrating (and, if necessary, allowing adjustment of) the pointing error output gradients.

Test signals covering a programmed range of amplitudes and frequencies will be inserted into the loop at the points designated on Figure 9.6.5-2 as E_1 (error output of pre-amplifier), E_2 (input to beam deflector) and E_3 (input of gimbal torque motor drive amplifier). For each of these test inputs, the following quantities will be monitored (Figure 9.6.5-2):

V_1 - error output of pre-amplifier

V_2 - output of integrator

V_3 - error signal to gimbal drive.

θ_G - gimbal angle readout

Ground station beam pointing error outputs

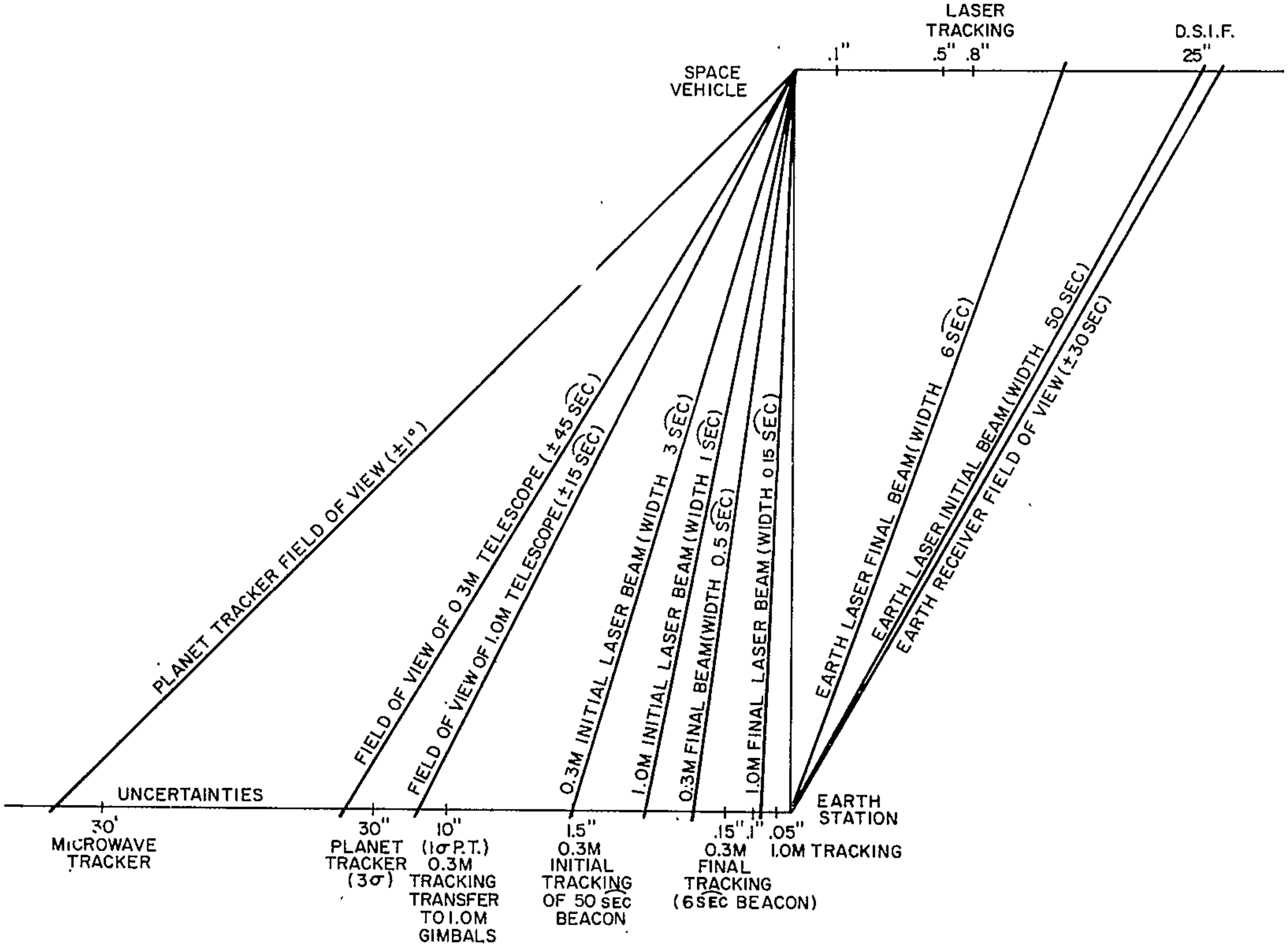

Figure 9.6.5-1. Laser Tracking Experiment Relationships of Uncertainties, Fields of View and Beam Widths (1/2 Cone Angles Shown)

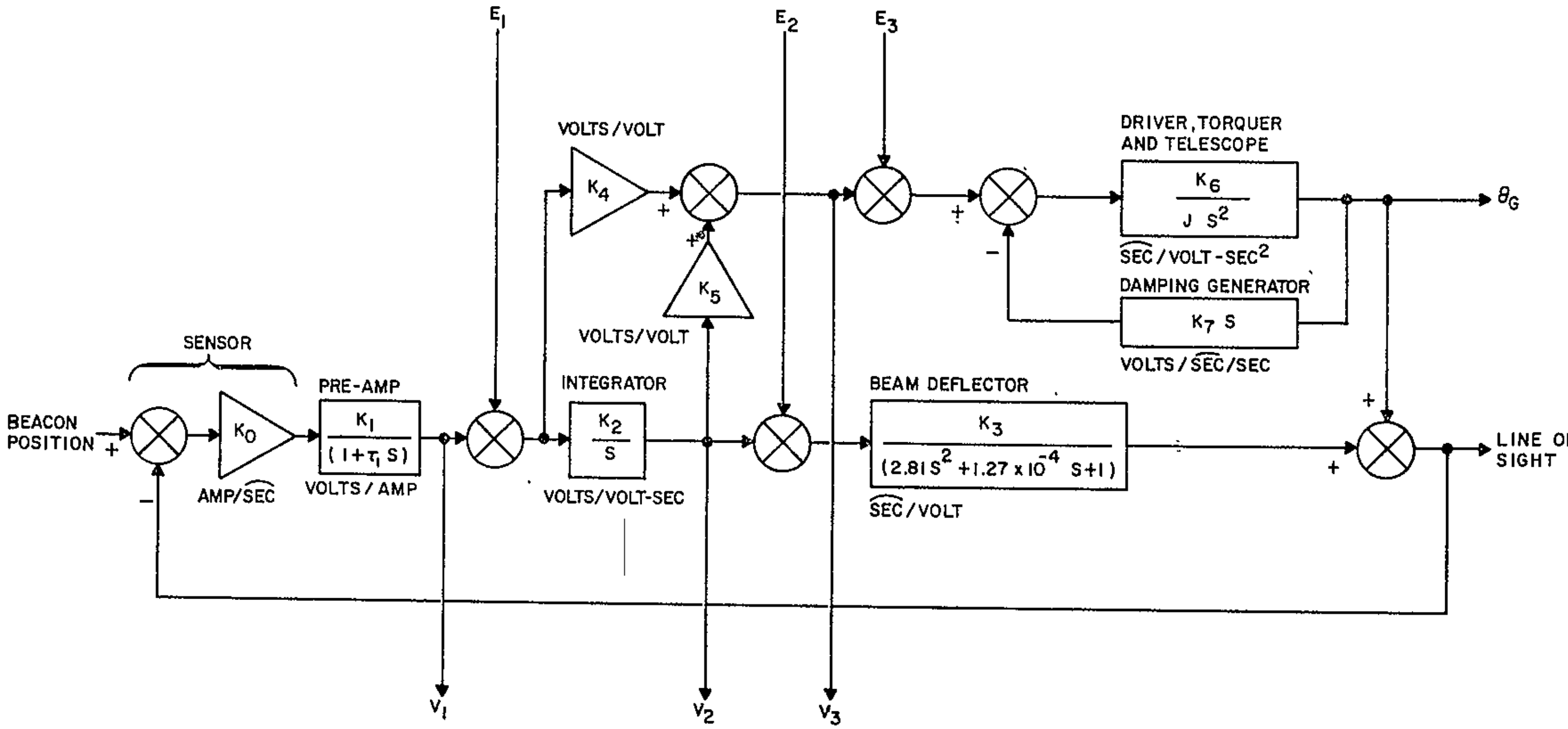

Figure 9.6.5-2. Tracking Loop Performance Test, Block Diagram

These tests will be performed for both the synchronous orbit condition, and for the simulated deep space condition (reduced beacon power).

9.6.5.1.2.4 Acquisition and Tracking in Varying Earth Shine Conditions

The acquisition and tracking function at the spacecraft must take into account the varying earth shine conditions present at earth for differe illumination phases of earth as seen from Mars. This requires that the tracking and acquisition procedures will be performed under different light levels. Thus acquisition and tracking will be performed under the varying earth shine conditions which will be naturally present in synchronous orbit over a diurnal cycle. A numerical analysis of the effects of earth shine on acquisition and tracking is presented in section 9.9.

9.6.5.2 Experiment Measurement Objective

9.6.5.2.1 Precision Tracking of A Ground Beacon

In tracking the ground beacon from space, the beam will be perturbed from a number of sources, both internal and external. Tracking is implemented by a quadrant detection scheme. For the purpose of stabilizing the spacecraft transmitted beam, internal disturbances must be separated from external ones since the former is the source of down-beam jitter. The nature of the disturbance and the method for measuring and cancelling the disturbance are listed:

a. Mechanical vibrations - the spacecraft motion transmits vibration to the various optical components which in turn perturb the optical line of sight to both receiver (tracker) and transmitter. The amplitude and frequency of the vibrations are sensed differentially on the paired quadrant sensors. The precise power spectrum of these disturbances during space flight will be very difficult to predict, and only a preliminary specified range can be determined for tracker design purposes.

b. Atmospheric perturbation of ground-to-space laser beam. The ground transmitted laser beam will be subject to both angular and translatory fluctuations from the earth's atmosphere. Only angular fluctuations will be present at the spacecraft and they will be sensed as amplitude fluctuations or scintillation in the image. By summing all 4 quadrants of the detector, the spectrum of scintillation can be determined and thus separated from other disturbances.

9.6.5.2.2 Spacecraft Acquisition of Earth Laser Beam Under Varying Earthshine Conditions

a. Determine capability of acquiring laser beam under varying amounts of earthshine.

b. Measure tracking accuracy degradation as a result of increase in background light levels.

c. Relation to optical design parameters: on the basis of evaluating tracking performance with different background light levels, design parameters such as maximum allowable spectral filtering, and optimum tracker field of view can be determined.

9.6.5.3 Experiment Equipment Design

The equipment required to perform this experiment is divided into ground station equipment and spacecraft equipment. The ground station equipment consists of microwave tracking and communication capability for coarse acquisition, a 4880A laser beacon with variable beamwidth to illuminate the spacecraft and an optical receiver-tracker to locate the spacecraft more precisely and permit narrowing of the beacon beamwidth. The tracker is also used to verify the completion of the precision tracking and pointing experiment (Section 9.6.6). A description of the tracker and discussion of its capabilities are given in Section 9.6.6. Two types of tracking arrays are treated, heterodyne and direct, the latter not requiring any programmed movements (nutation) of the down-going beam.

The space station equipment required for this experiment comprises the transmitter and tracker sections of the 1.0 meter telescope and the 0.3 meter separately gimbaled telescopes, including the local oscillators and associated tracker balance and boresight calibration circuits. The remaining equipment of the laser telescope group, i.e., receiver units, heterodyne and direct, and the entire 0.3 meter strapped-on telescope, have no application to this experiment. The telescopes are completely described in the preceding section (9.5).

9.6.5.4 Data Management

The function of the precision tracking experiment is to acquire, lock on and center precisely in the field of view of the telescope the line of sight to the ground station beacon. This is to be done despite the effects of spacecraft and telescope vibration and jitter, and effects of atmospheric perturbations.

The telescope pointing error appears on the tracker as a difference signal in the axis involved. The difference signal is processed and applied to the appropriate fine beam deflector axis. Building up of error in the fine beam deflector is prevented by sensing excessive input voltage and sending an appropriate correcting signal to the gimbal drives. Thus the telescope aligns itself with the ground station line of sight and the excessive excitation voltage on the fine beam deflector is relieved. The difference signals from the tracker as well as the fine beam deflector excitation and the telescope gimbal angles are all displayed and recorded for analysis. A steady error signal with no departures in excess of 0.1 second of arc is indicative of the required tracking precision. Atmospheric perturbations which are evidenced by scintillation are measured by recording the sum signal from all four detectors. From this signal the atmospheric perturbation spectrum can be derived. This signal also is telemetered to the ground station for analysis.

9.6.6 Point Ahead and Space-Ground-Space Loop Closure

In a two-way communications link for deep space missions the relative orbital velocity between the space vehicle and earth, coupled with the long signal transit delays, require that the spacecraft transmitter "point ahead" of the apparent spacecraft-ground transmitter line-of-sight in order that the ground receiver receive the spacecraft transmission. For a typical Mars fly-by the lead angle will be on the order of 40 arc seconds near the terminal phase. Continuous and accurate reception from the spacecraft requires that the "point ahead" be referenced to the coordinate reference frame established in the PRECISION TRACKING OF A GROUND BEACON experiment. The "point ahead" precision requires that control be effected through a closed space-to-ground-to-space feedback loop. Perturbations due to spacecraft disturbances must be compensated: low frequency disturbances by spacecraft and telescopic control; high-frequency disturbances by beam (deflector) control within the telescope.

Two types of optical detection at the ground receiver are investigated. Heterodyne (coherent) detection involves use of a matrix of small telescopes and a local laser oscillator signal beating against the incoming signal in each telescope. Direct (incoherent) detection using a four telescope array is also considered. Both methods are to detect gradients in intensity across the beam width intercepted, in order to "steer" the beam toward the center of the array by means of error signals transmitted to the spacecraft. State of the art techniques in balancing of detector sensitivities will be required for this, although angle detection proper (i.e., direction of the beam) is shown to be quite feasible by either method.

The space-ground-space loop is concluded stable by examination of analytic criteria developed in OTAES Interim Progress Report (Vol. IV, Appendix I-1).

Image dancing due to atmospheric disturbances operating in a manner analogous to that discussed in the PRECISION TRACKING OF A GROUND BEACON experiment, imposes the need for testing "point ahead" under the actual condition of a space mission, here proposed at synchronous altitude.

9.6.6.1 Experiment Design

9.6.6.1.1 Need for Closed-Loop Correction

The effectiveness of the Space-to-Earth Laser communication link and the precision to which spacecraft position can be determined by laser tracking on the earth are both highly dependent on the signal-to-noise ratio achieved at the earth station receiver. To achieve acceptable signal levels at the receiver using feasible power levels at the transmitter, at long ranges, requires the use of highly concentrated (very narrow dispersion) beams. The advantage of this concentration can be lost if the receiver is not illuminated by the peak-intensity center of the transmitted beam. (For example, if the receiver is illuminated by the half-power point in the transmitted beam, rather than the center, it will receive only one half as much energy from the laser, and the received signal-to-noise ratio will be reduced by 3 db.)

Factors tending to cause the beam center to be displaced from the receiver include the following:

a. Uncertainty in the knowledge of the direction from the spacecraft to the ground station. This includes tracking errors, such as those produced by noise on the tracking signal, disturbances trans mitted to the telescope through the gimbal system, and residual detector unbalance.

b. Residual boresight errors between tracking receiver and transmitte (at the spacecraft).

c. Uncertainty in the computed value of point-ahead required, due to perturbations of the spacecraft trajectory, for example.

d. Residual errors in the calibration of the point-ahead mechanism command mode.

e. Scintillation effects of the atmosphere.

The initial beam spread must exceed the expected rms sum of these factors, and is thus taken as 3 arc sec.

9.6.6.1.2 Closed Loop Pointing Control

If a signal can be developed which is proportional to the angle by which the beam center misses the receiver, this signal can be fed back to the point-ahead mechanism in such a manner as to reduce this error signal to a minimum by driving the beam center toward the receiver. This is, in fact, how the space-to-ground-to-space correction loop is intended to function.

When the center of the beam arrives at the center of the receiving array, the signals in corresponding telescopes on each side of the array will be equal (assuming telescope sensitivities have been precisely balanced). This symmetry is lost when the beam center moves away from the array, and a net signal gradient appears across the array (from side to side or from top to bottom, or both, depending upon the direction of the beam pointing error). It is this gradient, sensed by a differential measurement across the array, which is used an an error signal, and is fed back via an earth-to-space data link, to correct the pointing.

9.6.6.1.3 Closed Loop Performance

Figure 9.6.6.1-1 is a block diagram of the pointing correction loop, including the transmission lags due to the transit time required for a signal to travel between the earth station and the spacecraft and back.

Stability criteria and dynamic performance of this loop are analyzed and discussed in some detail in the OTAES Interim Progress Report Vol II Appendix I-1.

From this analysis it may be concluded that at a range of about one astronomical unit, a loop velocity constant, K_v ($=K_1K_2$) of about 5×10^{-4} sec $^{-1}$ would result in a loop damping ratio of about 0.7. The conclusion may also be drawn that loop gains of this order are adequate to maintain pointing error at a negligible value in the presence of normal variations of hardware parameters. Further details regarding stability of the space-ground-space loop are given in Section 9.9.1.7.

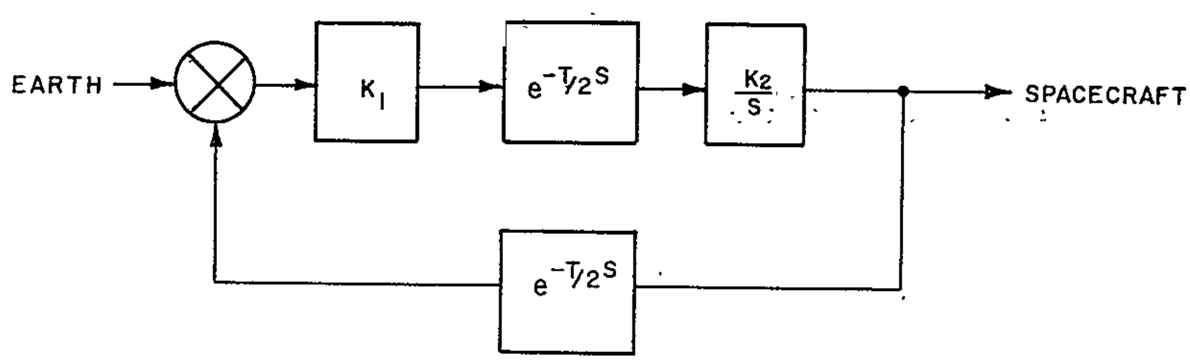

Figure 9.6.6.1-1 Pointing Correction Loop (with Transport Lags)

9.6.6.2 Experiment Measurement Objective

9.6.6.2.1 Point Ahead

The relative orbital velocities of the spacecraft and the signal transmission time require a point ahead capability for both spacecraft and ground station in order that mutual acquisition of laser signals be accomplished. The experiment will establish the degree of accuracy to which point ahead can be implemented.

The first parameter to be measured is initial point ahead accuracy. Prerequisites are: (1) the spacecraft's own knowledge of its attitude, established by Canopus LOS and earth laser LOS, and (2) the relative orbital velocities of spacecraft and earth station along with geographic position of earth station.

Point ahead is implemented by offsetting the transmitter LOS from the receiver LOS via the diasporameter rotation. The ground complex measures the incoming laser power gradient. Both temporal and spatial averaging is required to smooth out the effects in the down going beam, resulting from atmospheric turbulence.

The second parameter to be measured is point ahead capability as a function of tracking S/N. The point ahead capability is improved by the upgrading of the tracking LOS. However, the ground station must acquire the spacecraft's laser beam before it can narrow down its own beam and thus improve the spacecraft's laser tracking capability. The limits of point ahead capability as a function of tracking S/N can be determined by successive narrowing of both earth and spacecraft laser beams. The narrowing of the spacecraft laser beam will enable the ground receiver array to determine the incoming laser amplitude gradient. However, there will be limits on the narrowness of both laser beams at which the point ahead capability will not improve. At this limit, the effect of other parameters which can affect point ahead capability can be examined. Some of these additional parameters are listed below:

a. Spacecraft transmitter and tracker boresight accuracy

b. Precision of diasporameter subsystem

c. Accuracy of determining navigational parameters such as spacecraft attitude, position, and range

9.6.6.2.2 Space-to-Ground-to-Space Loop Closure

The improvement in the spacecraft's capability of pointing its laser at the ground array resulting from measured information fed back to the spacecraft will be determined in this experiment. The loop closure will be implemented with realistic deep space transmission delays.

Parameters to be measured are:

a. Improvement in beam pointing capability of spacecraft by virtue of a feedback loop.

b. Ability of ground receiver array to measure the incoming laser beam positions under varying ambient conditions. Correlations of beam pointing measurements with light level, and atmospheric conditions can be made.

9.6.6.3 Experiment Equipment Design

9.6.6.3.1 Spaceborne Equipment

The same equipment as in the preceding experiment section 9.6.5.3 is used for this experiment, except that now the pupil matching optics of both the

0.3 and 1.0 meter telescopes are employed to narrow the down going beams. The diasparameter servo loops of both instruments now receive input commands in response to error signals received from the ground station.

9.6.6.3.2 Ground Receiving Equipment

In previous reports, three types of ground receivers have been considered. One of these, namely, the use of a single large direct detection telescope ("photon bucket") with nutation of the spaceborne laser beam was not considered further, as it required the additional complexity of nutation in the spacecraft telescope equipment

Of the other two, one utilizes heterodyne (coherent) detection and the other direct (incoherent) detection of the received energy. The heterodyne detection technique employs a number of relatively small receiving telescopes arranged in an array, each combining the received energy with energy from a "local oscillator" laser, to produce a beat or I. F. signal at a frequency equal to the difference between the received and local oscillator laser frequencies.

The direct detection technique involves the use of four larger incoherent receiving telescopes, arranged in an array for detection of intensity differences across the beam.

9.6.6.3.3 Distributed Heterodyne Array

The distributed heterodyne array for reception from a deep-space probe would consist, typically, of 100 individual telescopes. For a synchronous orbit simulation the array would consist of 16 telescopes. Each telescope would be about 12.5 cm. in diameter, which is the largest aperture considered capable of receiving a coherent optical signal through the atmosphere without serious degradation of wavefront.(1) Figure 9.6.6.3.3-1 illustrates a typical array, including a co-mounted transmitter, containing 16 telescopes, as would be used for testing from synchronous orbit. Figure 9.6.6.3.3-2 illustrates a single heterodyne detector telescope, with typical signal processing. Signal processing for angle tracking follows the same logic as that applied to the spaceborne tracker (see figure 9.9.1.1-2). For beam pointing, the "presence" signals (sum of all four detector outputs) of all telescopes in one half-array (either horizontally or vertically) are combined, and the difference between opposing halves is used as a measure of beam pointing error. (See section 9.6.6.1.3)

(1) Jurgen R. Meyer - Arendt and Constantinos B. Emmanuel "Optical Scintillation; A Survey of the Literature" N.B.S. Technical Note 225

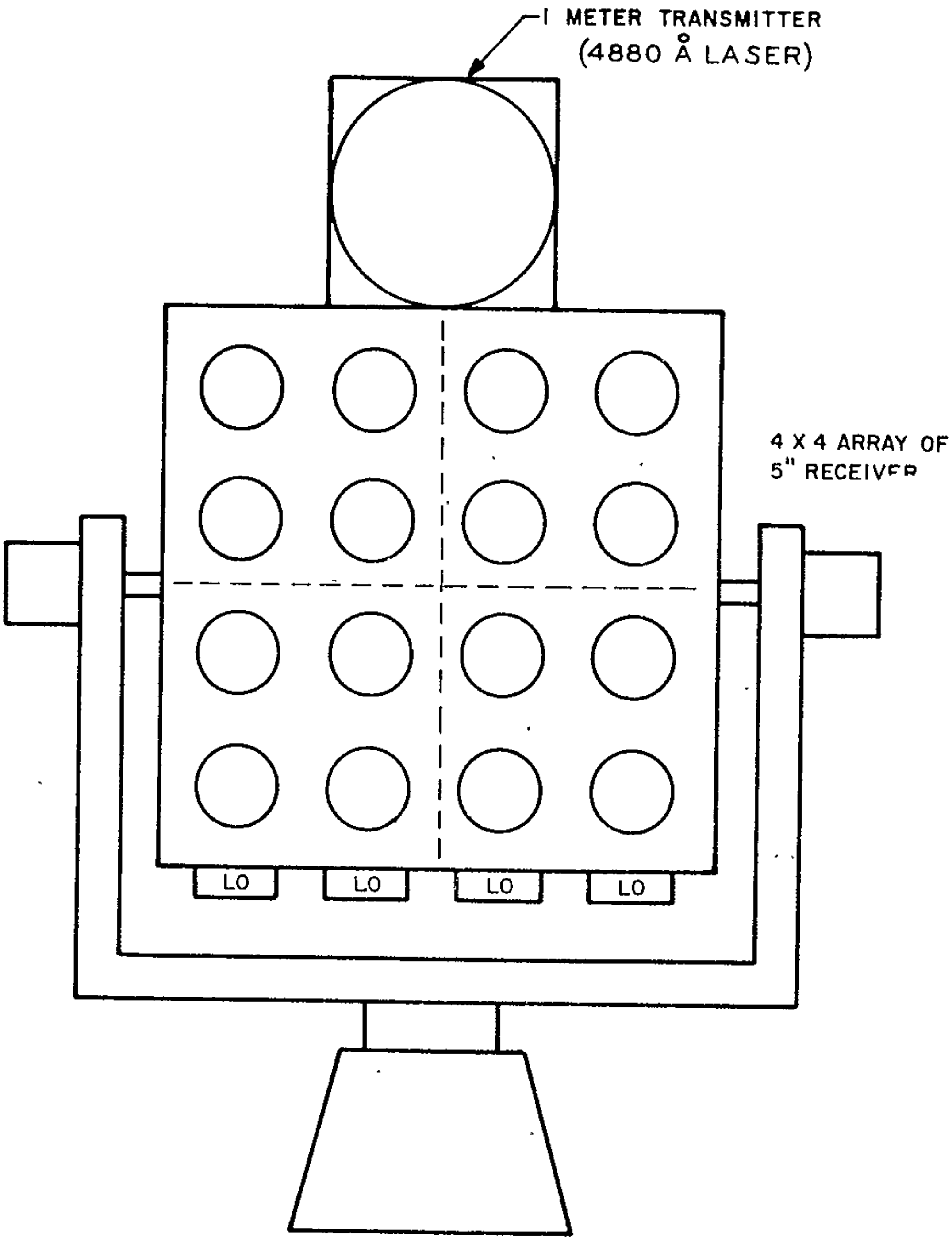

Figure 9.6.6.3.3-1 Earth Station Distributed Receiver-Tracker Array and Transmitter

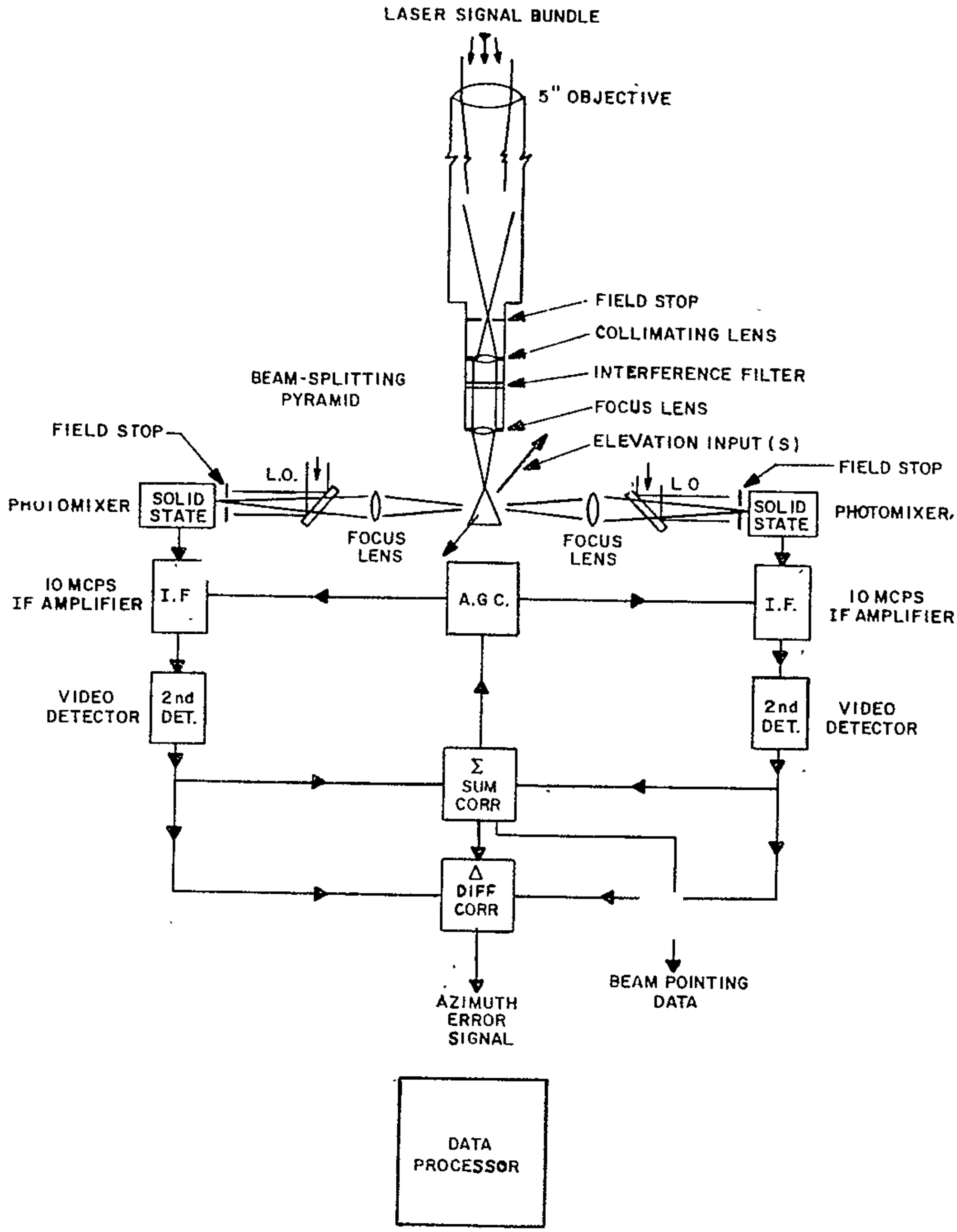

Figure 9.6.6.3.3-2 Single Channel Receiver-Tracker and Azimuth Error Channel

Superheterodyne detection makes it possible to realize an improved signal-to-noise ratio, by lifting a weak signal above noise resulting from background light, photodetector dark current, and thermal agitation in the resistive load circuit. Post-detection signal power, and the noise power component due to the local oscillator current are both proportional to the local oscillator power.

The general expression for the power signal-to-noise ratio is:

$$\frac{i_s^2}{i_n^2} = \frac{S\, P_{LO}\, P_r''}{e\, \Delta f\, (P_N + P_{LO})} = \frac{S\, P_r''}{e\, \Delta f\, \left(1 + \frac{P_N}{P_{LO}}\right)}$$

where:

i_s = R.M.S. signal current (I.F.)
i_n = R.M.S. noise current
S = sensor sensitivity
P_{LO} = local oscillator power (at sensor)
P_r = received signal power (at sensor)
Δf = effective noise bandwidth
P_N = input power required to produce noise equivalent to that from all other sources, including background
e = unit electron charge = 1.6×10^{-19} coulomb.

From this it may be seen that when the ratio P_N/P_{LO} is quite small the term $\left(1 + \frac{P_N}{P_{LO}}\right)$ becomes essentially unity, and the signal-to-noise ratio becomes a function only of the sensor sensitivity, the received signal level, and the equivalent noise bandwidth

9.6.6.3.4 Direct Detection Array

Figure 9.6.6.3.4-1 illustrates an arrangement for a direct detection array for earth reception of a spaceborne laser beam.

Each telescope contains a pyramidal reflector and four photomultiplier detectors (quadrant detector-see section 9.9.1.1), for angle tracking. The relatively large apertures of the telescope perform partial spatial averaging of perturbations caused by atmospheric effects, and additional spatial averaging is obtained by combining the error outputs of all four telescopes in angle tracking.

9.6.6.3.5 Equipment Effectiveness in Tracking

This is shown by the results summarized below, as developed in s 9.9.1.5 and 9.9.1.6. The large signal to noise ratios at 1 H_z bandwidth are especially indicative of tracking feasibility with either technique.

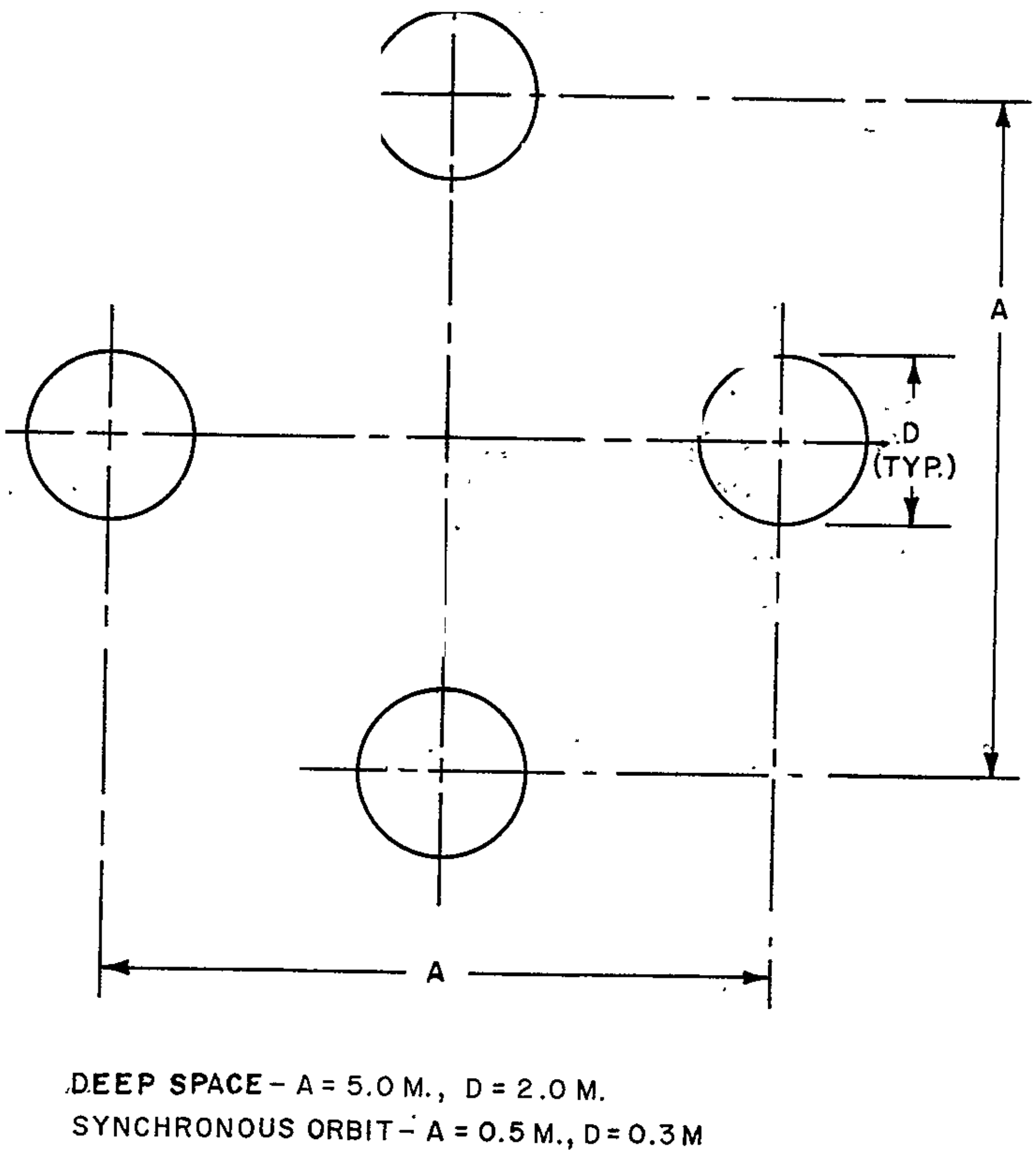

Figure 9.6.6.3.4-1 Direct Detection Tracker Array
(Earth Station)

TABLE 9.6.6.3-1

SUMMARY-GROUND TRACKING AND BEAM POINTING CORRECTION

Detection Technique	Quantity	Deep Space @ Beam Center	Deep Space @ Beam Edge	Synchronous Orbit @ Beam Center	Synchronous Orbit @ Beam Edge
Heterodyne Detection	Total Presence Signal (IF. Amps, RMS.)	2.06×10^{-6}	1.46×10^{-6}	117×10^{-6}	82.8×10^{-6}
	Presence S/N in 1 HZ. Bandwidth	5100	3620	7.26×10^{5}	5.14×10^{5}
	Maximum Tracking Signal (I.F. Amps, RMS.)	2.06×10^{-6}	1.46×10^{-6}	117×10^{-6}	82.8×10^{-6}
	Total Noise Power Spectral Density $\left(\frac{amp.^2}{HZ}\right)$	16.28×10^{-20}	16.28×10^{-20}	2.60×10^{-20}	2.60×10^{-20}
	Pointing Error Signal @ $\theta = 0.015$ sec. (I F.amps, RMS)	2.34×10^{-12}	—	—	—
	Pointing Error Signal @ $\theta = 0.075$ sec. (I.F.amps, RMS)	—	8.52×10^{-12}	—	1.04×10^{-6}
	1/2 Array (center-to-center) angular subtense, (radians)	6.1×10^{-12}	6.1×10^{-12}	1.27×10^{-8}	1.27×10^{-8}
Direct Detection					
	Total Presence Signal (Amp., D.C.)	1.14×10^{-6}	0.57×10^{-6}	3.4×10^{-3}	1.7×10^{-3}
	S/N in 1 HZ. Bandwidth	1.33×10^{6}	7.66×10^{5}	1.0×10^{8}	7.3×10^{7}
	Maximum Tracking Signal (Amp., D.C.)	1.14×10^{-6}	0.57×10^{-6}	3.40×10^{-3}	1.70×10^{-3}
	Total Noise Power Spectral Density, $\left(\frac{amp^2}{HZ.}\right)$	73.40×10^{-26}	55.3×10^{-26}	10.9×10^{-22}	5.45×10^{-22}
	Total "Non-Signal" D.C. (threshold) (Amp., D.C.)	0.291×10^{-6}	0.291×10^{-6}	14.4×10^{-9}	14.4×10^{-9}
	Pointing Error Signal @ $\theta = 0.015$ sec. (amp., D.C.)	6.98×10^{-12}	—	8.75×10^{-6}	—
	Pointing Error Signal @ $\theta = 0.075$ sec. (amp., D.C.)	—	1.8×10^{-11}	—	22.5×10^{-6}
	Center-to-Center Array Subtense, radians	3.33×10^{-11}	3.33×10^{-11}	1.39×10^{-8}	1.39×10^{-8}

Table 9.6.6.3-1 summarizes the results of calculations for several conditions, for both the deep-space case, and for the synchronous orbit condition. Assumed conditions are as follows:

Transmitted Power: From Deep Space = 1.0 watt

From Synchronous Orbit = 7.5×10^{-3} watt

Beam Divergence = 0.15 arc second (θ_B)

Heterodyne Detection:

Telescope Diameter = 12.5 cm

Deep-space - 100 telescopes in array

Synchronous Orbit - 16 telescopes in array

Local Oscillator Power - 5×10^{-3} watt/sensor, 4 sensors/telescope

Direct Detection:

Deep Space. - 4 telescopes, two on each axis. Diameter 2.0M., and separation along axis is 5.0M center-to-center.

Synchronous Orbit - 4 telescopes, two on each axis. Diameter = 0.3M., and separation along axis is 0.5M center-to-center.

9.6.6.4 Data Management

With precision tracking established in both directions, measurements of significant parameters for the pointing correction loop will be made, wit the loop still open, to provide a reference for comparison with closed loop data.

The pointing correction loop will then be closed. Again, the significant parameters will be measured. Programmed disturbances will then be introduced into the loop, and the effects on the performance measured.

Figure 9.6.6.4-1 illustrates the loop, and shows the points at which measurements are made, and those at which disturbances are introduced.

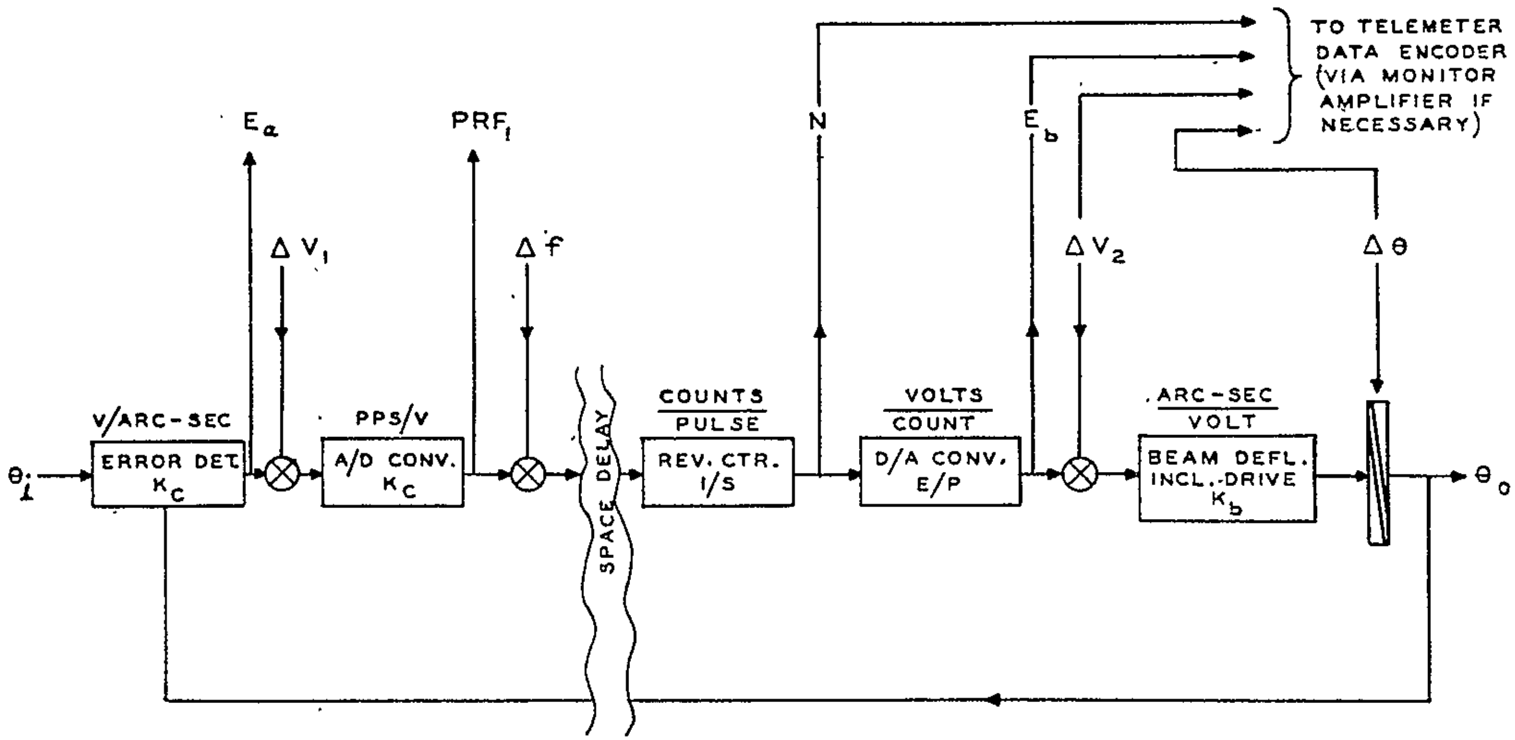

Figure 9.6.6.4-1 Analytical Model Space-To-Ground-To-Space Feedback Loop for Point-Ahead Experiment

Measured quantities include:

E_a - Pointing error output of ground array

PRF_1 - Digitized pointing error signal before transmission

N - Output of digital integrator (spaceborne)

E_b - Output of D/A converter, fed to diasporameter command input.

Programmed (and monitored) disturbances are introduced at:

ΔV_1 - input to pointing error A/D converter

Δf - input to ground station error transmitter

ΔV_2 - Command input to diasporameter

$\Delta \theta$ - Input to tracking loop beam deflector, controlling both transmitter and receiver lines of sight.

The actual lead angle required, about forty seconds of arc, can readily be simulated from a synchronous equatorial satellite, by a physical separation of the Earth's transmitting and receiving installation of approximately four miles. The receiving installation, which maintains angle track on the satellite, must, of course, communicate accurate angle information to the transmitter, in order to enable it to keep the satellite illuminated.

It is anticipated that the point ahead experiment will be conducted after tracking capability has been tested and verified. In order to co-locate the earth station receiver and transmitter, an initial point ahead bias must be maintained to allow for the tangential velocity difference at synchronous orbit and ground. At the start of the simulated deep space point-ahead test, the Earth station will command the point ahead mechanism to slew over the amount required to hit the new receiver, some four miles away.

It can be seen that, for the proposed mechanization, the overall loop is inextricably interwoven with the point ahead operation; the space-to-ground-to-space loop closure thus represents an integral part of the point ahead experiment, rather than a separate demonstration. Nevertheless, it would be of interest to open the feedback loop during the test (for periods that would have to be determined experimentally, gradually increasing), to see how far and how fast the transmitter beam will wander off the target without the benefit of correction.

The idea underlying the major portion of loop testing is the same one as in the PRECISION TRACKING experiment, namely that of introducing calibrated disturbances at several points of the loop. Amplitude and frequency of the disturbance, as well as that of the response are either metered on the ground, or monitored in the satellite and relayed back to the ground station.

Overall loop performance, as well as the functioning of individual blocks, will be considered. It should also be possible to adjust the loop gain by controlling the sensitivity of the error detector (volts per arc second), the scale factor of the analog-to-digital converter (pulses per second per volt) at the ground station, or the scale factor of the digital-to-analog converter, via telemeter control (figure 9.6.6.4-1).

9.6.7 Transfer Tracking from One Ground Station to Another

A deep space vehicle in optical communication with earth must possess the capability of transferring track between earth stations in order to maintain continuity of operation despite cloud overcast and the Earth's rotation. The acquisition and tracking between a spacecraft and a ground complex (beacon transmitter and ground receiver), which naturally precedes transfer tracking, is discussed in subsections 9.6.5 and 9.6.6. A chain of earth stations must be established and so located that a minimum of two stations with reasonable zenith angles and high probability of clear weather will have a direct line of sight to the vehicle. Meaningful experimentation with precision tracking of a ground beacon can only be conducted from altitudes above 2000 miles. The transfer tracking demonstration is predicated on accurate tracking, and consequently also requires such space testing.

The station spacing required to demonstrate the 11 arc-second tracking transfer from synchronous altitude-which is the altitude proposed for the PRECISION TRACKING OF A GROUND BEACON experiment- is one mile; however, a four mile separation is required for the POINT AHEAD AND SPACE-TO-GROUND-TO-SPACE LOOP CLOSURE experiment. Consequently the transfer will be performed at a four mile separation. Both stations, at a four mile separation, will have co-located receivers and transmitters for the tracking transfer demonstration.

Two techniques will be tested from synchronous orbit. One will involve transfer by commands to the 1.0 meter telescope beam deflection system. The other will involve transfer back to the 0.3 meter telescope in order to put both beacons in the field-of-view at the same time, and subsequent transfer to the 1.0 meter telescope after completion of transfer in the 0.3 meter.

9.6.7.1 Experiment Design

Adequate hand-over techniques must be developed before wide bandwidth laser communications can be utilized for either earth orbit or deep space vehicles which require uninterrupted communication. Certainly a function required for deep-space vehicle communication must be proven before actually undertaking such a mission. In order to make this possible, a chain of earth stations must be established, so located that a minimum of two, and preferably more stations will have direct line of sight to the vehicle, with reasonable zenith angles and high probability of clear weather.

One study[1] resulted in the recommendation for using a total of eight stations around the globe, with probability of clear reception greater than 90 per cent for the full rotation of the earth (if one site location in Red China is assumed to be accessible), and greater than 95 per cent for a very large portion of the diurnal cycle. This study is, however, based on communication down to zenith angles of 70° which may be excessive for high quality optical contact; it may be necessary to provide more stations to reduce required elevation coverage. For the sites listed in Ref. (1), the largest spacing is that between sites at 19°N - 156°W and 20°S - 113°E, a chord length of some 5200 statute miles, which may subtend as much as 11 arc seconds at vehicle range of 1 AU.

It is anticipated that the realistic spatial situation of the lead angle requirement in the point ahead demonstration, using a synchronous satellite requires a four mile separation of receiver and transmitter stations Ordinarily, the station spacing required to demonstrate tracking transfer from synchronous altitude would be one mile. Since the stations required for the point ahead demonstration would be available, these stations can be used to demonstrate tracking transfer. Obviously, a system that can transfer tracking between stations four miles apart will more than satisfy the normal requirement of one mile separation.

In the realistic deep-space case, two stations separated by 11 arc second will both fall well within the ±15 arc second field of view of the 1.0 meter telescope. Thus, when the second station's transmitter illuminates the spacecraft, the 1.0 meter telescope, which has been tracking the first station, will move over and track to a position representing the "center of gravity" of the intensity between the two beacons. When the first beacon is then turned off, the telescope will track the second beacon to the center of the field.

Since the two stations to be used for this experiment are separated by 40 arc seconds at the test (synchronous) altitute, the second beacon will not be in the field of view of the 1.0M telescope when the first is being tracked. For this reason, transfer will be accomplished first with one and then with the other of the following two techniques:

a. Direct transfer of the 1.0 meter telescope, using angle command to the beam deflection system. The appropriate angle commands can be computed on Earth, using the known coordinate frame of the vehicle attitude with respect to the stellar coordinates and earth line of sight.

---

(1) Kenneth L. Brinkman et al, Study on Optical Communication From Deep Space, Hughes Aircraft Co., Aerospace Group, Interim Progress Report, No. SSD 3166R, NASA Doc. No. N64-16770.

The angle commands are fed to the input of the angle tracking fine beam deflectors, with the tracking loop, including the coupling between the beam deflectors and the gimbals, disabled. Upon acquisition of the new beacon, the tracking loop is again activated, and the beacon is tracked to the center of the field in the normal manner, using both the gimbals and the fine beam deflectors.

The point-ahead angle requirement may change by as much as 0.7 arc second, or several beamwidths, between two earth stations, as a result of the difference in the relative velocities caused by a difference in latitude. Corresponding commands must also be computed and telemetered to the vehicle, so that the transmitter beam can be directed to the new station with a minimum of delay. The timing of the tracking and pointing transfer commands should be such that switchover of transmission from the old to the new station will occur immediately after the tracking transfer instructions have been issued, thus allowing the vehicle to track the new station. Reception must, however, continue at the old station for one transmission delay interval. The transmitter telescope at the new station must be directed by data radioed over from the old station and corrected for the angular difference. The new station's receiver, which will not begin operaation until one transmission delay later, can also be slewed into position upon the basis of such data.

This technique has the disadvantage that a momentary loss of contact in both directions will result from the time required to move the line of sight from one station to the other. The requirement for a precise open-loop angle command from the earth may also be considered a disadvantage of this technique. It does, however, allow the transfer to be accomplished entirely with the 1.0 meter telescope.

On the basis of the protracted tracking and angle smoothing operation preceding the optical communication process, and the refined tracking permitted by it, the angular computations required for the above should certainly be feasible. The exact form of the computations, as well as that of the commands remains to be investigated.

Transfer via the 0.3 meter telescope.

In this method, tracking is handed over from the 1.0 meter spaceborne telescope to the 0.3 meter spaceborne telescope. Since its field of view is ±45 arc seconds, the second beacon will be in the field of view when the first is being tracked, even though they are separated by 40 arc seconds. When the second beacon is turned on and illuminates the spacecraft, using pointing data transmitted from the first station, the 0.3 meter spaceborne telescope will track a point between the two, repsenting the center of illumination. The first station is now switched off, and the 0.3 meter telescope tracks the second beacon to the center of its field. Tracking data are next transferred from the gimbals and beam pointing system of the 0.3 meter telescope to the 1.0 meter telescope, which will now acquire and track the second station. At the same time, the new computed value of point-ahead is transmitted to the spacecraft, as outlined under alternative a) above. The transfer within the 0.3 meter telescope is directly analogous to the manner in which transfer would take place within the 1.0 meter telescope when the stations are only 11 arc seconds or less apart (i.e., in a deep space mission).

While space-to-earth contact is interrupted with this method also, as it is in method a), contact from ground to space is maintained continuously. This technique does not require the precise open loop angle command from earth. It does, however, require the extra complication of transfer from the 1.0 meter to the 0.3 meter telescope, and back again.

9.6.7.2 Measurement Objective

The purpose of the experiment is to compare the relative merits of the two techniques described above and to assess their applicability to the various phases of a deep space flight. To this end it is desired to obtain a time history of the tracking loops during the interval between the initiation and completion of the transfer.

9.6.7.3 Experiment Equipment Design

The instrumentation aboard the spacecraft is identical to that used in the Precision tracking and Point ahead experiments. The only added requirements - (which are in the form of design refinements to be incorporated subsequent to the conceptual design phase) are means to insert a calibrated offset into the fine beam deflector of the 1.0 meter telescope and a means of disabling the gimbal drive momentarily. In the ground complex, in addition to the tracking capability of the second station, there are also employed a steerable laser beacon transmitter and the communication link to the computation facilities at the first station.

9.6.7.4 Data Management

The data to be collected include the tracker error signals, the fine beam deflector deviations, point ahead angles, and the telescope gimbal angles for both telescopes. These quantities will be sampled at a high frequency and telemetered to the ground station where they will be recorded on a suitable strip chart. The high frequency variables, namely error signals and beam deflector positions will be sampled at a rate of 100 samples per second. The slower elements, point ahead angle and gimbal angles can be sampled a few times a minute.

9.6.8 10-Micron Phase and Amplitude Correlation

Although atmospheric effects on the propagation of electromagnetic waves have been the subject of scientific and engineering interest for hundreds of years, increases in the spectral capabilities, resolution, and sensitivity of available instruments and sensors have revealed gaps in the knowledge of the atmosphere (section 9.1), as well as renewed interest in measurements previously attained with great difficulty.

The effects on the transmission of optical frequencies can be determined by a detailed examination of the attenuation and refraction characteristics of the atmosphere. The absorption properties of the atmosphere have yielded much of the information now available. There is still much information to be gained, however, through measurement of refraction effects.

Temporally and spatially random variations in the index of refraction of the atmosphere have limited the performance of optical instruments. Now that optical wavelengths can be applied to communication, tracking, and mensuration, the need for detailed knowledge of these variations has become even more evident. Theoretical knowledge of the effect of these variations on optical wavefronts has progressed to the point (paragraphs 9.1.1 and 9.1.2.1) where measurements must be made of the physical quantities and their functional relationships. To date, theoretical derivations have been based on correlation and structure functions or extrapolated from the microwave frequencies in which the presence of water vapor is considerably more significant than at optical frequencies. Most available measurements at optical frequencies have been made with stellar or thermal sources that have such poor temporal coherence that extrapolation to the more coherent laser light applications is of questionable validity.

In this experiment, a technique for measuring the phase variations as functions of time and space, with a highly monochromatic CO_2-N_2 (10.6-micron) laser source, is proposed (figure 9.6.8-1). Amplitude correlations are also measured. From these measurements, the limitations on coherent apertures could be determined for ready application in the design of superheterodyne systems and an assessment made of the accuracy of scientific measurements that depend on signal frequency.

To correlate experiment and theory, which usually assumes a plane wave incident on a random medium, it is necessary that the turbulent medium be in the far field of the transmitting antenna. This cannot be done with a transmitting aperture located within the atmosphere. To make such measurements would require a monochromatic light source in orbit and a receiver that samples and correlates two points on a wavefront. To avoid spatial integrating effects, the measurements should be made with a small aperture.

The extent of spatial phase and amplitude perturbations imposed by the time-varying atmosphere are essentially unknown in the far infrared. Such measurements require a monochromatic light source in orbit and a receiver that samples and correlates two points on a wavefront. To avoid spatial integrating effects, the measurements should be made with small apertures. Signals from a spaceborne 10.6-μ transmitter will be measured with 2-cm apertures. Correlations will be made at various separation distances between 4 cm and 10 meters. An evacuated and seismically isolated instrument is required to avoid random differences in the optical paths following the initial sampling aperture.

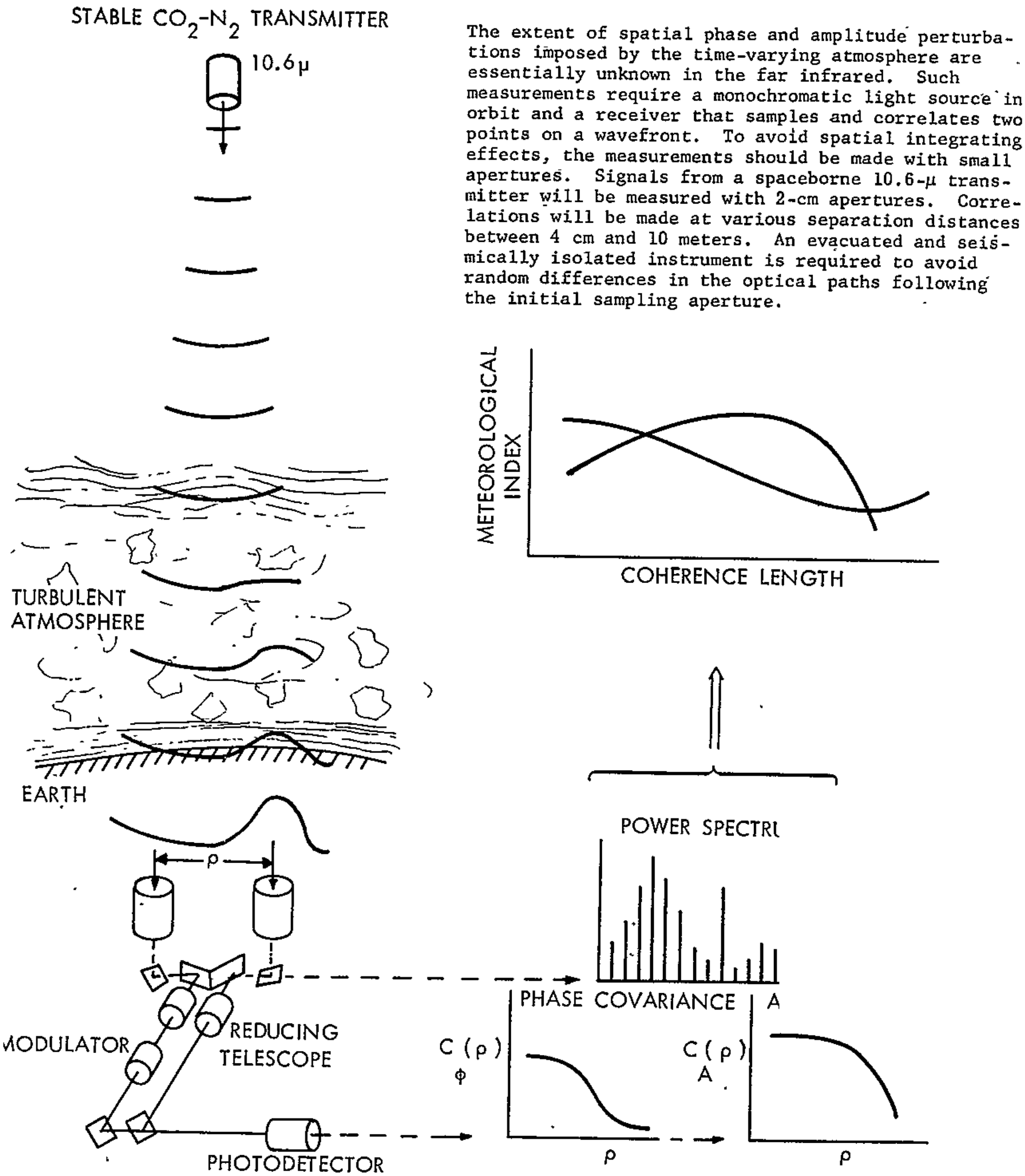

Figure 9.6.8-1. 10-Micron Phase and Amplitude Correlation

9.6.8.1 Justification

Horizontal tests (paragraphs 9.1.2.2) clearly show the existence of a maximum effective aperture which varies with turbulence conditions. In these tests, image quality or optical heterodyne receiver performance has been used as an indirect measure of phase covariance. The laser beam result for log-amplitude variance (paragraph 9.1.1) is one theoretical prediction that can be directly compared with experiment. The 10-micron Phase and Amplitude Correlation experiment seeks to measure the transmitter diffraction distance. For a horizontal path on Earth, this distance is predicted as $L/k\alpha$, where L is the range and α is the standard deviation of the amplitude distribution across the transmitter aperture. There may be no advantage to increasing transmitter apertures beyond $\alpha = (L/k)^{1/2}$. Such a result would have significant bearing on the efficacy of optical heterodyne communication.

In principle, the measurements proposed could be made on stellar sources. However, the actual measuring must be made with a resonable signal-to-noise ratio. The accuracy of measurement is further improved by the use of highly monochromatic light.

Measurements on starlight as well as ground-based measurements of laser light have shown a dependency on the distance to the receiver as well as to the transmitter of the disturbing elements of the atmosphere. Space testing would remove this doubt from the data obtained.

9.6.8.2 Experiment Design

The object of this experiment is to measure the phase and amplitude perturbations imposed by the time varying atmosphere on a signal transmitted at optical frequencies, and to determine the correlation in the phase front of two points as a function of their separation. Amplitude correlations should also be measured. Because the frequency deviations due to the atmosphere are of the same order of magnitude as those due to instability in the laser oscillator itself, it is important to measure these deviations as independent of the laser instabilities as is possible.

Short term relative stabilities of a laser oscillator in the order of 3×10^{-9} have been reported.(1) Theoretical studies(2) have also shown that the line broadening due to molecular scattering effects in the atmosphere is also in the order of 10^{-9}.

---

(1) R. Targ and W.D. Bush, "Automatic Frequency Control of a Laser Local Oscillator for Heterodyne Detection of Microwave-Modulated Light," Applied Optics, vol. 4, no. 12, December 1965.

(2) A. Consortini, L. Ronchi, A.M. Scheggi, and O. Toraldo di Francia, "Deterioration of the Coherence Properties of a Laser Beam by Atmospheric Turbulence and Molecular Scattering," Radio Sci., vol. 1, no. 4, April 1966.

In addition to the above effects, refractive index inhomogeneities moving relative to the receiving aperture will cause amplitude and angle modulation as well as undesirable image motion effects. Angular deviations of the phase front of the order of 1 to 3 seconds of arc have been observed in small apertures. If these deviations occur in 0.1 to 0.3 seconds with a 2-cm aperture, a phase shift, changing linearly across the aperture at about 1 to 2 hertz, is indicated.

The greatest instrumentation difficulties lie in the mechanical design of the rigid optics required. Random differences in the optical path following the initial sampling aperture are undesirable. The longer these paths are made the greater the chance for error. Processing of the data is simplified if two apertures can be separated enough to assure complete decorrelation between the two paths. At low altitudes this may be of the order of meters, but at higher altitudes separation of several meters may be required. It would probably be necessary to have evacuated optical paths to assure high accuracy. The other important calibration point is at minimum separation which should be made small for measurement under severe atmospheric conditions.

A method of measuring atmospheric perturbations that minimizes the effect of laser instabilities is shown in figure 9.6.8.2-1.

Two small apertures of diameter D are capable of being separated at distance ρ, which can vary from D to a distance large enough to assure that the phase perturbations at aperture 1 are uncorrelated with those at aperture 2. The operation of the instrument is as follows. Nearly monochromatic light from a spaceborne laser is collected by apertures 1 and 2. The signals at time t, denoted by the subscript at the two apertures, can be denoted by

$$A_1 \cos \omega (t - \tau_1) + \delta_{t - \tau_1}$$

$$A_2 \cos \omega (t - \tau_2) + \delta_{t - \tau_2}$$

where A_1 is the amplitude, ω the radian frequency, τ_i is the transit time from the source to the indicated aperture, and δ is a phase angle that is due to instability in the laser. Assume for the rest of this discussion that the phase delay in both arms of the instrument are equal so that time t can be the time when the delays are compared at any time in the system. The signal in arm 1 will be attenuated, and fall on the surface of the photomultiplier with a different amplitude, say

$$a_1 \cos \left[\omega (t - \tau_1) + \delta_{t - \tau_1}\right]$$

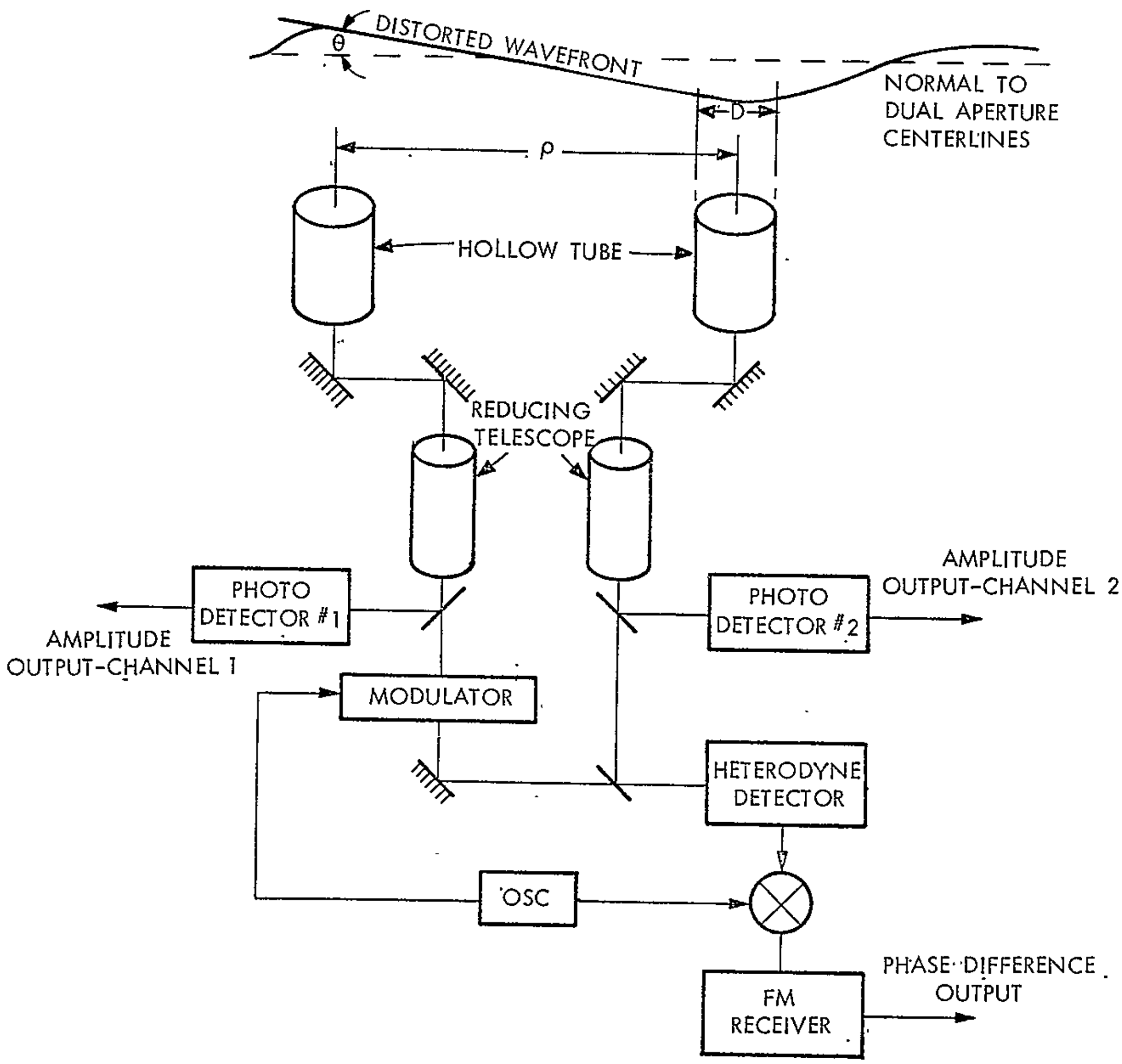

Figure 9.6.8.2-1. Atmospheric Measurement, Phase Correlation

The signal in arm 2 will be given an additional modulation ω_m ($\omega_m << \omega$) to aid in further processing of the signal, so that the signal in this arm becomes

$$a_2 \cos \left[\omega(t - \tau_1) + \omega_m t + \delta_{t - \tau_1}\right]$$

The square law action of the photomultiplier will mix the two signals, resulting in a dc term, higher frequency terms (which are assumed attenuated by the circuits following), and the difference frequency term, which is of interest. The term is

$$K \cos \left[\omega_m t + \omega (\tau_1 - \tau_2) + \delta_{t - \tau_1} - \delta_{t - \tau_2}\right] \tag{1}$$

Now if $\tau_1 - \tau_2$ is constant, the output of the filter following the photomultiplier will be at a constant frequency ω_m. If $\tau_1 - \tau_2$ is time varying, however, an angle modulation will result.

First, consider the relative value of the laser instability. Since $\tau_1 - \tau_2$ are travel times over very nearly the same path, they will not differ appreciably so that to a very good approximation

$$\delta_{t - \tau_1} = \delta_{t - \tau_2} + \dot{\delta}_{t - \tau_2} (\tau_1 - \tau_2)$$

where the dot indicates the derivative with respect to time. Equation (1) then becomes

$$K \cos \left[\omega_m t + (\omega + \dot{\delta}_{t - \tau_2}) (\tau_1 - \tau_2)\right] \tag{2}$$

where ω is the optical frequency and $\dot{\delta}$ is the instantaneous drift frequency.

A spaceborne laser may have $\dot{\delta}$ as great as 3×10^8 Hz. However, compared to the optical frequency of 3×10^{13}, $\delta << \omega$, and can be safely ignored, so that the signal of interest is

$$K \cos \left[\omega_m t + \omega (\tau_1 - \tau_2)\right]$$

If this signal is passed through a phase shift discriminator centered at ω_m, the input to the recorder will be a signal proportional to the

$$\omega\tau_1 - \omega\tau_2 = \psi_1 - \psi_2$$

where $\psi_1 - \psi_2$ is the difference in phase (averaged over the small aperture) at two points separated by a distance ρ. With proper design, phase shifts occurring at frequencies as high as 1000 Hz should be recorded. From this record of transit time delay, further processing will provide the following information. First, squaring and averaging,

$$\overline{(\tau_1 - \tau_2)^2} = \overline{\tau_1^2} + \overline{\tau_2^2} - \overline{2\tau_1\tau_2}$$

In that part of the record taken where ρ is large, $\overline{\tau_1\tau_2} = 0$, and assuming that

$$\overline{\tau_1^2} = \overline{\tau_2^2} \text{ , then } \overline{(\tau_1 - \tau_2)^2} = \overline{2\tau_i^2}$$

so that the variance in transit time can be determined directly. Having found $\overline{\tau_i^2}$, at other portions of the record where ρ is shorter, the correlation in transit times as a function of ρ can be found from

$$\overline{\tau_1\tau_2} = \overline{\tau_i^2} - \frac{\overline{(\tau_1 - \tau_2)^2}}{2}$$

It has been shown that it is possible, in principle, to measure the phase difference along a wavefront between two points separated by a distance ρ. If the two sampling apertures are exactly perpendicular to the line between the source and the center of the interferometer arm, the phase difference is caused by the path differences encountered by the light as it travels from the source to the receiving apertures. In the practical case, the arms of the interferometer cannot be aligned exactly. It is important to consider the effects of misalignment of the phase front as well as of the motion of the satellite relative to the apertures of the interferometer.

Although theoretical treatments are available in the literature, a quick appreciation of the magnitudes of phase front distortions involved can be obtained from the following considerations, As shown in figure 9.6.8.2-1, a distorted wavefront will have random displacements that will appear as a phase perturbation to any aperture parallel to the "average" phase front. For a sufficiently small aperture, the entire wavefront will arrive at an angle, θ, which will cause motion of the entire image in focal plane of the lens L. From measurements made by astronomers, θ has been found to be up to 3 arc seconds ($\approx 15 \times 10^{-6}$ radians) with the wavefront correlated up to a distance of 6 inches (15 cm) or more, in the visible spectral region ($\lambda \approx 0.5$ microns) under conditions of great image motion. Extrapolating the coherence diameter using the sixth-fifths power wavelength dependence predicted by the Obukhov-Kolmogorov turbulence theory,[3] a short calculation shows that the phase perturbation at any point

$$\frac{2\pi\rho\theta}{\lambda}\left(\frac{10.6}{0.5}\right)^{6/5} = \frac{2\pi\,(0.15)\;15 \times 10^{-6}}{10.6 \times 10^{-6}}\;(21)^{6/5} \approx 2\pi\,(12)\text{ radians}$$

which is greater than an optical wavelength. The phase difference measuring instrumentation must be capable of measuring and recording phase differences of greater than a wavelength. Because these phase jumps can occur in 1/10 second intervals or less, frequency shifts of greater than 30 Hz can be expected under rather ordinary conditions.

Because it is desirable to have the two apertures parallel to the average wavefront, the technique of tracking the source in angle was examined. Assuming that it was desirable to keep the tracking noise down to say 1/10 of the expected phase deviation to be measured, this would require, for a 1.0 meter interferometer, a tracking accuracy of better than 0.25 microradians ($\approx$ 1/20 sec), which is nearly the goal for the OTAES, and does not seem to be a reasonable objective for ground-based instrumentation unless absolutely required.

Another possible source of noise is that due to seismic activity. Observations have been made of the amplitude of seismic waves [4] of 1/2 to 1 micron with periods of 0.01 to 0.05 second during which intervals of high activity (winter months) with larger amplitudes for longer period waves. During microseismic storms the amplitudes can be much greater. It is estimated that the effects of these disturbances can be minimized in the design of the instruments.

Noise due to wind buffeting could also be a problem. Isolation from seismic noise will introduce a degree of flexibility that must be protected from the wind. Structures designed to reduce wind effects will serve as thermal sources, as well as wind deflectors, the effects of which must be considered in interpretation of the recorded data. Careful design is required to minimize turbulence due to the protective structure.

In addition to the random noise sources that will cause random errors in the measurement of the phase difference between the two apertures, there will be a bias component due to the motion of the source relative to the interferometer. A satellite in a 24-hour circular orbit inclined 20° to the equator could have an angular rotation relative to an interferometer; this represents a frequency difference of $\approx$16 Hz, which would be changing relatively slowly. Measurements made at this

---

(3) V.I. Tatarski, Wave Propagation in a Turbulence Medium, McGraw-Hill Book Co., Inc., New York, 1961.

(4) Handbook of Geophysics, pp. 12 and 49-50.

point in the orbit with a 3° field of view could cover an interval on the order of an hour or so. Subsequent processing of data containing this nearly steady frequency component should permit separation of the random phase errors from the steady components.

As previously discussed, expected phase variations can be several wavelengths. For a 1-meter baseline, an alignment to within microradians (at visible wavelength) would be required if the instrument were to be held parallel to the average wavefront. Wavefronts arriving at an angle will be delayed at the more distant aperture. However, assuming that the instrument is within 3° ($\approx$ 1/20 radian), the time delay (seconds per meter baseline length) is 1/20C, where C is the velocity of light. For a 6-meter baseline, the delay is 10^{-9} seconds, which is two to three orders of magnitude smaller than the period of the highest frequencies expected. Although this represents a phase delay of many optical wavelengths, the phase disturbances will occur over intervals usually greater than 10^{-3} seconds, and hence should be measurable. Misalignment to the wavefront of large angles could introduce time delays greater than desired, as well as reduce the base line separation by the cosine of the angular deviation.

As a result of the above considerations, it is concluded that the phase correlation measurements should be made without the aid of optical tracking because the tracking noise introduced is of the same order of magnitude as the effects being measured. A fixed interferometer of the type described, oriented within a few degrees of the average wavefront and properly protected from the wind and seismic disturbances, seems within the current capability of optical technology.

The associated phase difference measuring circuitry is considered within current technology although additional study is required to determine optimum circuit parameters. From information presently available on the power spectrum of phase variations, variations up to 1000 Hz rates should be measured.

Amplitude correlations can be measured by direct detection of the optical intensities as shown in figure 9.6.8.2-1. Subsequent signal processing is required to reduce the raw data to log-amplitude variance and covariance in order to compare results to theory. A block diagram showing the signal processing circuits is shown in figure 9.6.8.2-2. Log-amplifiers, differential amplifiers, and multipliers directly convert the data to log-amplitude covariance for recording and subsequent analysis.

GaAs optical modulators that will transmit roughly 60 to 70 per cent of the light input have been built. Photodetectors of sufficient sensitivity that will have a passband up to 100 MHz or so are available. The bandwidth of the phase perturbations should be less than 1000 Hz, and a local oscillator of the desired frequency could be readily available.

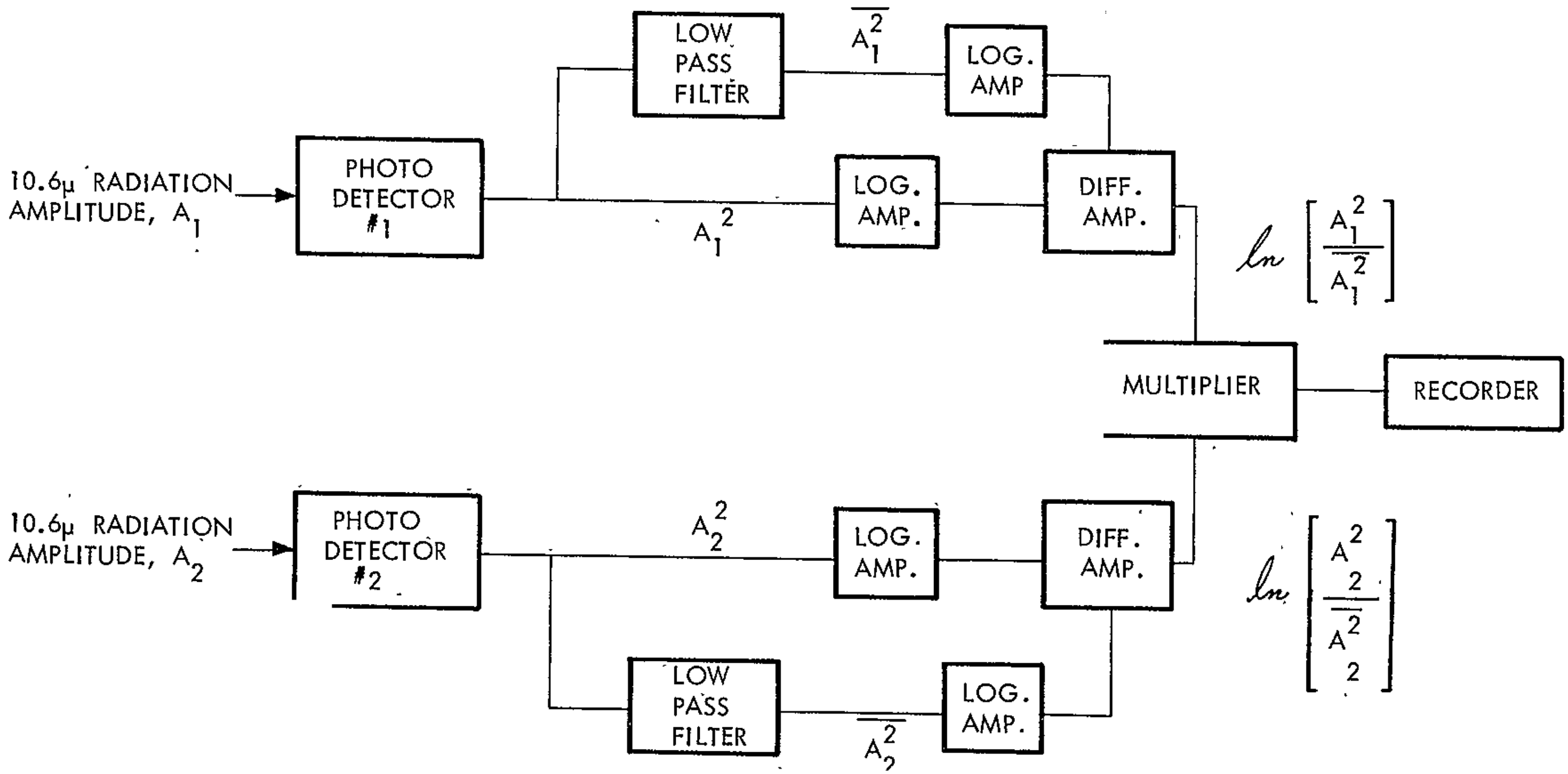

Figure 9.6.8.2-2. Amplitude Correlation Signal Processing

To reduce angular motion to a minimum, the experiment should be conducted at synchronous altitudes. A diffraction-limited aperture 0.3 meter in diameter, capable of tracking the receiving station on earth to an accuracy of about one arc second, is required to provide adequate signal to the narrow aperture required.

9.6.8.3 Measurement Objectives

This experiment will determine the phase and amplitude correlation functions for a 10.6-micron CO_2 laser after transmission through the atmosphere. CO_2 laser radiation transmitted from space-to-ground will be detected by a dual-aperture, adjustable ground receiver. Provision must be made for both direct and heterodyne detection through each aperture. These simultaneous phase and amplitude fluctuation measurements will be made in a variety of atmospheric conditions to obtain statistical data.

9.6.8.4 Equipment Design

The spacecraft equipment used for this experiment will be the same as used for the Heterodyne Detection on Earth experiment. The 10.6-micron CO_2 laser located in telescope no. 2 will be the experiment transmitter (figure 9.6.8.4-1).

Two folded optical telescopes evacuated with an aperture of 2 cm in diameter, capable of focusing their outputs on a common photodetector for the phase correlation measurement. Provision must be made to insert filters and attenuators or modulators in the optical path of either telescope. Separations up to 2 to 3 meters could probably be obtained with transportable equipment. Larger separations would require fixed installations, possibly having phase-compensated paths at large separations. This could be accomplished with an auxiliary laser, ground-based.

A high speed photodetector capable of operation at 10.6 microns with signals having a bandwidth of 2 kHz centered in the 10-80 MHz band is needed for the phase correlation measurements. For the direct detection amplitude fluctuations, a nominal frequency response of 1 kHz is adequate. An optical modulator will be used to frequency modulate an incoming laser signal with a 10 to 80 MHz offset frequency to enable filtering out the dc component of the received signal.

Additional equipment unique to this experiment includes

Equipment Control, Sequencing, and Measurements System

Phase Correlation Signal Processing Circuits

Amplitude Correlation Signal Processing Circuits

Signal Storage/Computational Facilities

Experiment Control/Display Console

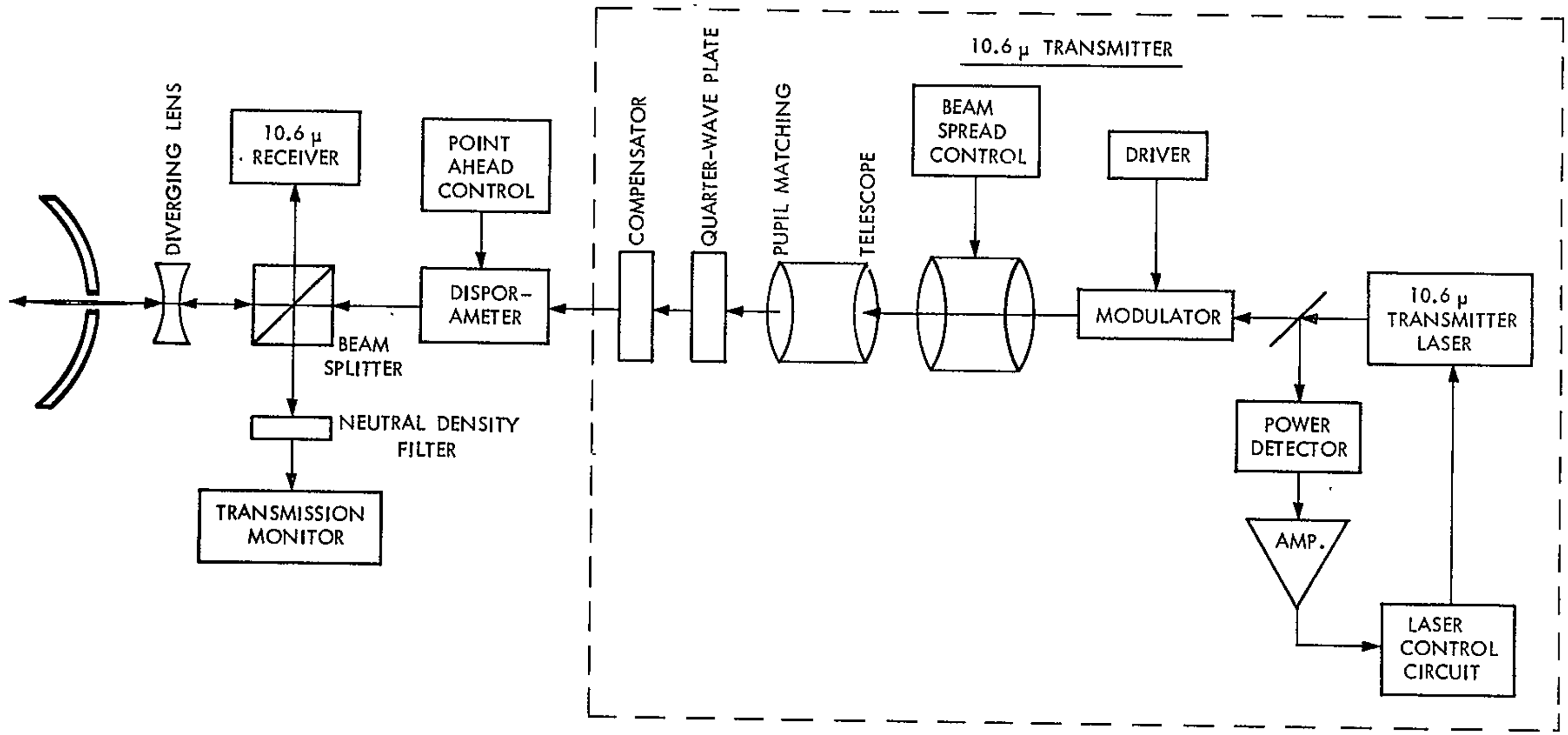

Figure 9.6.8.4-1. Block Diagram of Telescope No. 2: 0.3-Meter - Strap-On

9.6.8.5 Data Management

Optical transmitter power and fluctuations in power are telemetered for subsequent normalization of the received amplitude fluctuations. Ground measured data will be processed, recorded and displayed as desired at ground console.

The recorded analog data will be analyzed to provide:

a. Atmospheric transmission losses

b. Power spectrum of signal fluctuations

c. Variance and covariance of amplitude fluctuation versus dual aperture spacing

d. Variance and covariance of phase fluctuations versus dual aperture spacing

e. Dependence of data on synoptic conditions.

The equipments aboard the spacecraft that must be operated include:

a. An 0.6328-micron stabilized laser transmitter

b. A 10.6-micron stabilized laser transmitter

c. The 1.0 meter telescope, in a tracking mode

d. An 0.4880-micron tracker for telescope no. 1

e. The 0.3-meter strap-on telescope (no. 2) in transmit mode

f. Transmission monitor for telescope no. 2

g. Transmitter beam spread control for telescope no. 2

h. Transmitter beam point-ahead control for telescope no. 2

j. RF telemetry and beacon system.

The astronauts can operate these equipments using the laser control panels, figure 9.6.8.5-1 (and figures 9.8.1-1 through 9.8.1-3). Alternatively, this experiment can be operated from the ground OTTOS-OTAES Control Room (figure 9.6.2.4.2-3) using consoles 1 and 3 (figures 9.6.1.5-6 and 9.6.8.5-2). The OTTOS panels used to operate experiment 1 are shown in figures 9.6.1.5-8 through 9.6.1.5-13.

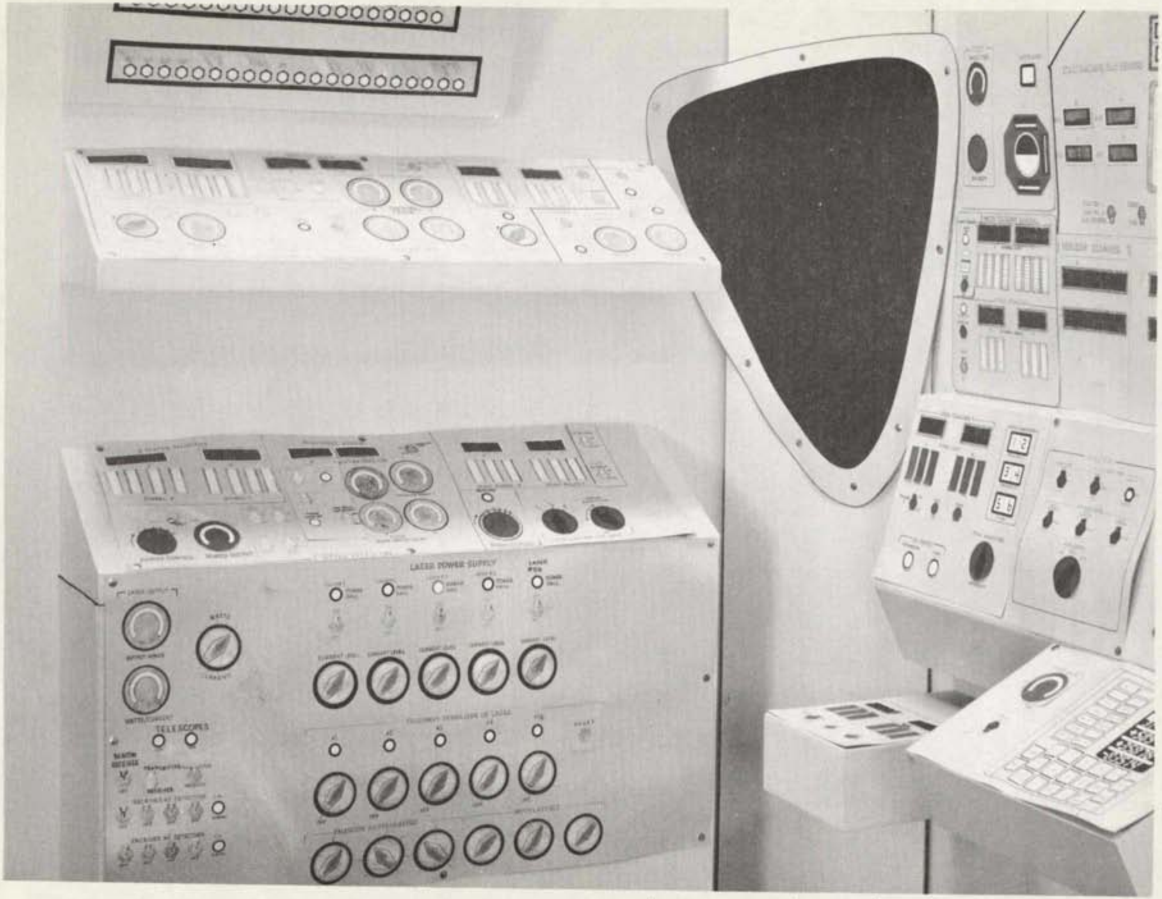

Figure 9.6.8.5-1. Star Tracker/Sun Sensor Display Panel

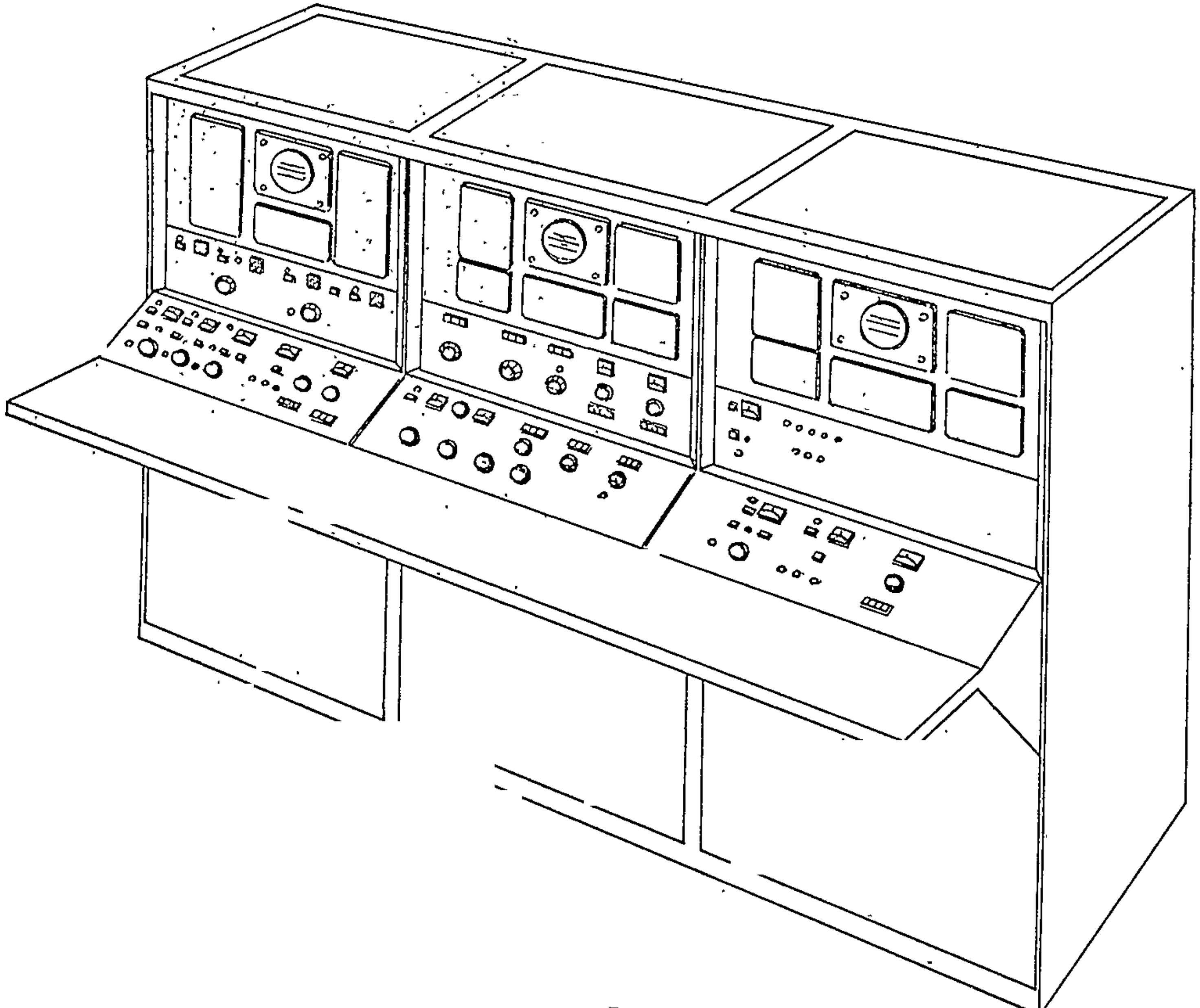

Figure 9.6.8.5-2. Console - Experiments 1, 2, 8 and 9

The ground-based equipment required for this experiment will include:

a. The 10.6-micron interferometer -- phase comparator

b. The 8.0-meter aperture direct detection telescope, or the 1.0-meter aperture heterodyne detection telescope, for use in signal acquisition and boresighting procedures

c. Pointing and positioning equipment

d. 10.6-micron direct or heterodyne receivers

e. Receiving electronics and data handling equipment

f. Control and display consoles for receiving telescopes, receivers, interferometer, data processing, and recording equipment.

g. 0.4880 laser beacon transmitter

h. Microwave tracker to provide pointing information

i. Spacecraft telemetry command and display.

The ground-based equipment will be checked for operability before the experiment is begun. All of the lasers (0.4880-micron beacon and 10.6-micron local oscillator) will be turned on and thermally stabilized, and AFC circuits turned on. Cryogenic cooling will be supplied to the 10.6-micron heterodyne receiver and to the interferometer -- phase comparator. Internal checking of the receiving electronics will be done by injecting an optical signal directly into the photodetectors and checking the output against the input for gain and distortion. These functions will all be controlled from the ground station control consoles. Signal processing electronics will be self-checked in a similar manner.

The beacon modulator will be operated with selected test signals, and the beacon output will be measured. Pointing of the beacon will be done by using the inputs from the RF tracking stations such as Goldstone, and the RF tracking equipment at the optical ground site.

The interferometer and one of the receiving telescopes is pointed at the spacecraft, using the same pointing signal inputs. More accurate pointing will be done after the spacecraft signal is acquired by the receiving telescope, and the spacecraft transmitter boresight error is corrected.

The RF telemetry system will be checked for operational status at the spacecraft status display and control console.

9.6.8.5.1 Experiment Performance

Radiosonde balloons will be released over a period of several hours prior to, and during, optical measurements, in order to record upper air conditions. Local meteorological conditions will be measured near the interferometer. When there is no interference from clouds, the spacecraft will be commanded to acquire the 0.4880-micron ground beacon, to begin fine tracking, and to transmit test signals on the 10.6-micron downlink. The pointing of the ground receiving telescope, the beacon transmitter, and the interferometer are updated, so that spacecraft and ground station are accurately illuminating each other. The modulation of the transmitted beam will be a selected narrow-band signal so that the receiver bandwidth may be narrowed accordingly, giving a good signal-to-noise ratio for the reduced signal intensities obtained with wide transmitter beamwidths.

The 10.6-micron transmitter is commanded to scan around its line-of-sight, in order to measure, and correct, its boresight error. As the pointing accuracy and the boresight of the spacecraft are improved, the transmitter beam may be narrowed in increments, and a high signal-to-noise ratio achieved in the interferometer system, which has a smaller receiving aperture diameter. The auxiliary receiving telescope may then be turned off, unless required for another simultaneous experiment.

The effective received coherence diameter at 10.6 microns will be measured over extended periods of time by varying the separation of the interferometer entrance apertures and measuring phase fluctuations. These will be displayed at the interferometer control console, and automatically recorded.

The duration of the phase and amplitude correlation measurement experiment will be determined primarily by weather conditions, and secondarily by the conflicting needs of other experiments, such as the transfer of tracking from one ground station to another. Data should be taken over periods of several hours at a time, especially when weather conditions are changing.

9.6.9. Pulse Distortion Measurements

The atmosphere, as a propagation medium, has been studied intensively by communications engineers. Several methods have evolved for measuring the maximum bandwidth which the medium can support. One of these, the impulse response technique, promises additional insight into the physical structure of the atmosphere as well as a measure of channel capacity, when adapted to optical propagation studies.

Measurements described in the preceding experiments would provide the spatial and narrow-band characteristics of atmospheric optical transmission. It would be desirable to transmit a very wideband signal to observe whether conditions for selective fading exist. Knowledge of the fading characteristic of the medium can assist an instrument designer to choose between an analog or digital system, and may lead to a preference for non-thresholding detection techniques and redundant coding. Multipath transmission caused by scatters in the atmosphere introduces a transit time spread that can limit resolution or distort a message. Time spread can also be introduced by index of refraction variations, and this effect can vary drastically with frequency. All these effects tend to limit the laser communication channel bandwidth or information rate. They are not important in the megahertz range but are important for gigahertz bandwidths. Time dispersion is especially important in modulation techniques such as FM and PCM, where ultrawide bandwidths are essential to efficient transmission of megahertz information bandwidths.

One method of determining the phase and amplitude characteristics of a channel is to transmit a known wideband waveform through the channel and compare the received waveform phase and amplitude characteristics with those of the transmitted characteristics. By accounting for changes due to the equipment used, the characteristics of the channel can be determined. The transmission, reception, and display of very narrow pulses are within the capability of present technology (figure 9.6.9-1). In fact, a pulse shorter than 10^{-9} seconds has been demonstrated in the laboratory using a mode-locked helium-neon laser. This technique will permit the determination of channel characteristics up to bandwidths in the order of 10^{9} Hz, well beyond presently definable needs.

The difficulty in instrumenting such a technique lies in the signal strength, hence, in received signal processing. This difficulty can be circumvented by adopting sampling oscillograph techniques. Present sampling rates are lower than the high repetition rates produced by the mode-locked laser, but the required sampling rates can be generated if development effort is expended. The effects on a wideband channel are expected to be negligible so that the trace sampled at currently attainable rates would be truly representative of all pulses transmitted. Rapidly varying effects would be revealed by a noisy presentation which would be difficult to analyze without a real time display. Because effects are expected to be negligible or

One method of determining the phase and amplitude characteristics of a channel is to transmit a known wide-band waveform through the channel and compare the received waveform phase and amplitude characteristics with those transmitted. The transmission, reception, sampling techniques, and display of very narrow pulses are now possible. In fact, a 0.6×10^{-9} second pulse has been demonstrated with a helium-neon laser; and sampling gates 100 picoseconds wide have been operated at a PRF of 100 MHz. This technique will permit an examination of channel characteristics up to bandwidths of 10^9 Hz.

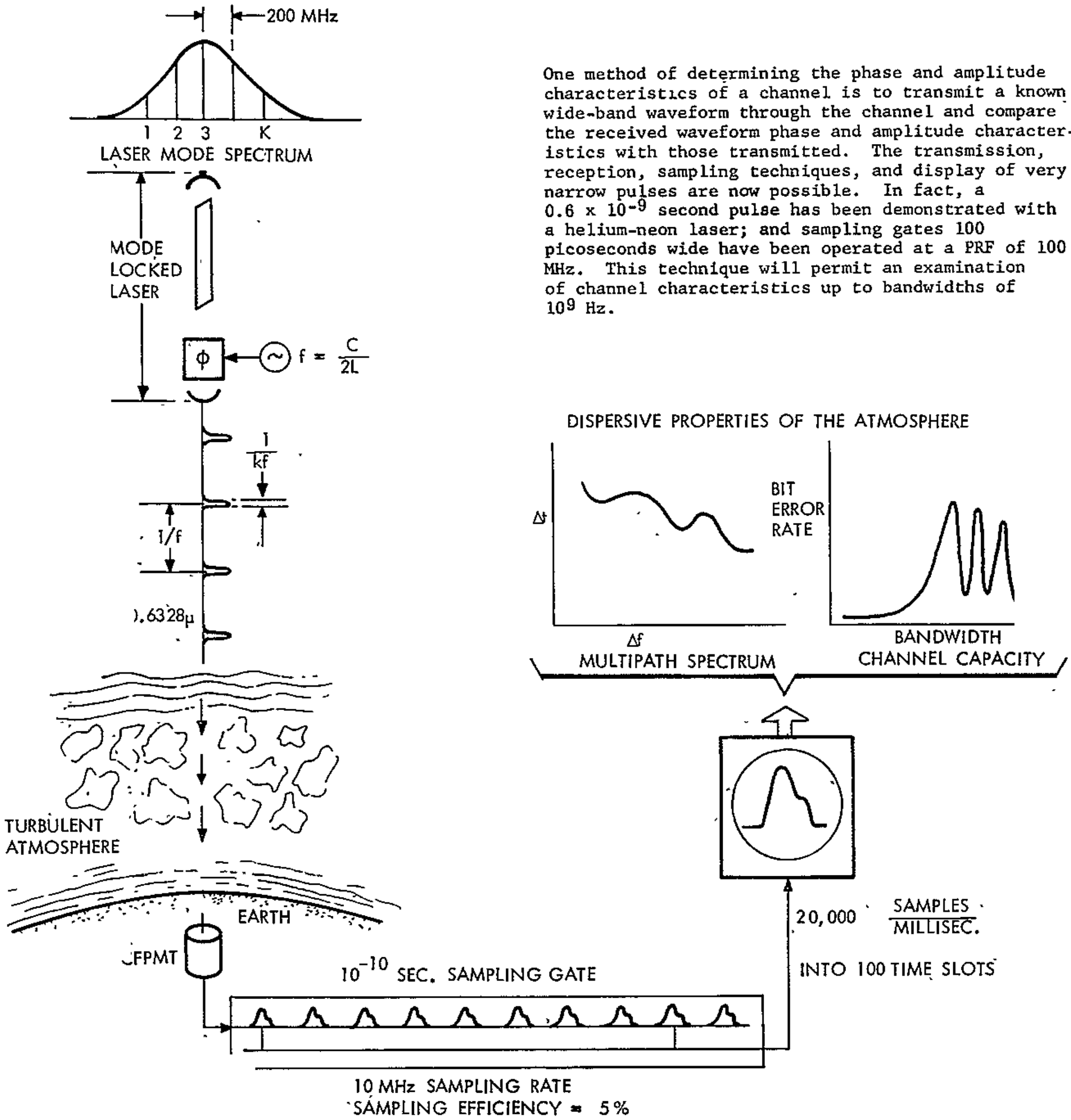

Figure 9.6.9-1. Pulse Distortion Measurements.

slowly changing (at less than kilohertz rates) the pulse distortion experiment proposed for OTAES will explore a bandwidth more than adequate for presently definable needs and may reveal unanticipated limits imposed by atmospheric effects.

9.6.9.1 Justification

The central physical quantity of the theory of turbulence is the refractive index. The Obukhov-Kolmogorov correlation function (paragraph 9.1.1) is a rigorous description which divides refractive index variations into macroscale and microscale disturbances. However, the optical propagation solutions by this theory are quite incomplete. Some authors have elected to ignore the microscale. This approach leads to the Gaussian formulation and application of geometrical optics, but omits the mutual interference of beamlets, restricting its applicability to ranges of, typically, a few hundred meters.

The Rytov approach, which allows the use of physical optics, extends the solution to account for refracted beam components but includes approximations which must be confirmed by experiment at ranges beyond a few kilometers. These approximations are circumvented by the modulation transfer function formulation. However, this formulation contains only limited information since the wave equation need not be involved. The modulation transfer function for laser beam propagation has not been obtained.

Computations of the scattering loss at the frequency considered for this experiment show that such effects would normally be so small as to be undetectable at the power densities required for the other laser experiments. It is possible, however, that a particularly favorable geometry combined with an unusual concentration of scatterers that are large compared to the wavelength would result in a measureable effect which would reduce the potential bandwidth of optical links.

In order to provide the data required in the design of such links, the characteristics of the transmission channel must be determined as independently of equipment characteristics as is possible.

One way to examine channel characteristics would be to observe the behavior, at several suitably spaced radio frequencies covering the bandwidth of interest, of a modulated optical carrier after transmission over a space-to-ground path. This technique would require a number of stable RF generators with a fixed phase relationship in the spacecraft, so that there would be no large gaps in the spectrum.

An alternative way of examining the channel would be to transmit a very short pulse, of the order of a nanosecond, and observe changes, if any, in the pulse shape received after transmission through the atmosphere. Such a pulse contains harmonics which cover a frequency span of the order of the reciprocal of the bandwidth, in this case, $\approx$ one gigahertz. Nonlinearities in the phase characteristics of the channel will be revealed as pulse distortions which can be analyzed to determine the phase shift characteristics of the channel.

In addition to providing useful information on the phase characteristics of the channel, a short pulse will reveal the presence of scatterers which could contribute to multipath effects over the optical channel. Aerosols of various sizes are known to be present at altitudes of around 70 to 100 km. Scattering from these aerosols form the "aureole" around the sun's image.(1) Aerosols have also been detected from back scattered measurements with a high powered laser radar. Because some of these aerosols are larger than the optical wavelengths at visual frequencies, they may be scattered more in the forward direction, perhaps by orders of magnitude, than they are in the backward (toward the transmitter) direction. If the forward scattering is sufficient to cause delayed pulses (computations of the path geometry required for this to occur are in paragraph 9.6.9.2) to appear on the display, the effects on communication rates can be calculated. In addition, these measurements will describe the amplitude and phase characteristics as well as the time delay characteristics of the transmission channel. Additional ground based instrumentation will permit a measurement of the height of the scattering layers if sufficient scattered power is received.

9.6.9.1.1 Considerations on Pulse Stretching due to Frequency Dispersion in the Atmosphere

A pulse 10^{-9} seconds long will have a bandwidth of the order of 10^9 cycles. If the index of refraction in the atmosphere is such that the frequency component at one end of the band is delayed by 10^{-9} seconds compared to the other end of the band, the pulse would be smeared out to roughly twice its length. It is of interest to compute the rate of change with frequency required for this dispersion to take place.

The travel time for a particular frequency component to travel a path distance, L, is

$$\tau = \frac{1}{c} \int_0^L n(\lambda)\, dx$$

where τ is travel time, n is the index of refraction which is a function of λ, as well as position, and temperature, pressure, and water vapor content, and c is the velocity of light. The dispersion in time between the two extreme frequencies traveling the same path would be

(1) E. J. Chatterton, "Optical Communication Employing Semi-Conductor Lasers," M.I.T. Lincoln Laboratory, Technical Report 392, June 9, 1965.

$$\Delta\tau = \tau_1 - \tau_2 = \frac{1}{c}\int_0^L (n_1 - n_2)\ dx$$

Data on index of refraction is usually given as the "Refractive Modulus" (2)

$$N = (n-1)\ 10^6$$

so that

$$\Delta\tau = \frac{1}{c}\int_0^L (N_1 - N_2)\ 10^{-6}\ dx$$

If it is assumed that $N_1 + N_2$ are constant over the path for this short (at optical frequencies) range of frequencies

$$\Delta\tau = \frac{(N_1 - N_2)\ L\ 10^{-6}}{c} = \frac{\Delta NL\ 10^{-6}}{c} \tag{6}$$

$$\Delta N = \frac{\Delta\tau c\ 10^{+6}}{L} \tag{7}$$

and since the frequency spread ΔF (of 10^{+9}) Hz sec is given by

$$\Delta F = c\left(\frac{1}{\lambda_1} - \frac{1}{\lambda_2}\right) \approx \frac{c\,\Delta\tau}{\lambda_2} \tag{8}$$

the required gradient is

$$\frac{\Delta N}{\Delta\lambda} = \frac{\Delta\tau c^2\ 10^{+6}}{L\,\Delta F\,\lambda^2} \tag{9}$$

---

(2) Handbook of Geophysics, revised ed., U.S. Air Force, Air Research and Development Command, Macmillan, New York, 1961, p. 13-1.

To approximately double the pulse length, $\Delta\tau \approx \frac{1}{\Delta F}$ and with $\frac{c}{\lambda} \approx F$, the above becomes

$$\frac{\Delta N}{\Delta \lambda} = \frac{10^6 \; F^2}{L \, (\Delta F)^2} \tag{10}$$

If L is given in microns, Eq. (10) shows the change in N no. per unit change in wavelength (in microns) required to double the pulse length. For the nanosecond pulses at 0.6328 micron over a 100 km path, Eq. (10) results in

$$\frac{\Delta N}{\Delta \lambda} \approx 25 \times 10^5 \quad \frac{\text{N nos.}}{\mu \text{ of wavelength}} \tag{11}$$

To compare the above with what is expected, use the approximate formula[3] for N

$$N = N_\infty \left[1 + \frac{7.52 \times 10^{-3}}{\lambda^2} \right]$$

where N_∞ is the refractive modulus for wavelengths $> > 20\ \mu$ and λ is given in microns. Assuming $N_\infty \approx 300$, differentiating with respect to λ, results in

$$\frac{dN}{d\lambda} = - \frac{3 \times 300 \times 7.52 \times 10^{-3}}{(.6328^3)} - \frac{27 \text{ N nos}}{\mu \text{ of wavelength}}$$

The required gradient is 5 orders of magnitude greater than would be expected in a uniform atmosphere. The approximation made in these computations tend to err on the conservative side, so that the conclusion is that there will be no distortion of the pulse due to frequency dispersion in the atmosphere.

If the transmitted frequency were on the edge of molecular absorption band it would be possible for some pulse distortion to occur because of the unequal absorption of the component frequencies. As shown in published high resolution (0.2A) atmospheric absorption spectra[4], a number of sharply absorbing bands exist in

(3) op cit., p. 13-2.

(4) J. A. Curcio, L. F. Drummeter, and G. L. Knestrick, "An Atlas of the Absorption Spectrum of the Lower Atmosphere from 5400 Å to 8520 Å," Applied Optics, vol. 3, no. 13, December 1964.

the visible range. The wavelength of 0.6328 micron is not near any known absorption band, however, so that no pulse distortion from this effect is expected.

9.6.9.2 Experiment Design

The characteristics of the transmission channel must be determined as independently of equipment characteristics as is possible. It is the objective of this experiment to describe the "impulse response" of the atmosphere in order to describe the character of the communication channel provided by the atmosphere under a variety of transmission conditions.

One method of determining the phase and amplitude characteristics of a channel is to transmit a known wideband waveform through the channel, and compare the received waveform phase and amplitude characteristics with those of the transmitted characteristics. By accounting for changes due to the equipment used, the characteristics of the channel can be determined. In this experiment, short pulses can be generated in the spacecraft at optical frequencies, using a multi-mode laser in the mode-locked condition. The effect of the atmosphere on these pulses is measured on the ground. Mode-locked lasers have been tested in the laboratory at this frequency, and considerable success has been achieved in the display of nanosecond pulses in certain nuclear applications. This technique will permit the determination of channel characteristics up to bandwidths in the order of 10^9 Hz.

9.6.9.2.1 Possible Multipath Delay

If it is assumed that the center of the transmitter beamwidth (ϕ) is accurately aligned with the center of the angle of view (θ) cone angle, the geometry shown can be used to compute possible multipath delays. Misalignment of the beam and viewing cone angle could lead to larger delays than computed here. Although scatterers could be located anywhere within the beamwidth and view angle, the greatest delay will occur when the scatterer is at S, the intersection of the view angle cone and the transmitting beamwidth cone. As indicated in figure 9.6.9.1-1 the maximum path difference $\Delta\rho$ (Path TSR - r) is given by

$$\sqrt{(r-h)^2 + h^2 \tan^2 \frac{\theta}{2}} \qquad \sqrt{h^2 + h^2 \tan^2 \frac{\theta}{2}} - r \doteq \Delta\rho$$

Assume, for space to ground transmission, that $r > 2h$. If $\theta/2$ is less than 10 milliradians, so that $\tan\theta/2 = \theta/2$, and using the approximation $\sqrt{1+X^2} \simeq 1 + X^2/2$ for $X < 1$, the above equation reduces to

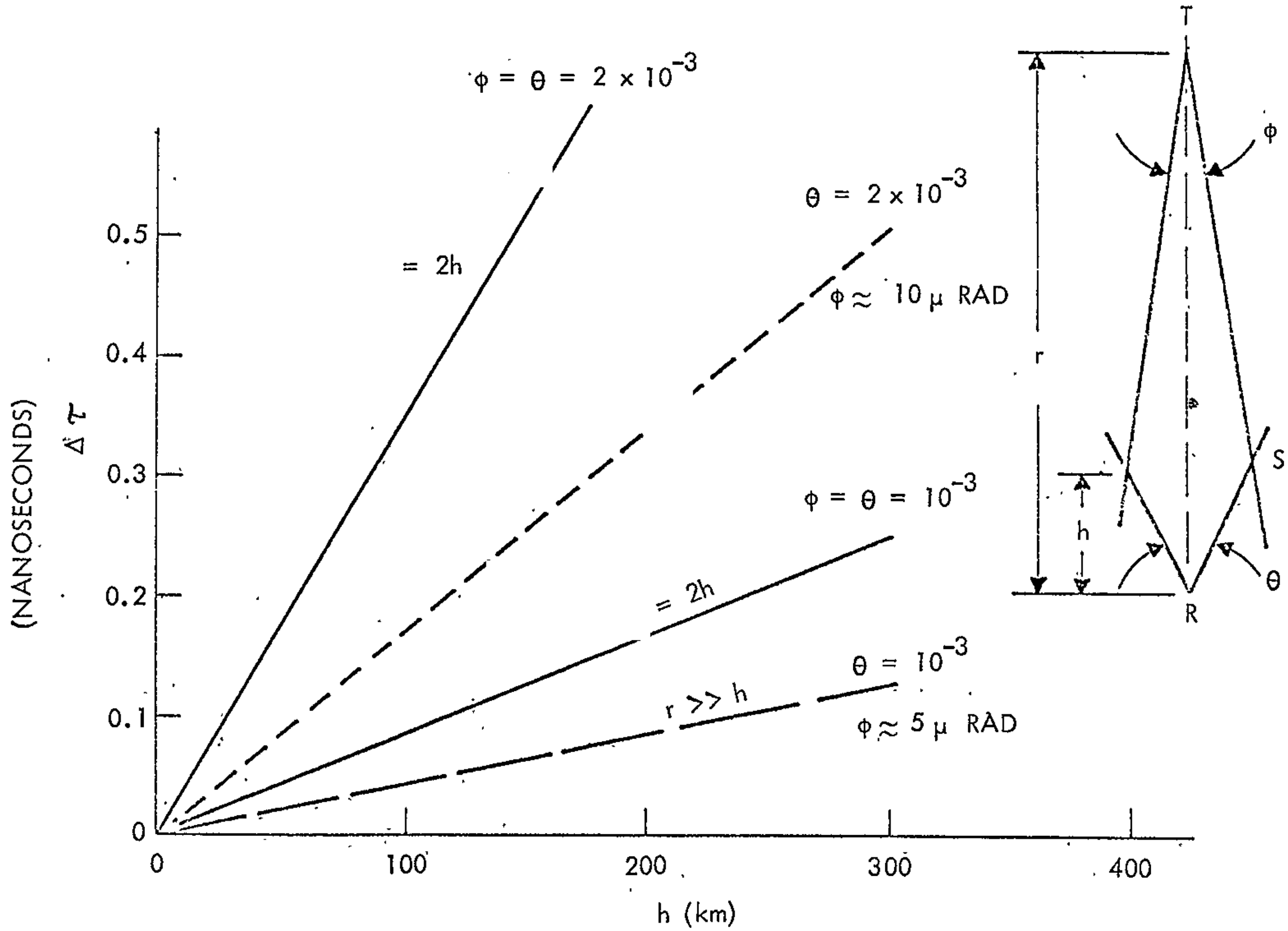

Figure 9.6.9.1-1. Multipath Delay.

$$(r - h) \left[1 + \frac{h^2 \theta^2}{8(r-h)^2}\right] + h \left[1 + \frac{\theta^2}{8}\right] - r = \Delta \rho$$

$$\frac{h^2 \theta^2}{8(r-h)} + \frac{h\theta^2}{8} = \Delta \rho$$

since $\frac{1}{2} \leq \left(1 - \frac{h}{r}\right) \leq 1$, the worst case for an r is when r = 2h, so Eq. (1) becomes

$$\frac{\theta^2}{4} \cdot h = \Delta \rho \qquad (2)$$

and $\Delta \tau$, the path delay, is given by $\frac{\Delta \rho}{C}$ where C is the velocity of light.

$$\Delta\tau = \frac{\theta^2}{4} \cdot \frac{h}{C} \qquad (3)$$

If h is 100 km, $\theta = 10^{-3}$ radians

$$\Delta\tau = \frac{10^{-6}}{4} \cdot \frac{100}{3 \times 10^{-5}} \cdot 109 = \frac{1}{12} \text{ nanoseconds}$$

and probably could not be detected. However, at certain slant paths, h could be 500 km, and if θ is say 3×10^{-3} radians, $\Delta\tau$ increases by a factor of 45 to become $\approx$ 4 nanoseconds, which could possibly be measured if the scattering cross sections are sufficient.

In the foregoing computations it is assumed that the scatterers are located at the intersection of the beam angles. Normally this will not be true, so that the actual multipath will probably be less than indicated in figure 9.6.9.1-1. If the scatterers are in a layer, at some distance other than that defined by the cone intersections, one beam or the other will limit the maximum multipath delay. As shown in the figure, the transmitting beamwidth, ϕ, is given approximately by

$$\phi = \frac{h\theta}{r-h} \qquad \theta, \phi < 0.01 \text{ radians} \qquad (4)$$

For earth-space applications θ will be kept as small as is consistent with system considerations. For a given θ, reducing ϕ to as small a value as possible forces a reduction in h, the range to possible scatterers, which reduces the duration of possible multipath delay. Values of multipath delay for various distances to the scatterers are plotted in figure 9.6.9.1-1. Values of ϕ on the $r >> h$ curves are computed for synchronous altitudes. As shown by the curves of figure 9.6.9.1-1, possible multipath delays are expected to be very small. A very short pulse is required for their measurement. If scatterers are found in sufficient number, of the proper size, and in a favorable geometry, some multipath might be observed. Computations of the scattering cross sections required show that the probability of this event will be low.

If Eq. (1) and Eq. (4) are used, and dividing by the velocity of light, the maximum multipath delay (scatterers located at the intersection of the cone angles, $\Delta\tau$) becomes, for small angles,

$$\Delta\tau = \frac{\theta \ \phi \ r}{8 \ C} \tag{5}$$

This form of the equation is not particularly adaptable to earth-space applications, however; if it is assumed that the maximum height of scatterers is of the order of 100 km, a maximum range to the scatterers on a slant path is 500 km. In Eq. (5) the distance to the scatter is not explicit.

9.6.9.3 Measurement Objective

This experiment will determine if laser beam transit-time fluctuations are caused by the atmosphere. Ultrashort optical pulses transmitted from space-to-ground will be sampled and compared with reference waveforms to detect any pulse shape degradation or distortion. Harmonic analysis of distorted pulse shapes will determine the maximum information bandwidth limitation of the atmosphere. Pulses will be transmitted in a variety of atmospheric conditions to obtain statistical data.

9.6.9.4 Equipment Design

The spacecraft equipment used for this experiment will be the same as used for the Heterodyne Detection on Earth experiment (paragraph 9.6.1 and figure 9.6.9.4-1). One of the two dual He-Ne transmitter units located in telescope no. 1 will be mode-locked to generate the short optical pulses. Figure 9.6.9.4-2 shows the dual He-Ne transmitter unit.

9.6.9.4.1 Pulse Generator with the Mode-Locked Laser

An He-Ne laser longer than about 10 cm has enough gain to oscillate at several frequencies simultaneously. The actual frequencies are determined by the laser resonator cavity, i.e., the separation between the laser cavity mirrors. The frequency spacing between oscillating modes is given by C/2L, where C is the velocity of light, and L is the length of the cavity. A laser 0.75 meters long will have mode spacing frequency of 200 MHz.

A laser of this length will have a number of independent modes oscillating, spaced by 200 MHz, over the whole region in the optical band where the laser gain is sufficient to support oscillation. The He-Ne transition at 0.6328 microns has a Doppler broadened gain curve that is about 1600 MHz wide, so that a family of about 10 separate oscillations can be sustained by a 0.75-meter laser.

It should be noted that these are independent oscillations. Their frequencies and phases are only weakly coupled to other oscillations, through such competition effects as "hole burnings," etc. If the light output is detected by a phototube, the beats between neighboring oscillations can be observed as 200 MHz modulation on the beam. Next-to-nearest neighbors generate a 400-MHz beat, and so forth. The phases of the modes are essentially random, however, so that the power of the 200-MHz beat signal does not increase linearly with the number and power of the contributing modes, but increases in a random-walk manner instead. The total output power fluctuates slightly because of mode competition effects, making the multimode laser a noisy transmitter.

This situation can be dramatically cleaned up by the use of an electro-optic phase modulator, placed within the laser cavity as shown in figure 9.6.9-1. When the modulator is driven by an external oscillator at exactly the mode spacing frequency, C/2L, each of the modes generates sidebands on top of all the others. In a very short time the original set of modes is quenched and is replaced by a new set of oscillations.

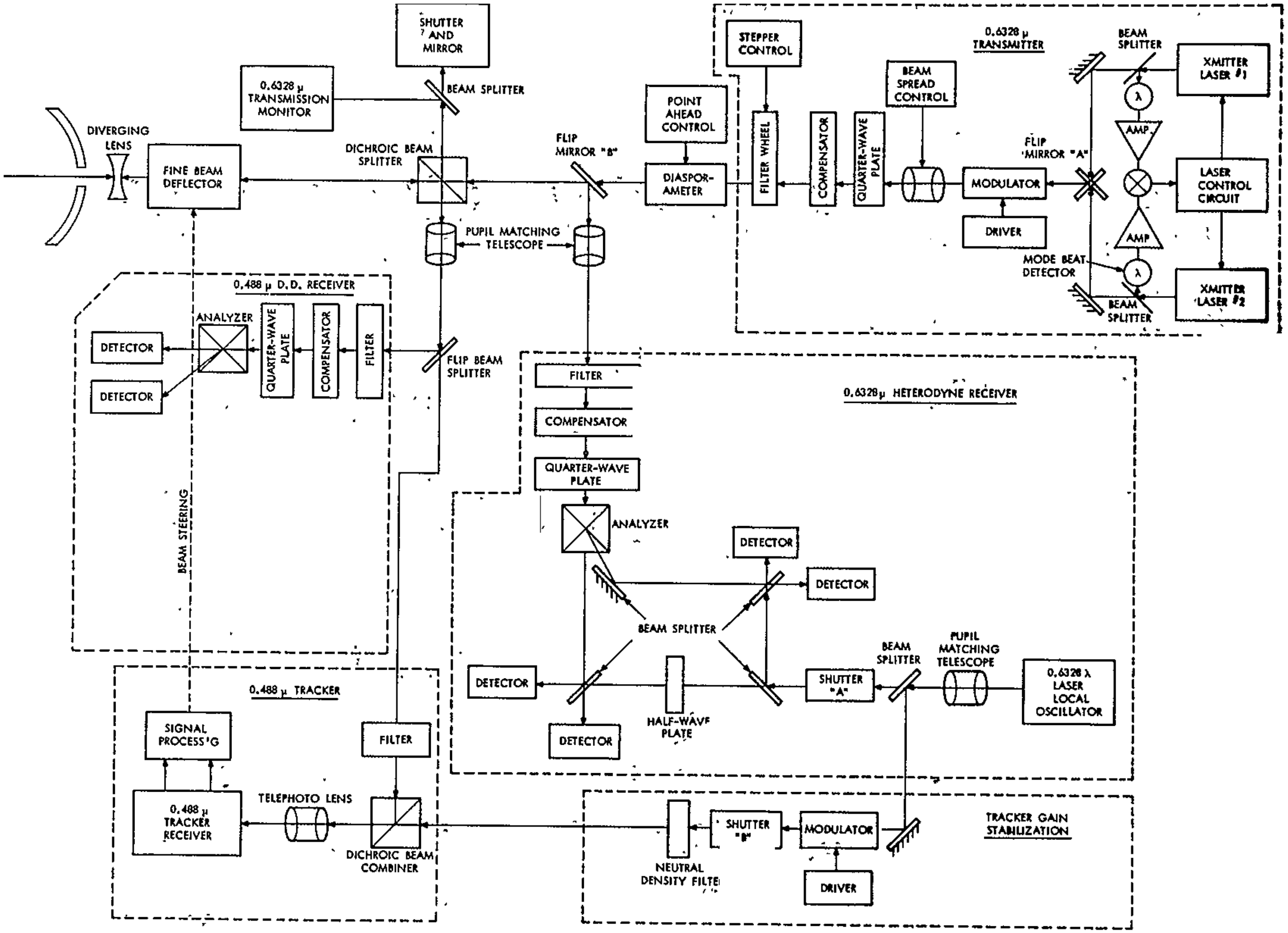

Figure 9.6.9.4-1. Block Diagram of Telescope No. 1: 1.0-Meter - Gimbaled

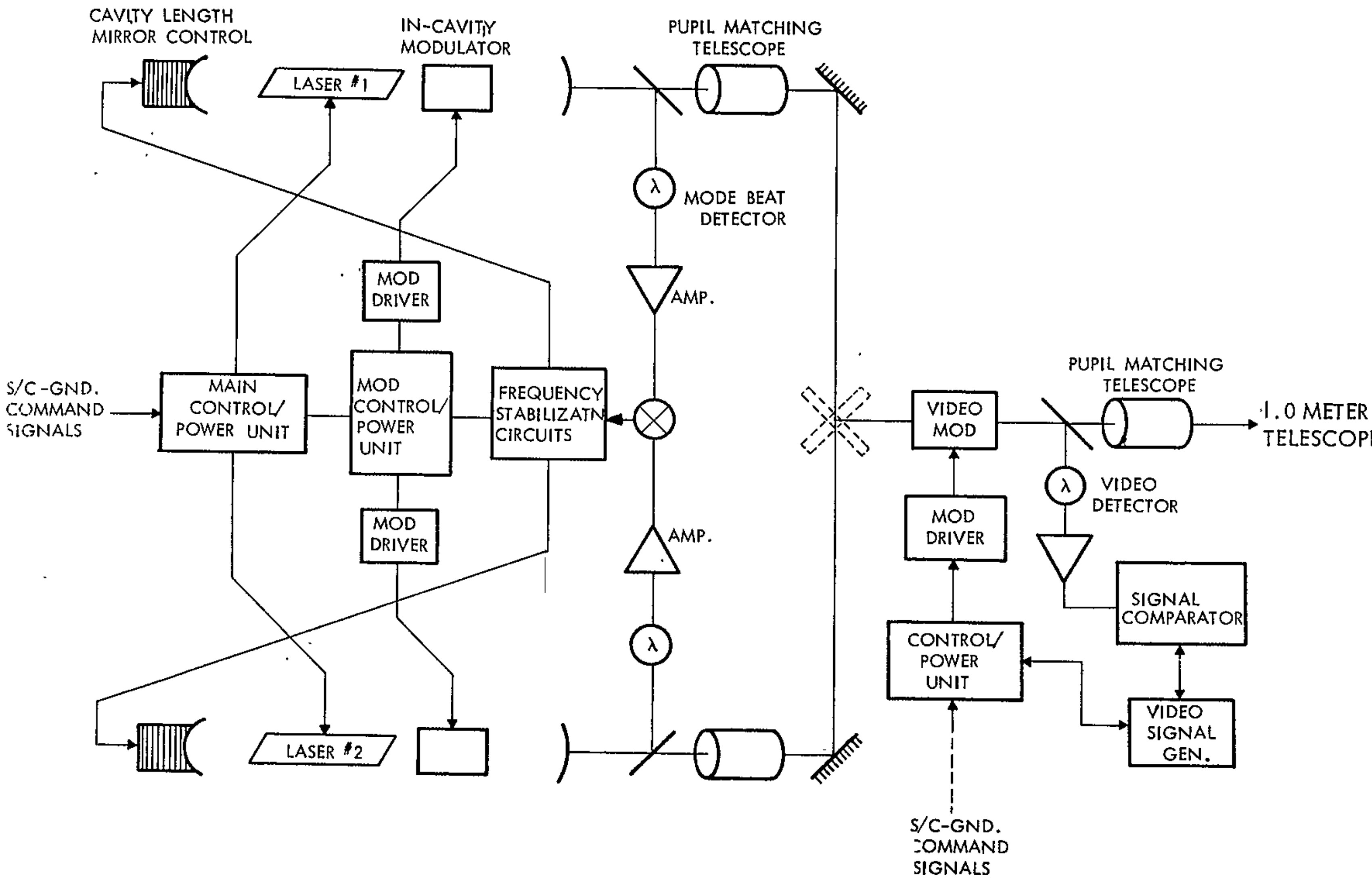

Figure 9.6.9.4-2. Dual 6328Å Laser Transmitter

The new set of modes are strongly coupled to each other, as the phase modulator is continually transferring energy between them. They are: (a) separated by exactly the frequency of the driving oscillator, and mode-pulling effects in the free-running laser are eliminated; and (b) their phases are not random but locked in step, so that the laser output becomes a series of very rapid pulses. The pulse width is roughly one nanosecond, and the PRF is 200 MHz, for the He-Ne laser described earlier, giving a duty cycle of 10 per cent.

The average power output of the laser is not changed during mode-locked operation. Thus the peak pulse power will be many times the average power -- higher by the reciprocal of the duty cycle, a factor of 10 in this case. The RF power required to drive the modulator is not large -- less than one watt.

The mode-locked laser is a unique transmitter source. It generates sub-nanosecond pulses at extremely high PRFs, and it can be easily implemented. The only requirements beyond those of a free-running laser are a low-loss modulator, its driver, and oscillator.

The presently designed spacecraft multimode He-Ne laser transmitters have approximately a 75-cm long optical cavity. In mode-locked operation, the transmitted pulsewidth is about 0.6 nanoseconds to the one-half intensity points with a PRF of 200 MHz.

9.6.9.4.2 Ground Receiver Signal Processor

The optical pulses are detected on earth with a wideband crossed-field photo multiplier and analyzed by high-speed sampling techniques to measure pulse distortion.

A very significant advance in ultra-wideband sampling devices, recently announced by H-P Associates, [5] is the development of a 28-picosecond wide sampling gate. This gate will permit very fine time resolution of the optical pulse. At the present time the sampling rate of the H-P gate is about 100 KHz. However, private communications with Dr. Cowley of Hewlett-Packard Associates, Palo Alto, California, indicate that a 10-MHz sampling rate can be expected in the near future. Fairchild Semiconductor, Mountain View, California, is also developing high PRF wideband sampling gates. In private communications to Sylvania, they have recently reported operation of a 100-picosecond gate at a PRF of 100 MHz. The high sampling rates of these gates insure that the incoming optical pulse is sampled before any atmospheric changes occur.

---

(5) "A DC to 12.4 GHz Feedthrough Sampler for Oscilloscopes and Other RF Systems," Hewlett-Packard Journal, October 1966, pp. 12-15.

The space-to-ground pulse propagation experiment is fairly easy to implement and requires no unique spacecraft equipment. The major equipment necessary to conduct the pulse distortion measurements is discussed below.

9.6.9.4.3 Equipment Required

9.6.9.4.3.1 Spaceborne Equipment

The spaceborne equipment is common to the space-to-ground heterodyne link. The optical pulses are obtained by mode-locking either of the two He-Ne lasers located in the 1.0-meter aperture telescope. Verification of the mode-lock condition is telemetered from the laser mode beat detector used in the stabilization circuit.

9.6.9.4.3.2 Ground-Based Equipment

The 1.0-meter telescope used for the heterodyne downlink equipped with a wide-band crossed-field photomultiplier detects the optical pulses. Equipment unique to this experiment includes:

a. Experiment Control, Sequencing, and Measurements System

Pulse Distortion Signal Analysis Circuits

Signal Storage/Computational Facilities

Pulse Distortion Control/Display Console

9.6.9.5 Data Management

A simplified block diagram, figure 9.6.9.5-1, shows the ground station pulse distortion signal analysis technique. The optical pulse is photodetected by a cross-field phototube with frequency response from baseband to about 3 GHz. The electrical pulses are sent to a phase comparator/AGC unit which synchronizes the incoming pulse train to a local reference pulse and normalizes the pulse height.

The pulses are then sampled by an ultra-wideband, high PRF gate into approximately 100 resolution cells. The sampled pulse is temporarily recorded on a video tape recorder. The sampled pulse is then compared to a standard, nondistorted reference signal. If deviations in pulse shape due to transit-time dispersion are noted in the threshold/logic unit, a permanent tape of the incoming sampled pulse is recorded. Otherwise, the temporary recording is erased and the measurement cycle repeated. Transit-time dispersion is measured by subsequent harmonic analysis of the distorted pulse shape.

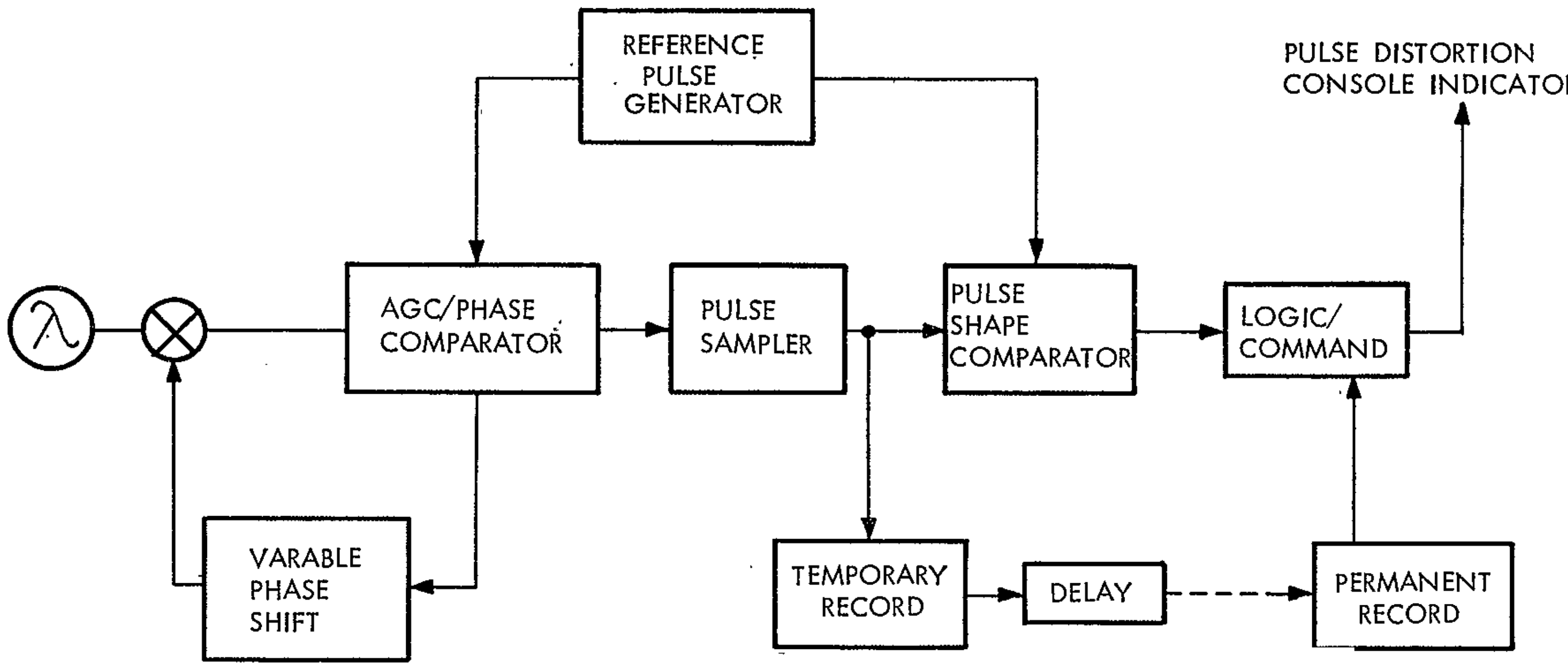

Figure 9.6.9.5-1. Pulse Distortion Signal Analysis

The equipment aboard the spacecraft that must be operated include:

a. An 0.6328-micron stabilized multimode laser transmitter

b. Either the 1.0-meter or the 0.3-meter gimbaled telescope, in a transmit mode

c. An 0.4880-micron tracker for telescope no. 1 or no. 3

d. Transmission monitors for telescope no. 1 or no. 3

e. Transmitter beam spread controls for telescope no. 1 or no. 3

f. Transmitter beam point-ahead controls for telescope no. 1 or no. 3

g. Transmitter optical attenuators for telescope no. 1 or no. 3

h. RF telemetry and beacon system.

The astronaut can operate these equipments using the laser control panels figure 9.6.9.5-2 (figures 9.6.1.5-2 through 9.6.1.5-4). Alternatively, this experiment can be operated from the ground OTTOS-OTAES Control Room (figure 9.6.9.5-3) using consoles 1 and 3 (figures 9.6.1.5-6 and 9.6.8.5-2). The OTTOS panels used to operate experiment 1 are shown in figures 9.6.1.5-8 through 9.6.1.5-13.

9.6.9.5.1 Spacecraft Equipment Test and Checkout

To assure satisfactory performance, the equipment alignment must be optimized and periodically repeated. Alignment of the laser and telescope can be determined by operating the boreshight error measurement equipment on the control panel and determining the magnitude of this error. Adjustment of diasporameter controls will be made to minimize the boresight error. Tuning of the laser to obtain optimum efficiency will be done by adjusting the laser mirror controls to maximize output power for fixed input power. Laser AFC and mode-locking circuits are automatic in operation and require only recheck of status indicator lamps. Telescope fine tracking functions are also automatic once they are initiated.

9.6.9.5.2 Ground Equipment Test and Checkout

The ground-based equipment required for this experiment will include:

a. The 1.0-meter aperture heterodyne receiving telescope

b. Pointing and positioning equipment

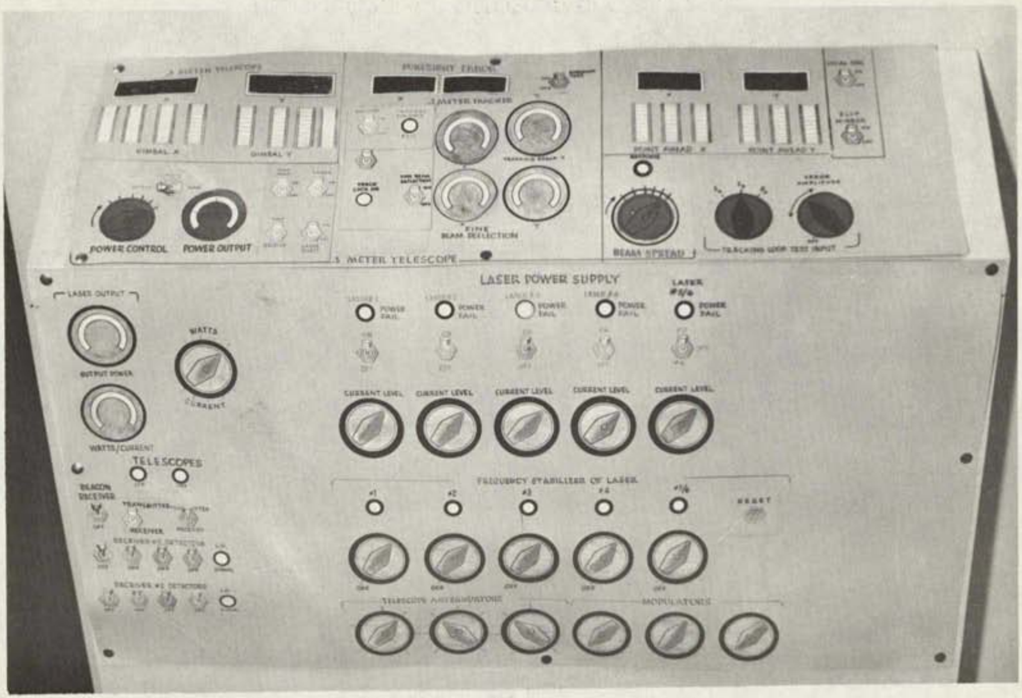

Figure 9.6.9.5-2. Laser Control Panel.

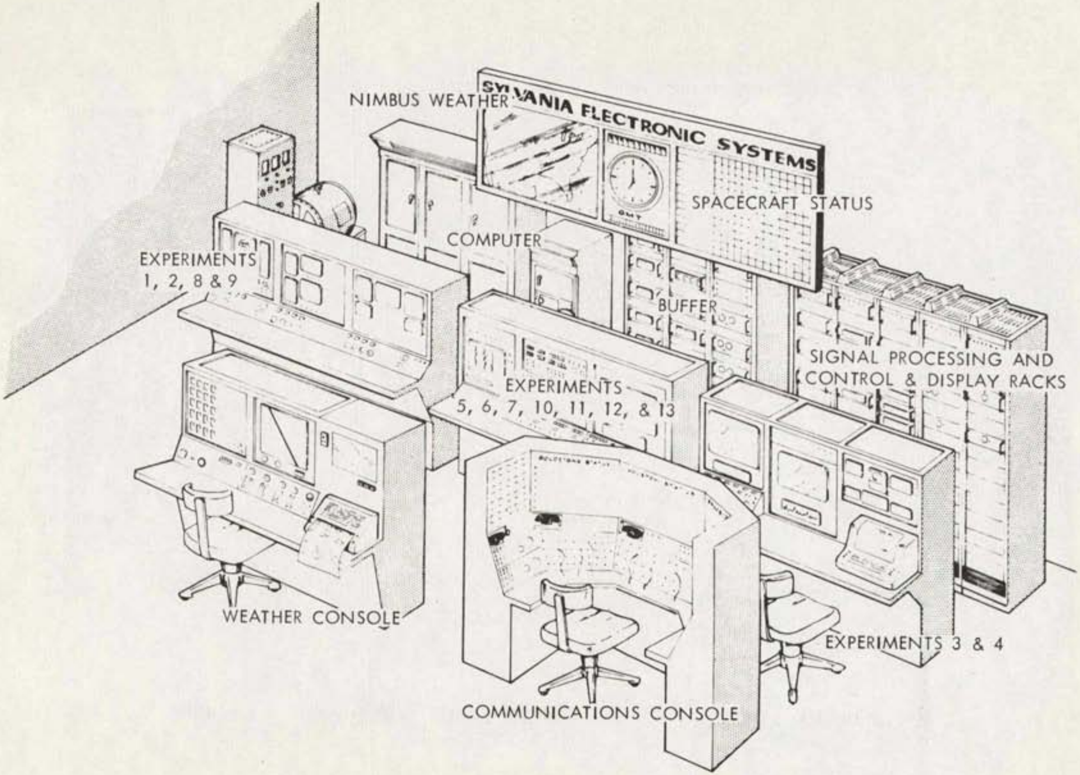

Figure 9.6.9.5-3. OTTOS/OTAES Control Room.

c. 0.6328 micron heterodyne receiver

d. The 8.0-meter aperture direct detection telescope

e. Pointing and positioning equipment

f. 0.6328 micron direct detection receiver

g. Receiving electronics and data handling equipment

h. High-speed sampling circuit for pulse shape analysis

i. Control and display consoles for receiving telescopes, receivers, data processing, and recording systems

j. 0.4880 laser beacon transmitter

k. Microwave tracker to provide pointing information

l. Spacecraft telemetry command and display.

The ground-based equipment will be checked for operability before the experiment is begun. All of the lasers (0.4880-micron beacon, 0.6328-micron local oscillator) will be turned on and thermally stabilized, and AFC circuits turned on. Internal checking of the receiving electronics will be done by injecting an optical signal directly into the photodetectors and checking the output against the input for gain and distortion. These functions will all be controlled from the ground station control consoles. Signal processing electronics will be self-checked in a similar manner.

The beacon modulator will be operated with selected test signals, and the beacon output will be measured. Pointing of the beacon will be done by using the inputs from the RF tracking stations such as Goldstone, and the RF tracking equipment at the optical ground site.

The 8.0-meter direct detection and the 1.0-meter heterodyne receiving telescopes are pointed at the spacecraft, using the same pointing signal inputs. More accurate pointing will be done after the spacecraft signal is acquired by the receiving telescopes.

The RF telemetry system will be checked for operational status at the spacecraft status display and control console.

9.6.9.5.3 Experiment Performance

Radiosonde balloons will be released over a period of several hours prior to, and during, optical measurements, in order to record upper air conditions. Local meterological conditions will be measured near the receiving telescope. When there is no interference from clouds, the spacecraft will be commanded to acquire the 0.4880-micron ground beacon, to begin fine tracking, and to transmit fast pulse signals on the optical down links. The pointing of the ground receiver and the beacon transmitter is updated, so that spacecraft and ground station are accurately illuminating each other. The receivers will be operated at first with narrow bandwidths centered at the fundamental PRF being transmitted from the spacecraft, giving a good signal-to-noise ratio for the reduced signal irradiance obtained with a wide transmitter beamwidth.

As the pointing accuracy of the spacecraft telescope is improved, the transmitter beam may be narrowed and the ground receiver bandwidth increased. This will include the higher harmonics of the PRF and allow the signal sampling circuits to analyze the pulse shape. Fading rate, signal dropouts, and signal-to-noise ratios will also be determined over extended periods of time. Fluctuations in beam polarization will be continually measured, and unexpected anomalies displayed and recorded.

Phase noise introduced by the atmosphere will be measured, and selected portions of data will be recorded.

Many of these measured quantities may be varying at up to 1 kHz. Extensive preprocessing will be used before data are recorded. It is expected that pulse distortion effects will be strongly dependent upon upper air scattering and turbulence conditions, so that a large fraction of the received pulses will be undistorted. Raw data from the direct detection of heterodyne receivers will be stored only while processing takes place, and then erased. Anomalous, or out-of-limit pulses will automatically be retained for later analysis. The magnitudes of, and the statistical distributions of the anomalous data are the most important information.

The duration of the pulse distortion measurement experiment will be determined primarily by weather conditions, and secondarily by the conflicting needs of other experiments, such as the transfer of tracking from one ground station to another. Data should be taken over periods of several hours at a time, especially when weather conditions are changing.

9.7 GROUND STATION REQUIREMENTS

Performance of the proposed OTAES optical propagation experiments will depend to a large degree on the optimization of the signal-to-noise ratio. Background illumination must be avoided, as must scintillation which gives rise to one form of signal fading. Hence, the ground-based experiment optics are designed to: (a) limit the field of view of the detector, thereby eliminating as much background illumination as possible, and (b) form as sharp an image as possible, which implies excellent seeing conditions and freedom from dancing. In this respect, the Optical Technology Test and Operations Station (OTTOS) requirements are similar to those for photography of stellar images; but the OTAES propagation experiments must operate in daylight as well as at night. The importance of high resolution is greatly accentuated for daytime experiment. As in image viewing, a large objective is desired to provide good image brightness (when the background is below detection level) and high resolution. The requirement for low sky brightness is similar to the requirements of a photometric observatory with the added provision that daytime sky brightness might well be the controlling feature. This imposes a requirement for low atmospheric haze and freedom from cloud, even thin cirrostratus. The requirement for minimum scintillation implies that the effects of the upper atmosphere will also come into play; this phenomenon does not trouble most other observatories.

An astronomical observatory is often concerned with the quality of its best observing conditions; the occasional outstanding result among many observations may justify months of observing. For the ground-based elements of the OTAES Optical Propagation Experiments, on the other hand, the opposite end of the performance scale becomes important; namely, the bad "observing" conditions or total outage. OTAES statistical data must be gathered over a period of many hours and repeated for many days. Signal distortion measurements must be made through the entire sensible atmosphere, along slant and near-zenith paths; and results must be correlated with observable meteorological parameters. To this end, it is desirable to have a site for which: (a) seasons of significant downtime due to weather are predictable; and (b) during other seasons, the probability of unpredicted downtime is low; and, particularly, the probability of an extended run of outage time is small. Astronomical observatories focus attention on the best of their performances, for these determine their best achievements. The OTTOS must be evaluated in terms of its worst unpredictable performance.

It is known, a priori, that certain regions are incompatible with the OTAES requirements. These are: (a) zones subject to commercial air traffic, (b) zones with high likelihood of jet contrail interference, and (c) zones subject to dense air pollution from urban centers. The objection to aircraft in flight rests not only on possible interference with experimental procedure caused by temporary interruption of the telescopic line-of-sight, but also upon the possible laser radiation hazard to airborne passengers and crew. The exclusion of airways tends to exclude a large fraction of the total land area, with increasing area eliminated around the larger coastal cities because of the convergence of air lanes near urban centers.

Positive OTTOS criteria would include an elevation over 6,000 feet above sea level, wooded surroundings, and a rock stratum for foundation support. The mechanics of providing an adequate foundation dictate that the ground must have a high bearing capacity, without the slipping or creeping which would be encountered with clay or silt. This is further emphasized by a finding of the Bureau of Mines, which has determined that solid unbroken rock strata attenuate the amplitude of an earth wave to one-tenth the amplitude through "normal ground." Earth-wave amplitudes through sandy soil may be three times greater than those through "normal ground."

Typical OTTOS sites which might satisfy these requirements are:

a. Atascosa Peak, Arizona

b. Capitan Mountains, New Mexico

c. Chiracahua Peak, Arizona

d. Chisos Mountains, Texas

e. Guadelupe Mountain Range, New Mexico

f. Kingston Peak, California

g. Mount Wrightson, Arizona

h. Sacramento Mountains, New Mexico

i. White Mountains, California.

9.7.1 Particular OTTOS Facility Requirements

The measurement precision required in certain of the OTAES optical propagation experiments implies seismic and meteorological isolation. These instruments include:

a. Two tracking telescopes of nominal 1.0-meter aperture. These instruments will have all-reflective optics and a fine-pointing capability of ±5 microradians. One of these tracking telescopes is to serve as the 0.488-micron transmitting aperture attached to the gimbaled telescope array.

b. An 8-meter segmented optical aperture capable of ±50 microradian tracking accuracy.

c. A similar 3-meter segmented optical aperture.

d. Two gimbaled arrays of sixteen 12.7-cm diameter telescopes. One array is to be separated by about four miles from the main (1.0-meter aperture) facilities.

e. An evacuated 10-micron optical interferometer having 2-cm receiving apertures which may be separated at sequential intervals to a distance of 10 meters.

f. A nominal 0.3-meter, all-reflective, transmitting telescope (0.6328-micron and 10.6-micron transmitter)

Each of these precision devices will require power supply/conditioning equipment and specialized experiment signal processors.

Because the laser propagation experiments, taken together, constitute a study of the optical properties of the atmosphere, a frequent closely spaced sampling of the state of the atmosphere is required. The OTTOS must therefore be equipped as a meteorological ground station, augmented for the coordination of rawinsonde/rocketsonde operations distributed up to 150 miles south of the optical instrumentation site (section 19).

Furthermore, to make maximum use of the NASA Tracking and Data Acquisition Networks, yet permit experiment control at the optical site during critical periods, the following experiment support facilities will be required as a minimum:

a. Three experiment control consoles adequate for hand-off control during critical experiment periods

b. Two 642B computers

c. Two data links to the DSIF and MSFN having a 51,200 bits per second capacity and a communication control console

d. A backup commercial video link (5 MHz) to the nearest LE-350 computer site (e.g., Goldstone, Houston, etc.)

e. A microwave tracker

f. Programmable pointing drive devices for the seven telescopes and arrays

g. Two video tape recorders.

During the period when the optical propagation experiments are active, the OTTOS test conductor will require access to spacecraft telemetry data which is being transmitted at a rate of 5×10^4 bits per second, video data which is a maximum of 0.5 MHz, and DSIF tracking and mensuration data which will not exceed 10^3 bits per second. Normal voice (typically 20 voice lines) and teletype (typically 16) communication between OTTOS and (a) the DSIF ground station and (b) the control center at MSC will be required. Facsimile communications from the NASA meteorological network will be required. Figure 9.7.1-1 shows an OTTOS concept which would satisfy the support requirements of the OTAES Baseline Mission.

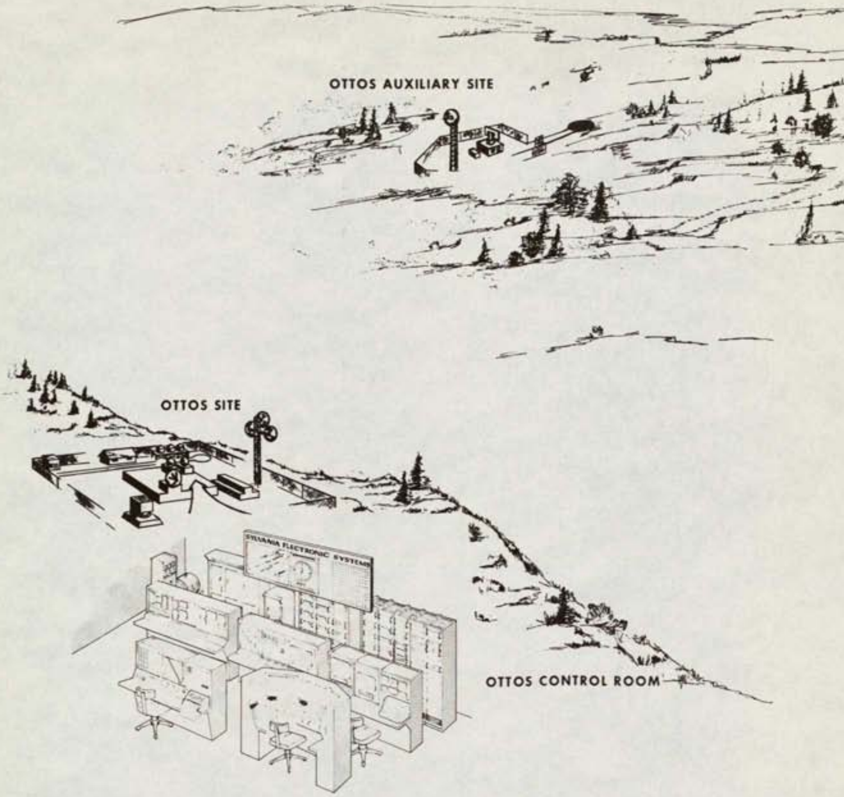
OTTOS AUXILIARY SITE
OTTOS SITE
OTTOS CONTROL ROOM

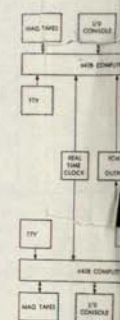
MAG TAPES
TTY
REAL TIME CLOCK
TTY
MAG TAPES

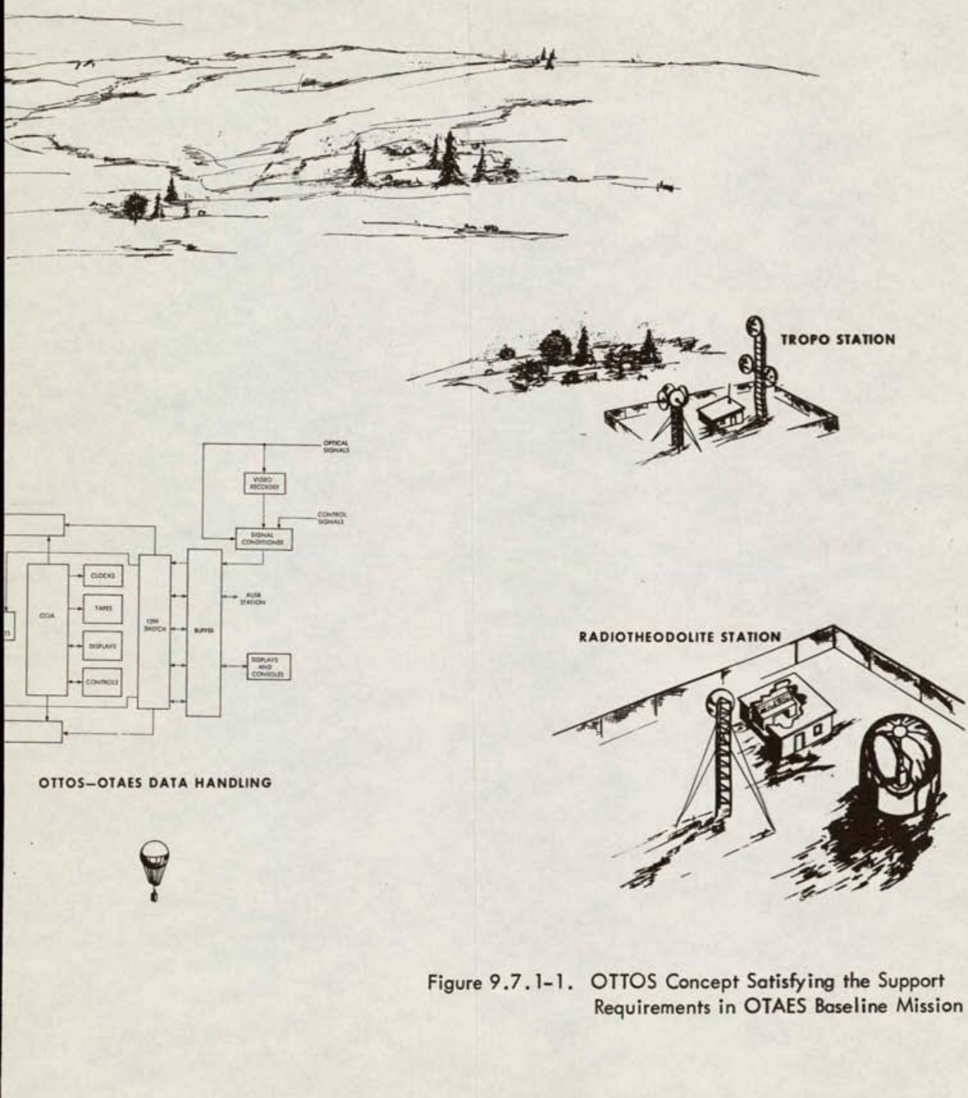

Figure 9.7.1-1. OTTOS Concept Satisfying the Support Requirements in OTAES Baseline Mission

9.8 EXPERIMENT PROCEDURE

9.8.1 Initial Conditions for the Optical Propagation Experiments

Performance of the Optical Propagation Experiments will require that the spacecraft roll axis be aligned to the sun line-of-sight and that the vehicle be stabilized on the sun and microwave tracker signal (figure 9. 8. 1-1). The ground station argon laser beam will be pointed at the spacecraft. All controls on the one-meter and 0. 3-meter telescope panels (figures 9. 8. 1-2 and 9. 8. 1-3) and the laser power supply panel (figure 9. 8. 1-4) will be in the off position.

9.8.2 Laser Transmitters

a. Turn on the 0.3- and 1.0-meter telescope laser transmitters.

b. Stabilize and evaluate performance by measuring laser input power, laser output power, and modulator performance. Input power will be measured with meters on the laser control panel and may be increased or decreased by knob controls on the panel. Output will be measured with the transmission monitor and will be displayed by a meter on the control panel. Output will be controlled by adjusting input power with the optical attenuator set in the open position.

c. Optimizing of output power may be done by operating controls that align the laser mirrors and adjust the cavity length to center the laser output in the fluorescent band. This latter function will be performed automatically by the laser AFC circuit.

d. Check proper operation of the AFC circuits with oscilloscope monitoring if the panel warning light for excessive AFC voltage is lit.

e. The modulator's performance will be determined by operating it with a selected drive signal and observing the transmission monitor outputs on an oscilloscope display or TV monitor. Time must be allowed for the lasers to come to thermal equilibrium within the telescope wells.

9.8.3 Coarse Acquisition

Acquire Canopus with star tracker. Canopus tracker gimbal angles will be requested from the ground station and inserted by thumbwheel control. The slew button will be pressed and lock-on observed to verify acquisition.

Acquire the white light beacon with the planet tracker. The 0.3-meter telescope gimbal angles will be requested from the ground station and inserted by thumbwheel control on the lower left on the center panel. Press the slew button and observe lock-on signal to verify acquisition by planet tracker.

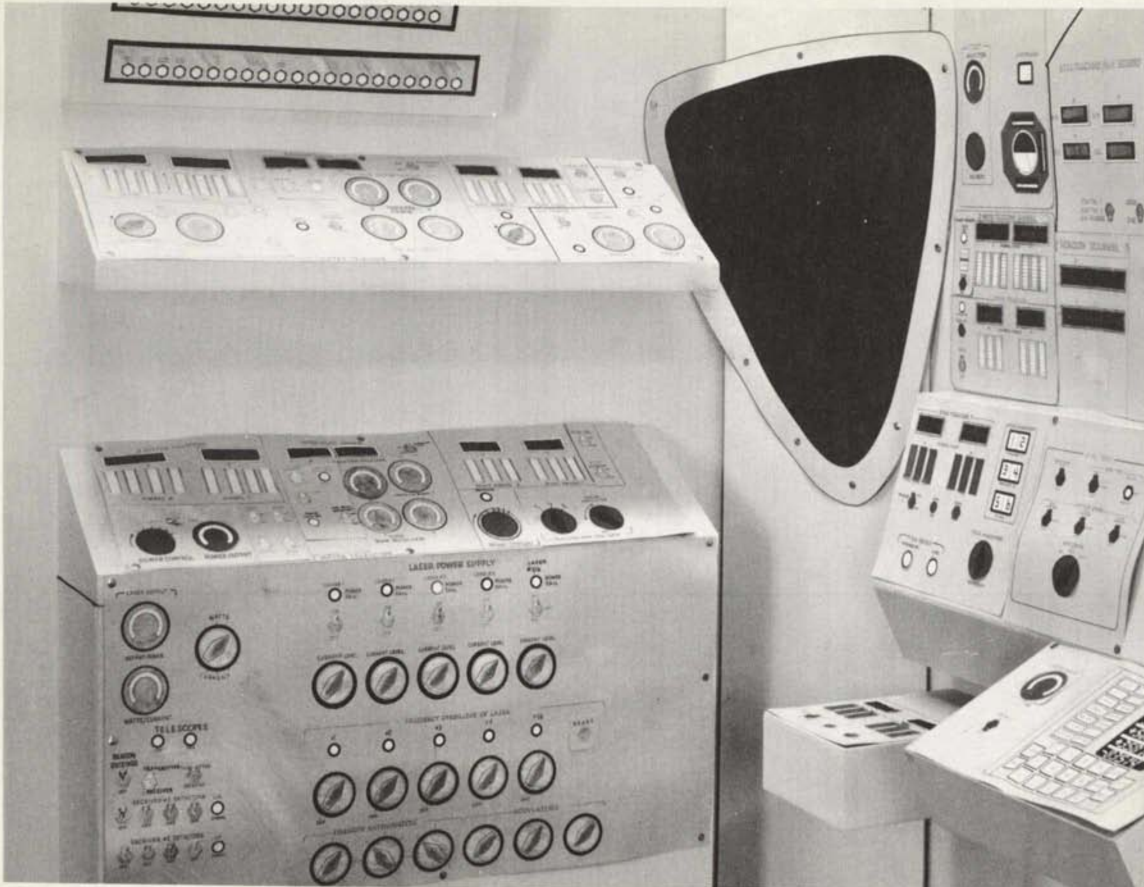

Figure 9.8.1-1, -2, and -3. 1-Meter and 0.3 Meter Telescope Panels and Laser Power Supply Panel.

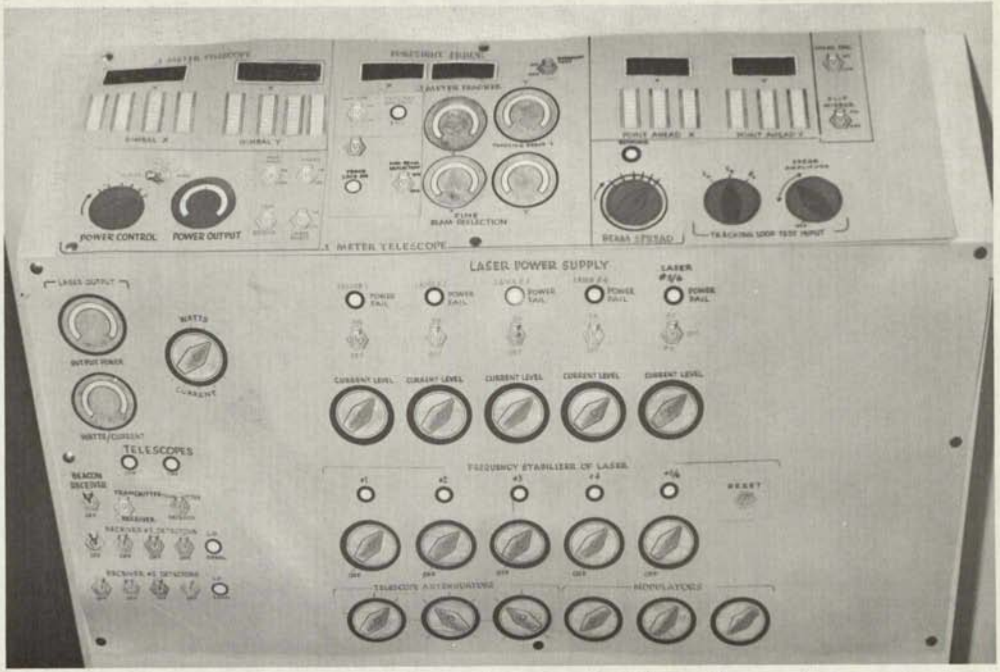

Figure 9.8.1-4. Laser Power Supply Panel.

At this point in the procedure, the Direct Detection experiment may be performed since the transmitter lasers are operating; and this experiment does not require precision pointing.

9.8.4 Boresighting -- Telescopes no. 1 and/or no. 3

a. Turn on 0.4880-micron laser tracker with switch on tracker control panel.

b. Turn on 0.6328-micron local oscillator laser, and open the shutter between local oscillator laser and tracker.

c. Turn on modulator in this beam, and balance the tracker electronics by adjusting phototube gain control knobs on tracker control panel. When the balance has been obtained, close the shutter.

d. Set beam spread control to "max" and set optical attenuator.

e. Open the shutter in front of reference optical flat, and activate boresight mode of point-ahead diasporameter control.

f. Set beam spread control to "min."

g. Verify correct execution of boresight by panel meters on telescope tracker control panel.

h. Deactivate boresight mode, close shutter.

9.8.5 Intermediate Acquisition and Fine Pointing

a. Acquire argon laser beacon with the 0.3-meter telescope tracker. This is done automatically without manual intervention. The tracking mode signal is observed to verify acquisition.

b. Direct the 0.3-meter down beam to ground station, with the 0.3-meter 0.6328-micron transmitter and the ground station receiver operating. Press the boresight button and relay the offset readout to the ground station. Request the point-ahead coordinate from the ground and insert by thumbwheel controls. Set the beamwidth of the telescope at 6 arc seconds and verify reception of the laser beam by the ground station.

c. Ground station acquisition. With the ground receiver, using a wide beam, the 0.6328-micron beam will be tracked optically and will then reduce the argon laser beamwidth to 6 arc seconds, improving the signal strength at the spacecraft.

d. Reduce telescope beamwidth. Manipulate the point-ahead thumbwheel to maximize received signal, and then reduce beam spread angle until the beam spread is set at 0.5 arc seconds, and the ground station verifies a satisfactory signal.

e. Switch control to the 1.0-meter telescope. Set the 1.0-meter telescope gimbal angle thumbwheel to agree with the 0.3-meter telescope gimbal angles and check that the tracking mode light of the 1.0-meter telescope is on. If it is not on, insert the fine beam deflector offset taken from the 0.3-meter telescope and observe light. The transmitting laser in the 0.3-meter telescope may be turned off.

f. Press the boresight button and relay offset readout to the ground station. Set the beam-spread control to 1.0 arc second, request point-ahead coordinates from the ground station, and insert by thumbwheel control. Verify acquisition of signal by the ground station.

g. Fine Pointing. Manipulate the point-ahead thumbwheel and the beam-spre selector switch until the beam has been narrowed to 0.1 arc second and the signal is satisfactorily received at the ground condition.

h. When fine pointing has been verified, the following experiments may be performed: (a) Heterodyne Detection on Earth, (b) Megahertz Optical Communication, (c) Atmospheric Scintillation Experiment, and (4) 10-micron Phase and Amplitude Correlation.

i. Deep Space Simulation. Repeat (e) with attenuator in place at all transmitters to simulate the deep space range and by insertion of signal delay.

9.8.6 Operation of Receivers

a. The beacon receivers are the direct detection receivers in telescopes no. 1 and no. 2. They are turned on by operating the appropriate switch on the left-hand side of the Laser Power Supply Panel. Application of power will also activate the telemetry channel for return of received data to the ground station and insert the flip beam splitter in the optical path for telescope no. 1.

b. The heterodyne receivers will be operated by turning on the local oscillator laser in telescope no. 1. This most likely will have been operating for som time to provide a reference signal for gain stabilization of the tracking receiver.

c. When the local oscillator laser is stabilized, the receiver no. 1 detectors will be turned on by operating the receiver no. 1 detector switches on the left-hand side of the Laser Power Supply Panel.

d. The flip mirror switch on the 1.0-meter telescope panel will be operated to direct the incoming energy to the receiver. This will also provide for the data processing of the detector output.

e. Proper operation of the receivers can be determined by observing the waveforms of each detector on the video monitor panel and measuring the dc component of the heterodyne detector to verify the local oscillator input.

f. With the operation of the receiver verified, the Heterodyne Detection on the Spacecraft Experiment may be performed.

g. The receiver operation procedure may be performed immediately after the boresight procedure so that the Heterodyne Detection on the Spacecraft Experiment may be initiated as soon as the precision tracking of the telescope has been verified.

9.8.7 Spacecraft Support Requirements

The Optical Propagation Experiments group will require supporting facilities from the spacecraft. This will include physical support, prime power, operating controls, information display and data handling.

a. Physical Support requirements are best illustrated by the telescope drawings in section 9.5, "Laser Telescopes."

b. Prime Power requirements will vary with time of operation of the experiments and are shown in graphical form in section 14.0, "Electrical Power Subsystems." and section 28.0, "Data Management."

c. Operating Controls and Information Displays in the spacecraft for these experiments are located on

   1) the 1.0-meter telescope panel

   2) the 0.3-meter telescope panel

   3) the laser power supply panel

   4) star tracker/sun sensor panel.

   These are shown in figures 9.8.1-1 through 9.8.1-4 of this section.

d. Data Handling will require a number of telemetry channels to return information to the ground station. The channel requirements and bandwidth characteristics are described in section 2.8, "Data Management Subsystem."

9.8.8 Ground Station Support Requirements

The ground station is described in detail in section 28.0. Certain facilities of the ground station are required specifically for this experiment group. This includes the several transmitting and receiving telescopes with their mounts and controls.

Special activities will be required at the ground station for the performance of these experiment

Radiosonde balloons will be released over a period of several hours prior to, and during, optical measurements, in order to record upper air conditions. Local meteorological conditions will be measured near the receiving telescope. When there is no interference from clouds, the spacecraft will be commanded to acquire the 0.4880-micron ground beacon, to begin fine tracking, and to transmit test signals on the optical downlinks. The pointing of the ground receiver and the beacon transmitter is updated, so that spacecraft and ground station are accurately illuminating each other.

9.9 SUPPORTING ANALYSES

9.9.1 Supporting Analysis - Pointing and Tracking

9.9.1.1 Detector Comparison

9.9.1.1.1 Image Dissector

In the image dissector tracker, laser light is brought to a focus on the image dissector cathode, forming an electron analog image. The electron image is electrostatically (or magnetically, depending on tube type) scanned along two orthogonal axes past an aperture, and the output i relayed to the anode via an electron multiplier section.

Consider the scan signal along a single axis when a sinusoidal signal is impressed on one pair of deflection plates. When the laser beam is imaged at the center of the scan oscillation, a presence signal is developed at twice the frequency of scan.

For an offset condition, the signal harmonic content shifts to the fundamental of the scan frequency, and the offset direction can be detected by synchronous phase detection. A serious problem exists, however, due to a number of tracking conditions which make the image dissection tracker very difficult to implement.

As will be shown, (section 9.9.1.2) earthshine, even after limiting with a 1 Angstrom filter, is brighter than the laser signal, for the deep space case. In fact, the earth will be imaged in the focal plane of the telescope and would cause an offset unbalance even for the quadrant photomultiplier detection system, unless the ground beacon is modulated. With modulation, the signals can be processed through a narrow-band filter whose center is the modulation frequency. The filter is made wide enough to pass the spectrum of angular disturbances that are to be tracked. As the image is jittered about in the focal plane due to the mechanical disturbances, each detector of the quadrant will "see" an AM signal, provided the carrier frequency is widely separated from that of the spectrum of mechanical disturbances and frequency modulation does not become a problem.

The signal processing techniques ordinarily used for the image dissector trackers will be quite complicated since there will be frequency modulation of the carrier as the image dissector scans the ground modulated laser image across the aperture. The signal will require additional multiplexing down from the ground modulated laser frequency to the image dissector scan frequency before standard synchronous detection techniques can be employed. A second difficulty arises as a result of the image dissector scanning across the Earth's limb and terminator as it will appear in the image dissector focal plane. The resulting step signal containing higher harmonics may be confused with the laser signal itself. Possible additional problems involve structural and electrical instabilities of the image dissector tube and its associated equipment.

These stability problems could possibly be alleviated through the use of a toroidal reflector in the imaging system. This technique would also avoid the problem of balancing the four separate detectors needed for the quadrant photomultiplier technique. The other image dissector problems, such as error due to modulation of the Earth's image, and signal processing complexity, remain, however.

9.9.1.1.2 Quadrant Photomultiplier Tracker

Figure 9.9.1.1-1 illustrates the operation of the quadrant photomultiplier tracker for one axis. Figure 9.9.1.1-2 illustrates the techniques used for developing the tracking error signals for both axes, and a presence signal, from the outputs of the four photomultipliers. The photomultiplier is conceptually used in the telescope trackers; further properties of these detectors are evident in the acquisition signal-to-noise analysis following.

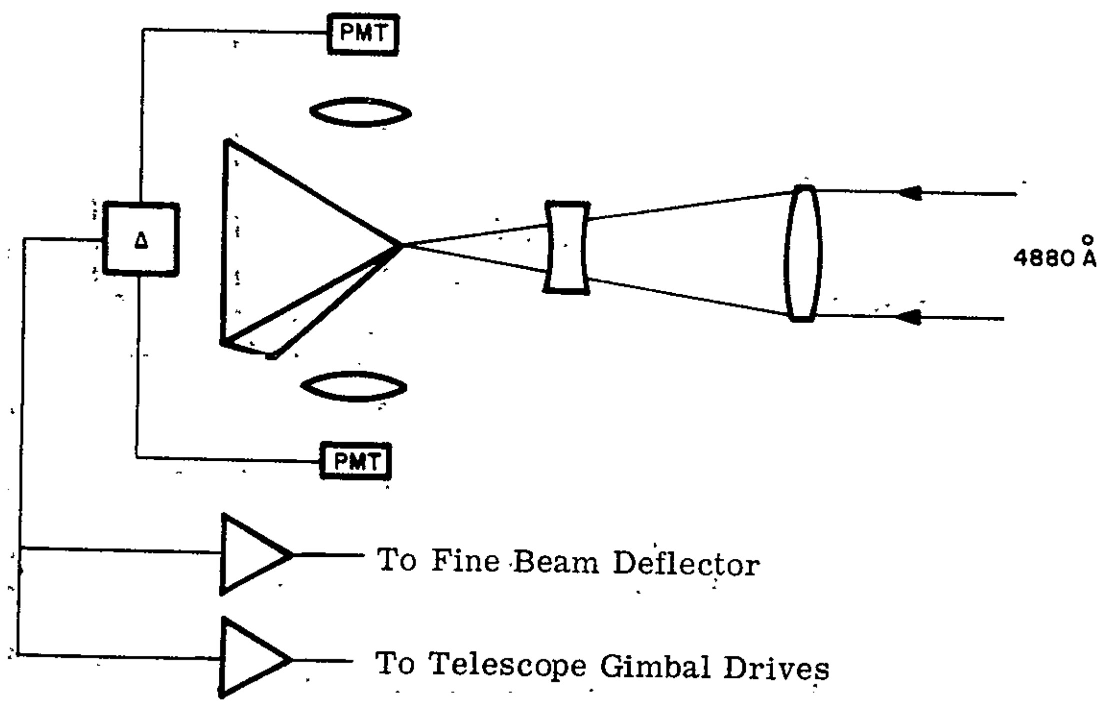

Figure 9.9.1.1-1 Quadrant Photomultiplier Space Tracker Configuration

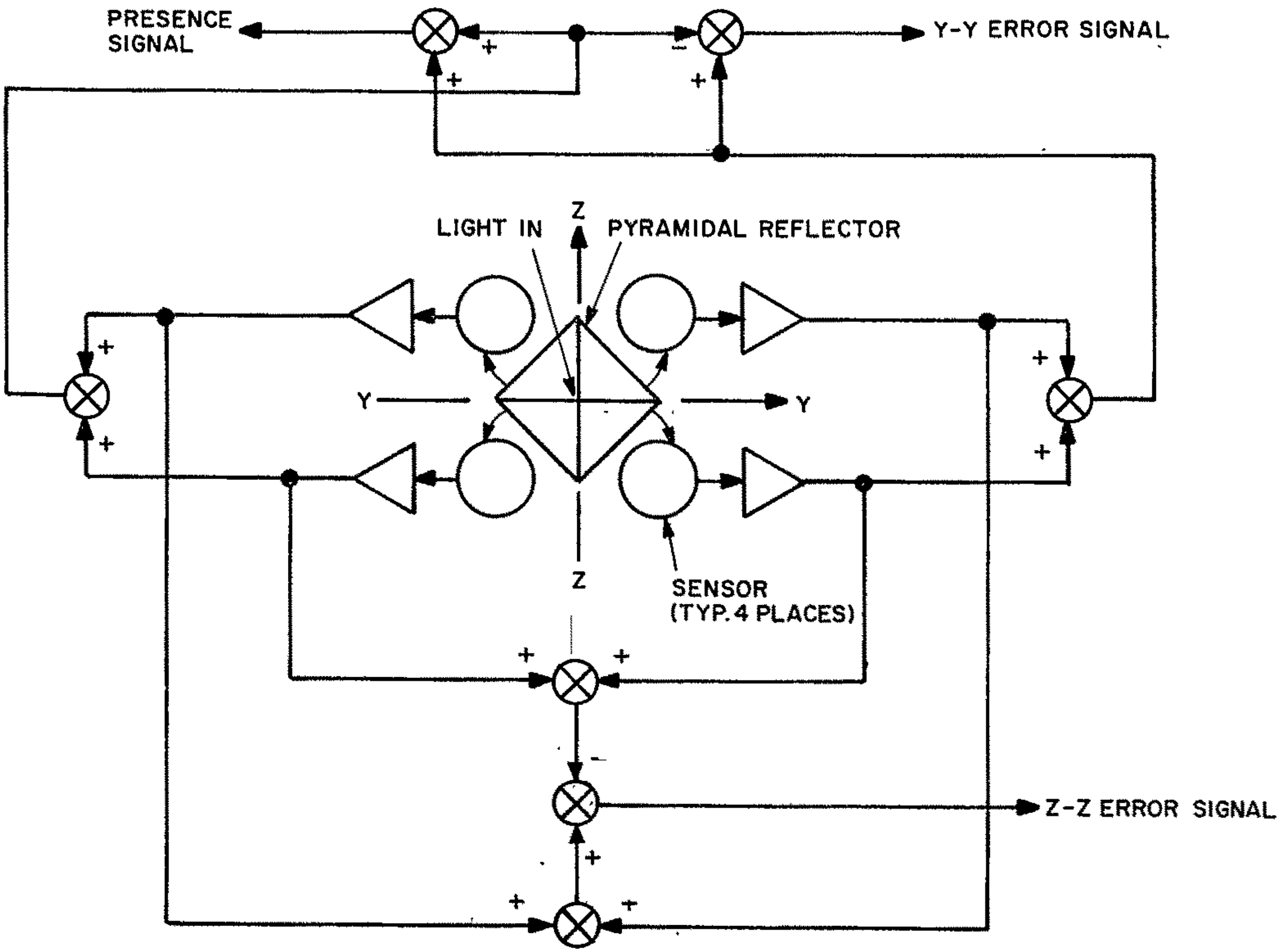

Figure 9.9.1.1-2 Laser Telescope Tracker Signal Development

9.9.1.2 Deep Space Acquisition

9.9.1.2.1 Signal Power

At the start of the acquisition process, the deep-space vehicle's angular position is known to the Earth Station to a 3 sigma error of about ±22.5 arc seconds[1]. A beam with divergence of 50 arc seconds is therefore used at the Earth-Station, to insure illumination. (See section 9.6.5.1.2.2.) The total power received by the space vehicle at range R, using a telescope with aperture diameter D is

$$P_r = P_t \times \frac{4}{\pi (R\theta)^2} \times \frac{\pi D^2}{4} \times A = P_t A \left[\frac{D}{R\theta}\right]^2$$

where:

θ is the divergence of the transmitted beam

A is atmospheric transmission

for:

$P_{t_1} = 10^3$ watts

$R = 1 \text{ AU} = 150 \times 10^9$ meter

$D = 38'' = 0.965$ meter (for 1.0 meter telescope)

$\theta = 50 \text{ arc sec} = 0.242 \times 10^{-3}$ rad

A = atmospheric transmission for 4880 Angstrom laser ≈ 0.7

$P_{r_{11}} = 4.95 \times 10^{-13}$ watt (for 1.0 meter telescope)

For the 0.3 meter telescope, this energy is reduced by the factor,

$$\left(\frac{0.3}{0.965}\right)^2, \quad \text{or} \quad P_{r_{12}} = (4.95 \times 10^{-13}) \left(\frac{0.3}{0.965}\right)^2 = 4.77 \times 10^{-14}$$

(1) G. Stauss, "Study of Laser Beam Pointing Problems," Fourth Bimonthly Technical Report, No. 000162-4, NASA Contract No. NASW-929, Kollsman Instrument Corporation, Elmhurst, N.Y., 15 April 1965, Section IIa.

The total light striking the four sensors will then be $P_r \times M_t$, where M_t = optical transmission factor, including that of tracker optics, collimating optics, 1 Angstrom filter, fine beam deflector, two dichroic mirrors, and obscuration losses due to secondary mirror.

$$M_t = M_{1\mathring{A}} \cdot M_B \cdot M_P \cdot M_O \cdot M_{DM}^2$$

where:

$M_{1\mathring{A}}$ = transmission of 1 Å filter ≈ 0.5

M_B = transmission of fine beam deflector ≈ 0.75

M_P = transmission of primary and secondary optics including secondary obscuration ≈ 0.85

M_O = optical transmission of refractive elements in galilean ocular, tracker telescope ≈ 0.8

M_{DM} = transmission of Dichroic Mirror, (2 used) ≈ 0.9 each

Thus $M_t = (0.5)\ (0.75)\ (0.85)\ (0.8)\ (0.9)^2$

$= 0.207$

and total incident power on four phototubes = $(0.207)\ (4.77 \times 10^{-14})$

$$P'_{r_{12}}\ I = 9.88 \times 10^{-15} \text{ watt}$$

Proceeding to the pulsed laser mode, an assumed duty cycle of 10 percent and peak power of P_{t_2} = 10 kw will result in a total peak received power (for the four detectors) of $P_{r_2} = (10)\ (9.88 \times 10^{-15}) = 9.88 \times 10^{-14}$ watt, at the beam center. At the edge (1/2 power point) of the beam, this is reduced to half,

$$P'_{r_2} = 4.94 \times 10^{-14} \text{ watt.}$$

9.9.1.2.2 Noise Power

For a photomultiplier detector, it may safely be assumed that load resistor noise is rendered negligible in comparison with noise due to light background, dark current and noise-in-signal (owing to the intervening dynode gain).

Background Noise Due to Earthshine

The noise contribution due to background light is evaluated on the basis of earthshine alone, because the amount of starlight which will appear in the restricted field of view does not begin to compete with the light reflection from earth. The maximum irradiance from the earth at the moon is a function of wavelength.(2) In the vicinity of 4,800 Angstroms, the wavelength of argon, it is 2×10^{-5} w/cm^2 - μ = 2×10^{-5} w/m^2 - Angstrom.

At the vehicle range of 1 AU, this reduces by the square of the range ratio, $(384 \times 10^6 \text{ m}/150 \times 10^9 \text{ m})^2$ to 13×10^{-11} w/m^2 - Å. In the case of a Mars mission the vehicle will not view a fully illuminated earth. In a typical situation, as there pointed out, the angle between space-vehicle, earth and sun might be $\beta = 68°$, and the amount of light will be proportional to $(\pi - \beta) \cos \beta + \sin \beta/\pi = 0.516$ times the value calculated above, assuming earth to be a Lambertian reflector. Each of the four detectors will thus receive:

$$P_b = \frac{12 \times 10^{-11} \text{ watts}}{\text{m}^2 \text{ Å}} \times \frac{\pi}{4} \times (0.965 \text{ m})^2 \times 1 \text{ Å} \times 0.25 \times \frac{1}{4} \times 0.516$$

$$= 3.06 \times 10^{-12} \text{ watt.}$$

Dark current for the new RCA C70038D photomultiplier tube (high quantum efficiency) is given as 2×10^{-9} ampere at the anode, with dynode gain of 5×10^4. Quantum efficiency at 4,800 Å is 22 percent and the cathode sensitivity $S = \eta e/h\nu$; $e = 1.6 \times 10^{-19}$ coulomb and $h\nu$ at 4,800 Å, is 4.15×10^{-19} joule; hence $S = 0.085$ ampere cathode current per watt incident power.

Total earthshine on all four detectors is, then, $4(3.06 \times 10^{-12}) = 1.224 \times 10^{-11}$ watt, for the 1.0 meter telescope, or, for the 0.3 meter telescope,

$$1.224 \times 10^{-11} \left(\frac{0.3}{0.965} \right)^2 = 1.18 \times 10^{-12} \text{ watt.}$$

(2) R.A. Rollins, Jr., "Investigation of Optical Spectral Regions for Space Communications," University of Michigan, ASD Technical Documentary Report No. 63-185, May 1963, figure 54.

The anode sensitivity of the detectors is $0.085 \times 5 \times 10^4 = 4.25 \times 10^3$ amps/watt. The current due to background light is then $i_b = 1.18 \times 10^{-12} \times 4.25 \times 10^3 = 5.02 \times 10^{-9}$ amp.

(for all 4 detectors), (0.3M telescope)

Dark Current $= 4(2.0 \times 10^{-9}) = 8.0 \times 10^{-9}$ amp, for all 4 detectors

D.C. Current due to signal, during "on" period (0.3M telescope)

$= (9.88 \times 10^{-14})\ (4.25 \times 10^3) = 4.19 \times 10^{-10}$ amp, at center of beam,

or:

$= (4.94 \times 10^{-14})\ (4.25 \times 10^3) = 2.095 \times 10^{-10}$ amp, at beam edge.

Total anode current, during "on" period of laser is then:

$5.02 \times 10^{-9} + 8.0 \times 10^{-9} + 4.2 \times 10^{-10} = 13.44 \times 10^{-9}$ amp,
at center of beam,

or:

$= 5.02 \times 10^{-9} + 8.0 \times 10^{-9} + 2.1 \times 10^{-10}$

$= 13.23 \times 10^{-9}$ amp, at beam edge,

Resulting in a noise power spectral density, during the "on" period of:

$2ei_{dc} = 2(1.6 \times 10^{-19})\ (13.44 \times 10^{-9})$

$= 43.0 \times 10^{-28}$ amps^2/Hz, at beam center,

or

$2(1.6 \times 10^{-19})\ (13.23 \times 10^{-9}) = 42.4 \times 10^{-28}$ amp^2/Hz, at beam edge.

9.9.1.2.3 Signal-to-Noise Calculation

Assuming the laser is pulsed at a repetition rate high enough to be well above the frequency region of interest for tracking (e.g., a PRF of about 10,000 pps with a tracking bandwidth on the order of 100 Hz), and also assuming the signal processing to be synchronously gated so as to be operative only during the laser "on" period, the following performance may be expected for the deep-space condition with a 50 arc second beam being received by the 0.3 meter telescope:

The fundamental component of the signal (that component which will be passed by a narrow-band filter centered at the prf of the laser) has, for a 10 percent duty cycle rectangular pulse, an amplitude of 0.197 times the maximum value of the pulse by Fourier theory,[1] so that the effective signal amplitude is equivalent to an RMS anode current of:

$$I_s = (0.707)\ (0.197)\ (9.88 \times 10^{-14})\ (4.25 \times 10^3)$$

$= 5.84 \times 10^{-11}$ amp at the beam center, and 1/2 this, or,

2.92×10^{-11} amp at the beam edge.

As a result of gating at a 0.1 duty cycle, the effective noise power spectral density in the frequency region of interest for tracking, would be reduced to 1/10 the maximum value, or

$\phi_{n-n} = 0.1 \times 43 \times 10^{-28} = 4.3 \times 10^{-28}$ amp^2/Hz, at the beam center,

and

$\phi_{n-n} = 0.1 \times 42.4 \times 10^{-28} = 4.24 \times 10^{-28}$ amp^2/Hz, at the edge of the beam.

---

(1) The magnitude of the fundamental component of a pulse train may be found from the Fourier coefficient,

$$C_n = 2A \frac{t_o}{T} \frac{\sin n\pi\, t_o/T}{n\pi\, t_o/T}$$

where:

$n = 1$

A = amplitude of pulse

T = period, (i.e., rising edge to rising edge)

t_o = pulse width

t_o/T = duty cycle = $\frac{1}{10}$

or

$$C_1 = 0.2\,A \left[\frac{\sin \pi/10}{\frac{\pi}{10}} \right] = 0.197\,A$$

If the effective noise bandwidth of the acquisition channel is limited to about 1 Hz, the signal-to-noise ratio for initial acquisition by the 0.3 M telescope would then be:

$$S/N = \frac{5.84 \times 10^{-11}}{2.1 \times 10^{-14}} = 2.8 \times 10^{3}$$

= 2800:1, at the center of the 50 arc second beam, and at the edge, or 1/2 power point of the beam, it is reduced to:

$$\frac{2.92 \times 10^{-11}}{2.07 \times 10^{-14}} = 1420{:}1$$

9.9.1.3 Tracking Resolution Analysis, at the Spacecraft

9.9.1.3.1 Initial Tracking Resolution

When the 50 arc second beacon has been acquired by the 0.3 meter telescope it must be tracked to the center of the field, before the next step in the acquisition process, which is transmission of a 3 arc second beam from space to earth.

The total field of view of the 0.3 meter telescope is ±45 arc seconds. If the linear range of the tracking error signals developed (see figure 9.9.1.3-1 for the error signal characteristics) is assumed to be ±10 arc seconds, then the gradient (slope), K_o will be:

$$K_o = \frac{5.84 \times 10^{-11}}{10} = 5.84 \times 10^{-12} \text{ amp/sec, at the center of the beam, or,}$$

$$K_o = \frac{2.92 \times 10^{-11}}{10} = 2.92 \times 10^{-12} \text{ amp/sec, at the edge of the beam.}$$

Tracking resolution may be estimated as the point at which the S/N ratio is unity. If it is assumed that the closed loop tracking bandwidth is 100 Hz, then this point, when tracking the beam edge (poorest S/N ratio), could be:

$$S/N = \frac{K_o \, \Delta\theta}{\sqrt{\phi_{n-n'} \, \Delta f}} = \frac{2.92 \times 10^{-12} \Delta\theta}{\sqrt{4.3 \times 10^{-28} \times 100}}$$

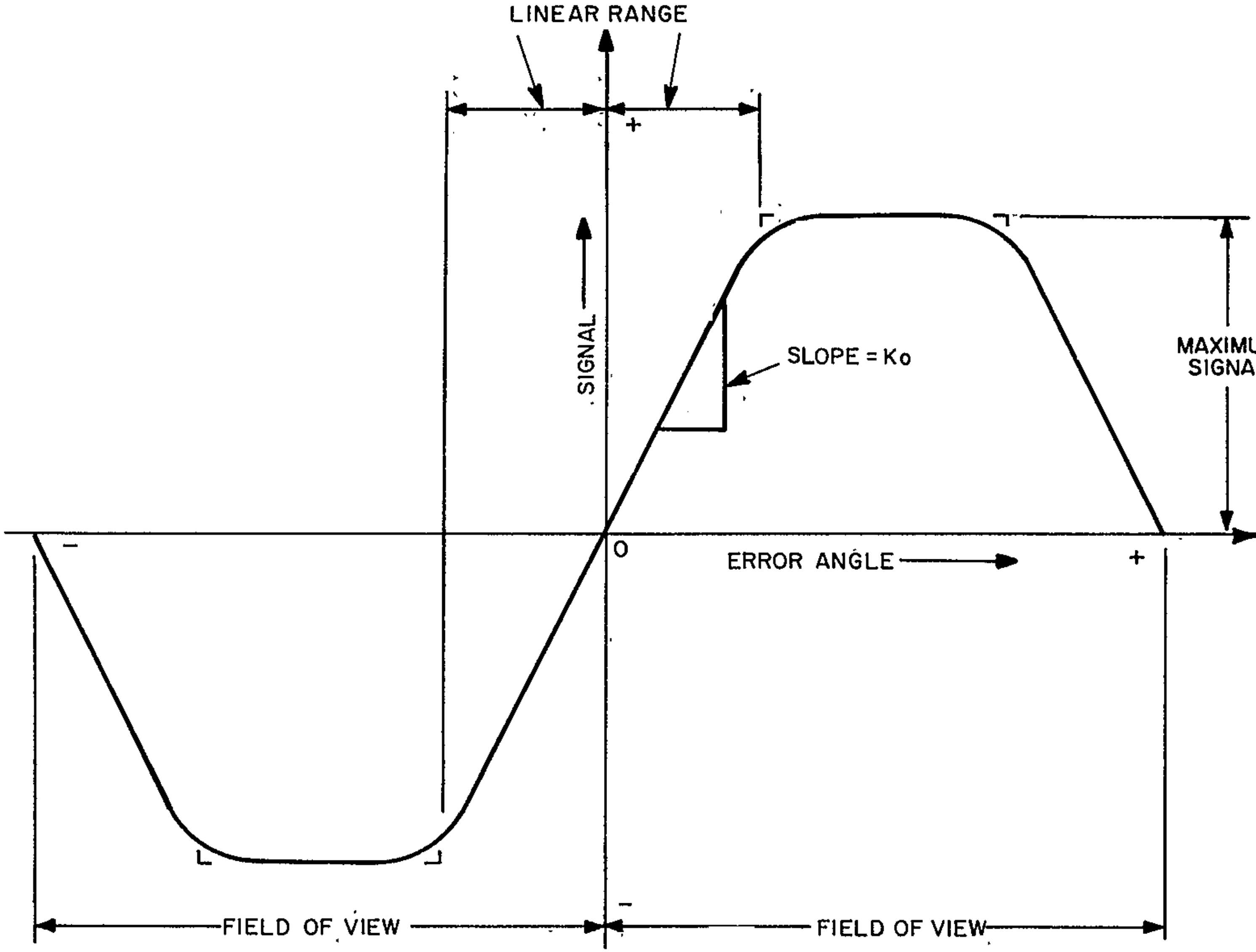

Figure 9.9.1.3-1 Laser Telescope Error Signal Characteristics

and

$$\Delta\theta = \frac{\sqrt{4.3} \times 10^{-13}}{2.92 \times 10^{-12}} = 0.071 \text{ arc second}$$

(This corresponds, approximately, to the RMS "jitter" due to noise.)

Thus the resolution at 100 Hz, and 50 arc beam spread is commensurate with the desired tracking accuracy, particularly when the beam is subsequently narrowed to 6 arc seconds.

9.9.1.3.2 Tracking on Earth

Upon receipt of a beam from the spacecraft on the earth, the earth station can track it. In section 9.9.1.2.4, it is shown that, for heterodyne detection on the earth, with a beam divergence of 0.15 arc second, the signal-to-noise ratio in a 1.0 Hz presence channel is 5100 to one at the center of the beam, and 3620:1 at the beam edge. Increasing the divergence to 3 arc seconds decreases the received energy by a factor of $\left(\frac{3.0}{0.15}\right)^2 = 400:1$. The RMS i-f signal is proportional to the square root of this value, and is therefore reduced by a factor of $\left(\frac{3.0}{0.15}\right) \doteq 20:1$, resulting in a signal-to-noise ratio, at the beam edge, of about 180:1, indicating that acquisition by the ground is theoretically feasible, even at the beam edge.

If the linear range of the ground receiver telescopes is ±5 arc seconds, and a tracking bandwidth at the earth station of 10 Hz is assumed, then the tracking resolution at the beam edge will be:

$$\Delta\theta = \frac{1}{180/\sqrt{10}} \times 5 \text{ seconds.}$$

$$= \frac{5\sqrt{10}}{180} = 0.088 \text{ second.}$$

To this must be added the effect of "image dancing" and scintillation to determine the uncertainty of the earth's knowledge of spacecraft position. Image dancing effect is estimated to be on the order of ±2 seconds for one telescope, or about $\frac{2.0}{\sqrt{100}} = 0.2$ second for the average effect on 100 telescopes in the array.

9.9.1.3.3 Narrowing of Earth-Space Beacon

The earth-to-space beacon is next narrowed down to 6 arc seconds divergence, increasing the signal at the spacecraft by a factor of $\left(\frac{50}{6}\right)^2 = 69.5$. Due to the noise effect of the increase in photomultiplier current resulting from the signal increase, the signal-to-noise ratio increases by a somewhat lower factor.

9.9.1.3.4 Transfer to 1.0 Meter Telescope

An additional improvement in S/N is obtained when tracking is transferred to the 1.0 meter telescope, by virtue of the larger aperture. The steeper signal gradient (K_o) resulting from a narrower linear range results in still finer resolution.

9.9.1.3.5 Acquisition and Tracking - Synchronous Satellite Case - Deep Space Simulation

In order to simulate the deep-space conditions from synchronous orbit, the transmitted power of the ground beacon will be adjusted to obtain a signal-to-noise ratio at the spacecraft tracker which is approximately equal to that anticipated for the deep space case.

9.9.1.3.5.1 Background and Dark Current

At synchronous satellite range, approximately 22×10^3 miles, the spectral irradiance due to earthshine is

$$\frac{2 \times 10^{-5}\ \text{w}}{\text{m}^2\ \text{Å}} \times \left[\frac{238 \times 10^3\ \text{mi}}{22 \times 10^3}\right]^2 = 2.34 \times 10^{-3}\ \text{w/m}^2 - \text{Å}$$

At the range of the synchronous satellite, 22×10^3 mi, earth (radius = 3.96×10^3 mi) subtends $2 \sin^{-1} (3.96/22.0) = 20.8° = 0.364$ radians. The solid angle is $\frac{\pi}{4} (0.364)^2 = 0.104$ steradian and the irradiance in terms of spectral power density per unit of solid angle is

$$\frac{2.34 \times 10^{-3}\ \text{watt}}{\text{m}^2 - \text{Å} \times 0.104\ \text{ster.}} = 22.5 \times 10^{-3}\ \text{watt/m}^2/\text{Å}/\text{steradian}$$

The earthshine which will be received by the 0.3 meter telescope will then be:

$$P_b = \frac{22.5 \times 10^{-3}\ \text{w}}{\text{m}^2\ \mathring{A}\ \text{steradian}} \times \underbrace{\left(\frac{\pi\,(0.3)^2}{4}\right)}_{\text{Telescope Receiver Area}} \times \underbrace{(1\ \mathring{A}}_{\text{Filter Bandwidth}} \underbrace{\times\ 0.25)}_{\text{x Transmission}}$$

$$\times \frac{\pi}{4} \times \underbrace{(90 \times 4.85 \times 10^{-6})^2}_{\text{solid angle field of view}}$$

$$= 5.95 \times 10^{-11}\ \text{watt}$$

The current resulting from this illumination is then :

$$i_b = 5.95 \times 10^{-11} \times 4.25 \times 10^3 = 2.53 \times 10^{-7}\ \text{amp},$$

dark current = $i_d = 8 \times 10^{-9}$ amp (for all four detectors),
and total current (exclusive of signal) = $i_b + i_d = 2.61 \times 10^{-7}$ amp

The noise power spectral density corresponding to this current = $2ei$ $= 2(1.6 \times 10^{-19})\ (2.61 \times 10^{-7}) = 8.35 \times 10^{-26}\ \text{amp}^2/\text{Hz}$. As a result of gating at a 10 percent duty cycle, this is reduced to $0.835 \times 10^{-26}\ \text{amp}^2/\text{Hz}$.

The RMS signal current to duplicate the deep space signal-to-noise (at the beam center) of 2800:1 in a 1 Hz bandwidth is approximately:

$$I_s = (2800)\sqrt{(0.835 \times 10^{-26})} \doteq 2.56 \times 10^{-10}\ \text{amp.}$$

This corresponds to a received pulse amplitude of:

$$P_r = \frac{2.56 \times 10^{-10}}{(0.707)\ (0.197)\ (4.25 \times 10^3)\ (0.207)} = 2.09 \times 10^{-12}\ \text{watt}$$

The amplitude of the pulse transmitted from the earth, with a beam divergence of 50 arc seconds, to produce this at synchronous satellite range of 22×10^3 miles is:

$$P_t = \frac{P_r}{A} \left[\frac{R\theta}{D} \right]^2$$

where:

$P_r = 2.09 \times 10^{-12}$ watt

A = atmospheric transmission at 4880 A ≈ 0.7

$\theta = 50$ arc seconds $= 0.242 \times 10^{-3}$ radians

$D = 22 \times 10^3$ miles $= 3.54 \times 10^7$ meters

Thus

$$P_t = \frac{2.09 \times 10^{-12}}{0.7} \cdot \left[\frac{(3.54 \times 10^7)\ (2.42 \times 10^{-4})}{0.3} \right]^2$$

$$= 2.43 \times 10^{-3} \text{ watt} \approx 2.5 \text{ mw}$$

This is the amplitude of the transmitted pulses required (with a 10 percent duty cycle) to simulate deep-space performance from synchronous orbit.

9.9.1.4 Accuracy Requirements for Reference Axes

The mathematical analysis of lead angle computation for aberration and transit time corrections is given here with numerical values corresponding to a Mars fly-by trajectory.

Typical values range from about 10 arc seconds at the beginning of the mission to about 40 arc seconds at fly-by.

The space vehicle is stabilized by means of the Sun Sensor and the Canopus Tracker. Assume that the initial Search-Acquisition process as previously described has been carried out using the DSIF, the earth station beacon, and the space vehicle beam pointing system. It is further necessary to use a precision celestial sensor to provide half of the reference axes, tracking on Canopus, for example, with the other half provided by the space vehicle track to earth.

A preliminary analysis of the precision needed for the reference axes' celestial sensor may be drived as follows, see Figure 9.9.1.4-1. The space vehicle track to earth station coincides with the Y-axis, and the X-Z plane is the plane at right angles to the tracker LOS to earth (established by the closed loop). The space vehicle transmitter beam is directed along vector OP at an azimuth angle α and an elevation angle β (in spherical polar coordinates). These angles represent the components of the space vehicle to earth transmission lead angle, and for $r = 10^8$ miles, $\alpha = 40$ arc seconds, $\beta = 0.2$ arc second, approximately.

The precision celestial sensor is used to determine the X-Y plane (i.e., the Z-axis). This might be the projection of the LOS to Canopus on the X-Z plane perpendicular to the LOS to earth (Y-axis). It is assumed for this analysis that the LOS to earth is errorless.

The analysis below shows that a 75 arc second error in the other reference axis (i.e., the Z-axis) is equivalent to a coordinate rotation about the Y axis. At a range of 100 million miles, the error is 7.3×10^{-8} radian which is one tenth of the 0.15 second laser beam width. The azimuth error angle is negligible. These error angles are small because the lead angles themselves are small, yielding small displacements of the radius vector OP at Earth.

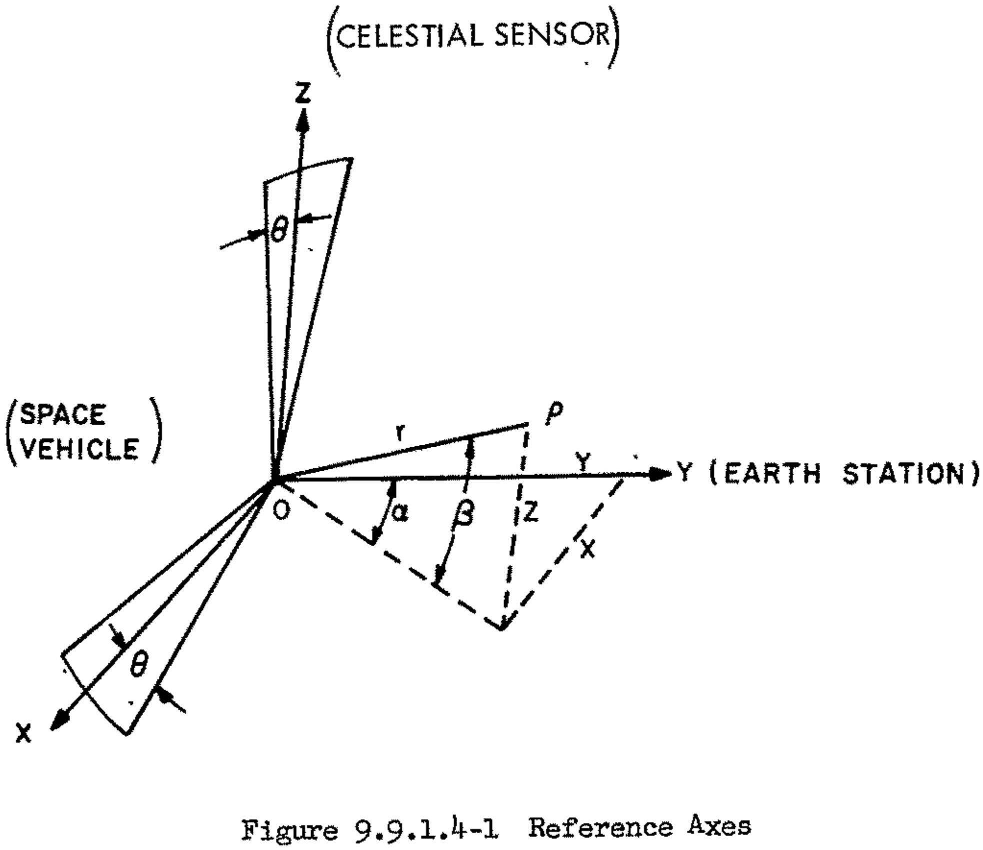

Figure 9.9.1.4-1 Reference Axes

It is clear that the geometry of the closed loop tracking to earth dilutes the requirement for extreme precision in celestial sensors which might otherwise be required for an open-cycle system. This analysis will eventually be modified to include the effects of atmospheric propagation in the loop, but it is not expected that the results for the space vehicle configuration will be significantly affected.

Coordinates:

$r \approx 10^8$ miles (range)

$\alpha \approx 40$ arc seconds $\approx 2 \times 10^{-4}$ radian (lead angle)

$\beta \approx 0.2$ arc second $\approx 10^{-6}$ radian (lead angle)

$x = r \cos\beta \sin\alpha \approx r\alpha \approx 2 \times 10^4$ miles

$y = r \cos\beta \cos\alpha \approx r \approx 10^8$ miles

$z = r \sin\beta \approx \beta \approx 100$ miles

Coordinate Rotation

$z^1 = z \cos\theta - x \sin\theta \approx z - x\theta$

$x^1 = z \sin\theta + x \cos\theta \approx z\,\theta + x$

thus:

$z^1 - z \approx - x\theta$, or, $\Delta z \approx -x\theta$

$x^1 - x \approx z\theta$, or, $\Delta x \approx z\theta$

X is the equivalent displacement of the beam along the X axis as projected to earth, and for $\alpha = 40$ arc seconds, $x \approx 2 \times 10^4$ miles; similarly, $z \approx 100$ miles. β is 200 times more sensitive than α to rotation about the Y axis due to star tracker error. Thus, $\Delta z \approx x\theta$ will be the essential error displacement of the beam in miles for the perturbation about the Y axis. For a perturbation of the lead angle corresponding to one-tenth of the beam width $\Delta\beta = 7.3 \times 10^{-8}$ radian, the permitted error, θ, is as follows:

$$x\theta = r\,\Delta\beta$$

Therefore,

$$\theta = \frac{10^8 \times 7.3 \times 10^{-8}}{2 \times 10^4} = 3.7 \times 10^{-4} \text{ radian}$$

$$\theta \approx 75 \text{ arc seconds}$$

9.9.1.5 Heterodyne Detection on The Ground

As discussed in section 9.6.6.3.3 above, heterodyne detection achieves the maximum improvement in signal-to-noise ratio when the local oscillator power is very high compared to the input power which would be required to produce noise equivalent to that present from all sources other than the local oscillator.

The sensor being considered is a silicon photodiode of the Philco L4501-L4504 series, with an assumed quantum efficiency of 0.5, making the sensitivity at 6328 Angstroms,

$$S = \frac{\eta e}{h\nu} = \frac{(0.5)\ (1.6 \times 10^{-19})}{(6.63 \times 10^{-34})\ (4.74 \times 10^{14})}$$

$$S = 0.254 \text{ amp/watt.}$$

9.9.1.5.1 Noise Contributions

The noise contribution due to dark current, and thermal agitation in a typical load resistor, may be estimated from the catalog value of N.E.P., where N.E.P. is defined as:

$$\text{N.E.P.} = \frac{\text{Incident Power}}{S/N\sqrt{\Delta f}}$$

With a cell area of 3.5 mm^2 and an incident power density of 6×10^{-9} watt/mm^2, the N.E.P. is given as 7.5×10^{-13} watt/$Hz^{1/2}$

For a 1 Hz bandwidth,

$$S/N = \frac{(6 \times 10^{-9})\ (3.5)}{7.5 \times 10^{-13} \times 1.0} = 2.8 \times 10^4$$

At this input level, the signal current is $(6 \times 10^{-9})\ (3.5)\ (0.254)$ $= 5.33 \times 10^{-9}$ amp.

$$\text{RMS Noise Current} = \frac{5.33 \times 10^{-9}}{2.8 \times 10^{4}} = 1.9 \times 10^{-13} \text{ amp.}$$

Since this is calculated for a bandwidth of 1.0 Hz, the Noise Power Spectral Density is the $\dfrac{(1.97 \times 10^{-13})^2}{1.0} \approx 3.6 \times 10^{-26}$ amp^2/Hz.

The component of this density due to the signal current is

$$2\ ei_s = 2(1.6 \times 10^{-19})\ (5.33 \times 10^{-9})$$

$$= 1.7 \times 10^{-27} \text{ amp}^2/\text{Hz.}$$

Therefore, Noise Power Spectral Density due to dark current and thermal effects is $3.6 \times 10^{-26} - 1.7 \times 10^{-27} = 3.4 \times 10^{-26}$ amp^2/Hz.

The incident power to produce this amount of noise would then be:

$$P_{dk + th} = \frac{3.4 \times 10^{-26}}{2\ eS}$$

$$= \frac{3.4 \times 10^{-26}}{2(1.6 \times 10^{-19})\ (0.254)} = 4.2 \times 10^{-7} \text{ watts.}$$

The background contribution is caused by the incident background power, P_b on each sensor,

$$P_b = \beta_d \Delta\lambda \Omega \frac{\pi D^2}{4} Mm^1 \times 1/4$$

where:

$\beta_d = 16 \times 10^{-8}$ watts/cm^2-sterad-Å

$\Delta\lambda = 10$ Å (at 6328 Å)

Ω (for 60 arc seconds field of view) $= (4.85 \times 10^{-6})^2 \; (60)^2 \left(\frac{\pi}{4}\right)$

$= 6.66 \times 10^{-8}$ sterad.

$M = m^1 = 0.5$

$D = 12.5$ cm

Therefore,

$$P_b = \frac{(16 \times 10^{-8})\,(10)\,(6.66 \times 10^{-8})\,(\pi)\,(12.5)^2}{4} \times \frac{(0.5)\,(0.5)}{4}$$

$$= 8.18 \times 10^{-13} \text{ watt.}$$

Contribution of Incident Laser Energy

From section 9.9.1.5.2.1 below, the laser energy incident on each sensor (at tracking null) would be 4.1×10^{-14} watt.

The total of all of these = P_n

$$P_n = 4.1 \times 10^{-14} + 8.18 \times 10^{-13} + 4.2 \times 10^{-7}$$

$$\approx 4.2 \times 10^{-7} \text{ watt.}$$

With $P_{LO} = 5 \times 10^{-3}$ watt, the

ratio $\dfrac{P_n}{P_{LO}} = \dfrac{4.2 \times 10^{-7}}{5 \times 10^{-3}} \approx 1 \times 10^{-4}$

is indeed negligible compared to unity (see section 9.6.6.3.3).

9.9.1.5.2 Deep Space (1 AU) Case

9.9.1.5.2.1 Received Energy

The laser energy detected by each receiving telescope will be

$$P_r = m' \ P_t \ MN \ D^2/(R\,\theta)^2 \text{ watts,}$$

where:

P_t = transmitted power = 1 watt

M = optical efficiency of transmitter and receiver combined (not including heterodyne beamsplitter) = 0.5

N = atmospheric attenuation factor, which varies with zenith angle and wavelength, and representative value assumed = 0.5

m' = beamsplitting factor, for heterodyne detection = 0.5

D = diameter of aperture = 12.5 cm

R = range = 1 AU = 150 x 10" cm

θ = angular divergence of laser beam at 1/2 power points = 0.15 arc seconds = 0.728×10^{-6} radians

and, at a tracking null, each photodetector will receive 1/4 of energy, or $P_r/4$

$$\frac{P_r}{4} = \frac{1 \ (0.5)\ (1.0)\ (0.5)\ (0.5)\ (12.5)^2}{4 \ (150 \times 10^{11} \times 0.728 \times 10^{-6})^2} = 4.1 \times 10^{-14} \text{ watt}$$

The mean square i-f current developed at each detector (at tracking null) would then be:

$$i_s^2 = 2\,s^2\,P_{LO}\frac{P_r}{4}$$

where:

i_s = average (rms) i-f current

$$S = \text{detector sensitivity} = \frac{\eta e}{H\nu}$$

= 0.254 amp/watt (section 9.9.1.5 above)

$P_{LO} = 5 \times 10^{-3}$ watt

$\frac{P_r}{4} = 4.1 \times 10^{-14}$ watt

Therefore,

$$i_s^2 = 2(0.254)^2 \, (5 \times 10^{-3}) \, (4.1 \times 10^{-14})$$

$$= 0.268 \times 10^{-16} \text{ amp}^2,$$

or, the rms i-f current is:

$$i_s = \sqrt{0.268 \times 10^{-16}} = 0.516 \times 10^{-8} \text{ amp.}$$

This is the current in each sensor, at tracking null. Each 1/2 array of 50 telescopes contains 4 x 50 = 200 sensors. The total i-f current in each half-array is then 200 $(0.516 \times 10^{-8}) = 1.032 \times 10^{-6}$ amp.

9.9.1.5.2.2 Presence Signal

The presence signal, consisting of the sum of the signals from all sensors of all telescopes, will be twice the above value, or $2(1.032 \times 10^{-6}) = 2.06 \times 10^{-6}$ amp.

This is also the maximum (or saturation) value of the angle tracking signal (See figure 9.9.1.1.3-1.)

9.9.1.5.2.3 Noise Density

The noise spectral density at each detector, due primarily to local oscillator power (section 9.9.1.5.1) may be calculated as follows:

$$\phi'_{nn} = 2e\ i_{dc} \approx 2e\ (S \times P_{LO})$$

$$= 2(1.6 \times 10^{-19})\ (0.254)\ (5 \times 10^{-3})$$

$$= 4.07 \times 10^{-22}\ \text{amp}^2/\text{Hz}$$

For the full array of 100 telescopes, the total noise power spectral density is then $\phi_{nn} = 100 \times 4 \times \phi'_{nn} = 400 \times 4.07 \times 10^{-22}$

$$= 16.3 \times 10^{-20}\ \text{amp}^2/\text{Hz}$$

9.9.1.5.2.4 Signal-to-Noise

The signal-to-noise ratio for the presence signal, assuming a 1 Hz bandwidth in the presence channel, is

$$S/N = \frac{2.06 \times 10^{-6}}{\sqrt{16.3 \times 10^{-20}} \times 1.0} = 5100$$

This is at the center of the beam. At the edge (1/2 power point) of the beam, the received power is reduced by a factor of 2, reducing the rms i-f current, and hence, the S/N ratio, by a factor of $\sqrt{2}$. Hence, at the beam edge,

$$i_s = \frac{2.06 \times 10^{-6}}{\sqrt{2}} = 1.46 \times 10^{-6}\ \text{amp},$$

and the presence channel $S/N = \dfrac{5100}{\sqrt{2}} = 3620$

The maximum signal-to-noise ratio for tracking, with a closed-loop equivalent noise bandwidth for the tracking loop of 10 Hz would then be:

$$\frac{5100}{\sqrt{\frac{10}{1}}} = \frac{5100}{\sqrt{10}} = 1620 \text{ at the}$$

center of the beam, and $\dfrac{3620}{\sqrt{10}} = 1140$, at the edge of the beam (1/2 power points).

The tracking resolution at the beam edge (poorest S/N) if the linear range of the tracking error signal is ±5 arc seconds, will be

$$\Delta\theta = \frac{1}{1140} \times (\pm 5) = \pm 0.0044 \text{ arc second.}$$

9.9.1.5.2.5 Development of Beam-Pointing Error Signals

The intensity distribution of the laser energy across the beam width in the far-field is essentially gaussian, so that

$$I = I_o\, e^{-(a^2\theta^2)},$$

where

I = beam intensity at an angular displacement θ from the center of the beam

θ = angle measured from beam center

I_o = intensity at beam center

$a^2 = \frac{2.776}{(\theta_B)^2}$, i.e., $\exp -\left(\frac{2.776\,\theta^2}{\theta_B^2}\right) = 0.5$ for $\theta = \theta_B/2$.

θ_B = beam width between 1/2 power points.

The intensity gradient may be found by differentiating this relationship:

$$\frac{dI}{d\theta} = -2 I_o\, a^2\, \theta\, e^{-(a^2\theta^2)}$$

With θ_B = 0.15 arc second = 7.28×10^{-7} radian, we find, at

$$\frac{\theta_B}{10} = 0.015 \text{ arc second } = 0.728 \times 10^{-7} \text{ radian}$$

$$\frac{dI}{d\theta} = -2\, I_o \times \frac{2.776}{(7.28 \times 10^{-7})^2} \times 0.728 \times 10^{-7} \times e^{-\left(\frac{2.776\,\theta_B^2}{100\,\theta_B^2}\right)}$$

$$= -7.43 \times 10^5\, I_o$$

and at $\theta = \frac{\theta_B}{2}$, (= 0.075 arc second)

$$\frac{dI}{d\theta} = -2\, I_o \times \frac{2.776}{(7.28 \times 10^{-7})^2} \times 0.364 \times 10^{-6} \times e^{-\left(\frac{2.776}{4}\right)}$$

$$= -1.91 \times 10^6\, I_o$$

At a range of 1 AU, the half-array width (center-to-center distance between half-arrays) of 91.44 cm (3 feet) subtends an angle of

$$\delta\theta = \frac{0.9144}{1.50 \times 10^{11}} = 6.1 \times 10^{-12} \text{ radian}$$

Thus,

at θ = 0.015 arc second,

$$\delta I = (-7.43 \times 10^5)(6.1 \times 10^{-12})\, I_o$$

$$= -4.54 \times 10^{-6}\, I_o$$

and at θ = 0.075 arc seconds,

$$\delta I = (-1.91 \times 10^6)(6.1 \times 10^{-12})\, I_o$$
$$= -1.164 \times 10^{-5}\, I_o$$

If i_{s_1} is the RMS signal current produced in one-half-array by an intensity I_1, and i_{s_2} is that produced in the other half array by an intensity

$I_2 = I_1 + \delta I = I_1 - k\, I_o$, and since $\frac{i_{s_2}^2}{i_{s_1}^2} = \frac{I_2}{I_1}$,

it may readily be shown that

$$\delta i_s = i_{s_1} - i_{s_2} = i_{s_1}\left[1 - \sqrt{1 - \frac{I_o}{I_1}\, k}\right]$$

further, at $\theta = \frac{\theta B}{10}$, $I_1 \approx I_o$. Therefore $\frac{I_o}{I_1} \approx 1$,

and at $\theta = \frac{\theta B}{2}$, $\quad I_1 = \frac{I_o}{2}$, $\quad$ or $\frac{I_o}{I_1} = 2$

Substituting into the equation gives the differential RMS signal current:

at $\quad \theta = 0.015$ arc second,

$$\delta i_s = 1.032 \times 10^{-6} \left[1 \quad \sqrt{1 - 4.54 \times 10^{-6}} \right]$$

$$= 2.34 \times 10^{-12} \text{ amps,}$$

and at

$\theta = 0.075$ arc second, $\quad$ where $\quad i_s = \frac{1.032 \times 10^{-6}}{\sqrt{2}} = 0.732 \times 10^{-6}$ amp

$$\delta i_s = 0.732 \times 10^{-6} \left[1 - \sqrt{1 - 2(1.164 \times 10^{-5})} \right]$$

$$= 8.52 \times 10^{-12} \text{ amp.}$$

9.9.1.5.3 Simulation From Synchronous Orbit

9.9.1.5.3.1 Received Energy

Using the equation and definitions from section 9.9.1.5.2.1 above, but substituting:

$$P_t = 7.5 \times 10^{-3} \text{ watt}$$

$$R = 360 \times 10^7 \text{ cm}$$

the energy detected by each receiving sensor (at a tracking null) is found to be:

$$\frac{P_r}{4} = \frac{\frac{1}{4}\ (0.5)\ (0.5)\ (0.5)\ (7.5 \times 10^{-3})\ (12.5)^2}{(360 \times 10^7 \times 0.728 \times 10^{-6})^2} = 0.534 \times 10^{-8} \text{ watt, at the center of the beam}$$

The RMS signal current produced in each sensor is then:

$$i_s = \sqrt{2(0.254)^2 \; (5 \times 10^{-3}) \; (0.534 \times 10^{-8})}$$

$$= 1.86 \times 10^{-6} \text{ amp.}$$

Since each half-array consists of 8 telescopes, each with 4 sensors, the total RMS signal current in each half-array will be

$$8 \times 4 \times 1.86 \times 10^{-6} = 59.5 \times 10^{-6} \text{ amp,}$$

at the center of the beam.

At the edge (1/2 power point) of the beam, this will be reduced to

$$\frac{59.5}{\sqrt{2}} = 41.4 \times 10^{-6} \text{ amp.}$$

9.9.1.5.3.2 Presence Signal

The presence signal, as in section 9.9.1.5.2.2, will be twice the above values, or:

$$2 \times 59.5 \times 10^{-6} = 119 \times 10^{-6} \text{ amp, at the beam center,}$$

and

$$2 \times 41.4 \times 10^{-6} = 82.8 \times 10^{-6} \text{ amp, at the beam edge.}$$

These are also the maximum (saturation) values of the angle tracking signal (figure 9.9.1.1.3-1).

9.9.1.5.3.3 Noise Density

As in the deep-space case, the noise spectral density at each detector, due primarily to the local oscillator power, is 4.07×10^{-22} amp^2/Hz. (See section 9.9.1.5.2.3.)

For the full array of 16 telescopes the total noise power spectral density is then:

$$\phi_{nn} = 16 \times 4 \times 4.07 \times 10^{-22}$$

$$= 2.60 \times 10^{-20} \text{ amp}^2\text{/Hz.}$$

9.9.1.5.3.4 Signal-to-Noise

The signal-to-noise ratio for the presence signal, in a 1 Hz bandwidth, is

$$S/N = \frac{119 \times 10^{-6}}{\sqrt{2.6 \times 10^{-20}}} = 7.4 \times 10^{5}$$

at the beam center, and at the beam edge the $S/N = \dfrac{7.4 \times 10^{5}}{\sqrt{2}} = 5.2 \times 10^{5}$.

Tracking resolution, even at the beam edge, with a 10 Hz. Closed loop equivalent noise bandwidth (see section 9.9.1.5.2.4) is:

$$\Delta \theta = \frac{1}{5.2 \times 10^{5}/\sqrt{10}} \times (\pm 5) = \pm 3 \times 10^{-5} \text{ arc seconds}$$

9.9.1.5.3.5 Beam Pointing Error Signals

From section 9.9.1.5.2.5, at

$$\theta = \frac{\theta B}{2} = 0.075 \text{ arc second,}$$

$$\delta I = 1.91 \times 10^{6}\ I_o\ \delta\theta$$

At a range of 3.60×10^{7} meters, the angle subtended by the half-array distance of 45.52 cm (1.5 feet) is:

$$\delta\theta = \frac{(0.4552)}{(3.60 \times 10^{7})} = 1.27 \times 10^{-8} \text{ radians}$$

Therefore,

$$\delta I = (-1.91 \times 10^{6})\ (1.27 \times 10^{-8})\ I_o$$

$$= 0.0243\ I_o$$

and the differential RMS signal current between the two halves of the array is

$$\delta i_s = 41.4 \times 10^{-6} \left[1 - \sqrt{1 - 2(0.0243)} \right]$$

$$= 1.04 \times 10^{-6} \text{ amp.}$$

9.9.1.6 Direct Detection on the Ground

The direct detection on earth of a laser beam from space is accomplished as described in section 9.6.6.3.4, using an array of receiving telescopes in an arrangement typified by that illustrated in figure 9.6.6.3.4-1. The dimensions shown on that figure are those used in the following analysis.

The detector used is a quadrant photomultiplier type (see section 9.9.1.1). Signal development is also the same as that used for spaceborne detection of the ground beacon (see figure 9.9.1.1-2), except that no pulsing will be used.

The photomultiplier used is the same one applied in the spaceborne telescope (see sections 9.9.1.1 and 9.9.1.2). The cathode sensitivity of this tube at 6328 Angstroms, from manufacturer's curves, is about 0.068 amp/watt, which, at a dynode gain of 5×10^4 results in an anode sensitivity of $5 \times 10^4 \times 0.068 = S$ or, $S = 3.4 \times 10^3$ amp/watt.

9.9.1.6.1 Deep Space (1 AU) Case

9.9.1.6.1.1 Tracking Resolution

The laser power detected by the four tubes of one telescope, at the center of the beam is

$$P_r' = \frac{MNP_t D^2}{(R\theta)^2}.$$

where:

$M = N = 0.5$

$P_t = 1.0$ watt

$D = 2.0$ meters

$R = 1 \text{ AU} = 1.50 \times 10^{11}$ meters

$\theta = 0.''15$ arc second $= 0.728 \times 10^{-11}$ radian

$$P_r' = \frac{(0.5)\ (0.5)\ (1.0)\ (2.0)^2}{(1.50 \times 10^{11} \times 0.728 \times 10^{-6})^2} = 8.37 \times 10^{-11} \text{ watt.}$$

The signal current corresponding to this energy (at the anodes of the PMT's) is:

$$i_s = (8.37 \times 10^{-11})\ (3.4 \times 10^3)$$

$= 2.84 \times 10^{-7}$ amp (dc) (at the beam center) and, at the beam edge, this is reduced to one half this value, or

$$i_s = \frac{2.84 \times 10^{-7}}{2} = 1.42 \times 10^{-7} \text{ amp (dc)}$$

Dark current for this tube is given as 2×10^{-9} amp (at the anode). For the four tubes used in one telescope, this will amount to $4 \times 2 \times 10^{-9}$ $= 8 \times 10^{-9}$ amp.

Background illumination incident on the four tubes of one telescope amounts to:

$$P_b = \beta_d \Delta\lambda \Omega \frac{\pi D^2}{4} \text{ Mm}'$$

where:

$\beta_d = 16 \times 10^{-8}$ watt/cm^2-steradian-Å

$\Delta\lambda$ = optical filter bandwidth = 1.0 Å (at 6328 Å)

Ω , (for 60 arc second field of view),

$$= \frac{\pi}{4} (60 \times 4.85 \times 10^{-6})^2 = 6.66 \times 10^{-8} \text{ steradian}$$

M = optical efficiency, without filter = 0.5

m^1 = optical filter efficiency at 6328 Å center wavelength = 0.5

D = aperture diameter = 200 cm.

$$P_b = 16 \times 10^{-8} \times 1.0 \times 6.66 \times 10^{-8} \times \frac{\pi}{4} \times (200)^2 \times 0.5 \times 0.5$$

$$= 8.36 \times 10^{-11} \text{ watt,}$$

which produces an anode current of $(8.36 \times 10^{-11})\ (3.4 \times 10^3) = 2.83 \times 10^{-7}$ amp.

The total d-c anode current for all four tubes of one telescope is then:

$$i_{DC} = 2.83 \times 10^{-7} + 2.84 \times 10^{-7} + 0.08 \times 10^{-7}$$

$$= 5.75 \times 10^{-7} \text{ amp.}$$

This is at the center of the received beam. At the edge, it is reduced to

$$i_{DC} = 2.83 \times 10^{-7} + 1.42 \times 10^{-7} + 0.08 \times 10^{-7}$$

$$= 4.33 \times 10^{-7} \text{ amp.}$$

The noise power spectral density (for one telescope) corresponding to this current is:

$$\phi^{1}_{nn} = 2e\, i_{DC} = 2(1.6 \times 10^{-19})\ (5.75 \times 10^{-7})$$

$$= 18.35 \times 10^{-26} \text{ amp}^2/\text{Hz, at the center of the beam,}$$

$$= 2(1.6 \times 10^{-19})\ (4.33 \times 10^{-7})$$

$$= 13.8 \times 10^{-26} \text{ amp}^2/\text{Hz, at the beam edge.}$$

The presence signal, and the maximum value of the tracking signal, consisting of the combined outputs of the four telescopes in the array is equal to $4 \times 2.84 \times 10^{-7} = 1.14 \times 10^{-6}$ amp dc, at the center of the beam and $4 \times 1.42 \times 10^{-7} = 0.57 \times 10^{-6}$ amp dc, at the edge of the beam.

The total noise power spectral density for the four telescopes is

$$\phi_{nn} = 4 \times 18.35 \times 10^{-26} = 73.4 \times 10^{-26} \text{ amp}^2/\text{Hz, at the center of}$$

the beam, and

$\phi_{nn} = 4 \times 13.8 \times 10^{-26} = 55.2 \times 10^{-26}$ amp^2/Hz, at the edge of the beam.

The signal-to-noise ratio in a 1.0 Hz presence channel is then

$$S/N = \frac{1.14 \times 10^{-6}}{\sqrt{73.4 \times 10^{-26} \times 1.0}} = 1.33 \times 10^{6} \text{ at the center of the beam.}$$

$$S/N = \frac{0.57 \times 10^{-6}}{\sqrt{55.2 \times 10^{-26} \times 1.0}} = 7.66 \times 10^{5} \text{ at the edge of the beam.}$$

Tracking resolution (point where S/N = 1) for a 10 Hz tracking loop equivalent noise bandwidth and a ±5 arc second linear range is:

$$\theta = \frac{1}{1.33 \times 10^{6}/\sqrt{10}} \times (\pm 5) = \pm 1.2 \times 10^{-5} \text{ arc second at the}$$

center of the beam, and

$$\theta = \frac{1}{7.66 \times 10^{5}/\sqrt{10}} \times (\pm 5) = \pm 2.1 \times 10^{-5} \text{ arc second at the}$$

edge of the beam.

9.9.1.6.1.2 Development of Beam-Pointing Error Signals

The relationships are used as derived in section 9.9.1.5.2.5, for the intensity gradients, i.e.,

$$\frac{dI}{d\theta} = -7.43 \times 10^{5}\, I_o \text{ at the center of the beam, and}$$

$$\frac{dI}{d\theta} = -1.91 \times 10^{6}\, I_o \text{ at the edge of the beam, and}$$

the angle subtended at the range of 1 AU by the telescope separation of 5.0 meters, is

$$\delta\theta = \frac{5.0}{1.50 \times 10^{11}} = 3.33 \times 10^{-11} \text{ radian.}$$

It may then readily be shown that, since signal current is proportional to intensity for direct detection,

$$\delta i_s = -7.43 \times 10^5 \times 3.33 \times 10^{-11} \times 2.84 \times 10^{-7}$$

$$= 6.98 \times 10^{-12} \text{ amp}, \quad \text{at } \theta = \frac{\theta B}{10} = 0.015 \text{ arc second,}$$

and:

$$\delta i_s = -1.91 \times 10^6 \times 3.33 \times 10^{-11} \times 2.84 \times 10^{-7}$$

$$= 1.80 \times 10^{-11} \text{ amp}, \quad \text{at } \theta = \frac{\theta B}{2} = 0.075 \text{ arc second.}$$

It should be noted also, that the noise power spectral density corresponding to these signals, since each pointing error detection channel uses only two of the four telescopes, is half that in the presence and tracking channels, or:

$$\varphi_{nn} = 2 \times 18.35 \times 10^{-26} = 36.7 \times 10^{-26} \text{ amp}^2/\text{Hz}$$

at

$$\theta = \frac{\theta B}{10} = 0.015 \text{ arc seconds, and}$$

$$\phi_{nn} = 2 \times 13.8 \times 10^{-26} = 27.6 \times 10^{-26} \text{ amp}^2/\text{Hz},$$

at

$$\theta = \frac{\theta B}{2} = 0.075 \text{ arc seconds.}$$

9.9.1.6.2 Simulation From Synchronous Orbit

9.9.1.6.2.1 Tracking Resolution

Using the equations and definitions from section 9.9.1.6.1, but substituting:

$P_t = 7.5 \times 10^{-3}$ watt

$R = 3.60 \times 10^{7}$ meters

$D = 0.3$ meter,

the energy detected by the four phototubes of one telescope is, at the center of the beam:

$$P_r' = \frac{(0.5)\ (0.5)\ (7.5 \times 10^{-3})\ (0.3)^2}{(3.60 \times 10^{7} \times 7.28 \times 10^{-7})^2} = 2.5 \times 10^{-7} \text{ watt.}$$

The signal current (at the PMT anodes) produced by this energy is:

$$i_s = 2.5 \times 10^{-7} \times 3.4 \times 10^{3} = 8.5 \times 10^{-4} \text{ amp}$$

and, at the edge of the beam, it is half this amount, or

$$i_s = 4.25 \times 10^{-4} \text{ amp.}$$

The anode dark current, as in the previous case (section 9.9.1. 8×10^{-9} amp for four tubes.

Background illumination, using the equation and definitions of section 9.9.1.6.1.1, but substituting $D = 30$ cm, is

$$P_b = 16 \times 10^{-8} \times 1.0 \times 6.66 \times 10^{-8} \times \frac{\pi}{4} \times (30)^2 \times 0.5 \times 0.5$$

$= 1.89 \times 10^{-12}$ watt, which produces a current at the anode of:

$$i_b = 1.89 \times 10^{-12} \times 3.4 \times 10^{3} = 6.4 \times 10^{-9} \text{ amp.}$$

The total anode current for one telescope is then:

$$8.5 \times 10^{-4} + 8 \times 10^{-9} + 6.4 \times 10^{-9} = 8.5 \times 10^{-4} \text{ amp,}$$

at the beam center and

$$4.25 \times 10^{-4} + 8 \times 10^{-9} + 6.4 \times 10^{-9} = 4.25 \times 10^{-4} \text{ amp,}$$

at the edge of the beam.

The noise power spectral density (for one telescope), corresponding to this current is:

$$\phi^{1}_{nn} = 2e\, i_{DC} = 2(1.6 \times 10^{-19})\ (8.5 \times 10^{-4})$$

$$= 2.72 \times 10^{-22}\ \text{amp}^2/\text{Hz}, \text{ at the center of the beam,}$$

and

$$2(1.6 \times 10^{-19})\ (4.25 \times 10^{-4}) = 1.36 \times 10^{-22}\ \text{amp}^2/\text{Hz},$$

at the edge of the beam.

The total noise power spectral density for the four telescopes is:

$$\phi_{nn} = 4 \times 2.72 \times 10^{-22} = 10.9 \times 10^{-22}\ \text{amp}^2/\text{Hz}, \text{ at the beam center,}$$

and

$$\phi_{nn} = 4 \times 1.36 \times 10^{-22} = 5.45 \times 10^{-22}\ \text{amp}^2/\text{Hz}, \text{ at the edge of the beam.}$$

The signal-to-noise ratio in a 1 Hz presence channel is thus

$$S/N = \frac{(4)\ (8.5 \times 10^{-4})}{\sqrt{10.9 \times 10^{-22} \times 1.0}} = 1.0 \times 10^{8}, \text{ at the center of the beam}$$

and

$$S/N = \frac{(4)\ (4.75 \times 10^{-4})}{\sqrt{5.45 \times 10^{-22} \times 1.0}} = 7.3 \times 10^{7} \text{ at the beam edge.}$$

Tracking resolution (S/N = 1) for a 10 Hz tracking loop equivalent noise bandwidth and a ±5 arc second linear range is:

$$\Delta\theta = \frac{1}{1.0 \times 10^{8}/\sqrt{10}} = \times\ (\pm 5) = 1.6 \times 10^{-7} \text{ arc second}$$

at the center of the beam, and

$$\Delta\theta = \frac{1}{7.3 \times 10^{-7}/\sqrt{10}} = \times\ (\pm 5) = \pm 2.2 \times 10^{-7} \text{ arc second at the beam}$$

edge.

9.9.1.6.2.2 Beam Pointing Correction Signals

As in sections 9.9.1.6.1.2 and 9.9.1.5.2.5, $\frac{dI}{d\theta} = 7.43 \times 10^5 I_o$ at the beam center and $\frac{dI}{d\theta} = -1.91 \times 10^6 I_o$ at the beam edge.

The angle subtended by the telescope separation of 0.5 meter at a range of 3.60×10^7 meters is $\frac{0.5}{3.60 \times 10^7} = 1.39 \times 10^{-8}$ radian, so that similarly to section 9.9.1.6.1.2,

$$\delta i_s = -7.43 \times 10^5 \times 1.39 \times 10^{-8} \times 8.5 \times 10^{-4}$$

$$= -8.75 \times 10^{-6} \text{ amp, at}$$

$$\theta = \frac{\theta B}{10} = 0.015 \text{ arc second, and}$$

$$\delta i_s = -1.91 \times 10^6 \times 1.39 \times 10^{-8} \times 8.5 \times 10^{-4}$$

$$= -22.5 \times 10^{-6} \text{ amp, at } \theta = \frac{\theta B}{2} = 0.075 \text{ arc second}$$

The noise power spectral density in these channels is, as in section 9.9.1.6.1.2, one half the corresponding values in the presence and tracking channels, or

$$\phi_{nn} = 5.45 \times 10^{-22} \text{ amp}^2/\text{Hz, at}$$

$$\theta = \frac{\theta B}{10} = 0.015 \text{ arc second, and}$$

$$\phi_{nn} = 2.2 \times 10^{-22} \text{ amp}^2/\text{Hz, at}$$

$$\theta = \frac{\theta B}{2} = 0.075 \text{ arc second.}$$

9.9.1.7 Stability Requirements of Point-Ahead Correction (Space-Ground-Space) Loop

Stability criteria and dynamic performance of this loop, including the effect of the transmission delays, are discussed in some detail in Appendix I-1 of the OTAES Interim Progress Report, Volume IV.

Utilizing the root-locus plot, Figure I-3 on page I-6 of that report, it will be found that a gain margin of 10 decibels, and a damping ratio of about 0.71 correspond to a value of $K_v T = 0.495$, where K_v is the loop velocity error coefficient, and T is the transit delay (round trip)

At a range of 1 AU, the round trip delay, $T \approx 16$ minutes = 960 seconds, making $K_v = \frac{0.495}{960} = 0.515 \times 10^{-3}$ sec^{-1}, or approximately 5×10^{-4} sec^{-1}, to achieve the desired stability. Use of a higher value of K_v at this range will decrease the stability margin. The loop gain will therefore be controlled to insure stability.

Since the stability criterion is a limitation on the product, $K_v T$, it may be seen that higher values of gain (and hence, of K_v) can be tolerated for lower values of the transit delay, T, which occur at shorter ranges.

From the results of sections 9.9.1.5 and 9.9.1.6 it may be seen that the actuating error gradients are an inverse function of range, hence loop gain increases with decreasing range. Some additional control is anticipated however, to insure that the stability of the loop is maintained at all ranges.

9.9.2 Optical Propagation Experiment Analysis

9.9.2.1 Space Qualified Laser Considerations for OTAES Program

9.9.2.1.1 Introduction

This subsection covers some aspects of the problem associated with the space qualification of the He-Ne and CO_2-N_2 gas lasers chosen for use in the OTAES experiments. The discussion includes some of the lifetime, thermal, mechanical, electrical, and optical problems associated with space qualification. The object of this report is to present a solid foundation from which a detailed design can be developed during a later phase of the program. Primary emphasis has been placed upon the thermal and life time problem associated with both the He-Ne and CO_2-N_2 lasers.

The proposed version of the space qualified laser package is essentially that presented in the previous OTAES reports and is shown in figure 9.9.2.1.3.1. The outer shell and package configuration are the same (except for dimensions) for each of the He-N_2 lasers and the CO_2-N_2 laser. The laser dimensions are presented in table 1. The difference between the He-Ne laser package and the CO_2-N_2 laser package is in the method of heat transfer from the laser discharge tube to the shell, and in the discharge tube support. This difference primarily affects the internal design of the laser package, and is required because the CO_2-N_2 laser has a more critical temperature dependence than the He-Ne.

Each of the four laser packages is mounted to the telescope in the same fashion. A collar with a quick disconnect capability holds the mounting flange of the laser package firmly against a rigid disk which is extended from the telescope well. Except where other components interfere the disk has a surface area approximately equal to the telescope aperture. A detailed drawing of the mounting arrangement is shown in section 9.5.

The collar will be capable of holding the laser in alignment yet allow for easy removal under flight conditions. The disk and the telescope support structure provide the heat sink for the laser package.

9.9.2.1.2 Telescope Structure Thermal Environment

The purpose of this section is to provide a brief description of the laser telescope structure thermal interaction. For a detailed telescope thermal analysis see section 27.

The laser mounting flange, and hence the shell of the laser package will tend to reach the temperature of the telescope structure. It will be greater than that value due to the power generated in the laser itself, and the temperature rise developed across the thermal impedance of the circular support disk and the laser flange contact surface. The telescope structure is subject to a thermal environment which is a function of the heat generated internally by the electro-optical equipment, the thermal radiation and albedo from the earth's surface, and the thermal radiation from the telescope sunshield. In general all of these inputs vary with time. Preliminary analysis[(1)] has shown that over a ten-day period of synchronous orbit the temperature of one portion of the telescope support structure can range from -268°C to +235°C when starting from a 25°C initial temperature prior to launch. The computations used to obtain this temperature range were influenced by the fact that two lasers were operating in the telescope well during the run, and that the insulating characteristics of the laser package were not considered. A more reasonable temperature range might be -73°C to 155°C over both the launch and operation conditions.

In order to maintain reliability lifetime, and nearly constant output power (small fluctuations can be controlled by adjusting the input power), the laser discharge tube for both the He-Ne and CO_2-N_2 lasers should operate at a nearly constant temperature after the initial warm-up period. Thus under some operating conditions the laser package will perform the dual function of insulator and conductor of heat between the laser discharge tube and telescope structure.

9.9.2.1.3 Laser Package

An important requirement for the He-Ne and CO_2-N_2 space qualified lasers for the OTAES program is that in addition to the thermal considerations the mounting must maintain beam axis alignment to within the range of the boresight correcting apparatus under the shock, vibration, and acceleration environment. Of several ways for obtaining this objective, the most direct is to mount the laser rigidly to the telescope frame (see figure 9.9.2.1.3-1) to prohibit relative motion of the laser and telescope axis. The beam may then be redirected as required by optical steering mechanisms also attached to the frame. A single mounting point was chosen so that any external forces exhibited on the laser package would produce only a translation of the package about the mounting axis which could be corrected by the laser beam steering mechanism. In this way bending or twisting moments produced along the laser package can be predicted during the design and corrected for by the internal mirror alignment transducers.

Cooling is accomplished by conduction through the thick walled cylindrical aluminum tube to the telescope mounting flange. Heat transfer from the discharge tube to the cylindrical shell is accomplished by conduction and radiation.

(1) Telescope Thermal Analysis OTAES Interim Progress Report, vol. IV, Appendix J, NAS8-20256, March 8, 1966.

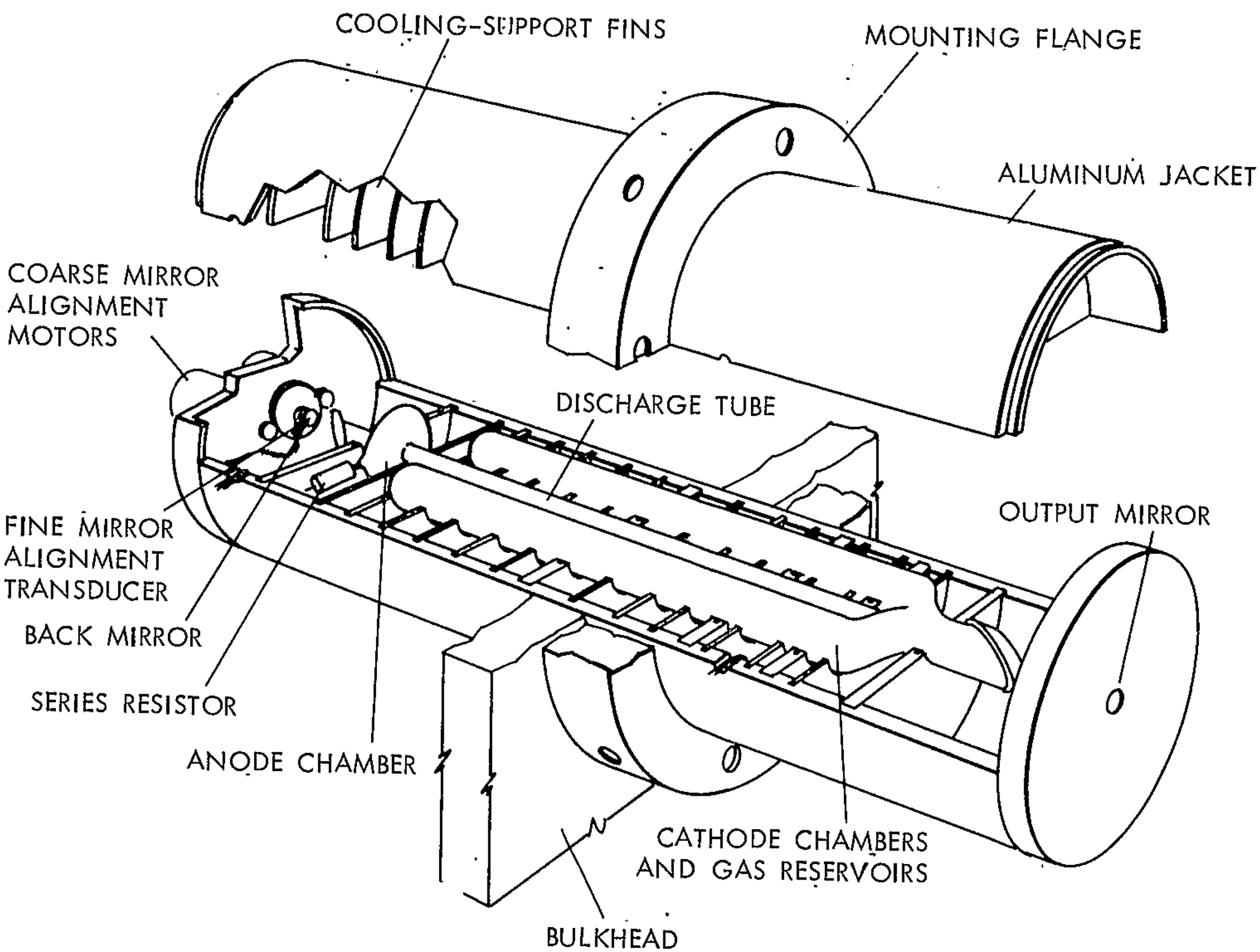

Figure 9.9.2.1.3-1. Spacecraft Laser Package.

The He-Ne version of the space qualified laser is shown in figure 9.9.2.1.3-1 with a detail of the discharge tube shown in figure 9.9.2.1.3-2. Typically the discharge tube has a thick-walled quartz capillary section about 45-cm long. A helium-neon tube with a 3-mm bore would be capable of over 15-mW output power at 6328 Å. Brewster windows, optically contacted and fused, terminate the discharge tube. The windows are in the parallel (rather than opposed) configuration and sufficiently thick so that cumulative refraction of the windows causes the cavity to be misaligned for the lines at 3.39 microns and 1.15 microns. This construction prevents spurious oscillation at these wavelengths without the need for incorporating Q-spoiling magnets around the discharge tube.

The connections to the laser discharge are through close-spaced parallel wires, twisted pairs, or coaxial cable to prevent the generation of spurious magnetic flux. An enlargement at one end of the laser tube contains an anode plate or ring; at the other end are two long tubular appendages which serve as gas reservoirs and cathode chambers.

The resonator is formed by a plane output mirror and a large-radius spherical back mirror. The output of the laser will be maintained in a TEM_{00} transverse mode and at an output power of 15 mW (transmitter taken as example). The 2-mm output beam will be collimated and diffraction limited at the output of the flat mirror. The required power output, mode configuration, spatial coherence, and beam diameter will be achieved with a 45-cm long, 3-mm diameter discharge tube, a plane output mirror and a spherical back mirror of about 100-meters radius. The divergence of the output beam will result entirely from diffraction. Mode and power output stability will be obtained by use of an alignment transducer upon which the spherical back mirror is mounted. The alignment transducer serves a multiple function: (a) it controls the normal changes in cavity alignment over the operating temperature range, and (b) it provides a method for applying a remote correction to the cavity alignment to compensate for contingencies such as inelastic deformation during launch, etc. The plane output mirror will be installed into a precise recess with no provisions for adjustment. This rigid mounting will insure that angular deviation will be held to a minimum, since use of a plane output mirror causes the output to be precisely orthogonal to the mirror plane. This method of mounting the mirror is used to insure that the laser design will meet the shock and vibration environmental conditions discussed in the Optical Heterodyne detection report.[2]

In order to insure that the output polarization of the laser is compatible with the various optical modulators used in the system, attention will be paid to making the polarization linear to one part in 1000. Measurements performed at GT&E Laboratories and elsewhere have indicated that this can be achieved.

---

(2) Optical Technology Apollo Extension System, Final Technical Report, Part I, Chrysler Corporation Space Division, October 21, 1966.

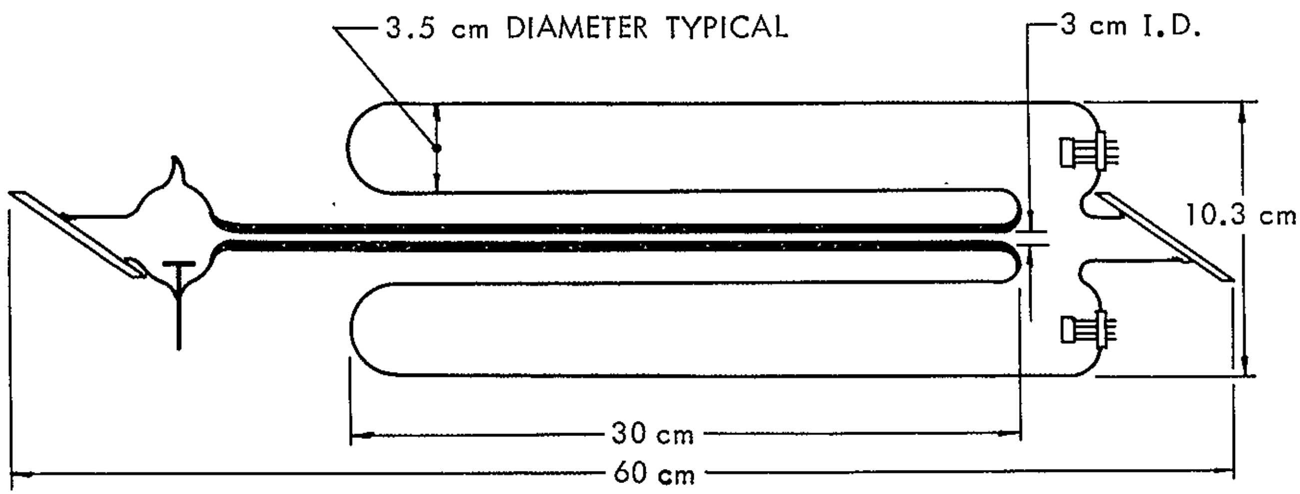

Figure 9.9.2.1.3-2. Laser Discharge Tube and Gas Reservoir.

The aluminum jacket seen in figure 9.9.2.1.3-1 serves as: (a) the principal mechanical support for the laser tube and resonator; (b) a radiation shield to keep stray light, radiant heat, and ac magnetic fields from interfering with the operation of nearby optical instruments; and (c) a path for conducting heat to the mounting flange and then to the bulkhead on which the package is mounted. In addition, a thermal shroud or wrap will be placed around the cylindrical aluminum jacket to reduce heat radiation effects and insure transfer by conduction through the flange only.

The mounting of the discharge tube within the package poses some problems. The quartz capillary tube is very elastic with low damping and could be excited under shock and vibration to large amplitude strains which might break it. This problem is solved by the use of mounting fins attached to the laser tube. The mounting fins are installed in the jacket half-cylinders. The tube is placed in one half cylinder and the other half is closed down over it. These fins will serve the dual function of conducting some of the heat to the jacket and holding the tube accurately in position, yet will yield sufficiently to avoid damage by differential expansion on temperature cycling. In addition, the fins will provide a number of supporting points for the tube and will restrict the magnitude of strain present at any point on the tube during launch. This construction technique makes it possible to minimize the weight of the shell and supporting structure while still maintaining rigidity.

It is not fully resolved at this point to what extent the supporting fins will provide cooling for the discharge tube. For the supporting fins must conduct the heat from the discharge tube at a rate which will maintain the walls of the discharge tube within a narrow limit over the operating temperature range. Changes in the temperature of the discharge tube produce gain variations which are a function of the gas density and the collisional transfer process between the helium and neon. The gain variations due to changes in gas density are the more predominant.

Because the discharge is occurring in the narrow bore of the laser while none occurs in the larger volume of the cathode and anode bulb area (see figure 9.9.2.1.3-2), the temperature rises in the bore. This causes the gas density in the area of the discharge to drop, while the gas density in the bulb increases. Since the volume of the discharge tube is small compared to the bulb area, a large density gradient is set up at the ends of the tube. This density gradient produces a less than optimum gas fill condition in the discharge bore and a corresponding drop in output power. Therefore, in addition to just conducting heat from the laser discharge tube, the fins must have their thermal impedances adjusted so that the laser tube is operating at a nearly uniform temperature. Some of the fins would be made up of concentric rings of insulating and conducting material. This would serve to adjust the thermal impedance as well as maintain the steady state operating temperature of the discharge tube within reliable operating limits for variations in the mounting flange temperature over the environmental range. It is assumed that in the steady state the walls of the laser package will tend to reach the specified operating temperatures by conduction through the package mounting flange.

Although it has a lesser effect on the gain than the density change, variations in the kinetic gas temperature in the discharge must be considered in the design if the gain and, hence, the output and efficiency are to be maintained over the operating range. The upper laser level population of the $3S_2$ state in neon is populated by collisional transfer of excitation from the 1S metastable level of helium (which, in turn, is originally excited by electron collisions in the discharge). The effectiveness of this collisional transfer process, and consequently the laser gain and output increase with the kinetic gas temperature. Conversely, if the laser jacket temperature is reduced to too low a temperature (e.g., -100°C) by cooling, a reduction in laser gain and output may follow.

To estimate practical effects on a laser in a spacecraft environment, the limiting case of a laser tube with unit emissivity surrounded by a black body is considered. Under these conditions a typical laser discharge tube 30-cm long by 9-cm o.d. and dissipating 50 watts would attain a wall temperature and therefore gas temperature of 300°C. Operation in an atmospheric room temperature environment would further cool the laser tube walls by convection to approximately 100°C. At these ranges of temperature the effect on laser output would be negligible. In the temperature environment encountered by the laser package there is no convection to reduce the temperature and all thermal controls must be performed by conduction through the support fins and radiation from the discharge to the laser package shell. To aid in heat transfer by radiation the inner surface of the cylindrical laser package will be made to look like a black body. The low temperature region is of sufficient importance that this point will be considered in sufficient detail in the next phase to insure the proper design of the support and cooling structure. This is necessary to insure that the laser discharge tube wall temperature does not drop below -50°C. The design will include provisions to protect other components internal to the laser package from extreme temperatures. One component that requires special attention is the anode resistor used to suppress relaxation oscillation. High-voltage insulation will be provided for the anode circuit within the laser package as well as between the laser package and the power supply. Insulation will surround the laser tube envelope near the anode to prevent voltage breakdown from occurring at any of the pressure levels encountered.

A thermal analysis is presented in paragraph 9.9.2.2. This paragraph analyzes the problem of conducting heat from a laser discharge tube to a cylindrical laser package constrained to a specific temperature. Since this analysis is meant to cover the general case of removing heat from within the package to a flange of known temperature, a single flange temperature was chosen. The analysis can be applied to any other flange, and hence telescope structure temperature, by adding to or subtracting from the referenced temperature.

9.9.2.1.4 Gas Tube and Mirrors

The proposed laser will employ a dc discharge from a directly heated cathode. The discharge tube will contain a spare cathode which will be switched on automatically if the first cathode should fail. A getter will be used to reduce the quantity of impurity gases in the laser. All supporting structures, cathodes, anode, reservoirs, and discharge tube will be ruggedized. Narrow-band dielectric coated mirrors will effectively prevent any detectable laser output at 1.15 and 3.39 microns. The exact dimensions of the discharge tube and the associated gas pressures will be determined during the design phase of the program for the particular He-Ne lasers shown in table 9.9.2.1.4-1.

This tube design is projected to provide a coherent output power of approximately 15 mW (depends upon the laser requirements) with a minimum gas reservoir volume over a lifetime in the order of 5,000 hours. The data for this projected figure was derived from data obtained by Watson and Fowler[3] on a previous study contract on binary gas plasmas. This study showed that the two major causes of laser tube failure were (a) gas cleanup (gas pressure loss) due to ion penetration of the tube walls and cathode and (b) outgassing of impurity ions which contaminate the tube. A considerable increase in the lifetime of cold-cathode He-Ne lasers was achieved by overfilling the laser tube beyond the pressure at which maximum output power was achieved, and then allowing the gas pressure to drop naturally as the tube ages until a state of maximum efficiency is reached. It was found that the pressures for maximum output power were 1.6 torr He and 0.16 torr Ne and that it took approximately 250 hours to reach this state from the pressures mentioned above. This investigation showed that the laser output deteriorated quickly beyond this time and lasing terminated after another 100 hours.

The space qualified laser lifetime will be extended over that of the laser investigated by several means. First, use will be made of heated cathodes which clean up the gas at one quarter the rate of cold cathodes.[3,4] The reasons for this is the substantially lower electron emission of cold cathodes. As a result of low emission efficiency, the electric field at a cold cathode must be kept large, and this causes the ions to impinge upon the cathode at high velocities and to bury themselves within. This source of ion loss is substantially lower in a heated cathode laser.

(3) W. Watson and V. Fowler, "Optical Properties of Binary Gas Plasmas," Technical Report AFAL-TR-66-7, January 1966.

(4) W. Watson and V. Fowler, "Optical Properties of Binary Gas Plasmas," Technical Report AFAL-TR-64-289, November 1964.

TABLE 9.9.2.1.4-1

LASER PACKAGE PARAMETERS

	Local Oscillator	Transmitter (single) 15 mw	Transmitter* (2 units) 15 mw each	CO_2-N_2	Symbol
Wavelength (μ)	0.6328	0.6328	0.6328	10.6	
Length (cm)	20	80	80	90	L
Input power (watts)	10	50	50	50	P
Diameter (cm)	15	20	25	25	$2r_2$
Radius (cm)	7.5	10	12.5	12.5	r_2
Outside Radius of flange (cm)	8.5	11	13.5	13.5	r_3
Thickness of flange or cap (cm)	1.0	1.0	1.0	1.0	t
Surface (cm^2)	1296	5020	7265	8050	S
Weight (g)	1207	≈8000	10,330	12,330	W

Note: * Internal optics provided to bring laser beam out coaxial with long axis of package.

A further increase in lifetime is obtained by using a large gas reservoir in the proposed laser. The lasers studied by Watson et al. had a total volume of 66 cm^3 of gas. Increasing this volume by a factor of ten should lead to a proportionate increase in lifetime. The space qualified laser has a tube and reservoir, shown in figure 9.9.2.1.3-2, whose total volume is approximately 660 cm^3

9.9.2.1.5 Cooling Requirements for the CO_2-N_2 Laser

In addition to the three He-Ne lasers a space qualified CO_2-N_2 laser with a minimum of 1 watt is required for use with the 0.3-meter telescope. This laser is subject to the same environmental conditions as the He-Ne lasers. The CO_2-N_2 laser will be housed in a cylindrical structure of aluminum similar to the design presented for the He-N_2 laser.

9.9.2.1.5.1 Wall Temperature and Lifetime Problems of CO_2 Laser

In the CO_2 laser, it is well recognized that the translational temperature of the gaseous constituents play an important role through collision processes in determining laser output and efficiency. It is now understood that to improve efficiency it is necessary to keep the translational gas temperature, which is largely determined by laser tube wall temperatures, as low as possible.

The physical basis for this requirement may be understood briefly as follows. Since the lifetimes of the excited molecular levels associated with lasering are long (order of 1 msec) they are determined by collisional processes rather than by spontaneous radiative processes. In the various collisions, vibrational energy is transferred from molecule to molecule and converted to translational energy, and vice versa, thus the system will tend to thermalize. Total thermalization would of course prevent laser action, thus operation is necessarily at lower pressures. Partial thermalization, however, is not harmful and can help in fact. Partial thermalization occurs when the various subsets of the molecular system are so strongly self-coupled that they may individually be described by a Boltzman distribution and temperature, yet several temperatures may be necessary to describe the whole system. Basically it is the rotational levels which are strongly coupled to the translational gas temperatures, whereas the vibrational levels are more strongly coupled to the electron temperature by virtue of their larger excitational cross sections. This situation satisfies the criteria for molecular laser action,[5,6] i.e., $T_{vib} \rightarrow T_{electron}$, $T_{rot} \rightarrow T_{gas}$, therefore, $T_{vib} >> T_{rot}$.

---

(5) C.K.N. Patel, "Interpretation of CO_2 Optical Maser Experiments," Phys. Rev. Lett., vol. 12, no. 12, May 1964.

(6) T. J. Bridges and C. K. N. Patel, "High-Power Brewster Window Laser at 10.6 Microns," Appl. Phys. Lett., vol. 7, no. 9, November 1965.

Thus, the population of the upper level in the CO_2 (00°1 vibrational level) has a Boltzman distribution among the rotational levels which is characterized by a rotational temperature (T_{rot}) approaching the translational temperature of the CO_2 molecules. For transitions on which inversion is sufficient for oscillation, variation in power among the laser lines will follow the same Boltzman distribution. The translation temperature of the CO_2 which determines this Boltzman distribution is determined by the tube wall temperature. This is even more so the case where helium is an additive; due to its higher velocity and higher thermal conductivity, it produces (by collision with the CO_2 molecules) an even lower rotational temperature (again linked to the wall temperature) which shifts the center of the laser action to a lower P-branch transition. This leads to an improvement in the maximum gain available for a few transitions near the center of laser action and a decrease in the gain for the remaining transitions. The helium further enhances this process by increasing the thermalization rate among the rotational levels; as well as dropping the rotational temperature. First order analysis shows (5) gain to improve approximately as $T^{-3/2}$.

Experiments have since verified this. However, due to the large variation in the laser parameters, such as amount of additive gasses used, it is too early to give general results, and these can only be quoted for specific cases.

Bridges and Patel[6] show that for a pure CO_2 laser and a CO_2 - N_2 laser with outputs of 2-5 watts and efficiencies of approximately 2 percent the efficiency improves by a factor of 2 when the jacket temperature is lowered from 40°C to -60°C.

In a more optimum tube, with the He additive and a power output of approximately 10 watts, Moeller and Rigden[7] found that efficiency dropped by 50 per cent when the tube temperature increased from 35°C to 110°C for a flowing gas system. This is also borne out approximately by measurements at Spectra Physics ranging from -20°C to 50°C.

From the various data the following figures may be reasonably deduced for a CO_2 laser with optimum additives of nitrogen and helium. For a power input of 50 watts output

at 0°C $\approx$ 5 watts

50°C $\approx$ 2.5 watts

130°C $\approx$ 1.3 watts

---

(7) G. Moeller and J. Dane Rigden, "High Power Laser Action in CO_2-He Mixtures," Appl. Phys. Lett., vol. 7, no. 10, November 1965.

Thus for the space requirement in question, with an output of at least 1 watt, the laser tube jacket needs to be kept below 130°C.

The dimensions of such a laser tube could be typically 75-cm long and 1-cm in diameter. By laser tube jacket we are referring to the discharge tube axial with the laser housing.

9.9.2.1.5.2 Window Temperature

At the moment the most promising window materials appear to be germanium. These however need to be maintained at approximately 20°C. This may be achieved by cooling the window-mirror housing. Possibly with a separate thermoelectric type device.

Irtran has too high an absorption which reduces efficiency by a factor of two. Salt windows would need to be hermetically sealed on the ground and further, they have a tendency to crack.

GaAs appears promising; but there is a difficulty, however, of making large enough crystals.

9.9.2.1.5.3 Lifetime Problems of CO_2 Lasers

Sealed-off life of CO_2 lasers is governed by the irreversible dissociation of CO_2. The irreversibility of the process is believed to occur as a result of the cleanup of oxygen from the discharge.

Possible processes leading to depletion of O_2 in CO_2 laser tubes are:

a. Adsorption and absorption in the glass discharge tube.

b. Gas cleanup by electrodes.

c. Oxidation of sputtered material.

Recent work with tantalum electrodes shows that is the most plausible mechanism where newly sputtered material from the cathode surface is oxidized either by CO_2 or O_2, to form a stable metal oxide by either of the following reactions

$$5\,O_2 + 4\,Ta \rightleftarrows 2\,Ta_2O_5$$

and

$$5\,CO_2 + 2\,Ta \rightleftarrows 5\,CO + Ta_2O_5$$

when stable oxides are formed such as Ta_2O_5, this leads to the irreversible depletion of O_2, and the decomposition of CO_2 to CO and oxygen.

Other processes such as oxygen trapped by sputtered cathode material on tube walls or on the cathode surface are temporary. The sputtered material will diffuse back from the walls to the cathode surface where it is resputtered, freeing the trapped oxygen.

9.9.2.1.5.4 Methods of Extending Life Time

The depletion of CO_2 may be offset by either introducing a fresh supply of CO_2 or by adding extra oxygen to the discharge.

This may be done in two ways.

a. Gas reservoir bottles.

b. Active chemical elements, or bulk sorbtion getters.

In more detail:

a. Gas reservoir bottles may be used in conjunction with an electrically controlled leak valve. This may be a very simple device where resistive heating (requiring very little power) of a taut thin wire normally holding the valve closed, permits it to open and leak the required gas into the laser tube.

b. A continuous and controllable supply of CO_2 can be liberated from $BaCO_3$ and $SrCO_3$ which are commonly used in vacuum and discharge tubes as basic materials for oxide coated nickel cathodes. When heated to a temperature of 1000°C these alkaline earth carbonates decompose to form stable oxides, and release CO_2 by

$$BaCO_3 \rightarrow BaO + CO_2$$

and

$$SrCO_3 \rightarrow SrO + CO_2$$

For example a folded nickel tape with an area of 5 cm^2 with a Ba - Sr - CO_3 coating of the type used in typical vacuum cathodes gave a gas evaluation of 8 liter torr. This corresponds to about 10 times the CO_2 required to fill a 75-cm long, 1-cm diameter CO_2 laser tube.

9.9.2.1.5.5 Oxygen Source

Sources of oxygen may also be used, such as sodium peroxide which begins to decompose at 300°C to sodium monoxide and oxygen.

$$2\,Na_2O_2 \rightarrow 2\,Na_2O + O_2 \quad (\text{at } T \geq 300°C)$$

With these resources available it is not expected that life time will pose a problem.

9.9.2.1.5.6 CO_2 Laser Package Considerations

In order that the CO_2-N_2 laser be practical for space applications one of the forms of sealed-off tube designs must be employed. Each of the designs discussed places a severe requirement on the thermal characteristics of the laser package. For the discharge tube requires operating temperatures below 130°C for long life and a minimum of 2 per cent efficiency (based upon 50-watts input), a lower efficiency would place a more severe requirement on the cooling since the additional heat would have to be removed. In order to remove the excess heat efficiently and keep the discharge tube wall temperature below 130°C, a more sophisticated approach than cooling - conducting fins must be employed. This includes the use of liquids and liquid solid (fine particles) mixtures.

The low temperature environment is not the serious problem in the CO_2-N_2 laser. The problem lies in the fact that under certain environmental conditions the mounting flange temperature might exceed the laser discharge tube wall temperature. This would make heat exchange from the discharge tube to the cylindrical shell of the laser package very difficult. One simple solution to this problem is to operate the laser only when the flange temperature falls within a certain range. Since the flange temperature takes upwards of 10 days, or more, to reach steady state with the laser generating heat, this should not place a serious restriction on the conducting of experiments. This approach could allow the CO_2 laser package detailed design to incorporate conducting fins combined with a particle filled silicone oil which acts as a good heat conductor while providing excellent vibration isolations.

To operate the CO_2-N_2 laser with flange or telescope structure temperatures above that required at the discharge tube wall for 1-watt output would require complete heat transfer equipment external to the laser package. This would require additional prime power and space. For example, if the heat exchanges were 20 per cent efficient, and the temperature of the flange was 130°C, an additional 250 watts of prime power would be required during the operating period. In addition, the flowing of liquid through flexible tubing tends to reduce the reliability of the equipment.

9.9.2.1.5.6.1 Alignment Transducer

The optical cavity of the Space Qualified Laser will consist of a fixed flat-surface mirror, which couples the beam out of the cavity; a spherical back mirror, which is mounted on an alignment transducer with two degrees of control. The choice of this transducer, whether it be piezoelectric or motor controlled, will be determined during the design phase. A servo motor alignment transducer draws power only when correction is being applied but is limited in speed of response.

The alignment transducer serves a multiple function: (a) it controls the normal changes in cavity alignment over the operating temperature range, and (b) it provides a method for applying a remote correction to the cavity alignment to compensate for any contingencies, such as inelastic deformation during launch or reentry. A discussion of the two axis servomechanism which drives the transducer is presented in the electronics section.

9.9.2.1.5.6.2 Laser Electronics Package.

The functional electronics package is shown in the block diagram of figure 9.9.2.1.5.6.2-1. Its function is to operate, monitor, and control the laser cavity and discharge tube. The package will consist of: (a) a solid-state converter-current regulator with a high-voltage starting circuit to initiate discharge current, (b) a regulated filament supply, (c) alignment control servomechanisms, (d) telemetry sensors consisting of thermocouples and a quadrant photodetector for generating alignment error signals and for monitoring the output power, and (e) telemetry and amplifiers.

9.9.2.1.5.6.3 Laser Power Supply

The laser power supply presented in this discussion is applicable to all the lasers being considered for the program. The voltage, current, and power being different for the different lasers.

The power supply contains a converter-regulator for the discharge current. A second converter-regulator or rectified 400 Hz can be used for the filament supply where applicable. (Not required for CO_2-N_2.) This approach allows standby operation at maximum power supply efficiency and simplifies the starting circuit design. A switching-type regulator is used to maintain high efficiency. A block diagram of the converter-regulator portion of the power supply is presented in figure 9.9.2.1.5.6.3-1.

The current regulator, with a few-thousand ohm series resistor, provides a high impedance source for the laser tube to minimize the laser noise and prevent relaxation oscillations. The series resistor is just large enough to suppress

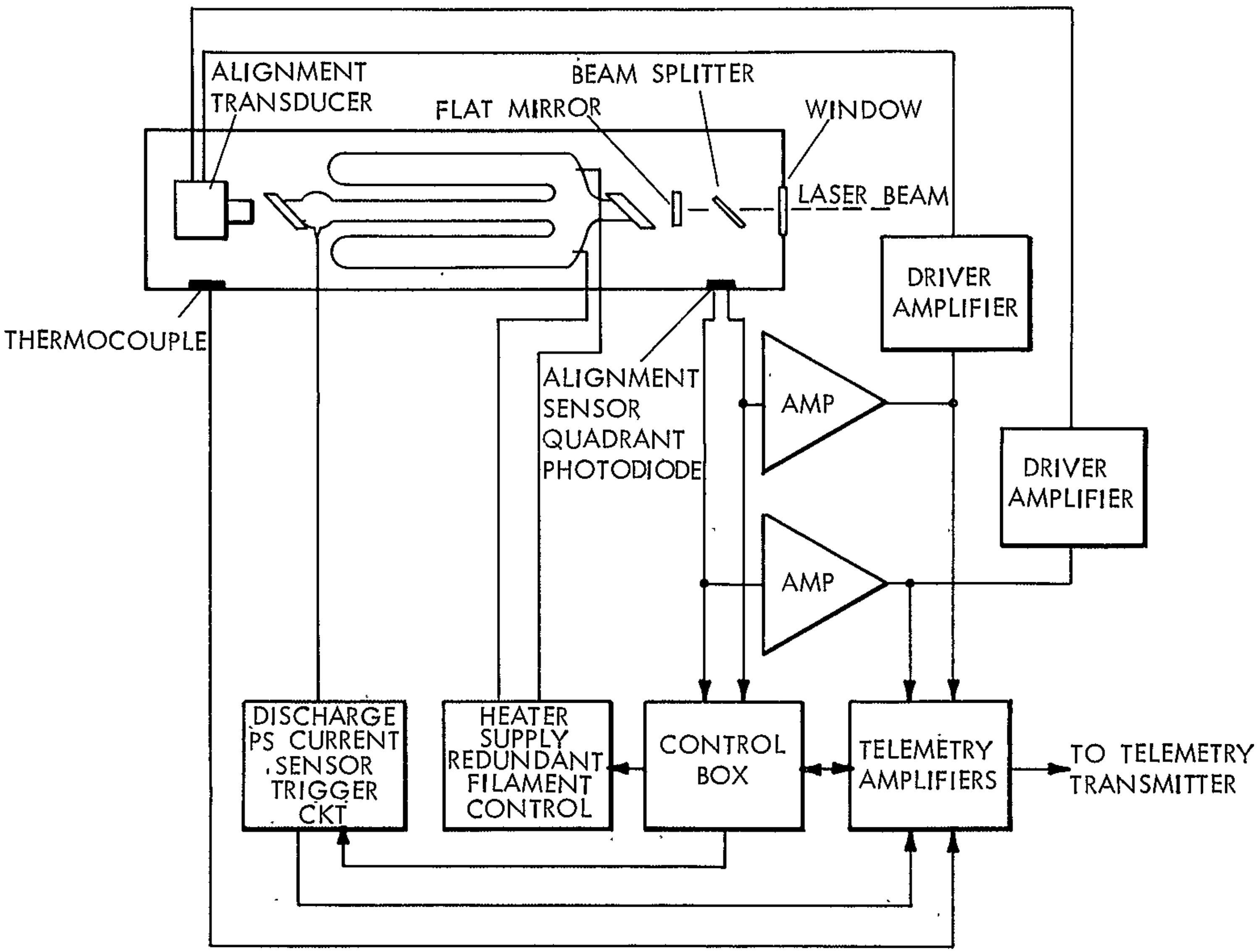

Figure 9.9.2.1.5.6.2-1. System Block Diagram.

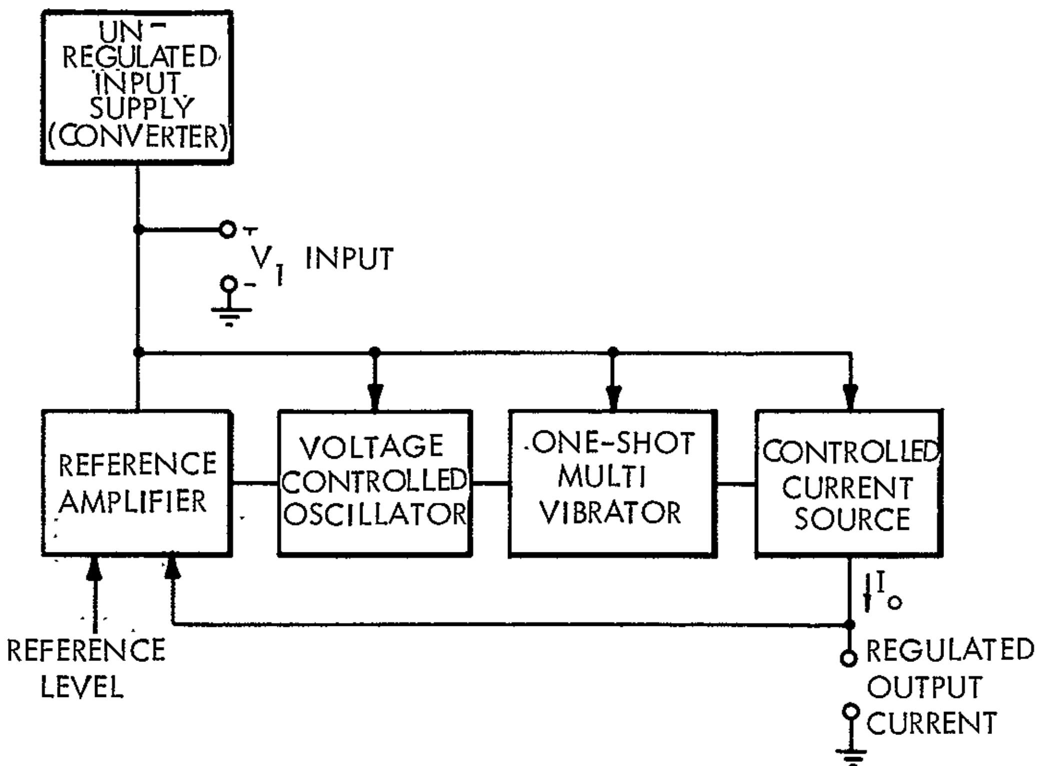

Figure 9.9.2.1.5.6.3-1. Block Diagram of Converter-Regulator.

relaxation oscillations associated with the negative dynamic resistance of the laser tube and parasitic capacitance from the laser anode to ground. The resistor is integral with the laser package, being located close to the anode to minimize stray wiring capacitance.

The laser tube starting or trigger circuit is part of the discharge power supply. The trigger voltage generator is in series with the power supply and the laser tube. Upon command, the trigger voltage is impressed across the circuit as a train of 20-millisecond pulses. When discharge current is sensed, the pulses are removed. Long high-voltage pulses are used in preference to RF pulses to minimize interference radiation during the starting period.

The two-axis alignment transducer is part of a two channel Type I servomechanism driven by error signals from a quadrant photodetector. The quadrant photodetector performs four monitoring functions associated with the laser beam. These are: power output, noise level, mode purity, and beam alignment. A circuit associated with the diode separates the monitored beam parameters and channels them to the appropriate section of the electronics package. The quadrant photodetector is needed to provide the error signals for the servomechanisms which control the two-axis alignment transducer. After laser action has been achieved, the photodetector samples part of the laser beam falling on the beam splitter and causes the alignment transducer to deflect the beam independently in each axis until it is centered in the field of view of the quadrant photodetector. When this occurs, a null voltage is impressed at the input to the servo amplifier. A separate circuit (part of monitor circuit) samples the presence of an error at the detector. If no signal is present at the photodetector and discharge current is flowing, the transducer servomechanism is placed in a search mode. A helical scan will be searched out by applying quadrature voltages of changing amplitude to each axis of the servomechanisms until a signal is detected by the photodetector.

Other parameters that will be monitored in the laser system include: discharge current, filament current, and cavity wall temperature.

9.9.2.2 Thermal Properties of a Laser Package

Three lasers are considered in the following package design calculations. For each of the packages the weight, temperature distribution thermal time constant, dimensions and other parameters are tabulated in table 9.9.2.2-1. The choice of parameters reflects a general design approach rather than a complete and detailed design. The generalized package design (figure 9.9.2.2-1) for each will be a cylindrical sleeve that is closed on the ends by caps and is mounted to a bulkhead by an annular flange around the middle of the cylinder.

TABLE 9.9.2.2-1

Laser No.	Local Oscillator #1	Transmitter 2 Units #2	CO_2-N_2 #3	Symbol
Wavelength (cm)	$6.328\text{x}10^{-5}$	$6.328\text{x}10^{-5}$	$1.06\text{x}10^{-3}$	λ
Wavelength (μ)	0.6328	0.6328	10.6	
Length (cm)	20	80	90	L
Input power (watts)	10	50	50	P
Output power (milliwatts)	0.1	15	1000	P
Heat flow (cal/sec)	2.39	11.9	11.9	q_0
Diameter (cm)	15	25	25	$2r_2$
Radius (cm)	7.5	12.5	12.5	r_2
Inside Radius of shell (cm)	7.463	12.057	12.0	r_1
Shell thickness (cm)	0.035	0.443	0.500	(r_2-r_1)
Outside Radius of flange (cm)	8.5	13.5	13.5	r_3
Thickness of flange or cap (cm)	1.0	1.0	1.0	t
Surface (cm^2)	1296	7265	8050	S
Weight (g)	1207	10,330	12,330	W
Ambient & flange temp. (deg. C)	20	20	20	T_0
Mean temp. rise (deg C)	8	8	8	$\overline{T}-T_0$
Expansion (cm)	$3.7\text{x}10^{-3}$	$15\text{x}10^{-3}$	$17\text{x}10^{-3}$	ΔL
Expansion λ	58	233	16	$\Delta L/\lambda$
Thermal time constant (sec)	$9\text{x}10^{2}$	$16\text{x}10^{2}$	$19\text{x}10^{2}$	χ
Thermal time constant (min)	15	27	32	
Thermal conductivity $\left(\frac{\text{cal}}{\text{sec}}\frac{\text{cm}}{\text{cm}^2}\frac{1}{\text{deg C}}\right)$	0.29	0.29	0.29	k
Density (g/cm^3)	2.77	2.77	2.77	δ
Specific heat $\left(\frac{\text{cal}}{\text{g}\cdot\text{deg C}}\right)$	0.23	0.23	0.23	C
Shell cross section (cm^2)	1.717	34.19	38.46	A

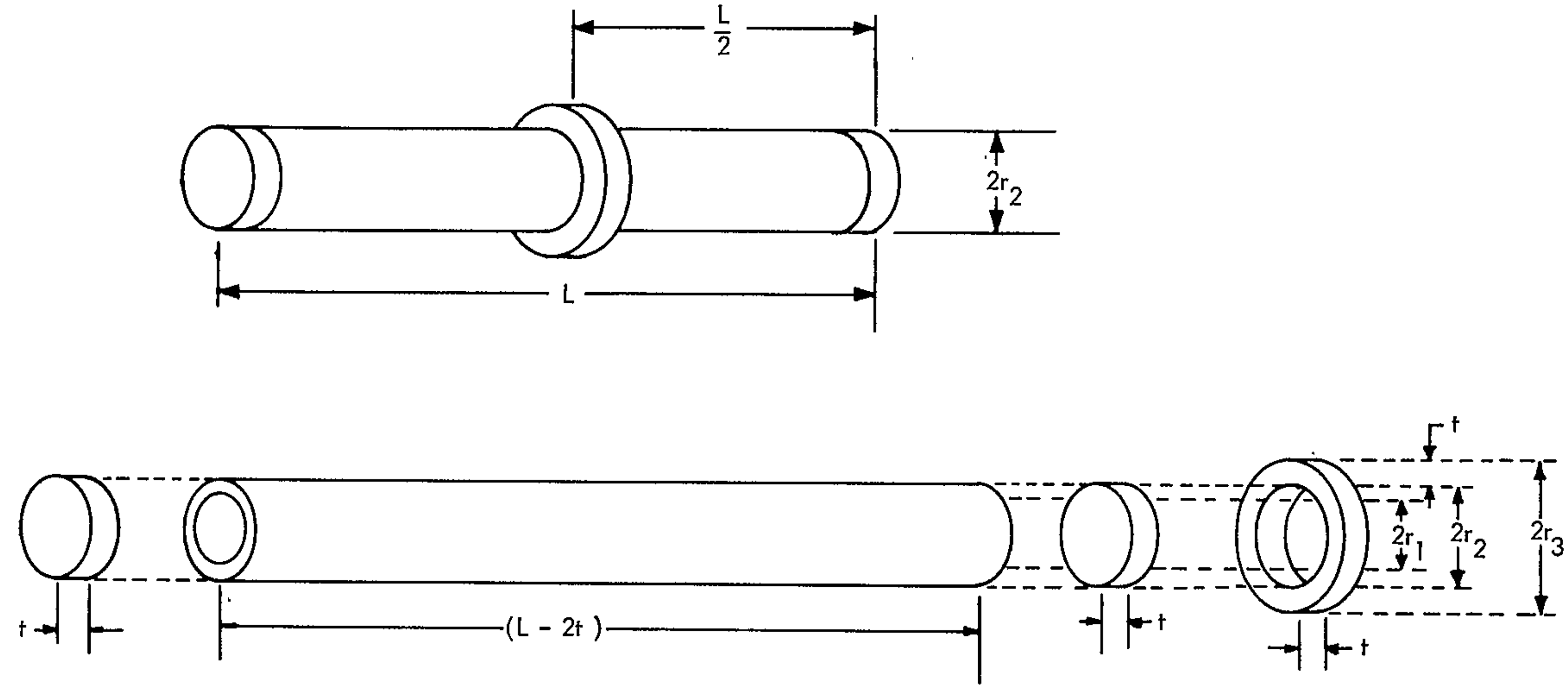

Figure 9.9.2.2-1. Generalized Laser Package Design

The rate of heating of the package q_0 (cal/sec) is assumed to result from complete conversion of the electrical input power P(watts) to heat.

$$q_0 = P/4.186 \quad \text{(cal/sec)} \tag{1}$$

This heat is assumed to be transferred to the shell uniformly along its length by radiation from the laser tube or by other means. Heat is also assumed to be removed from the shell only by conduction at the flange. (To reduce the effect of radiant heat transfer, a thermal shroud is placed over each of the shells.) This is most effective in minimizing the effects on the remainder of the optical system during ground operations. The longitudinal heat flow q(z) at a distance z from the middle of the package is given by Eq. (2)

$$q(z) = \frac{q_0}{2} + \frac{q_0}{L} z \tag{2}$$

By symmetry only the right-hand portion of the package need be considered so at the origin of the z-coordinate the heat flow has the magnitude $q_0/2$ and is in the minus-z direction at any z. The heat flow in this one-dimensional case is also a function of the thermal conductivity, k, the cross-sectional area, A, and the temperature gradient, dT/dz, as given in Eq. (3).

$$q(z) = -kA\, dT/dz \tag{3}$$

The temperature T(z) is obtainable from the temperature of the flange T_0 and the integral of the gradient along the shell to the point at z.

$$T(z) = T_0 + \int_0^z \frac{dT}{dz}\, dz \tag{4}$$

Eliminating q(z) between Eqs. (2) and (3), one obtains the following expression for the temperature gradient

$$dT/dz = \frac{q_0}{2kA} \left(1 - \frac{2z}{L}\right) \tag{5}$$

One now obtains an expression for the temperature rise with respect to the temperature of the flange by carrying out the integration of Eq. (4).

$$T(z) - T_0 = \frac{q_0 L}{2kA} \left(\frac{z}{L} - \frac{z^2}{L^2}\right) \tag{6}$$

For convenience we use normalized variables for the fractional distance ξ and for the fractional temperature rise θ as defined in Eqs. (7) and (8).

$$\xi = 2z/L \tag{7}$$

$$\theta = \left[T(z) - T_0\right] / \left[T\left(\frac{L}{2}\right) - T_0\right] \tag{8}$$

In terms of these variables Eq. (6) is represented by Eq. (9).

$$\theta = 2\,\xi - \xi^2 \tag{9}$$

From this it is clear that the temperature rises quickly at first and then more slowly as one passes from the flange ($\xi = 0$) to the end of the package ($\xi = 1$).

The mean temperature rise of the shell is required for estimating the thermal expansion of the cavity. In terms of θ this is simply $\bar{\theta}$.

$$\bar{\theta} = \frac{\int_0^1 \theta\, d\xi}{\int_0^1 d\xi} = \int_0^1 \left(2\xi - \xi^2\right) = 2/3 \tag{10}$$

From this the mean temperature rise of the package above the flange temperature is obtained.

$$\bar{T} - T_0 = \frac{2}{3}\left[T\left(\frac{L}{2}\right) - T_0\right] \tag{11}$$

It is seen that the mean temperature rise and the temperature rise to the end of the package are not independent; the values used for example will be:

$$T_0 = 20 \tag{12a}$$

$$T\left(\frac{L}{2}\right) = 32 \tag{12b}$$

$$T\left(\frac{L}{2}\right) - T_0 = 12 \tag{12c}$$

$$\bar{T} - T_0 = 8 \tag{12d}$$

The length, L, and outside diameter of the packages, $2r_2$, have been taken as specified. It is now required to determine other package dimensions consistent with the temperature given under Eqs. (12). Evaluating Eq. (6) at z = L/2 gives:

$$T\left(\frac{L}{2}\right) - T_0 = \frac{L\, q_0}{8k\, A} \tag{13}$$

For Eq. (13) the quantities L, q_0, k, and $\left(T\left(\frac{L}{2}\right) - T_0\right)$ are tabulated in table 9.9.2.2-1 and the cross sectional area of the shells A have been determined and tabulated.

$$A = 0.431\, L\, q_0 \left[T\left(\frac{L}{2}\right) - T_0\right] \tag{13b}$$

$$A = \pi\left(r_2^{\,2} - r_1^{\,2}\right) \tag{14}$$

$$r_1 = \sqrt{r_2^{\,2} - \frac{A}{\pi}} \tag{15}$$

The inside radius of the shell has also been calculated by Eq. (15) as a function of the results of Eq. (13b) and the specified outside diameters ($2r_2$). The wall thickness for package No. 1 is clearly too thin (0.035 cm) but that is of no consequence at the moment; the wall would be made thicker for mechanical reasons and this would reduce the temperature rise along the package below the assumed value of 12°C: [see Eq. (6)] . The thickness t for the flange and end caps has been taken as 1.0 cm and is thus about twice the thickness of the wall of the shell of package No. 3.

The weight of each package was also calculated using the density δ of aluminum and the tabulated sizes.

$$\delta = 2.77 \text{ g/cm}^3$$

$$W = \boldsymbol{\delta} \cdot V = \pi\,\delta \left\{- r_1^{\,2}\,(L - 2t) + r_2^{\,2}\,(L - t) + r_3^{\,2}\, t\right\} \tag{16}$$

The expansion of the length of each package from the time that the laser is turned on until it reaches a steady state is of interest as this affects the tuning of the laser cavity unless the mirror spacing is decoupled from this expansion. The expansion Δ L that has been calculated is the change in length that would occur if the initial temperature is uniform at T_0 and the final temperature is the T(z) of Eqs. (12). As the thermal expansion depends linearly on temperature, within the present degree approximation, the mean temperature rise ΔT is the significant quantity.

$$\Delta T = \bar{T} - T_0 = 8 \tag{17}$$

$$\frac{\Delta L}{L \Delta T} = k = 23 \times 10^{-6} \tag{18}$$

$$\Delta L = 1.84 \times 10^{-4} L \tag{19}$$

Equation (18) defines the coefficient of linear expansion k, and Eq. (19) gives the change of length. The values of ΔL are given in table 9.9.2.2-1 both in centimeters and in units of the respective wavelengths.

The time during which the rising temperature affects the length of the cavity is significant with respect to warm up times that must be allowed for the operation to become stable. A time constant, τ, can be estimated on the basis of the heat stored at equilibrium and the rate that heat is flowing through the system.

$$\tau = \frac{W \cdot C \cdot \Delta T}{q_0} \tag{20}$$

The mass, W, and heat flow, q_0, have been given in the table, while ΔT is the mean rise from the initial temperature T_0; thus the numerator of Eq. (2) gives the stored energy and q_0 gives the heat flow. The values of τ calculated by Eq. (20) are given in the table.

9.9.2.3 Direct System Trade-Offs

The purpose of the direct system for OTAES is to trade off laser power, beam-pointing accuracies, and beam-collimation requirements in the spacecraft at the expense of enlarging the ground-based optical collector. This trade-off is extremely significant because it provides a means by which spacecraft tolerances and requirements can be relaxed. It thus serves to enhance the reliability of the spacecraft-to-ground communication link.

Since the direct detection communication system is independent of the atmosphere coherence diameter limitation, a large aperture collector can be used. A large receiving aperture will provide an excess of aperture gain that may be traded off to relax the pointing requirements both on the earth and in the spacecraft, preserving the capability for megahertz bandwidth communications. The direct detection system technique accepts a detector efficiency of 10^{-1}, laser efficiencies of 10^{4}, pointing accuracies of tens of microradians, and nondiffraction-limited optics. The signal-to-noise ratio for an optical communication link using direct detection, neglecting dark current in the photodetector, is[8]:

$$\frac{S}{N} = \frac{\rho P_s^2}{2e\Delta f \left| P_s + P_B \right|} \tag{1}$$

where:

ρ = The responsivity of the photo-surface = $e\eta/h\nu$

P_S = The signal power received at the photomultiplier (watts)

P_B = The background power received at the photomultiplier (watts)

e = The electronic charge

Δf = The electrical noise bandwidth of the system (hertz)

η = Quantum efficiency (number of charge carriers per photon)

h = Planck's constant

ν = Optical frequency (hertz)

The receiver signal power is:

$$P_s = \frac{P_t}{\Omega_t} \frac{A_r}{R^2} T_o T_A \tag{2}$$

where:

P_t = Transmitted power (watts)

Ω_t = Transmitter half-power solid angle beamwidth (steradians)

A_r = Effective area of the receiver collecting optics (Square meters)

T_O = Optical transmission

T_A = Atmospheric transmission

R = Range (meter).

(8) G. Biernson and R. Lucy, "Requirements of a Coherent Laser Pulse Doppler Radar," Proc. IEEE, vol. 51, January 1963, pp. 202-213.

For a ground receiver, the background power due to air scattering is given by the expression:

$$\left(P_B\right)_{\text{blue sky}} = A_r T_o \Omega_r (N_\lambda)_{\text{sky}} \Delta\lambda \tag{3}$$

where:

Ω_r = The field of view of the receiver

N_λ = Average spectral radiance of the sky in the optical filter bandwidth, $\Delta\lambda$, as measured at the telescope receiver aperture, A_r.

Using Eqs. (1), (2), and (3), the signal-to-noise power ratio at the ground receiver system output may be written as:

$$\left(\frac{S}{N}\right)_{\text{Space to Ground}} = \left(\frac{P_t \rho A_r T_o T_A}{2e\Delta f \Omega_t R^2}\right) \left\{\frac{1}{1 + \dfrac{\Omega_r N_\lambda \Delta\lambda}{\dfrac{P_t T_A}{\Omega_t R^2}}}\right\} \tag{4}$$

The term in the first parentheses is the expression for signal photon noise-limited operation. The term in the second parentheses represents the effect of background in reducing the signal-to-noise ratio for signal photon noise-limited operation.

Typical parameters for the system are given in table 9.9.2.3-1. A graph of the space-to-ground performance as a function of the transmitter radiant intensity is shown in figure 9.9.2.3-1.

In the curves, a typical transmitter power and beamwidth are indicated for a 30-dB signal-to-noise ratio. In this case, operation will be signal photon noise-limited. Note that all the system parameters are within the state-of-the-art.

Figure 9.9.2.3-2 shows the ground-based optics diameter plotted as a function of the spacecraft transmitter beamwidth for different laser transmitter powers. The curves are derived from Eq. (4). The system is photon noise-limited when operating against a daytime blue sky background at a distance of 32,000 km. A signal-to-noise requirement of 30 dB and a 10-MHz bandwidth have been specified. The other parameters are given in table 9.9.2.3-1.

TABLE 9.9.2.3-1
TYPICAL VALUES REQUIRED FOR DIRECT DETECTION EXPERIMENT

SYSTEM PARAMETERS	SPACE-TO-GROUND NONCOHERENT
Range	3.22×10^{7} meters (20,000 miles)
Laser Power[(a)]	10^{-3} watts
Beamwidth[(a)]	1.4×10^{-5} radians
Wavelength	6.328×10^{-7} meters (6328 A)
Filter Bandwidth[(b)]	2 A
Modulation Type	Polarization
Filter Transmission[(b)]	0.4
Nominal Optics Efficiency	0.75
Nominal Atmospheric Transmission[(c)]	0.5
Typical Background Radiance Observed by Receiver[(d)]	Blue Sky at Zenith* 2×10^{1} watts/m^2-stermicron
Optical Collector Area	50 meters^2
Minimum Receiver Field of View	5×10^{-4} radians
Phototube Type	S-20 (C70038D)
Peak Signal to RMS Noise[(a)]	30 dB
System Bandwidth	10 MHz

(a) Possible system parameters as indicated on curve.
(b) Spectralab mica interference filter.
(c) Less than standard clear atmosphere at 60° from zenith.
(d) Angle of sun and observer neglected for simplicity.

---

*F. Moller, "Optics of the Lower Atmosphere," Applied Optics, vol. 3, no. 2, February 1964, p. 161.

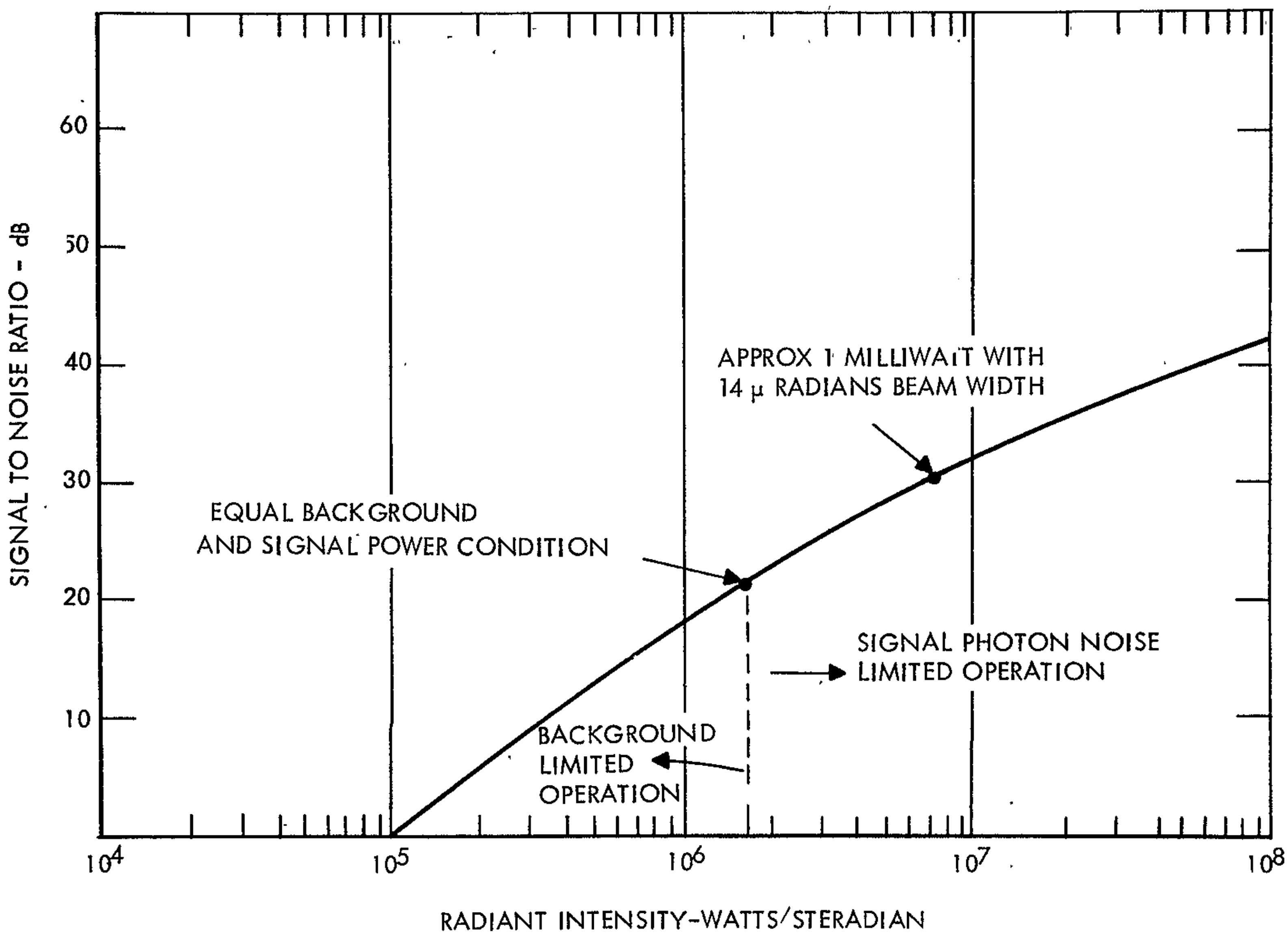

Figure 9.9.2.3-1. Performance of Direct Detection Ground Based Receiver Against Blue Sky Background.

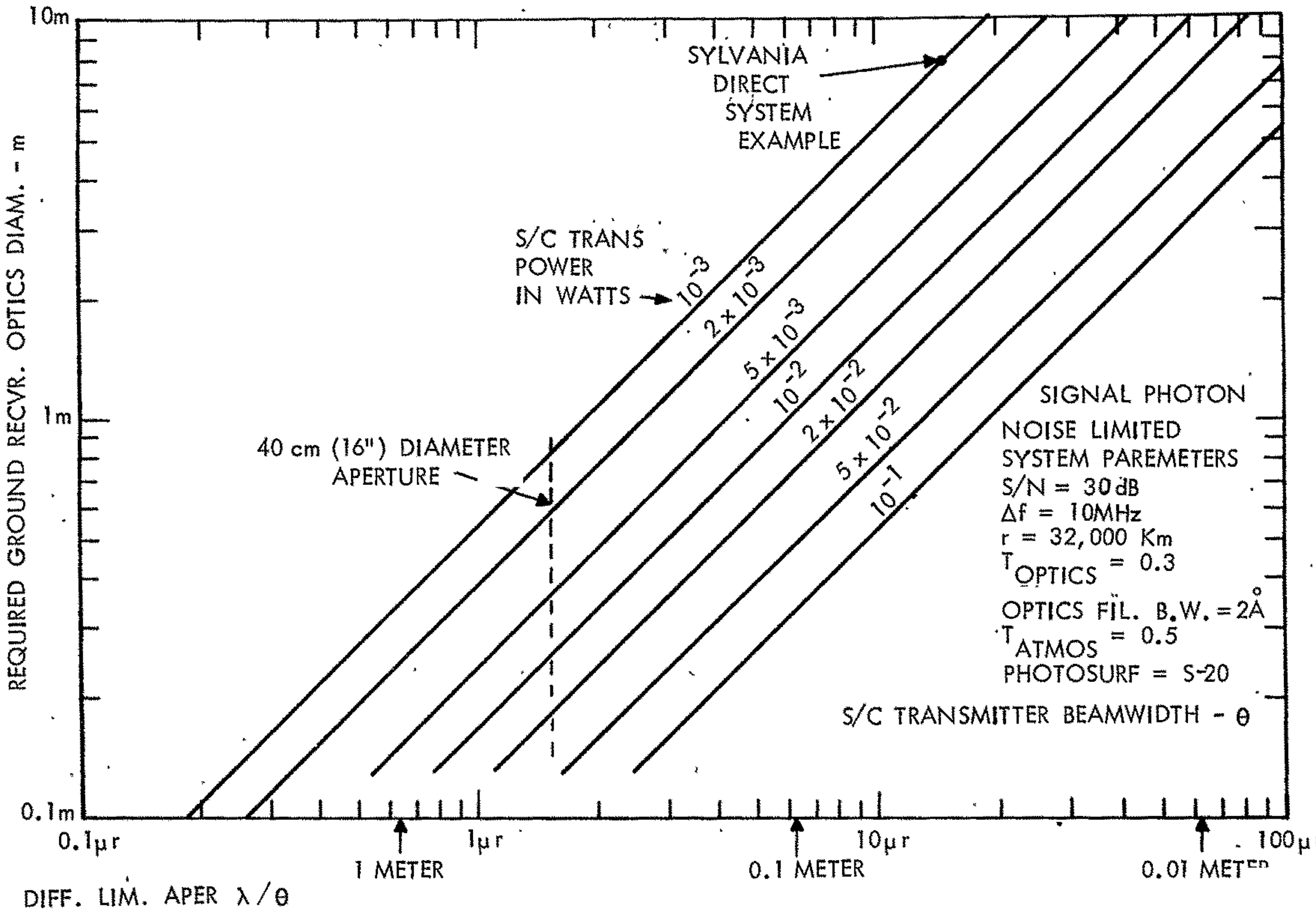

Figure 9.9.2.3-2. Direct System Tradeoffs for 6328 Å.

9.9.2.3.1 Evaluation of Direct Detection at 10.6μ

Because of the high power and efficiency of operation ($\epsilon \cong 10^{-1}$ for CO_2-N_2 vs. $\epsilon = 10^{-3}$ for HeNe) and relaxed tolerance requirements, the 10.6 microns, CO_2-N_2 laser may prove useful as another choice of wavelength of operation. A simple comparison of the 0.63-micron system to the 10.6-micron system may be made.

The background problem at 10.6 microns is less severe than at 0.63 micron. The background power incident upon the detector is:

$$P_B = N_\lambda \Omega_r \Delta\lambda A_r T_o T_F \tag{5}$$

A typical radiance value for clear sky at 10.6 micron is:

$$N_\lambda = 1 \text{ watt/m}^2\text{-micron-steradian}$$ [9]

If we assume a 2-per cent bandwidth interference filter and the ground-based receiver values of table 9.9.2.3-1, the background power incident upon the detector is:

$$\left(P_B\right)_{10.6} = 10^{-6} \text{ watts}$$

This amount of power is small compared to the total blackbody radiation from the optical antenna that is viewed by the detector. For a detector limited by excess noise due to its surroundings,[10] the detectivity D* is defined as:

$$D^* = \frac{\left(\frac{S}{N}\right)_v}{P_s} \left(\Delta f A_c\right)^{1/2} \tag{6}$$

where:

$\left(\frac{S}{N}\right)_v$ = The voltage signal-to-noise ratio

P_s = The signal power in watts

Δf = The noise bandwidth in hertz

A_c = The detector area in cm^2.

---

[9] "Background Measurements during the Infrared Measuring Program," 1956, AFCRL-TN-60-692, November 1960, p. 149.

[10] The aperture ratio of the detector must match the aperture ratio of the optical antenna in order to collect all the energy coming from the optical antenna. To improve the detector, a cooled spectral filter would be desirable.

Substituting Eq. (2) for P_S in Eq. (6) and solving for the transmitter radiance gives:

$$\frac{P_t}{\Omega_t} = \frac{R^2 \left(\frac{S}{N}\right)_v (\Delta f A_c)^{1/2}}{D^* T_o T_A A_r} \tag{7}$$

Typical D* values of Ge-Hg[11] are 3×10^{10} cm $(Hz)^{1/2}$/watt for an f/1.3 detector aperture ratio and a 4^{o}K operating temperature. The minimum area of the detector, determined by the optics circle of confusion, would be 0.25 cm^2.

Using the parameters from table 9.9.2.3-1 in addition to those properties of the detector, and requiring a 30-dB signal-to-noise ratio, the required transmitter radiant intensity is:

$$\frac{P_t}{\Omega_t} = 7 \times 10^7 \text{ watts/steradian} \tag{8}$$

Detectors can be improved by incorporating cooled spectral filters such that the detector does not see the total blackbody radiation from the optical antenna surface. Ideally the detectors could then become photon noise-limited in their operation and the ultimate limitation would be the photon noise of the signal and background radiation in the field of view of the optics. However, it has been found that as the detector field of view is reduced, other excess noise in the detector besides background will limit sensitivity. Thus, at present, Eq. (7) describes most aptly the performance of a direct detection system at 10.6 microns rather than Eq. (4) which describes only the photon noise-limited operation.

9.9.2.3.2 Deep-Space Performance of Direct Detection with State-of-Art Components

If the results of the analysis are extended to the Mars mission distance, then the transmitted signal powers must be increased by the square of the ratio of the Mars/OTAES distances or other improvements made.

Assuming the development of the critical pointing and beam-forming goals, and also having developed data from the successful operation of the direct detection system, a deep-space laser communication system becomes realizable.

---

(11) W. Wolfe, "Handbook of Military Infrared Technology," Office of Naval Research, Dept. of Navy, Washington, D.C., 1965.

An important example is the maximum Mars-to-Earth distance of 236 million miles. Ideal operation would be in the signal photon noise-limited mode. However, in any direct system application where the transmitter radiant intensity is limited and the range is continually increasing, the background radiation must be considered as the noise source limiting the ultimate system performance or guiding the system design.

At 6328 Å where the maximum laser power is about 200 milliwatt and optical filters are presently limited to 2 Å, then it becomes necessary to improve the receiver performance. In the previous example an 8-meter diameter aperture having a resolution or minimum field of view of 0.5 milliradians was recommended for the direct system. The Hale telescope at Mt. Palomar has a 5-meter diameter and a resolution of 6 microradians. Thus, an apparent immediate improvement would be to upgrade the resolution of the large aperture optics and perform a fine tracking of the signal in the focal plane to solve the pointing problem. Increasing the diameter would produce complications because increasing size and weight would make better resolution more difficult.

Column 1 of table 9.9.2.3-2 shows a typical set of parameters for an improved direct detection system at Mars distances. Beam pointing, beam forming, large aperture optics, and other vital developments have been assumed and Eq. (4) has been used in this calculation to determine the system bandwidth. Both blue sky and Mars have been included as contributing to background, and the calculation has been made for a field of view of 27-microradian at which the background power is equal to the signal power. Requiring a 20-dB signal-to-noise ratio in a PCM communication system allows a noise bandwidth of 53 kHz with an error rate of 1 in 10^6.

Column 2 of table 9.9.2.3-2 shows a typical example for 10.6 microns using the 8-meter collector aperture on the ground. The detector for this case is limited by its inherent noise and not blue sky or Mars background radiation. Assuming improved optical resolution, the detector size has thus been reduced to match the optics resolution and, consequently, has improved the detector sensitivity.

The small bandwidth of 230 Hz at 10.6-microns, compared to 53 kHz at 6328 Å, is representative of the present state-of-the-art with the indicated optics and pointing requirements. In this example the laser input power for each wavelength is approximately equal. It has been assumed that the CO_2 laser is approximately 500 times more efficient than the He-Ne laser at 6328 Å, and the parameters are representative of a direct comparison between the two wavelengths at the present time.

9.9.2.3.3 Future Performance

In table 9.9.2.3-2 the 6328 Å direct system example is near optimum. Improvements in detectors and filters might conceivably increase the bandwidth to the order of 0.1 MHz. However, at 10.6 microns significant improvements are possible. At 10.6 microns the received signal power incident upon the detector is 1.4×10^{-10} watt.

TABLE 9.9.2.3-2

TYPICAL VALUES FOR A DIRECT DETECTION COMMUNICATIONS SYSTEM BETWEEN MARS AND EARTH AT 236 MILLION-MILE RANGE

System Parameters		
Wavelength	0.63μ	10.6μ
Laser Power-Transmitted	0.2 watt	100 wat
Transmitter Aperture (1)	1 meter	1 meter
Pointing Accuracy (1)	0.1 sec.	0.1 sec
Atmospheric Transmission	0.65 (2)	0.5
Mars Background	1×10^{-8} watt/m^2-μ	1×10^{-9} watt/m^2-μ
Mars Angular Size (36-μ-radians)		
Blue Sky Background	2×10^{1} watt/m^2-μ-ster	1 watt/m^2-μ-ster
Collecting Aperture Diameter	8 meter	8 meter
Receiver Field of View (3)	27×10^{-6} radian	27×10^{-6} radian (4)*
Filter Transmission	0.4	0.85
Optics Efficiency	0.75	0.75
Detector	Improved S-20	Hg-Ge at 4°K and f/1.3 aperture
Optical Filter	2A	2000 A
Signal-to-Noise Ratio (5)	20 dB	20 dB
Noise Bandwidth	53 kHz	0.230 kHz

(1) Optics Requirements
(2) Standard Clear Atmosphere 60° from Zenith
(3) For Equal Signal and Background Power
(4) Corresponds to Detector Area of 7.8×10^{-4} cm^2, i.e., (2.8×10^{-2} cm x 2.8×10^{-2} cm)
(5) PCM Error Rate = 1 in 10^6

* This resolution is not necessary at 10.6 mircrons because the largest background component originates from the optics radiation, but is employed only to define a minimum detector size.

If a signal photon noise-limited system could be made by the realization of a photon noise-limited detector and narrower optical filters to eliminate background, then the ultimate bandwidth could be several megahertz. For example, using Eq. (4) and neglecting background power, the resultant bandwidth is 3.5 MHz at 20-dB signal-to-noise ratio and 10 per cent detector quantum efficiency.

To achieve only a 1-MHz bandwidth background photon noise-limited operation will be sufficient. To achieve this mode of operation the detector must be background limited when operating under the direct detection system conditions and narrower bandpass optical filters will be required. Background limited detectors (Blip) are nearly realizable at 10.6 microns.

The background, P_B, limiting the detector operation will be the sum of the blue sky thermal emission, scattered sunlight from Mars, and black body radiation from the direct detection optics. Table 9.9.3.3-3 shows the calculated power values for the direct detection system example. It is apparent that the optics radiation is the limiting background. Using Eq. (1), the maximum allowable value of P_B for a 1 MHz calculated to be 3.5×10^{-10} watt. To achieve this the optical filter bandwidth would have to be reduced from 2000 Å to 13 Å.

TABLE 9.9.2.3-3

CALCULATED RECEIVER POWER LEVELS FOR DIRECT DETECTION AT 10.6 MICRONS FOR MARS-TO-EARTH EXAMPLE OF TABLE 9.9.2.2-2 ($\Delta\lambda$ = 2000 Å)

Signal Power	$= 1.4 \times 10^{-10}$ watt
Sky Emission	$= 3.7 \times 10^{-9}$ watt
Mars Reflected Sunlight	$= 7 \times 10^{-9}$ watt
Optics Emission*	$= 5.5 \times 10^{-8}$ watt

*Temperature	= 295° K
Emissivity	= 0.1
Angular Size viewed by detector	= 44°
$\Delta\lambda$	= 2000 Å

Detectors can be improved by incorporating cooled spectral filters such that the detector does not see the total black body radiation from the optical antenna surface. Ideally, the detectors could then become photon noise limited in their operation, and the ultimate limitation would be the photon noise of the signal and background radiation in the field of view of the optics.

An alternative approach at 10.6 microns is also possible. The 1.0-meter transmitting aperture produces a diffraction-limited 10-microradian beam. Pointing accuracies of the order of 0.5 microradian will be realized by OTAES. An increase in aperture size to 3.1 meters will increase the signal power by a factor of 10 and still remain within pointing capabilities. Under these conditions a calculation shows that only a Blip detector would be required to achieve a 1-MHz bandwidth.

A photoconductive detector must have sufficient noiseless gain in order to be properly matched to the following amplifier. The requirement is that the photon-noise output of the detector be greater than the amplifier noise. Equation (78) of Reference (8) describing this requirement may be written as:

$$G > \sqrt{\frac{\pi f_{hi} C(FKT)\,(h\nu)}{Qe^2\,(P_S + P_B)}} \tag{9}$$

where

G = photoconductive gain

f_{hi} = 3-dB high-frequency cutoff required

C = detector output and amplifier input shunt capacity

FKT = amplifier noise spectral power density.

Typical values are:

f_{hi} = 1 MHz

C = 10 pfd

F = 1

T = 300° K

Q = 0.1.

Using Eq. (9) when

$$P_S + P_B = 5 \times 10^{-10} \text{ watt}$$

$$G > 50$$

which corresponds to the 10.6-micron example using narrower spectral filters.

For the 3.0-meter aperture case

$$P_S + P_B = 5.6 \times 10^{-8}$$

$$G > 5.$$

These values are representative of the gain required in the Blip detectors to assure a 1-MHz bandwidth.